AFCRL-67-0075
JANUARY 1967
SPECIAL REPORTS, NO. 57

AIR FORCE CAMBRIDGE RESEARCH LABORATORIES
L. G. HANSCOM FIELD, BEDFORD, MASSACHUSETTS

Proceedings, Fourth AFCRL Scientific Balloon Symposium

Editor
JAMES F. DWYER

OFFICE OF AEROSPACE RESEARCH
United States Air Force

DISCLAIMER NOTICE

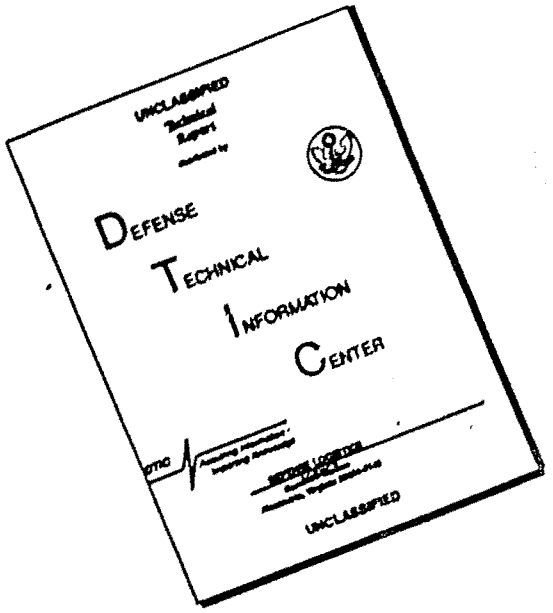

THIS DOCUMENT IS BEST QUALITY AVAILABLE. THE COPY FURNISHED TO DTIC CONTAINED A SIGNIFICANT NUMBER OF PAGES WHICH DO NOT REPRODUCE LEGIBLY.

AFCRL-67-0075
JANUARY 1967
SPECIAL REPORTS, NO. 57

AEROSPACE INSTRUMENTATION LABORATORY PROJECT 6665

AIR FORCE CAMBRIDGE RESEARCH LABORATORIES

L. G. HANSCOM FIELD, BEDFORD, MASSACHUSETTS

Proceedings, Fourth AFCRL Scientific Balloon Symposium

Editor

JAMES F. DWYER

OFFICE OF AEROSPACE RESEARCH
United States Air Force

Abstract

This document is comprised of a series of papers presented at the Fourth AFCRL Scientific Balloon Symposium in September 1966. The range of subject matter was purposely selected to cover both the major branches of balloon technology and a limited number of topics having a common disciplinary background. It was intended to provide, thereby, the exchange of information on capabilities and requirements essential to the orderly advancement of this technology.

Contents

Contents

1. Recent Developments in High-Altitude Meteorological Balloons

Eric Nelson
Kaysam Corporation of America
Paterson, New Jersey

Two years ago I was accorded the privilege of speaking to you here about two new types of special-purpose balloons which had recently been developed. It is gratifying to be asked to talk to you again for two reasons. First, because I must conclude that the previous address was of interest to at least a few of you. Second, because it is good to know that the humble, rather shabby looking, dusty meteorological balloon still finds its place among its glamorous polyolefin sisters and its noisy boisterous brothers, the rockets.

During this two-year interval we have been concentrating on providing balloons capable of reaching ever higher altitudes with greater reliability. It is my purpose to acquaint you with the vehicles which are now available for high-altitude soundings and research. At the same time, I want to describe a technique which resulted from the development of the ML-566 fast-rise balloon that simplifies the launching of large balloons and further improves their reliability and performance.

The largest balloons which are supplied in high volume quantities are the ML-537 balloons, which are purchased by the Armed Forces, and its counterpart purchased by the U.S. Weather Bureau and identified as the 1200-g balloon. The ML-537 is required to reach an altitude of 110,000 ft by day and by night at an

(Received for publication 18 January 1967)

ascensional rate of at least 1,000 ft/min. The altitude requirement for the Weather Bureau is slightly lower, being 31,500 m or 103,500 ft. Considerable data is, of course, available for this type of balloon, and in order to demonstrate the reliability of this vehicle we are using the test data obtained by the U.S. Weather Bureau during the course of the last production contract. These balloons were manufactured by the Kaysam Corporation of America and the flight data presented as Table 1 were obtained with balloons selected at random from production lots by Weather Bureau inspectors and flown by Weather Bureau personnel.

Table 1. Flight Performance of 1200-g Balloons

		Percentage of Flights Reaching			
		105,000 ft	110,000 ft	115,000 ft	120,000 ft
Total of 140 flights		89	81	56	30
October 1965	Day	86	57	50	21
	Night	93	93	71	43
November	Day	72	57	29	0
	Night	100	100	80	40
January	Day	100	100	75	50
	Night	40	40	20	0
February	Day	67	50	17	0
	Night	67	50	17	0
March	Day	100	100	63	25
	Night	73	64	18	9
April	Day	100	94	67	19
	Night	89	89	67	45
July	Day	93	93	62	54
	Night	92	92	67	42

In all cases a nozzle lift of 2,800 g was employed and the flights were conducted over a period of about eight months, including midwinter. Rather than list the individual flights, we have grouped them in altitude ranges, showing the number of flights which exceed a given altitude as a percentage of the total number of flights conducted.

The reliability of this balloon is clearly demonstrated by these results; almost 90 percent of the flights reach the minimum altitude required by the specification and 30 percent flew to altitudes of more than 120,000 ft. It is interesting to observe that although the balloons perform almost equally well by day and by night, there is a noticeable improvement in the altitudes reached during the summer months. We will make further reference to this phenomenon.

The next largest balloon which carries an Armed Forces nomenclature is the ML-564. This balloon has a day and nighttime altitude requirement of 120,000 ft and a weight specification of 1,800 ± 100 g. This balloon is purchased in relatively small quantities and the data available are, therefore, much more limited than that for the ML-537 balloon. However, it is possible to present sufficient data to illustrate this balloon's capabilities and the results of a series of carefully monitored flights is shown in Table 2.

Table 2. Flight Performance of 120G and 120GH Balloons
120 GH Ballons

Type	Altitudes Reached	
	Day Flights	Night Flights
120GH	140,597	136,808
	126,896	131,620
	135,076	143,205
	129,902	131,903
	129,665	131,502
120G	125,933	42,146
	140,092	135,860
	132,917	127,953
	133,789	65,282
	135,984	123,432
	131,542	124,292
	137,005	127,618
	134,938	123,050
	124,016	133,927
	131,220	118,438
	139,879	133,730
	127,195	130,850
	133,234	134,003
	140,308	
	127,759	

These flights were conducted under the supervision of Air Force Cambridge Research Laboratories and we would point out that the data presented are for this entire group of balloons and not a collection of carefully screened flights. Only if a flight were terminated because of the inability of the tracking equipment to follow the balloon were the results omitted from this tabulation.

It is again clear from the data that a vehicle which is very reliable to the 120,000-ft level is now available with equal performance and capabilities at night and during the day. It should be noted that the first five balloons in each group were substantially heavier than the remaining balloons and that these balloons appear to be somewhat more consistent in performance. Although they were no larger than the other balloons, it appears that the somewhat greater wall thickness does result in a more reliable balloon. By increasing the length somewhat further, however, a balloon capable of reaching an altitude of at least 130,000 ft can be obtained. Less data are available for this balloon, but Table 3 gives an indication of the performance obtainable from this type of balloon which weighs about 2,500 g and has a length of approximately 160 in.

The same compound was used for the manufacture of all the balloons described so far. As in many other fields, however, making a balloon which will reach still greater altitudes is not simply a question of increasing the size. Numerous other factors, including the ability of the heavier balloon to carry its own greater weight and the duration of the flight itself, necessitate building certain characteristics into the balloon compound. In order to reach altitudes of 140,000 ft and higher, a specially designed compound for use at such altitudes was developed in the laboratories of the Kaysam Corporation of America. Calculations showed that a balloon made from this compound, weighing in the order of 4,000 g, and having a flaccid length of about 240 in., should be capable of reaching an altitude of at least 150,000 ft. At the time of the original manufacture of these balloons the altitude reached for an expanding meteorological balloon was 146,000 ft, which had been attained by a balloon weighing about 6,000 g. Other balloons of this weight had also exceeded altitudes of 140,000 ft, but their performance was generally very erratic.

Table 3. Flight Performance of 130G Balloons

Day Flights	Night Flights
146,283	136,778
123,812	134,360
130,659	139,180
135,636	113,707
147,844	139,340
137,470	136,253
139,314	138,500
147,000	114,300
127,953	135,500
114,000	124,500

The size of these balloons is a basic cause of their erratic performance. A balloon having a flaccid length of 240 in. has a surface area of over 500 sq ft. In order to reach an altitude of 150,000 ft the balloon has to be capable of expanding uniformly until its surface area has increased to almost 8,000 sq ft. One small defect, such as a minute pinhole or small thin spot which prevents that particular area from expanding the required amount, can lead to premature rupture and more or less considerable reduction in bursting altitude. Hence, not only the manufacturing process itself must be conducted with meticulous care, but the inspection of the finished balloon must be carried out to the same exacting standards.

This balloon is for use in the daytime only and a limited number of flights were conducted by U.S. Army Electronics Research and Development Laboratories at Fort Monmouth, New Jersey. Five of six balloons were successfully tracked to burst and the altitudes ranged from 127,000 ft to 147,800 ft. Two of these five balloons reached altitudes in excess of 140,000 ft; the remaining three reached altitudes of 127,000, 135,000 and 139,000 ft. However, a much larger series of flights has just been completed in West Germany with this type of balloon.

The flights covered a period of about eight months and the results obtained are shown in Tables 4 and 5. The flights are given in chronological order with the date of the flight as well as the bursting altitude. Table 4 shows the performance of balloons from September, 1965, through April, 1966. The performance during the month of September was generally extremely good, and the balloon appears to be almost as reliable as the 1200-g balloon flown by the U.S. Weather Bureau, the performance of which was shown originally in Table 1.

During the winter months, however, there was a sharp deterioration in performance and as a result the number of flights was sharply curtailed, being restricted to a few evaluation flights. This situation persisted until April when there was a marked improvement in performance. Table 5 shows the results obtained during the months of May and June. It is immediately obvious that at this time of the year, and presumably from April through September, this balloon provides an extremely useful and reliable vehicle for high-altitude meteorological observations and research. Actually, during the month of June 67 percent of the balloons reached altitudes of over 150,000 ft, which surpasses the original performance in September of last year when 64 percent reached altitudes of more than 140,000 ft but only 27 percent reached the 150,000 ft level.

It has been noted that many of the problems associated with the manufacture of this balloon are due to its physical size. In a similar manner the size of the balloon also produces difficulties in inflation and launching. Furthermore, the duration of the flight can be a problem in itself. With a rate of ascent in the order of 1,000 ft/min, a flight to 150,000 ft takes 2-1/2 hr. This is uncomfortably close to the life of the battery in a standard radiosonde and there is a danger that the flight may

Table 4. Flight Performance of 140D Balloons Flown in West Germany from September 1965 to April 1966

Date Flown	Altitude	Date Flown	Altitude
9/1/65	152,000	1/20/66	26,000
9/3/65	155,500	2/21/66	46,000
9/6/65	148,500	3/29/66	23,000
9/8/65	152,000	4/1/66	26,000
9/11/65	148,500	4/5/66	144,000
9/13/66	111,500	4/7/66	125,000
9/15/65	148,500	4/19/66	111,000
9/16/65	121,500	4/22/66	147,000
9/17/65	135,000	4/25/66	157,000
9/20/65	148,500	4/26/66	95,000
9/22/65	42,000	4/26/66	131,000
11/5/65	137,500	4/27/66	141,000
12/22/65	135,000	4/28/66	75,500
12/28/65	142,000	4/28/66	137,500
1/6/66	30,000	4/30/66	154,000
1/7/66	132,000		
1/17/66	23,000		

Table 5. Flight Performance of 140D Balloons Flown in West Germany from May to June 1966

Date Flown	Altitude	Date Flown	Altitude
5/1/66	43,000	5/30/66	147,000
5/2/66	134,000	5/31/66	164,000
5/3/66	151,000	6/1/66	138,000
5/4/66	151,000	6/3/66	151,000
5/7/66	29,500	6/6/66	161,000
5/11/66	66,000	6/7/66	158,000
5/12/66	128,000	6/8/66	33,000
5/13/66	141,000	6/9/66	168,000
5/14/66	138,000	6/10/66	72,000
5/16/66	128,000	6/12/66	151,000
5/17/66	147,000	6/13/66	158,000
5/18/66	62,000	6/14/66	158,000
5/24/66	56,000	6/15/66	161,000
5/25/66	147,000	6/21/66	79,000
5/28/66	111,500		

terminate because of battery failure rather than balloon burst. Furthermore, if high winds are encountered aloft then the angle may become low enough to result in the signal being lost through ground interference.

It was felt that the carrier balloon technique which resulted from the development of the ML-566 balloon could be adapted to the high-altitude balloon with

advantage. The ML-566 balloon is designed to reach an altitude of 100,000 ft at over 1,700 ft/min. This balloon consists of a high-altitude balloon enclosed inside a two-piece streamlined balloon, as illustrated in Figure 1. The inner balloon, which is approximately twice the length of the outer balloon, is initially folded as indicated. In the case of the ML-566 the folds in the inner balloon have virtually disappeared when the assembly has been inflated and is ready for launch (see Figure 2). As the assembly rises the streamlined outer balloon provides for rapid ascent during the early stages of the flight, and this balloon is designed to burst at about 50,000 ft.

Figure 3 illustrates the appearance of the assembly after the outer balloon has ruptured and fallen away. The inner ballon, which during the early part of the flight flies in a horizontal position, as it were, now turns through 90° and assumes the normal position for a meteorological balloon with the neck at the lowest point.

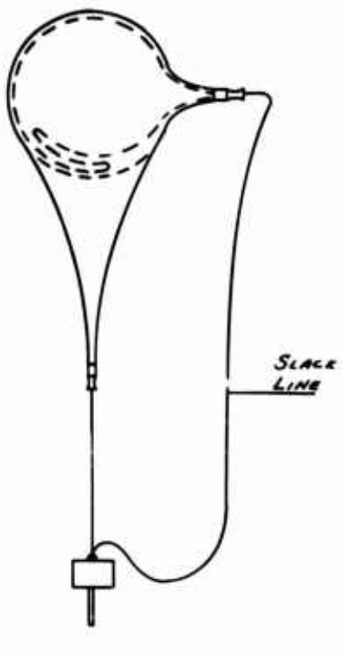

Figure 1. Carrier Balloon Assembly

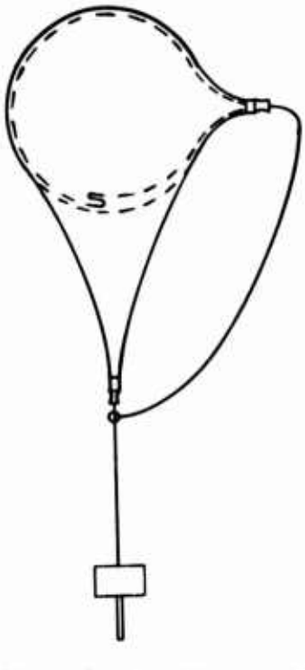

Figure 2. Carrier Balloon Assembly at Release

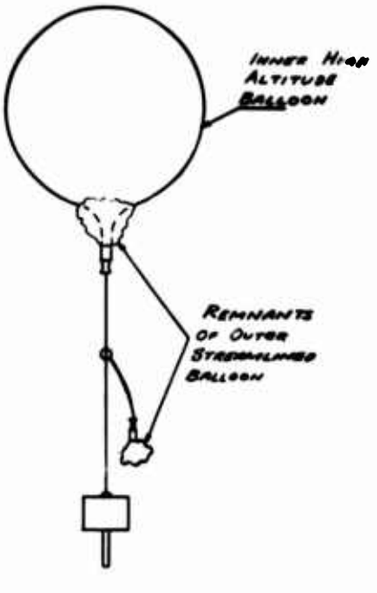

Figure 3. Carrier Balloon Assembly – Second Stage

Although the assembly was originally developed to provide faster rates of ascent, there are other advantages when it is used in conjunction with very high-altitude balloons. As already mentioned, the Kaysam 140D balloon has a flaccid length of about 20 ft. If inflated in the normal manner to a free lift of 2,000 g, which is recommended for this balloon, the balloon has a vertical height of a little

more than 20 ft. This is too great for most inflation shelters which usually have doors not more than 12 ft high. Therefore it becomes necessary to tie off the balloon near its equator during inflation and to take the balloon out of the shelter in this condition. The tie is then removed and the gas allowed to rise into the upper part of the balloon which is then released. The possibilities of damaging the balloon film by this procedure are substantial, particularly if winds exceed 10 knots.

By enclosing the high-altitude balloon inside a carrier balloon, however, the danger of damage to the inner balloon is eliminated. Furthermore, since the carrier balloon is much smaller than the inner balloon, the problem of its excessive length is also overcome and inflation and launching can be carried out in conventional shelters or from an automatic launching device.

In addition to the increased ease of handling and launching which the carrier technique provides, the outer balloon provides protection against atmospheric attack during the early part of the flight. This is admittedly a somewhat tenuous advantage in that there is little evidence that balloon flights do terminate as the result of atmospheric attack. However, it had been observed in the past that there appeared to be an upper limit of about 145,000 ft beyond which a meteorological sounding balloon was incapable of flying. One thought is that this limit was set by the duration of the flight or time of exposure of the balloon to the atmosphere. Should this be the case, then the protection afforded by the outer balloon during the early stages of the flight would permit the inner balloon to reach higher altitudes by reducing the length of time during which it was subject to atmospheric attack.

The fact that the carrier technique also increases the ascensional rate, thereby still further reducing the total flight time, also minimizes the possibility of failure by atmospheric deterioration of the balloon film. The reduction in overall flight time also decreases the possibilities of the flight being lost due to battery failure, and because the more rapid rate of rise provides higher angles from the ground tracking equipment the chances of a flight being lost due to interference from the ground are also substantially reduced.

The use of a carrier balloon system has, therefore, numerous practical advantages and flights are now being conducted with this type of assembly. At the present time the number of such flights is quite limited, and it is by no means clear that this technique is enabling the balloons to reach higher altitudes. Table 6 shows the performance obtained with these balloons so far. Although the highest altitude obtained in the United States by a meteorological balloon of the expanding type was with this type of assembly, there have been higher altitudes reported from West Germany with single balloons. However, the advantages in ease of handling and more rapid rate of ascent still render the carrier balloon system worthy of consideration, particularly where the inflation and launching

Table 6. Flight Performance of High-Altitude Carrier Balloon Assemblies

Altitude	Rate of Ascent
151,634	1309
145,000 F/A	1368
140,662	1240
133,244 F/A	1196
136,194 F/A	1345
143,842	1262
156,390	1511
139,215 F/A	1290

area is restricted. They could, for instance, be used successfully on ships where such conditions prevail. Furthermore, the reliability of the balloon appears to have been greatly improved; the lowest altitude recorded is 133,244 ft and not because of a balloon burst.

In conclusion, we may say that meteorological balloons of the expandable type are now available which are capable of reaching altitudes of as high as 120,000 and 130,000 ft with a high degree of reliability. By enclosing these types of balloons in carriers, the rate of ascent can be raised from as little as 1,000 ft/min to at least 1,300 ft/min with virtually no loss in altitude. In addition, there is also a balloon capable of reaching altitudes of over 140,000 ft and frequently over 150,000 ft with good consistency. Use of this balloon is limited at present to the hours of daylight. Research aimed at providing a similar vehicle for use at night is being conducted.

Acknowledgments

I should like to express my thanks to Mr. M. Sharenow of U.S. Army Electronics Research and Development Laboratories for his valuable advice during the course of this research that has led to the development of the balloons described. I also want to acknowledge Mr. R. Leviton of AFCRL and Mr. Sharenow for conducting the flights in the United States, and the U.S. Weather Bureau for making available the flight data on the 1200-g balloons, and Professor Scherhag of the University of West Berlin for the results of the 4000-g balloon flights carried out in West Germany.

II. Balloon Development for the Planetary Entry Parachute Program

James C. Payne
Air Force Cambridge Research Laboratories
Bedford, Massachusetts

Abstract

The Planetary Entry Parachute Program (PEPP) described by Mr. John McFall of NASA Langley Research Center necessitated the development of a high-altitude balloon capable of carrying the NASA payload to an Earth atmosphere comparable to that expected to exist about the planet Mars. The management of the balloon phase of the program was assigned to AFCRL and is the subject of this paper.

The initial balloon-design consideration for the program involved a 1500-lb payload that would float above 125,000 ft, with 130,000 ft the desired altitude. This could have been accomplished by using GT-11 material with a balloon volume of about 30 million cu ft, or by using GT-99-1 for a balloon of about 15 million cu ft.

As the discussions continued the payload underwent the normal growth to a final weight of 1650 lb for the NASA aeroshell, an additional allowance of 600 lb for the balloon control-and-safety equipment, plus 1200 lb of ballast to permit maneuvering the balloon over the White Sands Missile Range. We were then looking at a balloon that could carry 3500 lb at liftoff and achieve a floating altitude near

130,000 ft with a load of 2250 lb. Now, using GT-99-1, the balloon would be about 26 million cu ft in volume, but it would no longer have sufficient strength. A GT-11 balloon would be of the order of 65 million cu ft, and so would present launching problems as well as very high cost. It was obvious that this design was greatly over-reaching the state-of-the-art and that so ne other film would have to be developed that would reduce the balloon size without compromising the mission.

We had learned in another of our programs that the weight of reinforced film can be readily reduced by coating the threads with adhesive, rather than embedding the fibers in a layer of adhesive over the surface of the Mylar. It was recognized that there might be some benefit in having the layer of adhesive, but it did make up about 1/3 of the weight of a film like GT-99 (or, more generally, a weight equivalent to the basic film weight) and was not tolerable in this case.

The concept of coating the threads with adhesive was given maximum attention. The PEPP balloon has roughly 32 million ft of thread in the longitudinal direction alone. To coat the threads, dry them, and then respool them appeared to be impossible using the two available thread-coating machines because the best production rate was about 1000 ft/hr per coating machine. Schjeldahl Company then recommended a coating process which had been considered under an earlier AFCRL program: to coat each thread as it leaves the Flying Thread Loom and just prior to entering the laminator. This approach was tried and found to work well except that the longitudinal threads occasionally became slightly displaced and did not present a nice symmetrical pattern as in the GT-11 scrim. This concerned us at first but it appears to have no effect on the strength of the film.

Now that we were able to add reinforcing fibers to the Mylar without paying a great weight penalty for the adhesive, the next problem was to select the thread pattern. We worked with Schjeldahl on a paper study of 30 to 40 different patterns giving particular attention to theoretical weight, strength-to-gross load, strength-to-weight, and a safety factor. The main objective of this exercise was to select a balloon material that would produce the most reliable balloon. The safety factor (which was the most difficult to define) was computed by dividing the machine-direction (MD) strength (assuming 10-in. gore end sections) by the gross load. Cone angle was ignored for this initial comparison.

Table 1 shows a comparison of reinforced-scrim balloon designs that have been flown in the past. It is interesting to note that the Stratoscope II main balloon has the lowest value for the transverse-direction (TD) strength versus gross load. Among the nonwoven reinforced materials, the lowest TD strength/gross load ratio appears in the GT-50 balloon which was a 1.6 million cu ft balloon with 5600 lb of gross lift. This balloon also had the lowest strength-to-weight ratio.

Using the same comparative relationships, the following criteria were used for selecting the patterns for the PEPP balloon:

Table 1. Comparison of Reinforced-Scrim Balloon Designs

PROGRAM	MATERIAL	WEIGHT $K10^{-3}$ LBS/FT^2	BREAKING STRENGTH LBS/IN. M.D.	T.D.	BALLOON WEIGHT LBS.	PAYLOAD	GROSS LIFT LBS.	SAFETY FACTOR	STRENGTH/GROSS $x10^{-3}$ M.D.	T.D.	STRENGTH/WEIGHT $x10^{-3}$ M.D.	T.D.	BALLOON VOLUME $x10^{-6}$ FT^3
STRATOSCOPE	GT-11	12.0	45	25	2400	10,000	16,000	9.2	2.8	1.25	3.75	2.08	5.25
AF2929/TEST	GT-50	11.0	20	12	1000	4,000	5,600	8.0	3.57	2.14	1.82	1.09	1.60
AF2929/TANDEM	GT-12	12.0	45	25	1000	3,000	4,935	11.5	7.7	5.06	3.75	2.08	1.60
CORONASCOPE	GT-11	12.0	45	25	1600	1,700	3,500	10.0	11.8	7.15	3.75	2.08	3.20
NCAR GT-66	GT-66	2.7	5	5	567	690	1,750	5.5	2.86	2.86	2.04	1.85	6.00
AF4179	GT-99	5.6	12	12	835	950	1,600	8.3	7.5	7.5	2.14	2.14	1.60
PEPP	GT-111	5.5	33	15	3200	2,200	7,780	15.0	5.1	2.32	6.0	2.73	26.0

1. The Mylar film thickness was frozen at 1/3 mil, and the reinforcing fibers at 220-denier high-tenacity (HT), or 440-denier HT, or a combination of both; the suspended load at float altitude, at 2200 lb, and the balloon end sections at 10 in.

Table 2 shows the results of the PEPP material study. All of the patterns considered would have exceeded the strength ratios of the Stratoscope II main balloon. (Machine-direction strength data are based on the center 10-in. band.)

In Table 2, the lowest volume balloon that exceeds the GT-11 strength-to-weight ratio is shown as 6333 in the CNET column. The gore pattern consisted of 6 threads/ in. in the center 10 in. of the gore (machine direction), and 3 threads/in. to the outer edges; then 3 threads/in. in the transverse direction. The theoretical balloon volume would be about 21.5 million cu ft.

2. The highest TD-strength-to-gross-load ratio appears in design 6334 which also has the highest TD-strength-to-weight relationship.

3. It requires an additional million cu ft balloon volume to lift the added transverse direction fibers when the transverse density is changed from 3/in. to 4/in.

4. It also requires an additional one million cu ft to increase the number of fibers in the center 10-in. band from 6/in. to 8/in.

5. In the final analysis, the best choice among the all 220-denier-reinforced patterns was the 8664 design because it offered good strength characteristics and had a smooth transition in terms of strength from the center 10 in. to the remainder of the gore. In other words, going from 8 threads/in. to 3 threads/in. appeared to be too big a step!

6. The pattern 4334 (440 denier, high tenacity fibers in the machine direction) was then chosen over the 8664 (220 denier) pattern because it meant fewer fibers to handle and also was considered to offer better tear resistance.

7. The GT-99-1 pattern (6112) is shown only for comparative purposes.

The specifications of the final balloon system are shown in Table 3.

Knowing that we would probably find it necessary to inflate and launch with surface winds something less than ideal, we chose to allow the transfer of gas from the top balloon to the main balloon to begin at 10,000 ft MSL. This would be about 6000 ft above the proposed launch site. This choice allowed us to work with a relatively small balloon and maintain a tight bubble during the launch phase. Justin Smalley, formerly of Litton Industries, was engaged by Schjeldahl Co. to assist in the design of the balloons. (Mr. Smalley had previously made a computer study of tandem-system designs for AFCRL.) One of our greatest concerns was the effect of the weight of the launch balloon on the main balloon at ceiling. The launch balloon would have little or no lift and would very likely "lay over" on the main balloon. It also appeared that the EV-13 valve in the top of the launch balloon would probably be ineffective at the higher altitudes. However, this proved to be untrue because we were able to valve the first test balloon while it was at floating altitude.

Table 2. PEPP Balloon Material Survey

CNET	WEIGHT $\times 10^{-3}$ LBS/FT^2	BREAKING STRENGTH LBS./IN. M.D.	T.D.	BALLOON WEIGHT LBS.	PAYLOAD LBS.	GROSS LIFT LBS.	SAFETY FACTOR	STRENGTH/ GROSS $\times 10^{-3}$ M.D.	T.D.	STRENGTH/ WEIGHT $\times 10^{3}$ M.D.	T.D.	BALLOON VOLUME $\times 10^{-6}$FT^3
ADHESIVE ON THREADS (220HT)												
6333	4.4	26	12	2500	2200	6900	9.5	3.77	2.17	5.91	3.41	21.5
6334	4.7	26	15	2750	2200	7250	9.2	3.58	2.62	5.54	4.04	22.5
8334	4.9	33	15	2950	2200	7520	11.4	4.38	2.53	6.74	3.88	23.5
8664	5.5	33	15	3200	2200	7780	14.5	5.1	2.32	6.0	2.73	26.0
ADHESIVE ON THREADS (440HT M.D.--220HT T.D.)												
4334	5.5	33	15	3200	2200	7780	14.5	5.1	2.32	6.0	2.73	26.0
ADHESIVE ON FILM (220HT)												
6112	5.5	26	12	3200	2200	7780	11.1	3.86	1.85	4.55	2.18	26.0

At one time we considered separating the launch balloon from the system after sufficient gas had been transferred. However, this involves a separable fitting between the two balloons and the development of a large valve for the top of the main balloon. We had done this successfully on a smaller balloon system but considered that there was not sufficient time to develop a reliable valve, and it added complications to the system. Our decision was to retain the top balloon.

Mr. James F. Dwyer of AFCRL examined the final balloon design in great detail and recommended that three gores be added to the launch balloon and five gores to the main balloon. It was his concern that unusually high circumferential stresses would be built up in both balloons under certain flight conditions.

Normally when our laboratory undertakes a program of this magnitude a number of test flights would be made without the experimenter's equipment in order to ensure that our balloon design and launching concept will reliably do the job. However, when we are using balloons costing well over $100,000, some alternate means of evaluating the balloon must be found. For this program, we had an extra launch balloon built; then, to simulate the main balloon, a bag of GT-12 was made with heavy chain suspended from the top end fitting to give it weight much like the real balloon. This model permitted us to evaluate the launch method without the expenditure of a real main balloon.

To evaluate the chosen balloon material, we had a 3.2-million cu ft balloon manufactured and, combining it with a full scale launch balloon, we actually flew it in May from Holloman AFB. This flight went off very well, and because the lower winds were westerly and the higher winds easterly, we were able to observe the flight visually from launch to termination.

Since most of us are vitally concerned about getting balloons out of the air when the mission is completed, we were able to prove that with this tandem system the balloon would invert after the load was removed and descend immediately. Since the 26-million cu ft balloon would have an even higher center of gravity, we felt certain that this balloon would remove itself from the air without our adding a destruct system.

The first 26-million cu ft balloon was flown from Holloman AFB on the 18th of July, 1966. The surface winds were ideal and launching proceeded without any real difficulties. (I have a short movie of this launching.) Using 15 percent free lift, the balloon ascended at an average rate of 1345 ft/min to the tropopause; from the tropopause to the first float altitude, with 1200 lb of ballast aboard, the average ascent rate was 775 ft/min. The overall rate was 920 ft/min. The first floating altitude was about 122,000 ft measured by the on-board barocoder, and 124,900 ft, corrected radar altitude. The balloon was allowed to float at this altitude for about one-half hour, then all the ballast was poured. The final altitude achieved by the balloon was 128,400 ft (corrected) on the barocoder and 127,700 ft, corrected radar altitude.

Table 3. Tandem Balloon Design Specifications

PAYLOAD 2250 LBS.

ASCENT BALLAST 20%

FREE LIFT 20%

ASCENT VELOCITY 1500 FT. PER MIN.

MAIN BALLOON

VOLUME 26×10^6 FT^3

MATERIAL: GT-111-1 UNIT WEIGHT 0.0055 LBS/FT^2

BREAKING STRENGTH - 33 LBS./IN. (MACHINE DIRECTION)
15 LBS./IN. (TRANSVERSE DIRECTION)

Σ 0.3

GORE LENGTH - 568 FT. NO. OF GORES - 285

THEORETICAL SURFACE AREA - 476,500 FT^2

END SECTIONS - ASSUME SAFETY FACTOR OF 12

TOP - 10 INCHES PER GORE BOTTOM - 7 INCHES PER GORE

ESTIMATED WEIGHT - 3200 LBS.

LAUNCH BALLOON

TRANSFER ALTITUDE - 10,000 FT. MSL

VOLUME - 199,500 FT^3

MATERIAL: GT-12 UNIT WEIGHT 0.011 LBS./FT^2

BREAKING STRENGTH - 40 LBS./IN. (MACHINE DIRECTION)
20 LBS./IN. (TRANSVERSE DIRECTION)

GORE LENGTH - 110.5 FT. NO. OF GORES - 57

The first "hot" flight was flown on 30 August 1966 from Walker, AFB. In order to determine that the flight trajectory would pass over the target – the White Sands Missile Range – we began launching 87-ft diameter polyethylene balloons that carried AMT-12 radiosondes, long-duration battery packs and a timer. These balloons were designed to float at 130,000 ft. By adding about 3 lb of ballast it was possible to achieve a floating altitude nearer that expected of the big balloon. Figure 1 shows the trajectories taken by these balloons. Track number 1 was for a balloon launched at 1104 hr MST on 28 August. It floated at 129,000 ft and took a northerly path. The second balloon, launched approximately 24 hr before the 26 million cu ft balloon floated at 124,000 ft and followed a more southerly path. Balloon number 3 was launched at 2150 hr MST on the evening before and, floating at 126,000 ft, tracked more to the north. All three were within the assigned target area (north of the 30-mile area to the top of the 90-mile area). These pathfinder balloons had an average ascent rate near 900 ft/min with 15 percent free lift.

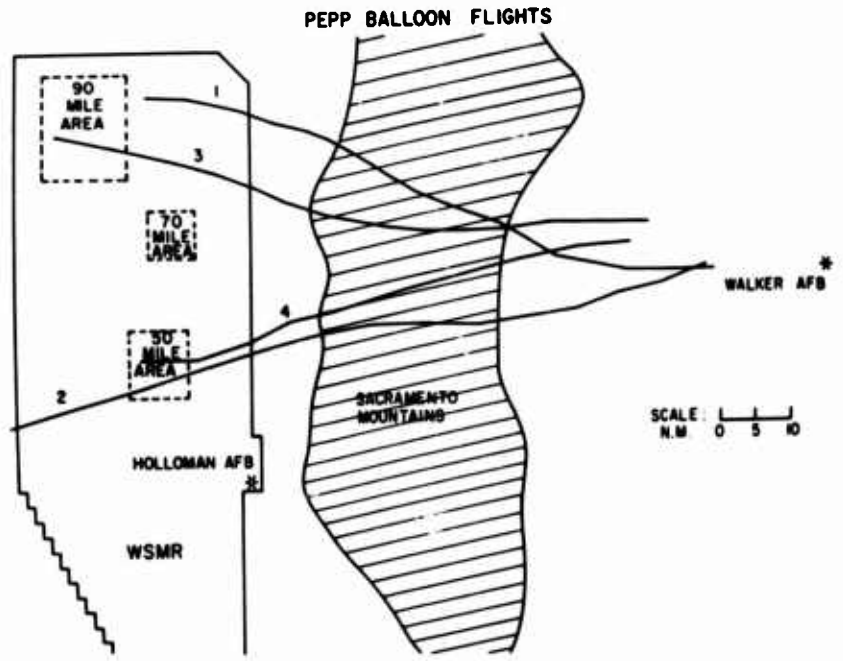

Figure 1. PEPP Balloon Flights

The path of the 26 million cu ft balloon is also shown in Figure 1. The 50-mile area is the most heavily instrumented area on the range and was the primary target. When we released the NASA aeroshell the balloon was positioned at 3 miles northwest of the center of the 50-mile area. The cooperation we received from the weatherman could not have been better!

III. Creep Characteristics of Polyethylene Film*

Harold Alexander
Department of Aeronautics and Astronautics
New York University

Abstract

In order to find the constitutive relations for polyethylene balloon film, an experimental investigation was conducted in which samples of polyethylene film were loaded both uniaxially and biaxially. The results of this investigation are presented as creep curves for strain versus time at constant true stress. The characteristics of these graphs are then discussed.

1. INTRODUCTION

High-altitude polyethylene balloons are today a common tool of scientists wishing to place a payload far into the upper reaches of the atmosphere. Their development and growth to present day prominence has occurred over a relatively short period of about fifteen years. In fact, polyethylene film was not available commercially until after the conclusion of World War II (Kresser, 1957).

*This paper is the result of research performed under Contract No. AF19(628)-4990 with the Air Force Cambridge Research Laboratories, Bedford, Mass. It constitutes part of a dissertation to be submitted in partial fulfillment of the requirements for the Degree of Doctor of Philosophy at New York University.

However, the demands put upon this relatively fragile "engineering material" are becoming greater with increased balloon size and payload, as is evidenced by the recent rash of costly balloon failures (Dwyer, 1965; Bilhorn, 1965). This report presents the results of an investigation into the basic properties of polyethylene film which should clarify the causes of some balloon failures as well as yield a deeper insight into the mechanical behavior of balloon films in general.

In the past there have been many experimental investigations into the uniaxial (Hahn, Macht, and Fletcher, 1945; Kolsky, 1949; Cary, Schulz, and Dienes, 1950; Anderson and Morfitt, 1958) and biaxial (Hopkins, Baker, and Howard, 1950; Anderson, Gear, and Morfitt, 1956; Hopkins and Wentz, 1960; McFedries, Brown, and McGarry, 1962) time-independent properties of polyethylene, as well as the uniaxial time-dependent properties of crystalline polymers, of which polyethylene is an example (Anderson, Gear, and Morfitt, 1956; Gohn and Cummings, 1960; Catsiff, Offenbach, and Tobolsky, 1956; Landzberg, 1966). However, results of biaxial time-dependent experiments, which do not seem to be available in the literature, are needed for the formulation of the problems in question. Also, the uniaxial time-dependent experiments listed above are not suitable for the contemplated analysis. It was therefore decided to undertake a complete experimental program that will yield the uniaxial and biaxial time-dependent properties of polyethylene film, and at the same time be used to study general failure patterns.

For a better understanding of the mechanical response to stresses it was found necessary to study the physical properties of the material (its microscopic as well as macroscopic structure). The first section of this paper is a presentation on the relevant structural characteristics of polyethylene film. This is followed by a description of the experimental program. In the last section the resulting creep characteristics are discussed with the aim of finding a model for the material response.

2. STRUCTURAL CHARACTERISTICS

Polyethylene is a polymer composed of long chains of methylene groups numbering 600 to 4000 per molecule. It is prepared directly from ethylene gas through a high-temperature, high-pressure polymerization process in the presence of a trace of oxygen. It is a thermoplastic (that is, it can be melted and hardened without change in molecular structure), and when formed into film has a "leathery" consistency at room temperatures (Kresser, 1957; Cary, Schulz, and Dienes, 1950).

In the unstressed state most of the molecules in a sample of polyethylene can be considered to be in partially curled configurations, neither tightly curled up nor rigidly extended to maximum length. There is a diffusion process occurring

at all times that is a motion of chain segments. The result of many such elementary processes is that the polymer molecule changes its shape (micro-Brownian movement). There is, however, no net discernible motion as these processes are entirely random (Alfrey, 1948, Chap. B). Upon the application of moderate stresses, this process becomes stress-biased in that the net motion of the molecules will now result in an orientation in the direction of stress. When the loading is removed, the diffusion process is again random. Eventually the molecules return to their random state of orientation. A permanent change of molecular configuration requires higher stress levels, causing a breaking up of complete chain entanglements.

Polyethylene is a partially amorphous, partially crystalline material at room temperatures. It has been found through X-ray diffraction studies (Bunn and Alcock, 1945; Treloar, 1958, Chap. I-9) that, in the unstressed state, single molecules can be partially in the amorphous state and partially in the crystalline state since the molecules are often larger than the crystals. This makes for a rather complicated composite. Upon straining, a first-order phase transition (increased crystallization) occurs. The crystallized areas formed during this process are mostly elongated, cylindrical, or flat bundles of parallelized chain molecules. This phenomenon is a result of increased molecular attraction caused by the orientation of the molecules.

A lowering of the temperature will also cause increased crystallization similar to that caused by straining. The crystals are randomly oriented and are formed as a result of decreased molecular motions. However, regardless of its origins the crystalline phase of polyethylene is characterized by a lower density (greater volume) and a greatly increased rigidity. The crystallization process is time dependent, its rate being proportional to the strain magnitude.

Decreasing the temperature to a point below about -80°C will result in what is referred to in the literature as a second-order phase transition. This transition is characterized by a sudden change of the intensive properties such as heat capacity and thermal expansion. The individual segments of the chain molecules no longer carry out rotational and vibrational movement as a whole, causing the material to become extremely brittle. It is much more fragile than the crystallized material due to the absence of "softer" amorphous regions (see Treloar, 1958, Chap. I-8).

The information presented above on the microscopic structure of polyethylene is used in the following to describe the reaction of tension sample. There are essentially four types of deformation that will occur. These are:

(1) An instantaneous shift of chain segments from their local potential energy minima (initial elastic response).

(2) A diffusion of the chain segments by the mechanism of micro-Brownian movement in the stress direction (retarded elastic response).

(3) A breaking down of the chain entanglements under stress (irreversible creep).

(4) An increased crystallization caused by increased molecular attractions due to (2).

The phenomenological results of these processes vary with the temperature.

Below about -80°C the material is in a brittle state. All segmental motions are very slow so that (2) and (3), and therefore (4), may be disregarded and only the instantaneous shift (1) need be considered. This results in a purely elastic reaction to stress with a high modulus of elasticity. However, the material is extremely fragile, as it lacks the mechanisms for absorbing sudden shocks.

Above about 100°C the material is viscous. The breakdown of entanglements (3) compares in rate with the diffusional movements (2) so that the chains progress as a whole in the stress direction, preventing crystallization (4). The deformation due to the instantaneous shift (1) is negligible compared to that of (2) and (3). Therefore, in this state, the reaction to stress is a flowing of the material like a highly viscous fluid (Meares, 1965).

For balloon considerations, the most interesting temperature range is that between -80°C and +60°C, the range encountered in balloon flights. At these temperatures polyethylene is in a "leathery" or "rubbery" state. In this state, the diffusion of chain segments (2) is slow compared to the instantaneous shift (1). In actual experimentation, however, it is difficult to establish which part of the deformation is caused by (1) and which part by (2). "Instantaneous" measurements are impossible and the time rate of (2) becomes very high at high stress and temperature levels. As the diffusion of free segments continues, crystallization (4) occurs causing a hardening of the material and a resultant decrease in the time rate of deformation. The breaking down of chain entanglements (3) occurs very slowly and has little effect on the deformation at moderate stress and temperature levels. However, at high stress or temperature this mechanism may account for a large part of the deformation response.

The above description of the response of polyethylene to an applied stress is unfortunately limited to one dimension.

It is not known whether or not increased orientation and crystallization will occur under biaxial loading and if there will be a resultant retarded elastic response and hardening. A study of uniaxial and equibiaxial tests performed at different strain rates reported by Anderson and Morfitt (1958) seem to indicate that the time-dependent response will be greatly decreased. However, Hopkins, Baker, and Howard (1950) have stated that high average molecular weight polyethylene sheets will "orient under complex stresses", resulting in large creep deformation in direct contradiction to the results of Anderson and Morfitt. The degree of orientation may also affect the brittleness properties of the film, possibly providing a clue as to the causes of many balloon failures (see Nielsen, 1962, p. 252).

The amount of irreversible time-dependent response is also not known for biaxial stressing. This will be determined by the present experimental program.

In view of the complications mentioned above, it might seem that the task of finding a realistic mathematical model for polyethylene is indeed a formidable one. However, in recent years, many advances have been made in the fields of viscoelasticity and creep (Kachanov, 1960; Lockett, 1965; Eringen and Grot, 1965; Halpin, 1965; Schapery, 1966), deformational anisotropy (Berg, 1958), and the mechanics of high polymers (Alfrey, 1948; Treloar, 1958; Meares, 1965; Ferry, 1961; Tobolsky, 1960). Even though the internal processes occurring during stressing of polyethylene are fairly complex, within the range of stress and temperature encountered in balloon technology it seems possible to represent the mechanical properties with reasonable accuracy with an appropriate mathematical model. A model of this type would have wide application in the analysis of some of the present problems of balloon design.

3. EXPERIMENTAL PROCEDURE AND RESULTS

The object of this experimental program is to obtain the uniaxial and biaxial, time-dependent as well as time-independent, properties of polyethylene balloon film. To satisfy this objective it was found necessary to obtain creep curves of strain in terms of λ, versus time t, at various values of true stress σ, and biaxial stress ratio n.* It was found that the most satisfactory procedure for the experimental investigation was to perform the experiments with long cylindrical tubes loaded by internal pressurization and axial loads for all ratios greater than zero (biaxial tension) and with thin rectuangular strips for n = 0 (uniaxial tension).

For the purposes of this and future experimental investigations specially prepared polyethylene cylinders were obtained from Raven Industries. These cylinders were formed by cutting 15-in. -wide strips from 54-in. layflat tubing, laying 2 identical strips on top of each other and heat-sealing both sides. They were prepared from various sections of the original tubes of various polyethylene films. The results presented here were obtained with 2 mil, new DFD-5500 film.

Uniaxial experimentation (n = 0) was performed on strips cut from the above-mentioned samples. These strips were 1/2-in. wide by 6-in. long and were cut in both the machine and transverse directions. Their thicknesses were measured with micrometer calipers. Bench marks, 2-in. apart, were drawn on the central region of each sample. This test area was made sufficiently small to eliminate end condition effects without loss of experimental accuracy. Each of 5 strips for each test series was clamped to a rigid upper support with a dead load weight hung

*Note: all symbols defined at the end of this chapter.

from the lower clamp (Figure 1). At various times between zero and a maximum of 32 hr, the distance between the bench marks was measured with calipers. The loads ranged from 1/2-lb to 1-5/8 lb causing an engineering or nominal stress range of approximately 500 psi to 1625 psi. The temperature in the test area was kept at approximately 75°F by the laboratory air conditioning system.

It has been indicated in the literature that polyethylene deforms as an incompressible material through most of its range of deformation. Carey, Schulz and Dienes (1950), treating polyethylene as a linearly elastic material, showed that the value of Poisson's ratio, ν, is very close to 1/2, the value obtained if the material is incompressible. However, polyethylene is by no means linearly elastic and, therefore, this method of proving incompressibility may not be valid.

Figure 1. Uniaxial Test Stand

Consequently, uniaxial, constant-load creep tests were performed on strips of polyethylene film during which all dimensions of the strips were measured at each reading. Referring to Figure 2, it can be seen that the assumption of incompressibility implies that

$$\ell\, w\, h = \ell_o\, w_o\, h_o = \text{const} \tag{1}$$

where the $(\,)_o$ quantities are those before loading. Assuming a state of constant stress and strain, the true stress σ_1 is defined as the force divided by the instantaneous cross-sectional area:

$$\sigma_1 = \frac{F}{A} = \frac{F}{w\,h} \tag{2}$$

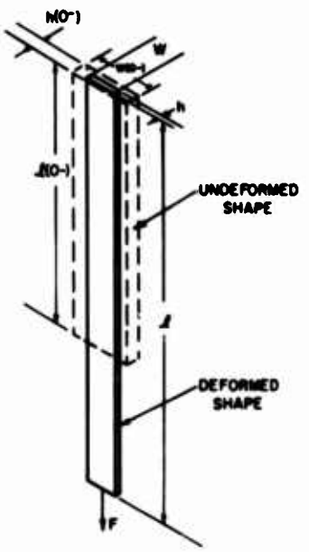

Figure 2. Undeformed and Deformed Shapes for the Uniaxial Sample

and, utilizing Eq. (1) to eliminate wh,

$$\sigma_1 = \frac{F}{A_o} \lambda_1 \tag{3}$$

where A_o is the original unstrained cross-sectional area and

$$\lambda_1 = \frac{\ell}{\ell_o} . \tag{4}$$

If the material is indeed incompressible under straining, then by Eq. (3) the extension ratio is linearly proportional to the true stress with the constant of proportionality being the engineering stress:

$$\sigma_{1_o} = \frac{F}{A_o} . \tag{5}$$

In Figure 3, Eq. (3) (solid line) is graphed on the same set of axes with the experimental values of σ_1 vs λ_1, obtained using Eqs. (2) and (4), for five different constant-load creep tests. These results seem to indicate rather conclusively that incompressibility is a valid assumption.

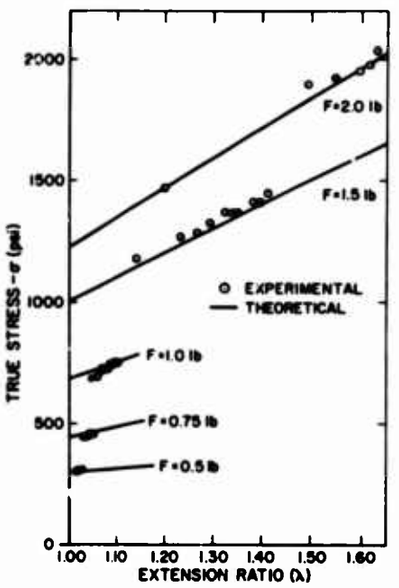

Figure 3. True Stress Vs Extension Ratio

It is extremely difficult to perform creep experiments at a constant true stress due to the continuously changing cross-sectional area, although for uniaxial testing there have been some rather ingeneous methods proposed (Tomashevskii and Slutsker, 1963). In order to obtain the creep curves for n = 0 (uniaxial tension), constant-load creep tests were performed at various values of the dead load, F. These tests yielded curves of λ_1 vs t for constant F, as shown in Figure 4a. At various values of $t = t_i$, $i = 1, m$, curves of λ_1 versus σ_1 (Figure 4b) were obtained using Eq. (3) to compute σ_1. The intersections of the lines σ_1 = const

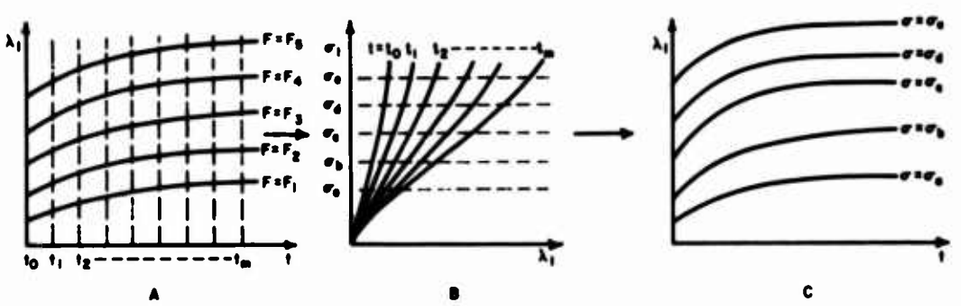

Figure 4. Procedure for Obtaining Constant Stress Curves

with the curves of Figure 4b yielded the creep curves in the desired form, as shown in Figure 4c. A computer program was written to perform the necessary calculations for the above procedure. The data from the tests were inputed into the program and the results for the machine and transverse directions are presented in Figures 5 and 6.

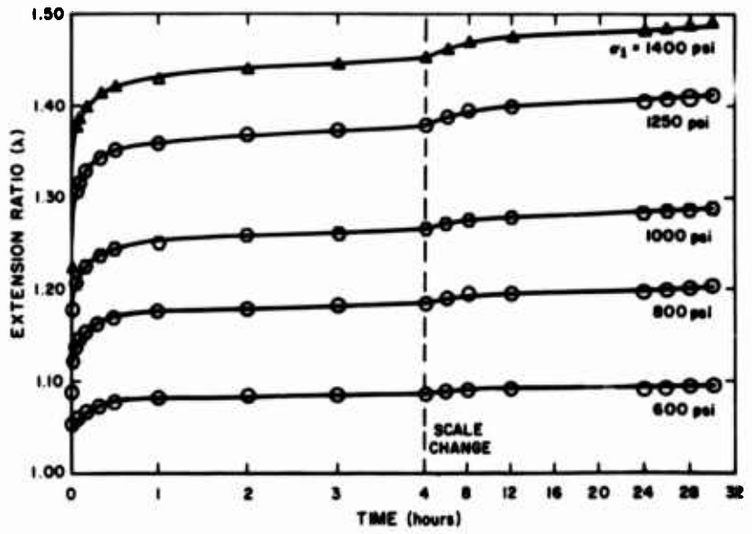

Figure 5. Extension Ratio vs Time (Uniaxial Creep, n = 0; Temperature = 75°F; Machine Direction)

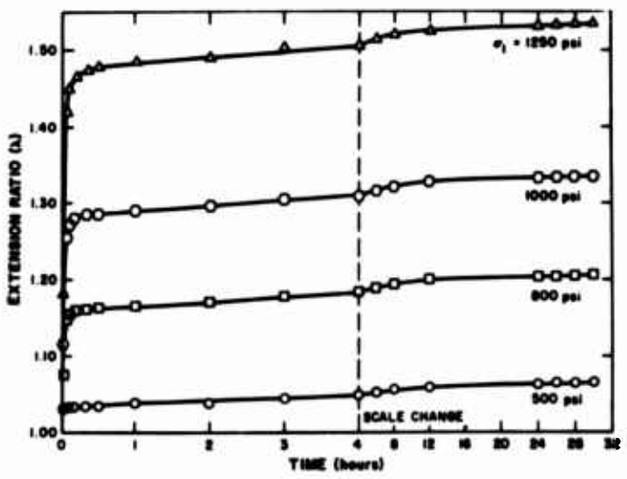

Figure 6. Extension Ratio vs Time (Uniaxial Creep n = 0; Temperature = 75°F; Transverse Direction)

For the biaxial tests (n > 0), 5-1/2-ft long tubes were cut from the master roll described above. Bench marks in the longitudinal and circumferential directions, 4 in. apart, were drawn on the center of one side of each sample and the average thickness of this test region was measured. Five of these tubes were hung on a specially prepared stand (Figure 7) by clamping one end of each to the upper fittings using hose clamps to insure an airtight seal. The lower end of each cylinder was sealed with a disk-like lower end fitting equipped with a hook for attachment of the dead load weights.

Compressed air was pumped into each sample through the upper fittings. The pressure in each tube was maintained at a different constant pressure ($p \pm 0.001$ psi) using a Model 40-2 Moore Nullmatic regulator. The pressures were monitored on a bank of straight-tube manometers filled with gauge oil (specific gravity = 0.826) dyed red for easy readability (Figure 8). The variable dead-load weights were provided by using pails filled with gravel. The temperature control was the same as mentioned above for the uniaxial tests.

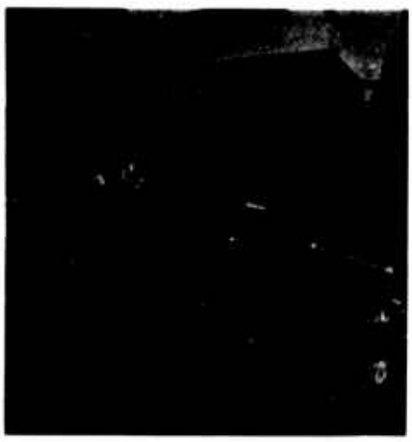

Figure 7. Biaxial Test Stand

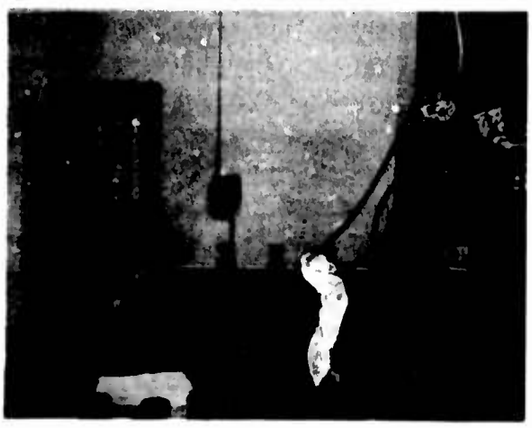

Figure 8. Pressure Regulating and Measuring System

The distances between the bench marks x and ℓ were measured with vernier calipers and the diameter of the cylinder D was measured with a specially prepared caliper-like machine at various times during the 32-hr testing period. The pressures in the samples ranged from 8 to 15 in. of oil, causing nominal stresses calculated on the basis of the original diameter ranging from 600 psi to 1100 psi.

The experimental procedure for the biaxial experiments is more complicated than that for the uniaxial investigations due to the existence of a multiaxial stress

state and the continuously changing radius of the cylinder. It was assumed that the central portion of the tube deformed as an infinite cylinder retaining a circular cross section. Due to the rather marked variations in film thickness, however, homogeneity of circumferential strain was not assumed around the whole tube, but only in a small region of arc length s and axial length ℓ .

Force equilibrium in the radial and axial directions (Figure 9) yields the two equilibrium equations for a cylinder:

$$\sigma_1 h = N_\theta = \frac{pD}{2} \tag{6}$$

$$\sigma_2 h = N_z = \frac{pD}{4} + \frac{F}{\pi D} \tag{7}$$

where h is the average film thickness in the small region under consideration.

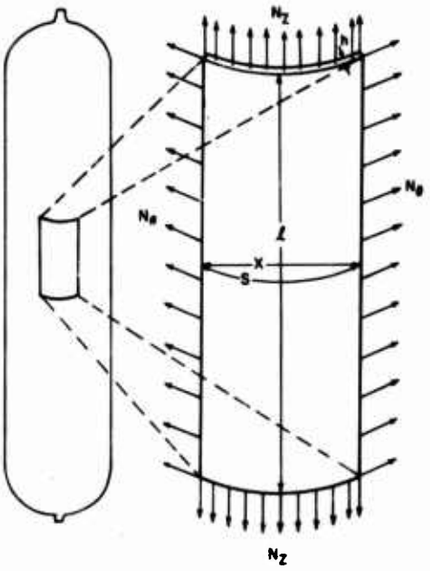

Figure 9. Test Cylinder

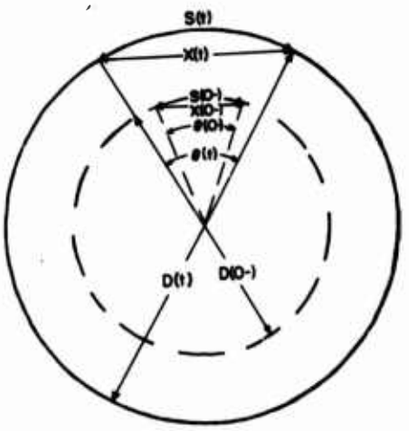

Figure 10. Cross-Sectional View of Cylinder

It can be seen (see Figures 9 and 10) that for this configuration the incompressibility condition of the region under consideration is:

$$\frac{\ell}{\ell_o} \frac{h}{h_o} \frac{\theta}{\theta_o} \frac{D}{D_o} = 1 \tag{8}$$

where, by geometry (Figure 10),

$$\theta = 2 \sin^{-1}\left(\frac{x}{D}\right) . \tag{9}$$

Therefore,

$$h = \frac{h_o \ell_o D_o \sin^{-1}\left(\frac{x_o}{D_o}\right)}{\ell D \sin^{-1}\left(\frac{x}{D}\right)} \tag{10}$$

and Eq. (6) can be written

$$\sigma_1 = \frac{p \ell D^2 \sin^{-1}\left(\frac{x}{D}\right)}{2 h_o \ell_o D_o \sin^{-1}\left(\frac{x_o}{D_o}\right)} . \tag{11}$$

The extension in the 1 direction is defined:

$$\lambda_1 = \frac{s}{s_o} = \frac{D}{D_o}\frac{\theta}{\theta_o} = \frac{D \sin^{-1}\left(\frac{x}{D}\right)}{D_o \sin^{-1}\left(\frac{x_o}{D_o}\right)} . \tag{12}$$

The biaxial stress ratio is defined:

$$n = \frac{\sigma_2}{\sigma_1} . \tag{13}$$

Using the equilibrium equations, Eqs. (6) and (7), the dead load F necessary to maintain a given value of n is found to be

$$F = (2n - 1)\frac{\pi}{4} p D^2 . \tag{14}$$

Experimentally, it is extremely difficult without the use of rather elaborate control equipment to maintain a constant true stress and biaxial stress ratio throughout the period of one creep test. It was therefore decided to perform many tests at constant pressures and to adjust the value of the dead load at each reading in order to maintain an approximately constant biaxial stress ratio. To obtain the desired curves of extension in the 1 direction versus time at a constant value of n, a procedure exactly analogous to that used for the uniaxial test results was utilized. A computer program was also written for this procedure so that in all of the experi-

ments the experimenter only had to card-punch his data for machine processing in order to obtain the data in the desired form. Experimental data for n = 1/2 (F=0) and n = 1 were inputed into the computer program and the results are presented in Figures 11 and 12

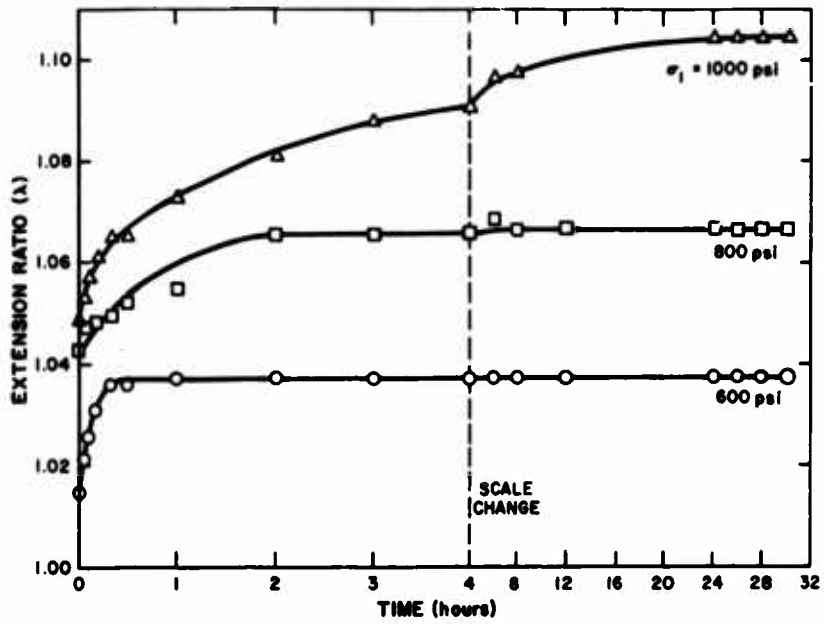

Figure 11. Extension Ratio vs Time (Biaxial Creep, n = 1/2; Temperature = 75°F)

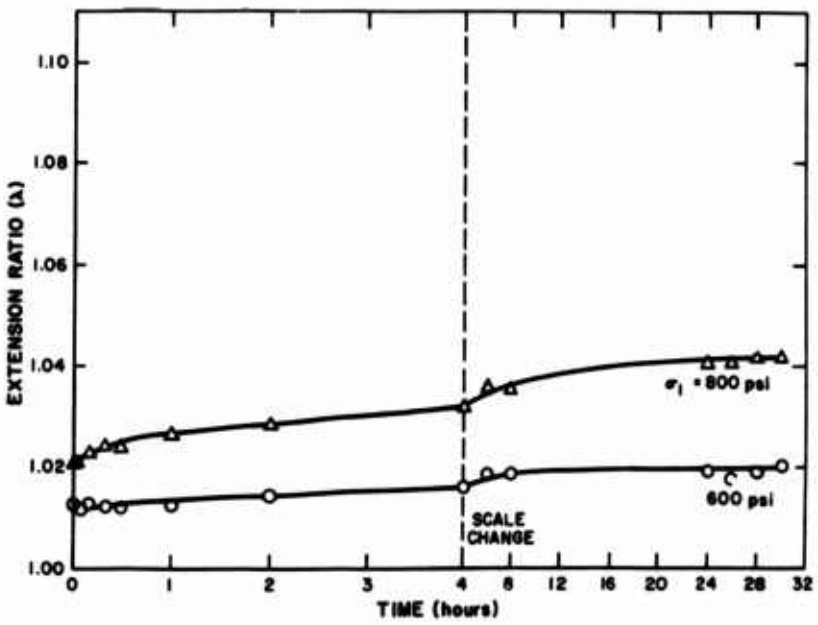

Figure 12. Extension Ratio vs Time (Biaxial Creep, n = 1; Temperature = 75°F)

As was indicated above, the time-dependent part of the material response to stress is due to three factors. One of these factors is of an irreversible nature. The other two are characterized by a retarded elastic or reversible response. A measurement of the test samples a long time after unloading ($t \approx \infty$) indicates what part of the total deformation is reversible. This information is presented in Table 1, where $\lambda_{1_{initial}}$, $\lambda_{1_{final}}$, and $\lambda_{1_{rec}}$ were measured immediately after loading was applied, at the time of unloading, and many days later, respectively.

Table 1

n		σ_{1_o}	$\lambda_{1_{initial}}$	$\lambda_{1_{final}}$	$\lambda_{1_{rec}}$
0	(machine)	500	1.047	1.064	1.016
0	"	1000	1.125	1.516	1.102
0	"	1250	1.221	1.823	1.267
0	"	1333	1.250	2.282	1.525
0	"	1500	1.550	2.888	1.930
0	(transverse)	500	1.023	1.063	1.008
0	"	666	1.050	1.109	1.023
0	"	750	1.055	1.242	1.031
0	"	1000	1.094	1.840	1.197
1/2		597	1.008	1.037	1.009
1/2		709	1.026	1.050	1.009
1/2		820	1.042	1.071	1.009
1/2		932	1.049	1.111	1.011
1/2		970	1.050	1.120	1.012
1		597	1.011	1.018	1.003
1		746	1.016	1.031	1.003
1		895	1.021	1.039	1.007
1		1045	1.028	1.051	1.010

4. DISCUSSION OF RESULTS

Upon examination of the curves of principal extension versus time at a constant true stress and biaxial stress ratio (Figures 5, 6, 11, and 12), it can readily be seen that all of the curves have the same basic characteristics. There is an initial time-independent elastic response followed by a time-dependent response with a relatively high creep rate. A rapid decrease in creep rate is evidenced during the first few hours of loading, followed by a region with an almost constant but quite small creep rate.

The instantaneous elastic response is similar to that of a neo-Hookean elastic material as described by Treloar (1958) and Rivlin and Saunders (1950). Indeed, an examination of the curves for t = 0 (Figure 13) seems to indicate a great resemblance to the stress-strain response suggested by Treloar and by Rivlin, even though their work was done for vulcanized rubber, a high polymer with prominent elastic response characteristics

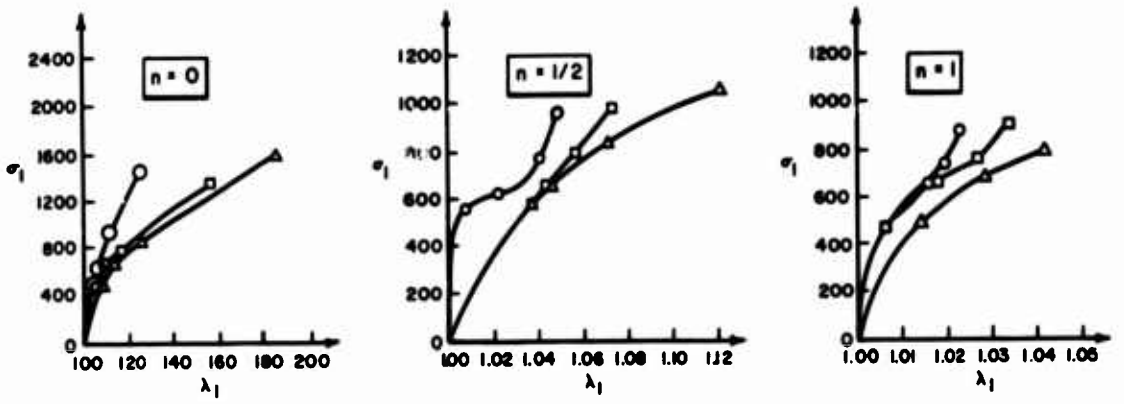

Figure 13. Comparison of Stress-Strain Characteristics for n=0, 1/2, 1

One part of the creep deformation may be considered as a retarded elastic response since it is recoverable after the load is removed. The remaining part is irrecoverable because of the breaking down of chain entanglements. This type of viscoelastic response is often represented by a model consisting of a linear spring, a linear dashpot, and a spring-dashpot parallel arrangement, all in series (Figure 14). Unfortunately, this combined Kelvin-Maxwell model yields a very poor quantitative representation of the response of this material. One of the fundamental assumptions of linear viscoelasticity is the linearity of the stress-strain relationship for all values of the time, t. An examination of Figure 13 indicates that this assumption is definitely not valid for polyethylene. The mathematical expression that would accurately represent this response would have to contain some type of non-linearity.

It was noted during the equi-biaxial experiments (Figure 12) that little creep occurred at stress levels up to approximately 800 psi. This phenomenon was unexpected since at stress ratios of n<1 there was appreciable creep at comparable stress levels. This seems to indicate that the creep response might be expressed by relating two-dimensional type deviators of strains, strain rates and stresses.

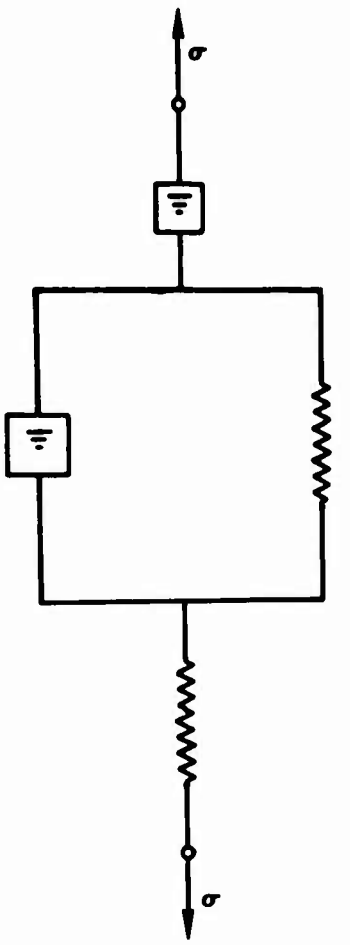

Figure 14. Combined Kelvin-Maxwell Model

When the equi-biaxial stress was increased to approximately 1000 psi, the material failed by a localized yielding. The yielded film thickness was found to have decreased to 1/20 of its original value. Connecting the yielded and unyielded regions, there was a sharp boundary that was always initiated along a line parallel to the machine direction.

The experimental results presented above yield a necessary guide for the determination of the constituitive relations for polyethylene film.

Acknowledgments

The author wishes to express his sincere gratitude to Professor Arnold D. Kerr whose invaluable guidance and personal interest made this work possible. Thanks are also due to Mr. James F. Dwyer and the Air Force Cambridge Research Laboratories for their support of this project, and to Mr. Michael Grubin for his assistance in the performance of the experiments.

Symbols

λ_i	Principal extension in i direction
σ_i	Principal true stress in i direction
F	Dead load force
A	Instantaneous cross-sectional area of strip
w	Instantaneous width of strip
h	Instantaneous thickness of strip or cylinder test region
ℓ	Instantaneous length of strip or cylinder test region
n	Biaxial stress ratio, σ_2/σ_1
N_i	Principal force per unit length of film in the i direction
p	Uniform, constant internal pressure in balloon samples
D	Instantaneous diameter of cylinder
θ	Instantaneous angle subtended by circumferential bench marks on cylinder
s	Instantaneous arc length subtended by circumferential bench marks on cylinder
x	Instantaneous straight-line distance between circumferential bench marks on cylinder

References

Alfrey, T. (1948) Mechanical Behavior of High Polymers, Interscience Publishers.

Anderson, A.A., Gear, E.C., and Morfitt, G.L. (1956) Balloon Barrier Materials, General Mills Inc., Mechanical Division, Rpt No. 1525, AFCRC-TR-56-262.

Anderson, A.A. and Morfitt, G.L. (1958) Balloon Barrier Materials, General Mills Inc., Mechanical Division, Rpt No. 1837, AFCRC-TR-58-211.

Berg, B.A. (1958) Deformational anisotropy, Appl. Math. Mech. 22(No. 1):90 (transl. of Russian Journal, Prikladnaia Matematika i Mekanika).

Bilhorn, T.W. (1965) Balloon Performance Analysis, Proc. AFCRL Scientific Balloon Workshop, 1965.

Bunn, C.W. and Alcock, T.C. (1945) The texture of polythene, Trans. Faraday Soc. 41:317.

Cary, R.H., Schulz, E.F., and Dienes, G.J. (1950) Mechanical properties of polyethylene, Ind. Eng. Chem. 42:842.

Catsiff, E., Offenbach, J., and Tobolsky, A.V. (1956) Viscoelastic properties of crystalline polymers: Polyethylene, J. Colloid Sci. 11:48.

Dwyer, J.F. (1965) Some polyethylene balloon statistics, Proc. AFCRL Scientific Balloon Workshop, 1965.

Eringen, A.C. and Grot, R.A. (1965) Continuum Theory of Nonlinear Viscoelasticity, Purdue Univ., School of Aeronautics, Astronautics, and Engineering Sciences, Tech. Rpt No. 32.

Ferry, J.C. (1961) Viscoelastic Properties of Polymers, Wiley and Sons.

Gohn, G.R. and Cummings, J.D. (1960) Creep characteristics of compression-molded polyethylene, ASTM Bull. No. 247.

Hahn, F.C., Macht, M.L., and Fletcher, D.A. (1945) Polythene, Physical and Chemical Properties, Ind. Eng. Chem. 37:526.

Halpin, J.C. (1965) Nonlinear Rubberlike Viscoelasticity: A Molecular Approach, Air Force Materials Laboratory, Tech. Rpt AFML-TR-65-107.

References

Hopkins, I. L., Baker, W. O., and Howard, J. B. (1950) Complex stressing of polyethylene, J. Appl. Phys. p. 206.

Hopkins, I. L. and Wentz, R. P. (1960) Stress-strain relations in cross-linked polyethylene, ASME Publ. No. 60-RP-14.

Kachanov, L. M. (1960) Theory of Creep, Fixmatgiz (in Russian).

Kolsky, H. (1949) An investigation of the mechanical properties of materials at very high rates of loading, Proc. Phys. Soc. (London) 62B.

Kresser, T. O. J. (1957) Polyethylene, Reinhold Publishing Corp.

Landzberg, A. H. (1966) Creep behavior of polymer films, Materials Research and Standards 6:232.

Lockett, F. J. (1965) Creep and stress-relaxation experiments for nonlinear materials, Intern. J. Eng. Sci. 3:59.

McFedries, R., Brown, W. E., and McGarry, F. J. (1962) Evaluation of brittle failures of polyethylene by subjection to biaxial stress, Trans. Soc. Plas. Engrs. 2:170.

Meares, P. (1965) Polymers: Structure and Bulk Properties, Van Nostrand.

Nielsen, L. E. (1962) Mechanical Properties of Polymers, Reinhold.

Rivlin, R. S. and Saunders, D. W. (1950) Large elastic deformations of isotropic materials, Phil. Trans. Roy. Soc. London, Series A 243:251.

Schapery, R. A. (1966) An engineering theory of nonlinear viscoelasticity with applications, Intern. J. Solids and Structures 2:407.

Tobolsky, A. V. (1960) Properties and Structure of Polymers, Wiley.

Tomashevskii, E. E. and Slutsker, A. I. (1963) Device for maintaining a constant stress in a specimen subjected to uniaxial tension, Industrial Laboratory, 29(No. 8):994-996 (transl. Russian J., Zavadskaya Laboratoriya).

Treloar, L. R. G. (1958) The Physics of Rubber Elasticity, Oxford at the Clavendon Press.

IV. Experimental Study of Balloon Material Failures*

Arnold D. Kerr
Department of Aeronautics and Astronautics
New York University

Abstract

Results of neoprene and polyethylene film tests conducted in the past year are presented with an emphasis on findings related to balloon failures. Planned tests to study fatigue failures of balloon materials at low temperatures are also described.

1. INTRODUCTION

In the search for possible causes of failure in balloons produced from neoprene or polyethylene films, it was found necessary to initiate an experimental program in addition to an analytical study of related phenomena. In this chapter the experimental program is described and some of the findings are presented.

*This publication is the result of research sponsored by the Air Force Cambridge Research Laboratories under Contract No. AF19(628)-4990.

2. ELASTICS AND VISCOELASTIC RUPTURE OF NEOPRENE BALLOONS

In a lecture presented at the past balloon workshop (Kerr, 1966) the author discussed the phenomenon of tensile instability of a spherical balloon which undergoes elastic as well as viscoelastic deformations. The presented analysis was based on the assumption that the balloon material is incompressible and that the deviatoric response obeys Maxwell's law for true stresses and logarithmic strains. In the meantime, tests were conducted on spherical neoprene balloons. It was found that, at room temperature, neoprene day balloons deform elastically for a large range of strains; whereas the night balloons, which contain plasticizers, do creep. Although it was established that the tested balloon materials obey more complicated constitutive equations than those assumed in Kerr (1966), it was found that the curves reproduced in Figure 1 do, in essence, represent the real behavior of the balloon except for very large strains where strain hardening plays a dominant role. In order to demonstrate the magnitude of the time-dependent deformations in question, a spherical plasticized neoprene balloon was subjected to a constant internal pressure and then photographed at eight progressing time intervals by a camera which was fixed with respect to the balloon center. The result is shown in Figure 2.

Using the test results as a guide, a new theory was developed for large elastic deformations that predicts the behavior of neoprene day balloons quite accurately. The experimental data, the corresponding analytical treatment, as well as a discussion of related published results, will be presented in a forthcoming paper.

Presently, tests are being conducted on neoprene balloons which contain plasticizers and which exhibit large creep deformations.

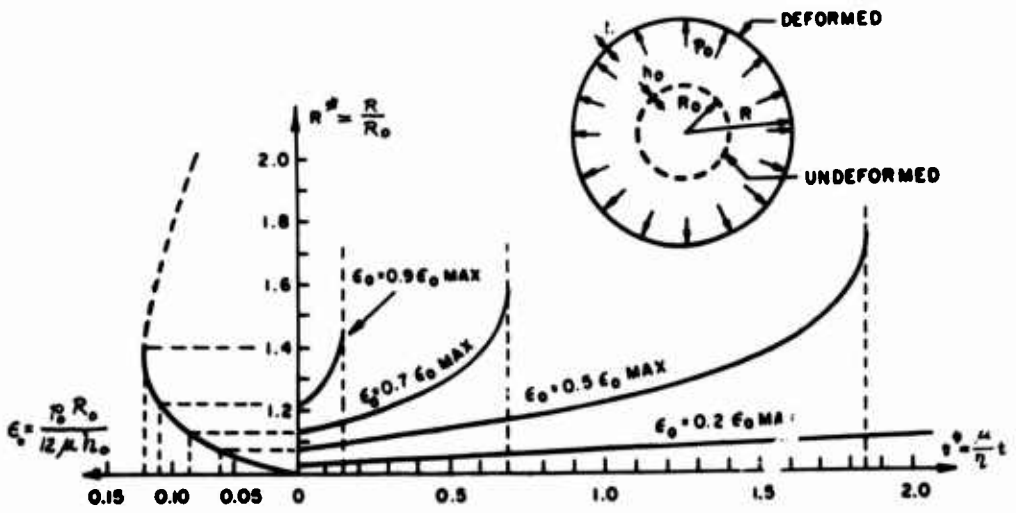

Figure 1. Plots of ϵ_o, R^*, t^* for a Spherical Balloon (μ, η are material parameters)

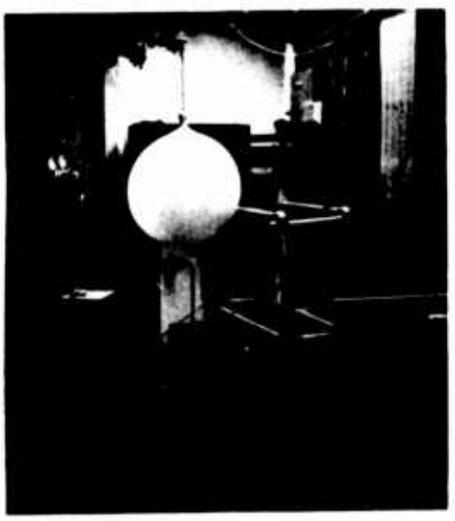

a. T = 0+ Minutes

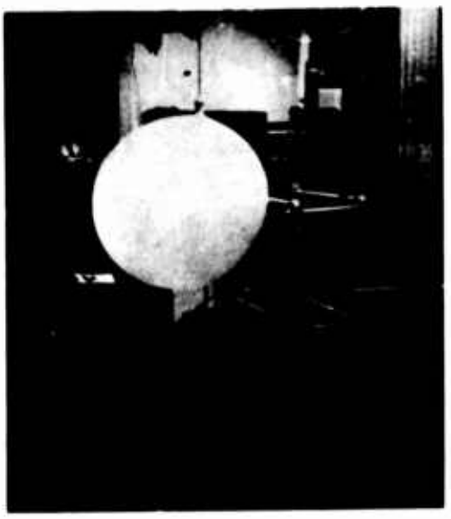

c. T = 60 Minutes

b. T = 30 Minutes

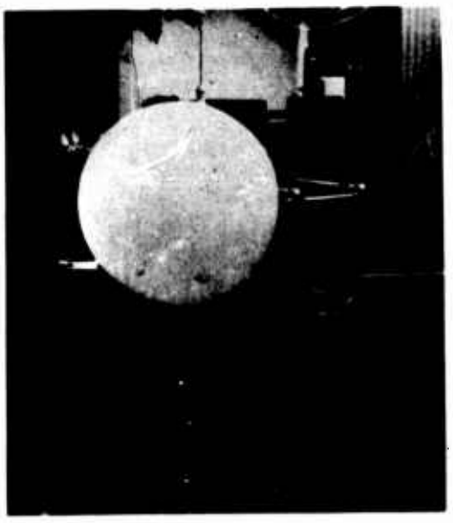

d. T = 90 Minutes

Figure 2. Creep of a Spherical Neoprene Balloon Under Constant Pressure

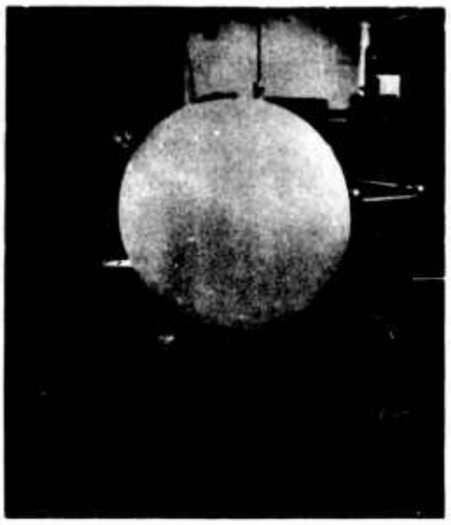

e. T = 120 Minutes

g. T = 300 Minutes

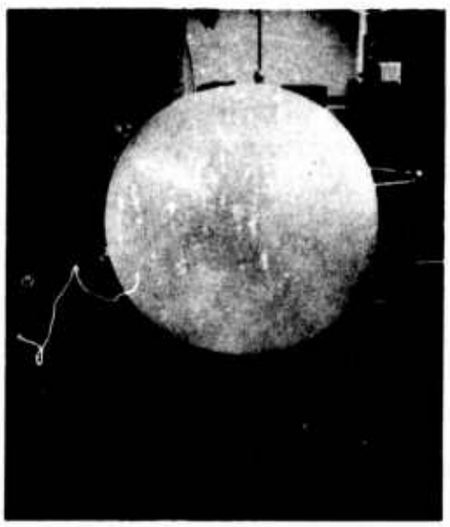

f. T = 180 Minutes

h. T = 420 Minutes

Figure 2. (Continued)

3. TESTS OF POLYETHYLENE BALLOON MATERIALS AT ROOM TEMPERATURE

This study focuses on deformation and failure patterns of polyethylene film subjected to uniaxial and biaxial states of stress, as well as behavior of seals, die lines, and creases.

In order to test polyethylene films and seals biaxially, it was found convenient to use polyethylene cylinders subjected to an internal pressure and an additional axial force. The experimental setup is shown in Figure 3. In this setup, compressed air is fed into five pressure regulators, which in turn are connected to five polyethylene cylinders. The pressures in the cylinders are measured by means of manometer tubes that connect directly to the regulators. The additional axial load consists of weights attached to the lower fitting. This arrangement makes it possible to test several cylinders simultaneously, each with a different internal pressure and axial load.

In order to establish the viscoelastic characteristics of polyethylene films which should serve as basis for the formulation of constitutive equations, a number of tests were conducted using the setup described above. These results and related comments are presented by Alexander (1966).

During these tests it was noticed that in all tested Startex cylinders (ten specimens) which were formed by heat-sealing two long strips, 20-in. wide (see Figure 3), one of the two seals consistently broke at a relatively low pressure. Uniaxial tests were then performed on 1-in. wide strips cut from these cylinders which contained the seal normal to the long axis of the strip. The tested samples did not fail at the seals, thus making the peel strength tests of seals using uniaxially stressed strips as described in "Standard Test Methods for Balloon Materials"(Hauser Research and Engineering Co., 1964, Sec. 2.1.5.1) rather questionable. It is also questionable if the uniaxial strength test as described by that report in Sec. 2.1.1.1 is a valid strength indicator for biaxially stressed polyethylene films because of the large deformations and the accompanying deformational anisotropy occurring in the uniaxial test.

In view of the above it is suggested to consider a new test for balloon films which uses, as specimen, the pressurized cylinder described previously. This test should integrate a number of tests such as the strength test, the peel test, and the gas permeability test, and additionally should check the behavior of die lines, creases, and other possible imperfections.

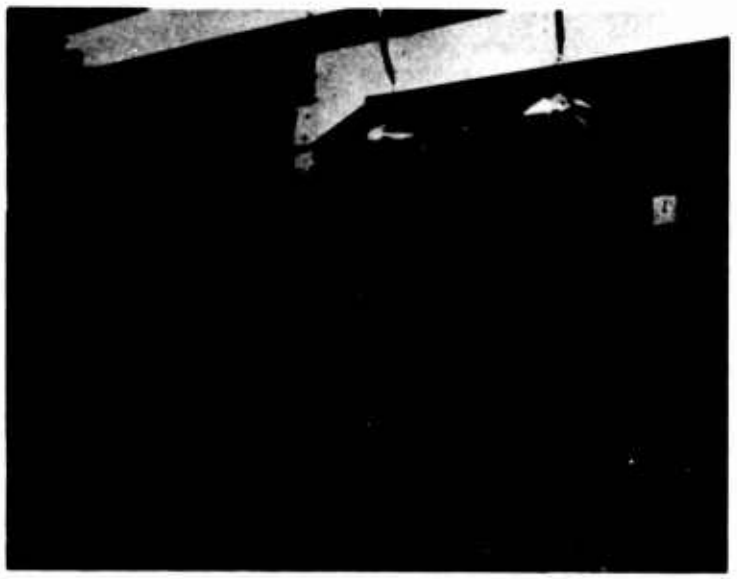

Figure 3. Testing Facility for Balloon Films

4. STRENGTH OF BALLOON FILMS AT LOW TEMPERATURES

The available data on balloon failures see for example Dwyer (1966) and Bilhorn (1966) indicate that a high percentage of balloons fail at altitudes between 35,000 and 60,000 ft.

Considering the temperatures through which the balloon has to pass during ascent (a schematic temperature profile is shown in Figure 4), it can be seen that from the launch altitude on the ground up to an altitude of 36,000 ft the temperature drops by more than 100°F. At 36,000 ft the temperature reaches about -65°F.

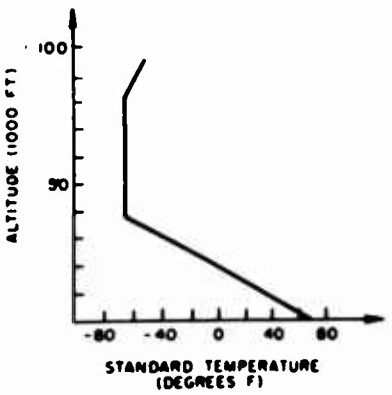

Figure 4. Atmospheric Height-Temperature Profile

This temperature distribution in conjunction with the observed failure altitudes suggests that a possible cause of balloon failures may be the effect of the low temperatures on the balloon film and seals.

To clarify this aspect, a systematic experimental study was initiated. Since during ascent the balloon material continuously deforms because of deployment and relative air motions, it was decided to use a test set up in which an axially loaded pressurized polyethylene cylinder is subjected to torsional oscillations. A schematic

drawing of such a fatigue tester is presented in Figure 5. The recently constructed testing machine is shown in Figure 6. Fatigue tests are presently being conducted at room temperature. It is planned to conduct similar tests in a cold chamber in the near future.

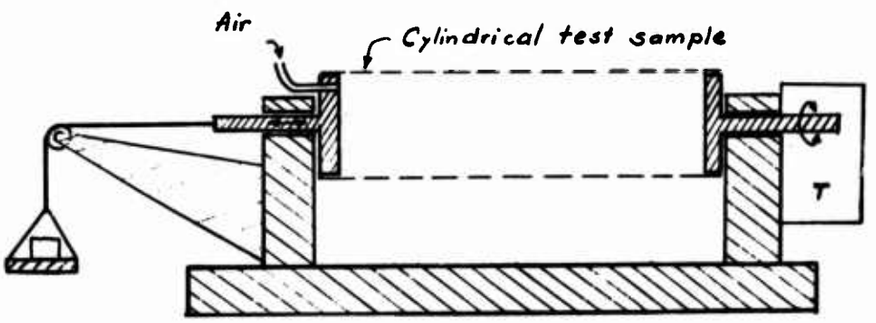

Figure 5. Torsional Fatigue Tester
(T - device which induces torsional oscillations)

Reviewing balloon failure statistics, J.F. Dwyer (1966) found evidence that creep deformations caused during launch may have a detrimental effect upon the strength of a balloon when it passes through lower temperatures. To study this aspect, it is planned to preload the test cylinder at room temperature after a time to lower the surrounding temperature, and then to determine the fatigue strength. A comparison of the obtained data with results of tests at which the specimen was not preloaded, should indicate the effect of creep deformations at launch.

Going out from the assumption that the low temperature level is a major cause of balloon failures, it was conceived that the raising of the temperature of the enclosed gas during the passage of the balloon through the critical altitude zone, may diminish balloon failures. To test this hypothesis, fatigue tests are planned during which the enclosed air is kept at a higher temperature than the cold air outside, and then the obtained results will be compared with results of corresponding tests at which the air inside and outside is kept at the same low temperature.

It is expected that the described tests will contribute to the clarification of the causes of a number of balloon failures.

(a)

(b)

Figure 6. Torsional Fatigue Tester (a - Front view, test sample mounted; b - Rear view)

Acknowledgments

The author wishes to acknowledge the assistance of Harold Alexander, Research Assistant, who conducted the tests described in this paper, and the constructive cooperation as well as the assistance of Mr. James F. Dwyer from AFCRL, who supervised the design and construction of the torsional fatigue tester.

References

Alexander, H. (1966) Creep characteristics of polyethylene film, Fourth AFCRL Scientific Balloon Symposium, 1966.

Bilhorn, T.W. (1966) Balloon performance analysis - NCAR Scientific Balloon Facility, Proc. AFCRL Scientific Balloon Workshop, 1965.

Dwyer, J.F. (1966) Some polyethylene balloon statistics, Proc. AFCRL Scientific Balloon Workshop, 1965.

Hauser Research and Engineering Company (1964) Standard Test Methods for Balloon Materials, NCAR Facilities Report FRB-2-64.

Kerr, A.D. (1966) On the creep failure of balloons, Proc. AFCRL Scientific Balloon Workshop, 1965.

V. Instrumentation for Balloon-Borne Infrared Spectral Measurements

David G. Murcray, Frank H. Murcray, and Walter J. Williams
Physics Department, University of Denver
Denver, Colorado

Abstract

Instrumentation has been developed for obtaining high-resolution infrared spectra from a balloon platform as it ascends through the atmosphere. These measurements have been made possible by the development of low noise, low frequency, time and temperature stable electronics, optically stable spectrometers and spectral radiometers, accurate solar pointing, and on-board digital magnetic tape recording.

Using this instrumentation high-resolution spectra have been obtained at a multitude of altitudes on ten balloon flights made from three geographic locations.

The instrumentation is described, with particular emphasis on problems associated with the balloon environment and the performance of the individual components evaluated.

Over the past decade the University of Denver Physics Department has conducted numerous infrared balloon experiments, gathering data pertinent to the study of atmospheric and solar physics. These experiments include the measurement of atmospheric transmittance, atmospheric backgrounds, atmospheric thermal flux,

solar radiance (and irradiance), terrestrial emission, and lunar emission. The study of atmospheric transmittance has continued throughout this period, and the experiments and data associated with it are perhaps the most complex part of the entire program. Much of the balloon-borne system has, as a consequence, been initially developed for this study and subsequently adapted to the others.

It is the purpose of this paper to describe the balloon instrumentation used in measuring atmospheric transmittance, with an emphasis on those aspects unique to the remote nature of the experiment.

In the course of the study, the transmittance of the atmosphere at various altitudes up to 31 km and throughout the spectral region from 1 to 15 μ has been measured. A prism spectrometer used in the earlier part of the study has been replaced on the last ten flights by a grating spectrometer with a significant gain in resolution. Data collected from more than 30 flights over New Mexico, California, and Alaska have been and are being published as scientific reports and journal articles.

There are several intervals in this spectral region which are strongly absorbed by the earth's atmosphere. In many cases balloon experiments have been designed to obtain data at high altitudes where these absorptions are not present. However, the variation of the absorption in these intervals with altitude is also of considerable importance and interest. The instrumentation described was therefore designed to obtain data pertinent to absorption at all altitudes from ground level to the balloon float altitude, rather than just at float altitude.

Several solar atlases have been published containing high resolution spectra observed from ground stations. One such atlas by Migeotte, Niven, and Swensson (1957) contains an infrared solar spectrum observed from the ground at the Jungfraujoch International Scientific Station, Switzerland. As mentioned above, many spectral intervals reported in this atlas are totally absorbed by minor atmospheric constituents such as CO_2, H_2O, O_3, and N_2O. Figure 1 shows a portion of their spectrum at the edge of the 2.7 μ CO_2 band. Similar data, measured with the balloon-borne grating instrument at about one-half the spectral resolution, are shown in Figure 2. Five spectra are plotted here, one above the other. Each covers the same spectral region, which is comparable to the region of Figure 1. Each succeeding record is at a higher altitude, ranging from 3.1 km to 16.8 km. The record at 5.8 km most closely matches the Jungfraujoch spectrum. The transmittance increases rapidly with altitude, and the N_2O band can be clearly discerned as the balloon rises above most of the tropospheric water vapor.

Figures 3 and 4 show, respectively, the spectrometer and coelostat used at the Jungfraujoch. The balloon-borne instrument (Figure 5) is fundamentally the same, although assembled for flight (Figure 6) it appears considerably different due to the spectral constructional details required for balloon application. Since the

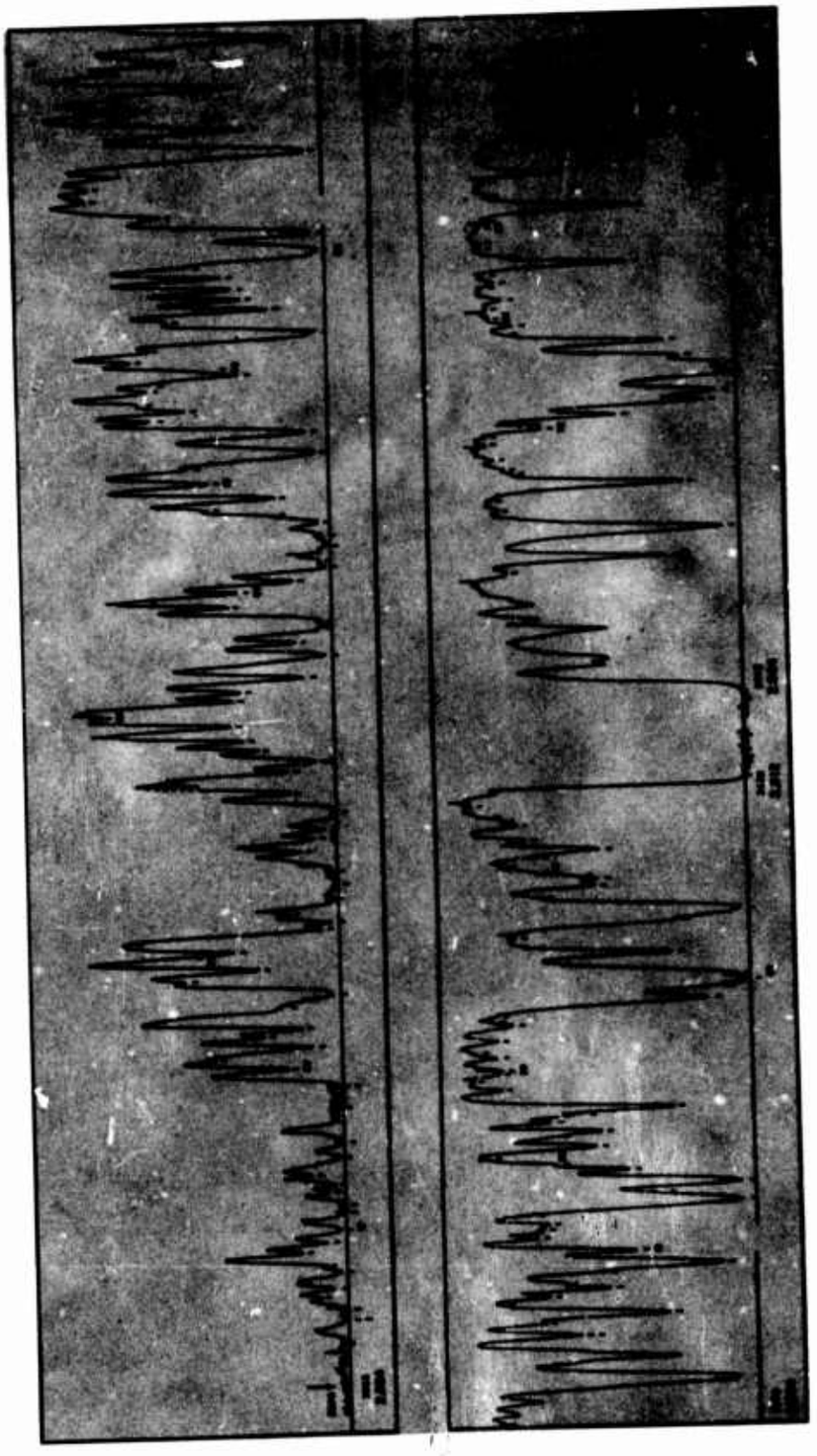

Figure 1. A Portion of the Solar Spectrum Near the 2.7 μ CO_2 Band (from Migeotte, 1957)

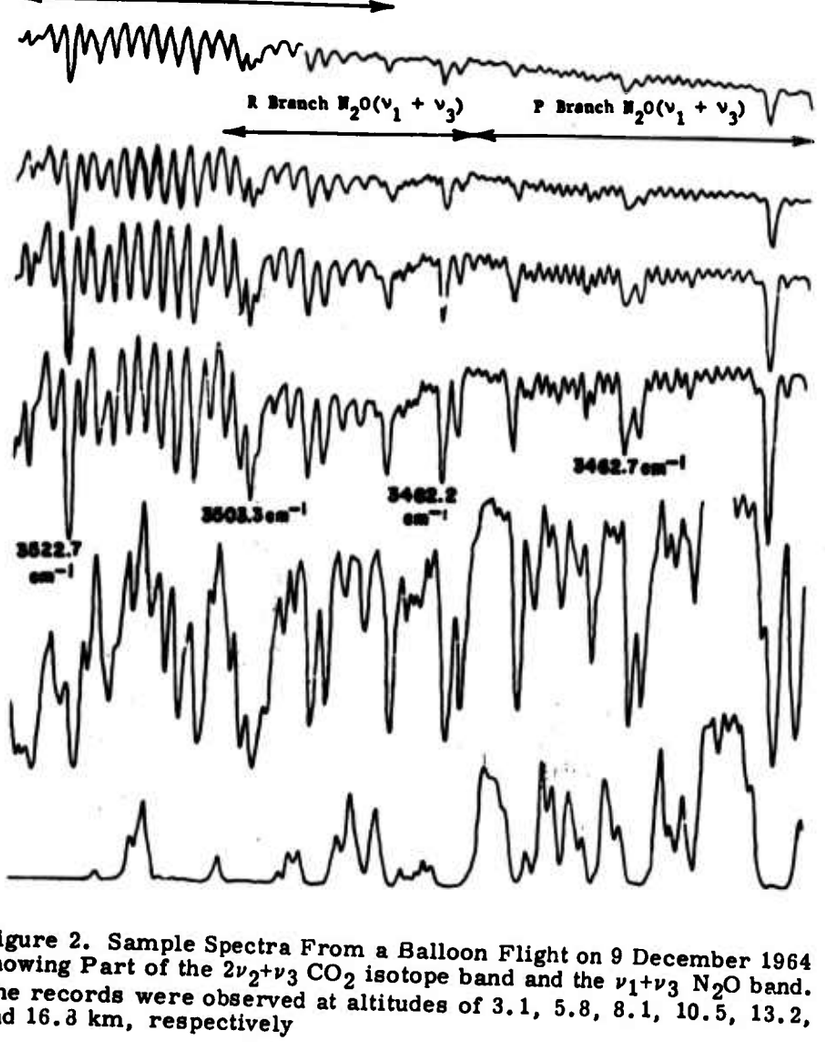

Figure 2. Sample Spectra From a Balloon Flight on 9 December 1964 Showing Part of the $2\nu_2+\nu_3$ CO_2 isotope band and the $\nu_1+\nu_3$ N_2O band. The records were observed at altitudes of 3.1, 5.8, 8.1, 10.5, 13.2, and 16.8 km, respectively

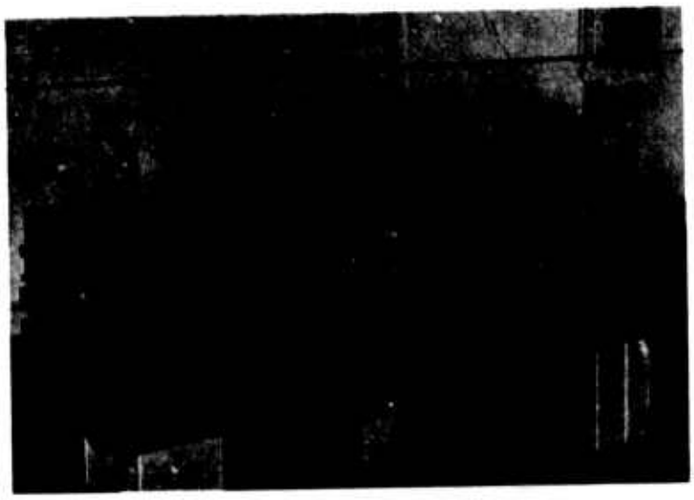

Figure 3. Photograph of the Grating Spectrometer Used at the Jungfraujoch to Obtain Data in Figure 1 (from Migeotte et al., 1957)

Figure 4. Photograph of the Coelostat Used at the Jungfraujoch in Connection With the Grating Spectrometer (Migeotte et al., 1957)

Figure 5. Photograph of the Balloon Grating Spectrometer Assembled in Its Gondola. Note the spring suspension

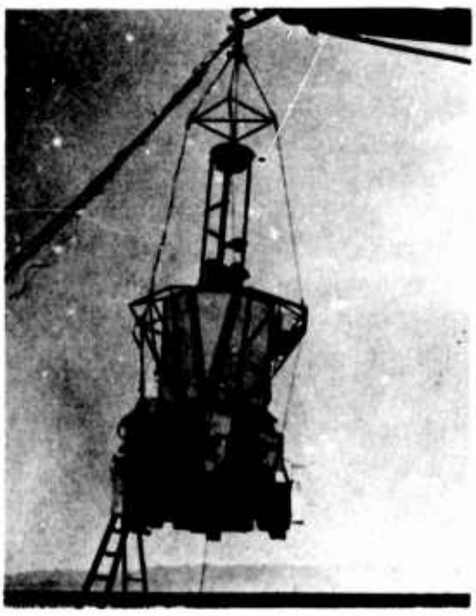

Figure 6. Photograph of the Balloon Grating Spectrometer Payload in Flight Configuration

balloon is not a stationary platform, a servo system instead of a coelostat is required to track the sun, and can be seen in Figure 6 above the gondola framework.

Successful adaptation for balloon work of equipment similar to that used at the Jungfraujoch requires experience in balloon instrumentation, and often involves a compromising of the optimum conditions desired for ground performance. The necessary experience was gained in building earlier equipment; the nature of the compromises will become apparent.

The equipment is composed of three functional units: the spectrometer, the biaxial pointing control (Sun-Seeker), and the data recording system. Solar radiation is maintained on the spectrometer slit by the Sun-Seeker, and the output of the spectrometer is recorded both on board and via TM to a backup recorder. Auxiliary units include a battery power supply, a thin-walled tubing gondola, and associated hardware. The total instrumentation weight is 700 lb. During flight the assembled spectrometer and pointer are suspended inside the gondola by springs which provide nearly complete isolation from the gondola yet retain its protection.

The grating spectrometer is a 1/2-m Czerny-Turner type instrument which double-passes the incident radiation. The double-passing of the radiation within the instrument permits the use of an instrument half the length that would otherwise be required, and results also in a great reduction in the scattered light. The orders of the grating are separated by first passing the radiation through a small prism predisperser spectrometer mounted just above the grating instrument. To scan the spectral wavelength the grating is repeatedly rotated through 15° by a precision cam, producing a linear wavelength as a function of time. A second cam couples the motion of the grating to the rotation of the prism predisperser. Both cams are polished, and their dimensions are critical to better than 0.001 in. The mirrors are rigidly mounted with slight shock cushioning and a minimum amount of adjustment is available. Both spectrometers are contained in a rigid light-weight frame which is insulated and thermostatically maintained at 27 ± 1.5°C during the balloon ascent.

Both thermocouples and uncooled PbS cells have been used as detectors (leaving the added complication of cooled detectors for a future flight). The solid-state detector electronics have been designed for stable operation over a wide temperature range with low power consumption. They are free of microphonics for moderate-level vibrations, and are capable of measuring the Johnson noise of a 15-ohm thermocouple.

The signal from the spectrometer is rectified and fed both to an on-board digital tape recorder and to an FM-FM telemetry system as backup. The digital recorder was specifically designed for airborne use and has a 6-hr recording capacity of 200 samples per sec. The recording format is directly compatible with IBM computers, thus simplifying data reduction. The inputs consist of 8 channels

with 25 samples per sec each. Two of these channels are subcommutated with 16 positions each for sampling low-rate data such as thermistors. In practice several of the remaining channels are paralleled to increase the information rate of the prime spectral data.

As previously mentioned, it is necessary to make some compromises in a balloon experiment, as contrasted to a ground measurement. As an illustration, one can consider the basic problem. An attempt is being made to scan as large a wavelength interval as possible with as high a resolution as possible in a time sufficiently short that the balloon has not appreciably changed altitude. As the resolution is increased, the energy available at the detector is decreased. The system is usually operating, however, in the vicinity of the detector noise level, and it is desirable to maintain a signal-to-noise ratio of about 100:1. The only way to reduce the noise level is to increase the electronic integration, thereby increasing the required spectral scanning time. In practice, upwards of 2000 resolution elements are scanned in each spectral cycle. It is desirable to sample each element from 3 to 10 times with the digital recorder. If the interval is scanned in 3 min, recording at 100 samples per sec, each resolution element is sampled 9 times, and there are 18,000 prime data points per spectral scan. A 3-min scan rate will yield about 50 scans during a moderate ascent. On occasion, when the signal-to-noise ratio has not been adequate, the scan time has been increased to 6-min.

The following example illustrates the effect of changing the scan time. The spectral region scanned in 3 min by the balloon spectrometer was scanned by the Jungfraujoch spectrometer in a composite time of about 7 hours. The ratio of these two times is 1:140. The noise can be reduced by an amount proportional to the square root of this ratio, or 11.9. If the signal-to-noise ratio is already adequate, the resolution can be increased to maintain the signal-to-noise at a constant level. The energy at the detector is approximately proportional to the square of the resolution element. Therefore, by changing the scan time from 3 min to 7 hr and maintaining a constant signal-to-noise ratio, the resolution can be increased by a factor of 3.4.

These are only a few of the factors which must be considered when designing a balloon-borne experiment. One other parameter that enters is the accuracy of the biaxial pointing control. Since the sun is the source of infrared energy for these experiments, the solar image must be held on the spectrometer slit at all times. (This is especially true when long scan times are used since the number of spectral scans possible at any one altitude is limited.) Some compromise may again be required, depending on the attainable pointing accuracy. The pointer has reliably pointed within ±6 min of arc during ascent on 17 of 18 flights, and within ± 2 min of arc at float altitude. The pointer used is a biaxial system built by the Hi-Altitude Instrument Company of Denver and modified in accordance with technology

and experience. The clutch system, in particular, was changed by the manufacturer from powdered iron clutches to hysteresis clutches. University personnel have modified the electronics and pointing sensors to accommodate automatic gain compensation for the variation in solar intensity at the sensors.

The pointing accuracy of ±6 min of arc permits the use of a spectrometer slit height corresponding to just over 1/2 the diameter of the solar image. A slit height of about 1/3 the solar image diameter is used in practice to avoid fluctuations due to limb darkening of the solar disk.

There are many critical parameters for a successful balloon experiment. The major experimental ones have been discussed. Also of importance is the care given this equipment by University of Denver staff and personnel at the AFCRL launch facilities. The authors wish to express thanks to these persons for their active participation and interest.

Reference

Migeotte, M., Neven, L., and Swensson, J. (1957) The solar spectrum from 2.8 to 23.7 Microns, Part II – Measures and identifications, Memoires de la Société Royale des Sciences de Liege, Special Volume No. 2.

VI. Electronics for Around-the-World GHOST Balloon Flights

Ernest W. Lichfield and Robert W. Frykman
National Center for Atmospheric Research
Boulder, Colorado

1. INTRODUCTION

On April 10, 1966, a superpressure balloon 7 ft in diam and made of Mylar plastic completed the first around-the-world flight ever made by a balloon.

The GHOST (Global HOrizontal Sounding Technique) balloon had been launched ten days earlier from Christchurch, New Zealand in an experiment being conducted by the National Center for Atmospheric Research (NCAR), the Environmental Science Services Administration (ESSA), and the New Zealand Weather Service.

After it was launched, the balloon rose to an altitude of about 40,000 ft and floated across the South Pacific, propelled by air currents which exist at that altitude. Its progress around the Southern Hemisphere was monitored by a network of five tracking stations located in New Zealand, South America, Mauritius Island, Australia, and Africa. The balloon passed over South America, Australia, and vast expanses of empty ocean, and completed its circuit of the globe as it passed north of New Zealand over the Fiji Islands.

The first globe-circling GHOST balloon continued to travel around the Southern Hemisphere, and at the end of July, 1966, it had been up for 74 days and had made six complete circuits of the globe. Other GHOST balloons launched from Christchurch have also circled the globe several times and have had flight durations up to

97 days. Thus the Southern Hemisphere experiment is meeting with success in its primary purpose, which was to prove the feasibility in terms of life expectancy of GHOST balloons as platforms for meteorological sensing instruments to obtain data from previously inaccessible parts of the earth.

An operational GHOST system, which lies many years in the future, will utilize several thousand free-floating balloons as part of a global observing system which will also include conventional weather stations, buoy-mounted remote stations in the oceans, remote ground stations, and meteorological satellites.

The feasibility of an operational GHOST system will depend on the ability of superpressure balloons to stay aloft, at a constant density level, for long periods of time. Superpressure balloons, such as those used in the GHOST experiment, are spherical in shape and must be made of a very strong, inelastic, impermeable material such as Mylar. The GHOST balloons use a double lamination of Mylar to minimize permeation of helium through microscopic pin holes.

In operation, the balloon is partially inflated with helium and is then released. As it rises, and as the atmospheric pressure decreases with altitude, the helium in the balloon expands until the Mylar skin is fully distended. The balloon will continue to rise until it reaches an atmospheric density level which is equal to the density of the balloon and its payload. The balloon will then drift horizontally at that constant density level. Unlike a zero-pressure balloon which must release gas or jettison ballast to compensate for expansion and contraction of the helium caused by daytime heating and nighttime cooling, the superpressure balloon maintains a constant density and floats at a nearly constant atmospheric density level day and night.

2. INSTRUMENTATION

Theoretically, it should be possible for a superpressure balloon to stay aloft for months. The Southern Hemisphere GHOST experiment was designed to test this theory by actually flying the GHOST balloons with adequate instrumentation to locate the balloons and to telemeter performance data during the flight.

The instrumentation requirements for the Southern Hemisphere experiment presented an almost impossible set of design criteria. The instrument package had to be capable of locating and reporting the balloon's position over a range of 4,000 miles with an accuracy of ± 100 miles. The total weight of the package, including the power source, had to be 6 oz. or less, its operating lifetime had to be about 1 yr, and it had to be capable of operating at temperatures down to -55°C. Four channels of telemetry were required, and each unit had to provide a unique identification code, as the same transmission channel would be used by up to 20

balloons. In spite of these stringent performance requirements, each package had to cost less than $300 and operate with simple tracking stations. Figure 1 shows the electronics package which was developed to meet these criteria.

2.1 Power Supply

The electronics package is powered by a solar-cell panel consisting of 26 solar cells, each measuring 2 cm × 2 cm. Power is supplied directly from the solar-cell panel. Since no battery is included, the electronics package operates only during daylight hours.

2.2 Position Locating Device

A small sun-angle sensor is mounted in the center of the solar-cell panel pointing upward. The sun-angle sensor measures the elevation angle of the sun and converts this angle into an electrical resistance, which decreases as the sun angle increases. The sun-angle sensor is the rate-determining resistance in a unijunction pulse generator circuit. Therefore, the pulse rate from the circuit is proportional to the sun's elevation angle. An exploded view of the sun-angle sensor is shown in Figure 2.

2.3 Coding Circuit

A 16 counter and a group of gates are wired together to produce a Morse-code waveform. A different Morse code letter can be wired into each electronics package by rearranging the wiring of the gates. The coding circuit is driven by the pulses from the unijunction circuit. Since the timing is provided by the unijunction circuit, the rate at which the Morse code letters are generated is proportional to the sun's elevation angle. The electrical configuration of the GHOST balloon electronics package is shown schematically in Figure 3.

2.4 Radio Transmitter

The Morse code signal is used to key a transmitter operating in the CW mode on a frequency in the 15 MHz band. This frequency was chosen because of its consistent long-distance propagation characteristics. Using the CW mode at low bit rates allows signals to be separated with as low as 100 Hz differences. Power is provided by a panel of solar cells having an output of approximately 12 V and 150 ma at noon on the balloon. Since transmission on the 15 MHz band is most efficient during daylight hours, batteries were not included. This resulted in the transmission power varying between a maximum of 1 W at noon to as low as 50 mW just before sunset. At first glance these power levels, varying from "flea to gnat", seem to be too low to transmit beyond the horizon. In actual practice, however, the balloons have been monitored consistently over a 4000-mile range.

Figure 1. Photograph of GHOST Electronics Package

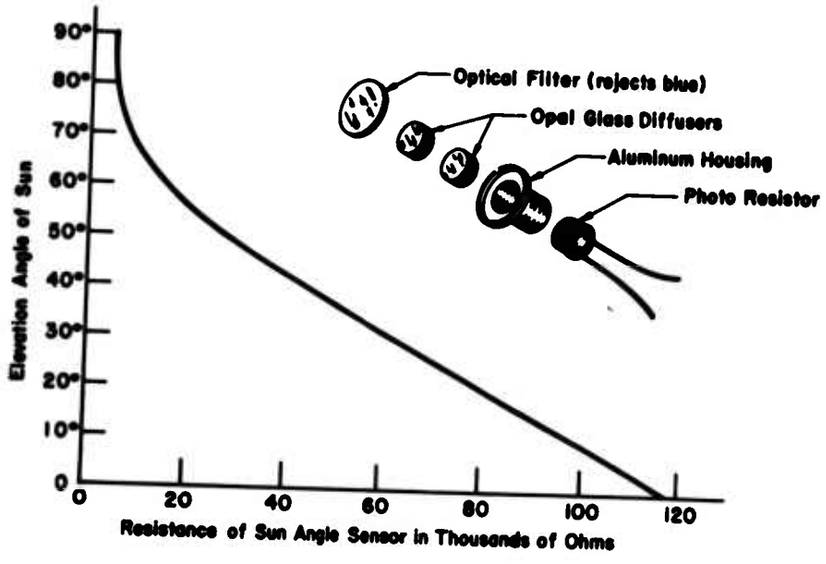

Figure 2. Exploded View of Sun-Angle Sensor

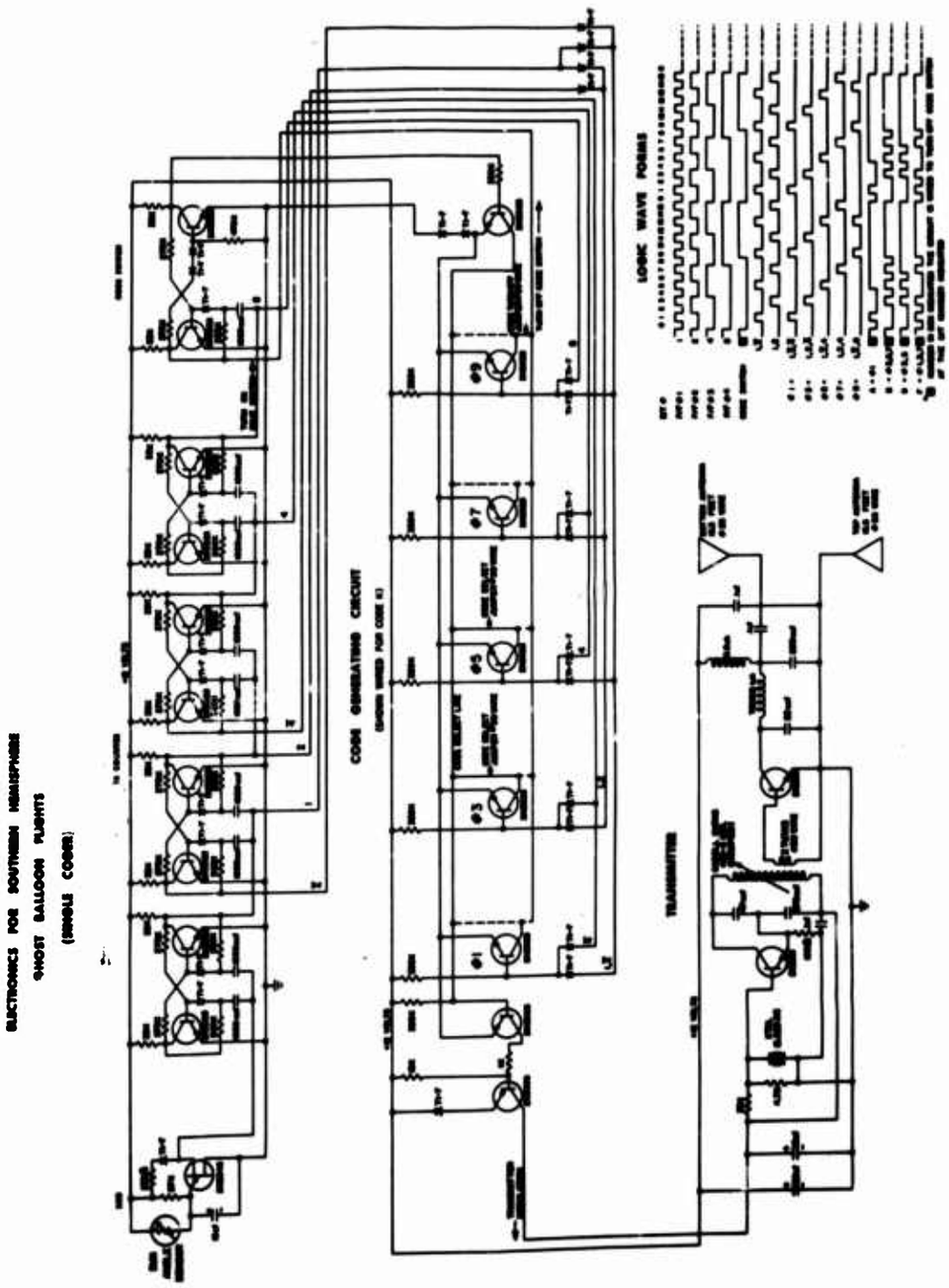

Figure 3. Electrical Configuration of GHOST Electronics

2.5 Antenna

The electronics package is suspended beneath the balloon by a quarter-wavelength section of antenna wire. An additional quarter-wave section is suspended from the bottom of the package to provide a center-fed dipole floating free in space.

3. CONSTRUCTION

The electronics package is assembled on a 0.005-inch-thick glass epoxy printed-circuit board. Miniature electronic components are used, but integrated circuits are not. The assembled circuit board weighs only 24 grams.

Solar cells are assembled on a 0.01-in.-thick glass epoxy printed-circuit board. The solar-cell panel weighs 45 grams. A plastic cover fits over the bottom of the package. The purpose of the cover is to provide a warm thermal environment for the electronics. Since the balloon and its package float with the wind, there is no relative wind blowing across the package to cool it. The temperature of the electronics is therefore determined primarily by solar radiation. A black plastic cover is used to maintain the temperature of the electronics package at about 15°C at an altitude of 40,000 ft. At 40,000 ft the average air temperature is -50°C.

4. TRACKING BALLOONS

The code-generating circuit produces a Morse code letter used to identify the balloon from which the signal is being received. Each balloon transmits a different code letter at a rate which is proportional to the elevation angle of the sun.

Tracking equipment for the sun-angle telemetry consists of a stop watch and a communications receiver. The operator tunes to the transmitted signal, using the CW reception mode on the receiver, and uses the stop watch to time the period of ten code letters. The operator then records the period and the time of observation. A calibration chart showing code rate as a function of sun angle is used to obtain the sun angle. Many such readings are taken each day for each balloon that is aloft.

Figure 4 shows an example of a three-day test flight launched from Boulder, Colorado, on April 24, 1965. The chart in the upper left of Figure 4 shows the sun elevation angle as a function of time of day. The curve labeled April 24 shows the sun angle for the day of launch. The divided line from 7:00 to 10:00 shows the envelope of sun-angle oscillations due to swinging of the package during ascent. Once the balloon is at altitude, the swinging stops and the balloon provides a very stable platform. On the first day the maximum sun angle recorded was 63° at

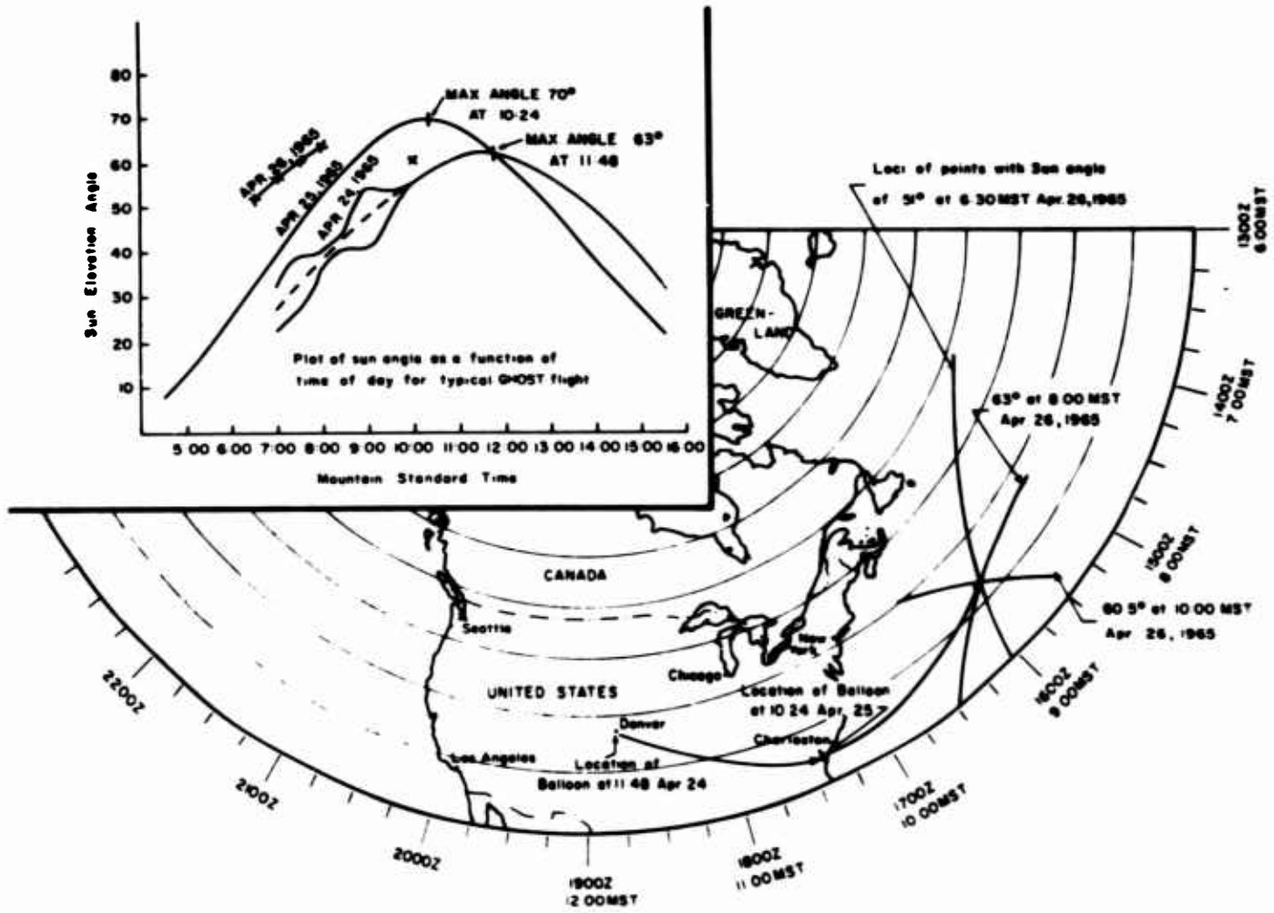

Figure 4. Technique for Locating Balloon Position

11:48 MST. The maximum sun angle determines the latitude and the time of maximum sun angle determines the longitude. At 11:48 MST on April 24 the balloon was 100 miles east of Denver. On April 25 the maximum sun angle was 70° at 10:24 MST, indicating a balloon position over Charleston, South Carolina. On the third day, April 26, only five data points were obtained so a different technique was used to obtain the balloon location. At 6:30 MST the sun's elevation angle at the balloon was 51°. Thus, it was known that the balloon was located somewhere on a line connecting all points with solar elevation angles of 51°. A segment of this line was drawn on the map. One and a half hours later, at 8:00 MST, the new sun angle was 63° and a new line segment was drawn. The intersection of the two lines gave the location of the balloon. A third line, drawn two hours later, gave additional confirmation of the location. This technique neglects the effect of balloon motion between readings, but this effect was negligible in the example given.

5. FOUR-CHANNEL TELEMETRY

On the majority of the balloon flights a single-channel telemetry system is used to telemeter sun angle, only. Additional channels of telemetry can be obtained by attaching an additional circuit board to the system. The add-on board provides 4-channels of telemetry. In operation, a 4-channel system transmits a given Morse code letter 16 times and then switches to a new letter for 16 transmissions. After the completion of the 4 code letters it starts over again at the first letter. The letter being transmitted identifies the data channel. The data is obtained by timing 10 code periods and referring to a calibration chart. A block diagram of this telemetry system is given in Figure 5.

6. CONCEPTS FOR THE FUTURE

The concept for a future GHOST system calls for thousands of balloons floating around the world-gathering meteorological information over remote portions of the globe. A satellite in orbit would be used to gather the data from the balloons and relay the information to ground stations. This will require a more advanced electronic system than the one presently being used. One consideration will be to devise an electronics package that will be nonhazardous to aircraft. The final electronics for this application may take the form of thin film circuits distributed over the skin of the balloon itself.

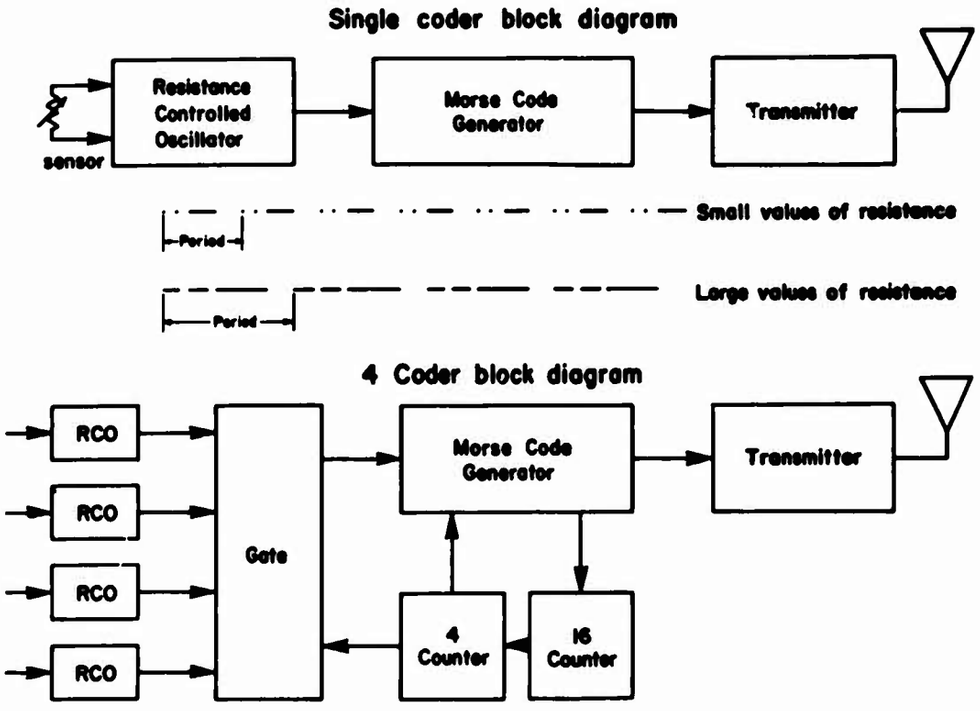

Figure 5. Block Diagram of GHOST Telemetry System

VII. Planetary Entry Parachute Testing Using a Balloon as a Launch Platform

J.C. McFall, Jr.
NASA Langley Research Center
Hampton, Virginia

Abstract

A 26 million cu ft balloon has been designed, constructed and tested for use as a launch platform in testing of planetary entry parachutes. The fabric weight of the balloon is less than 0.0055 lb/sq ft allowing a payload of 2,250 lb to be carried to an altitude of approximately 130,000 ft. The parachute tests to be conducted with this balloon system are a part of the NASA Planetary Entry Parachute Project in support of Project Voyager. In these tests, a 15-ft-diam simulated Voyager landing capsule with parachute system (84-ft constructed diameter parachute) will be launched with a tandem balloon system and carried to 130,000 ft. Following release from the balloon, rockets in the capsule will accelerate it to the required test conditions of Mach No. 1.2 and dynamic pressure of 5 lb/sq ft. The test parachute will be ejected from a mortar, and an aeroshell will be released from the instrumented internal body. On-board and ground-based instrumentation will record the system performance.

The purpose of the Planetary Entry Parachute Program is to furnish a technological background for selection of a parachute system for NASA Voyager Program missions, a program of planetary exploration to be conducted by means of unmanned spacecraft. The program includes flights to the planet Mars in the

1970-1980 time period to investigate the characteristics of the Martian atmosphere and the planet surface. Such missions will involve instrumented entry capsules, which will be detached from an orbiting spacecraft, descend through the atmosphere, and perform a survivable landing on the surface.

In one mission mode, deceleration of the lander capsule from the initial entry velocity to a subsonic or low supersonic velocity will be accomplished by the basic ballistic characteristics of the entry capsule. A parachute system will then be activated for deceleration of the instrumented payload to a low subsonic velocity to permit a dwell time in the atmosphere for atmospheric measurements, and to provide a low impact velocity for landing.

The purpose of the present flight program is to explore the characteristics of several types of parachutes under the expected conditions, and to provide information to enable selection of a parachute configuration and mode of operation for future development as part of the initial Voyager mission.

There will be two test techniques used in the PEPP flight program. One using conventional solid rocket boosters to test parachutes with diameters of about 30 ft and payloads of 200 lb. The other test technique is to use a balloon as a launch platform for parachutes having diameters of about 80 ft.

The reason for selecting the balloon method of getting the spacecraft to altitude is that, for these tests, the test parachutes will be deployed in the wake of a 120° conical body 15 ft in diam and weighing 1600 lb, and a balloon appeared to be the most economical means of getting this vehicle to approximately 130,000 ft.

Specific objectives of the flight tests are indicated in Figure 1. Primary data from tests of candidate parachutes will concern deployment dynamics (that is, shock loads and canopy inflation characteristics), stability or oscillation characteristics, and drag. In addition, every possible effort will be made to learn how the primary data is affected by the wake behind proposed entry shapes (parachute size varying between 30- and about 100-ft diam), possible detrimental effects of sterilization while in the packed condition, and the necessity for deployment aids.

PRIMARY - TO MEASURE AND OBSERVE:

- DEPLOYMENT DYNAMICS
- STABILITY
- DRAG

SECONDARY - TO OBTAIN SOME DATA ON:

- WAKE EFFECTS
- SCALE FACTORS
- STRUCTURAL EFFECTS OF STERILIZATION
- EFFECTIVENESS OF DEPLOYMENT AIDS

Figure 1. Planetary Entry Parachute Program: Transonic Configuration

The four configurations selected for this test program are shown in Figure 2. Note that all designs have geometric porosity and it is hoped that stability characteristics will not change with altitude. We have experience at Langley with the cross and DGB designs, and they both appear promising. The porosity of the basic ring sail design has been increased by removal of one row of sails for the first test. The annular design appears to have quite high drag potential. Dacron

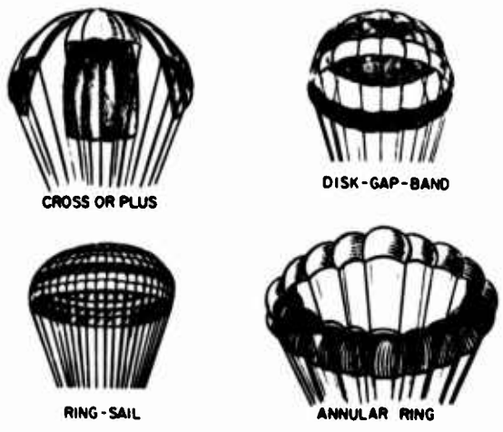

Figure 2. Promising High-Altitude Deceleration Configurations

material has been selected for fabrication of the first four test parachutes due to its ability to withstand sterilization temperatures.

The spacecraft utilized for the PEPP balloon launched series is shown in Figure 3. It is propelled by 12 M58A2 rocket motors arranged in a circular cluster about the internal payload section as shown in Figure 4. The motors have canted nozzles (33.5° off the longitudinal axis) such that the individual thrust vectors converge at a point between the iginition and burnout centers-of-gravity on the longitudinal axis. In the nominal case such an arrangement produces a resultant thrust vector along the longitudinal axis. Test data is recorded on-board and recovered. The recorded data includes accelerations, temperatures at several points within the payload, and certain events in the flight sequence. Five on-board cameras record the parachute deployment and also view the earth to provide data to aid in analysis of vehicle motions. Beacons are provided for in-flight tracking and for recovery aid. Ground photographic coverage of flight events is provided by the range.

Figure 3. Spacecraft Antenna Checkout

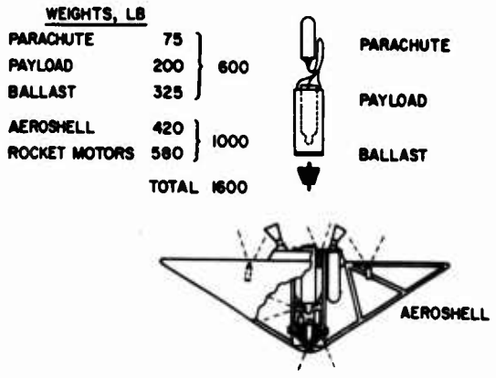

Figure 4. Balloon Launched Test Spacecraft

The C-band tracking beacon signal is modulated by the output from magnetometer instrumentation to furnish information on the azimuth attitude of the spacecraft. This information is intended to permit withholding of command release of the spacecraft if the spacecraft heading is such that landing outside the range safety limits is possible. This procedure should result in increased utilization of the range safety corridors specified for this program by effectively widening the permissible corridor from which spacecraft release is possible.

In our flight test of August 30, 1966, there was a noticeable effect of this instrumentation at the time the balloon ballast was dropped and some system motion apparently resulted. This portion of the data has not yet been analyzed, but is of considerable interest.

The nominal trajectory for the PEPP balloon-launched series is somewhat unusual when compared with conventional rocket vehicles. The mission sequence of events is generally as shown in Figure 5. The spacecraft is oriented at a 60° attitude angle (pitch up) beneath the balloon at launch. After the balloon has risen to 130,000 ft, the spacecraft is released and falls in a backward attitude (relative to downward velocity vector) for 4 sec. At this time, all 12 rocket motors are ignited simultaneously and the spacecraft is propelled to transonic velocity. After burnout a mortar is fired, ejecting the parachute, and the deployment sequence begins. Upon inflation the parachute withdraws the internal payload from the rear of the spacecraft. The payload descends by parachute and the remainder of the spacecraft (called the aeroshell) coasts over apogee on a separate trajectory until "hard" impact on the range. Experimental objectives and safety regulations require that that portion of the trajectory prior to mortar firing and parachute deployment, and the resulting aeroshell coast, be at a preselected area of the range.

The balloon system floated the spacecraft over a suitable drop point on the range and all flight test objectives were achieved.

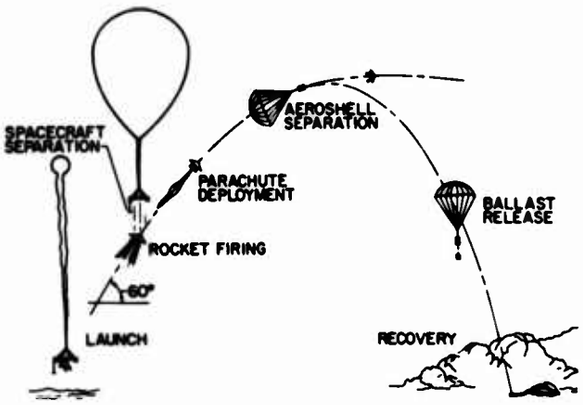

Figure 5. Balloon Launched Test Sequence

VIII. Balloon Stress-Band Analysis

Harold L. Baker
National Center For Atmospheric Research
Boulder, Colorado

Abstract

One of the tasks of the NCAR Scientific Balloon Facility is to advance the technology of ballooning. As part of this work, the Facility conducts a number of programs to improve standards for balloon materials, design, and fabrication. The present report covers a series of investigations carried out by Thomas W. Bilhorn, then Mechanics Section Manager, and Harold L. Baker, Development Engineer, in which balloon failures near the tropopause were photographed, and the data obtained were analyzed to provide better understanding of mechanisms of failure.

A test program to photograph tropopause-level balloon ascent failures unexpectedly revealed the presence of a circumferential stress band in certain balloons which failed catastrophically in flight. The band in each case was located between the top of the balloon and the equator of the bubble, and appeared to exert powerful transverse stresses on the envelope, culminating in failure near the tropopause level. The failure mechanismappeared to involve also the presence, beginning at launch, of a large asymmetrical pocket of undeployed material, which locally folded the envelope inward approximately as far as the vertical axis of symmetry of the balloon. With expansion during ascent this excess material was gradually deployed into the inflated balloon structure. Failure appeared to occur about at the point where there was no longer sufficient excess material to allow the pocket to extend to the vertical axis of symmetry. It is speculated that the additional work then involved in deploying the remainder of the pocket, together with film brittleness due to cold temperatures at tropopause level, and aided at least in some instances by shear winds, combined to produce failure by enhancing transverse stresses at the stress-band level. It appeared that development of the stress band might be modified or eliminated by variations in balloon design, and this suggestion was partially confirmed by balloon model tests.

1. INTRODUCTION

Since 1946 large polyethylene balloons have become standard vehicles for lifting many types of scientific experiments to high altitude. To accommodate desired experiments, scientists have asked for increasingly higher altitudes, heavier payloads, and longer duration flights, or combinations of these characteristics. Balloon manufacturers have responded by designing larger balloons. However, as balloon volumes have increased, the in-flight balloon failure rate has also increased. Such failures are most likely to occur during ascent, in the vicinity of the tropopause. The low temperatures encountered there evidently render the balloon film material brittle, while at the same time the envelope, still only partially inflated at tropopause altitudes, may be subject to stress from shear winds.

While these conditions offered some explanation of balloon failures, it seemed possible that balloon design, or manner of deployment during ascent, or both, could also contribute to failure. Experiments were devised to photograph large balloons during ascent, in the hope of obtaining detailed pictures of balloon failures. The experiments involved tandem balloons, tethered together. In one configuration the uppermost, or "tow", balloon carried down-looking cameras to photograph the lower "main" balloon. In a variation of the experiment, additional cameras were suspended below the main balloon and directed upward.

Three flights were attempted. Flight No. 1 yielded pictures of a catastrophic balloon burst. Flights No. 1 and No. 3 provided many additional pictures which gave evidence of stress in the balloon envelopes. Flight No. 2 was a ground failure. Two balloon model tests were carried out to test certain assumptions concerning balloon design that arose during the flight data analysis.

Each flight carried several cameras, in part to provide duplicate coverage and a range of exposure settings, but primarily to provide continuity of coverage: some cameras were pairs, set so that when all the film in the first camera was exposed, the second camera of the pair would begin taking pictures.

In the present text, the photographs from each flight appear in the Figures, in chronological flight sequence. Thus the figures will often be referred to out of numerical sequence.

Section 2 presents summaries of the test flights, and brief qualitative descriptions of the data secured. Section 3 presents the stress-band analysis, while Section 4 presents an analysis of the flight and model test photographs. The conclusions appear in Section 5.

2. TEST FLIGHT SUMMARIES

2.1 Flight No. 1, 13 November 1964

This flight carried down-looking cameras only. Tables 1 and 2 give the balloon and camera characteristics.

The main balloon was inflated to a gross lift of 2020 lb, representing a free lift of 6 percent. Launch was uneventful with the tow balloon very nicely taking position above the main balloon. Ascent rate from launch to 31,500 ft was 759 ft/min; from 31,500 to 46,800 ft (burst altitude), 933 ft/min. The tow balloon did swing from side to side, occasionally as much as 90° from vertical during ascent. Photographs showed that, starting one minute before burst and persisting until burst, shear winds apparently were blowing into the undeployed pocket and subpressure cavity, but no sailing of material was visible. At 46,800 ft the main balloon burst, in what appeared to be a typical tropopause failure. (Tropopause was at 47,000 ft, temperature -65°C.) The tow balloon was released from the main balloon by radio command. Payloads of both balloons were recovered in good condition.

Table 1. Balloon Characteristics, Flight No. 1

Parameter	Main Balloon	Tow Balloon
Volume, cu ft	2,940,000	58,000
Material	1.5-mil Hislip polyethylene	1.2-mil polyethylene
Load Tapes	650-lb strength Fortisan	
End Section Design	Taper tangent	
Balloon Weight, lb	1013	
Payload Weight, lb	890	

Table 2. Camera Specifications, Flight No. 1

Camera No.	Type (movie)	Pulse Rate frame/sec	Film	Aperture	Shutter Speed	Starting Altitude ft
1	8-mm	1/3	Kodachrome II daylight	self-adjusting	1/30 nominal	30,000
2,3	35-mm	1/5	Tri-X	f-16	1/200	30,000
4,5	35-mm	1/5	Tri-X	f-22	1/200	30,000
6	16-mm	32/1	Kodachrome II	f-16	1/60	balloon burst

Data Secured; Qualitative Impressions

The six cameras mounted on the tow balloon took pictures of the main balloon from 30,000 ft to burst altitude (46,800 ft). The photographs were of good quality, although geometric analysis was made difficult by the lack of reference points on the main balloon, and by related problems of depth perception. The only visible circumferential reference point was the inflation tube, and sometimes it was not visible.

The photographs showed a pocket of undeployed envelope material during ascent, and also revealed the unexpected development of a circumferential flattening of the balloon skin which we have termed the "circumferential stress band". The balloon failure appeared to originate in the region of this band, and within 90° azimuth of the pocket of undeployed material.

2.2 Flight No. 3, 24 August 1964

Tables 3 and 4 give the balloon and camera characteristics for this flight. The main balloon was inflated to a gross lift of 1270 lb, representing a free lift of 6 percent. The system was about 760 ft long and, just before launch, the tow balloon was subject to winds 3 to 5 times stronger than those affecting the main balloon. The tow balloon was blown over about 90°; however, launch vehicle maneuvers allowed the entire system to float off smoothly. Ascent rate from launch to 31,800 ft was 934 ft/min; from 31,800 to the burst altitude of 65,000 ft, 964 ft/min. (Tropopause was at 53,000 ft, temperature -74°C.)

The tow balloon was separated from the main balloon by a pressure switch at 58,400 ft. Payloads of both balloons were recovered in good condition.

Data Secured; Qualitative Impressions

The down-cameras took pictures from launch to 58,000 ft; the up-cameras from 10,000 ft to burst altitude. The photographs were of good quality, and geometric analysis was straightforward because the balloon was marked with a grid of red and green pennants located alternately each 10 ft down from the top end fitting through 80 ft and in vertical rows on every fifth gore's load tape.

The photographs revealed a definite circumferential stress band which was present from launch until the tow balloon separated. In addition, photographs taken by the up-cameras showed that, starting two minutes before burst and persisting until burst, shear winds caught undeployed material in the envelope and made it sail and flutter. The tow balloon swung from side to side, occasionally as much as 90° from the vertical. The burst itself was also photographed. The failure appeared to begin within 90° azimuth of the undeployed pocket.

Table 3. Balloon Characteristics, Flight No. 3

Parameter	Main Balloon	Tow Balloon
Volume, cu ft	9,000,000	58,000
Material	0.55-mil polyethylene	1.2-mil polyethylene
Load Tapes	75-lb strength Fortisan	
End Section Design	Cylinder end	
Balloon Weight, lb	727	
Payload Weight, lb	468.5	

Table 4. Camera Specifications, Flight No. 3

Camera No.	Type (movie)	Pulse Rate frame/sec	Film	Aperture	Shutter Speed	Starting Altitude ft
Down-looking from Tow Balloon						
1	35-mm	1/4	Medium-speed Ektachrome	f-8	1/360	launch
2	35-mm	1/6	Plus-X	f-11	1/200	30,000
3	35-mm	1/6	High-speed Ektachrome	f-16	1/200	30,000
Up-looking from Main Balloon Payload						
1	35-mm	1/5	Plus-X	f-8	1/200	10,000
2	35-mm	1/5	High-speed Ektachrome	f-11	1/200	10,000
3	16-mm	(a)	Kodachrome II	f-11	1/30	30,000
4	16-mm	(a)	Kodachrome II	f-16	1/30	30,000

(a) 16 frames/sec for 5 sec, at 30-sec intervals

3. STRESS-BAND ANALYSIS

Study of the photographs made it seem highly probable that the circumferential stress bands were crucially involved in the balloon failures. On both flights the band developed in the partially inflated bubble before launching, and persisted until burst. The band appeared in the zone between the top of the balloon and the effective balloon equator, and stayed in this zone during ascent. Since the balloon was expanding during ascent, the stress band both expanded in meridional width and moved downward on the balloon bubble.

The natural shape balloon envelope is intended to be circumferentially stress-free during ascent and at float altitude (that is, when the balloon is fully inflated and floating in the free atmosphere). Although before the present experiments it was known that a rising, partially inflated balloon was subjected to various stresses, such stresses had not previously been analyzed, so far as we are aware. The rising envelope has always been assumed to deploy the transverse excess gore material in equal pleats around the circumference for a stress-free balloon. However, the photographs made it clear that most of the excess balloon material in each of these flights was concentrated in a large asymmetrical pocket of material, folded inward and, in the early stages of the flight, reaching approximately to the balloon's vertical axis of symmetry. The pocket remained in the same relative azimuth position during ascent, while gores deployed uniformly from it on both sides.

As the envelope expanded, the pocket appeared to resist deployment, and this resistance evidently added to transverse stresses on the gores already deployed. Near burst altitudes the transverse stress increased, probably because so much excess material had then been used up that the pocket was being pulled outward, so that its inner margin opposite the stress band no longer hung approximately along the vertical axis of symmetry. Transverse stress could also have been intensified by shear winds, which apparently were blowing into the subpressure cavity, further increasing resistance to deployment.

3.1 Analysis of Excess Material

The analysis of possible failure mechanisms proceeded from these qualitative observations of the flight photographs. Figures 1 and 8 depict for Flights 1 and 3 the allocation of envelope material to deployed and undeployed material for a direct comparison with the material available, from the top of the balloon to the equator. Curve A in each figure shows the amount of material required at launch to contain the bubble. Curve B shows the additional material required to form the undeployed pocket. Curve C shows the material required to contain the bubble at burst altitude, and curve D shows the material required at that altitude for the undeployed pocket. Curves A and C are the theoretical natural shape of the bubble and were verified on the NCAR computer. Clearly, infinite families of curves representing progressive stages of expansion during ascent could be drawn between curves A and C, and between B and D on these figures.

Curve E is based on the actual design of the balloon, which for construction purposes deviates somewhat from the natural shape, particularly in the area of the balloon top fitting. Thus curve E shows the total material actually available at each gore station. The different shape of curves E on Figures 1 and 8 results from the different designs used in the two balloons.

Figures 2 and 5, from the flight photographic records, indicate the decreases in azimuth depth of the undeployed pocket from launch to near burst for Flight No. 1. Although pockets do not tend to form straight vertical folds, they did appear in these flights approximately to reach a uniform azimuth depth to the vertical axis of symmetry of the top hemisphere of the balloon at launch, and this depth has been assumed in the analysis carried out here.

3.2 Calculation of Circumferential Material

The desirability of exact measurement of the balloon dimensions was suggested during the program. The balloon for Flight No. 1 was not measured, but the balloon for Flight No. 2, made from the same design, was measured by the manufacturer during installation of pennants to provide a reference grid. Thirty gore widths were measured seal-to-seal, at each 10-ft gore station, and these values were averaged. The averaged values were multiplied by 75 (total number of gores) to obtain the total circumferential material. In the present analysis these dimensions were assumed to hold for the balloon of Flight No. 1.

The balloon for Flight No. 3, built to a different design, was measured during installation of the pennants. Twenty-two gore widths were measured seal-to-seal at each 10-ft gore station, and the values were averaged, and multiplied by 110 (total gores) to obtain the total circumferential material.

The as-built dimensions thus obtained differed negligibly from dimensions based on gore design patterns.

3.3 Stress-Band Mechanism

Figures 1 and 8 make it possible to locate the area on the balloon where a stress band might be expected. The circumferential envelope material between curves A and E, or between C and E, is termed "excess circumferential material", much or all of which will be contained in the undeployed pocket. Figure 8 shows quite clearly, and Figure 1 somewhat less so, that A and C approach E at a minimum in a region between balloon top and equator. This region provides a band of minimum excess circumferential material in relation to regions above and below.

In Figure 1, referring to the taper tangent gore design balloon used for Flight No. 1, curves B and D in their approach to E demonstrate more clearly than A and C the conditions for formation of a stress band. In Figure 8, based on the cylinder end gore design balloon used for Flight No. 3, the conditions are clearly seen for all four curves, A, B, C, and D.

The theoretical basis for stress-band analysis may be better understood if we assume the undeployed pocket is not present, and that excess material is distributed equally among the balloon gores so that a transverse radius of curvature exists at

each gore station. The stress band would still be present in an area where less excess material per gore was available than at stations above and below. The band would share the typical scalloped shape of the partially inflated gores, but the scallops would be shallower. Since the band could exist in this condition of equal deployment, shifting all of the gores circumferentially to accumulate the excess material into a pocket would increase the stress on the deployed gores. The stress band would change from a transverse scalloped shape to a flat band, squeezing the gas bubble, and with biaxial loading would occupy a balanced meridional width.

4. ANALYSIS OF PHOTOGRAPHS

4.1 Flight No. 1 (Figures 1 through 7)

Figure 1 indicates that at launch the stress band in this balloon should be located between the 16- and 20-ft gore stations. Figure 2 shows the band just above the bubble equator, approximately the position predicted by Figure 1. Figure 1 predicts that at burst the band will lie between the 24- and 28-ft gore stations. The geometric analysis performed on the balloon photograph of Figure 6 shows that the band is, indeed, in or slightly below this general area, and is about 10-ft wide.

In Figure 1, at burst altitude, curve D has crossed curve E indicating that there is no longer sufficient excess material to form a pocket to the depth of the balloon's vertical axis of symmetry. The pocket must be displaced outward; the necessary work involved adds to the transverse stress on the deployed material in the stress band. Figure 5 shows this outward displacement. As shown in Figure 2, the displacement began earlier in the flight than would have been predicted from Figure 1, presumably due to variations between actual conditions and the ideal assumptions made in Figure 1.

In Figure 5, depletion of excess material has pulled the inner margin of the pocket into a straight line in the region opposite the stress band, and the band itself is tending to pull the pocket outward and upward, with unknown biaxial forces. The excess material above the band is gathered into a typical rudder. Comparison of Figures 1 and 8 indicates the rudder should be smaller for Flight No. 1 at comparable stages for these balloons than for Flight No. 3, and comparison of photographs of the two flights confirms this prediction.

The sequence of flight photographs appeared to show the stress band moving downward by increasing in meridional width with increasing inflation. The band did become more evident on the photographs as ascent progressed; however, positive detection of movement was limited by the short range of photographic coverage and the lack of reference markers. The photographs clearly indicate that the transverse stresses represented by the band were more severe near the pocket corners (Figure 5). Some photographs showed the meridional width of the band to

increase at the pocket corners to as much as twice the width at other azimuth positions. At launch the pocket corners nearly touched, but during ascent the pocket corner gap and the transverse corner radii increased, indicating that the forces required to deploy the pocket were increasing (Figures 3 and 4).

Figure 6 shows the start of failure, in the stress-band region and near the pocket. Transverse loading is indicated by transverse displacement of gore seams. The orientation of the pocket upwind, and the displacement of the top balloon downwind, which started one minute before burst and persisted until burst, indicate that shear winds were blowing into the subpressure cavity and the pocket. The result would have been additional load on the stress band. Figure 7 shows the burst developing on both sides of the pocket.

4.2 Flight No. 3 (Figures 8 through 18)

Figure 8 indicates that at launch the stress band should be located between the 18- and 22-ft gore stations. The photograph in Figure 9 shows the band almost centered on the 20-ft gore station pennants, and approximately 4 ft wide. Figure 8 indicates that at burst the band should lie between the 22- and 28-ft gore stations, and Figures 13, 14, and 15 show that the band does lie between the 20- and 30-ft pennants. Curves D and E also cross in the burst altitude region, and the same conclusions may be drawn as for Flight No. 1. However, in Flight No. 3 the balloon was made of a different material, and was coated with cornstarch or polyethylene powder, with the result that the innermost part of the undeployed pocket is not visible on the flight photographs.

Down-cameras photographed Flight No. 3 from launch to separation of the tow balloon at 58,400 ft, 6600 ft below burst. The down-camera photographs show the stress band slowly widening from about 4 ft at launch to about 10 ft at 30,000 ft and above, as shown in Figures 12, 13, 14, and 15. As noted above, the band also moved downward by increasing in width during the ascent. This figure sequence again shows that the transverse stresses in the band area were intensified near the pocket corners, as they were on Flight No. 1.

Figures 10, 11, 12, and 15 show the changes in the pocket gap profile as the flight progressed.

Up-camera photographs taken immediately before burst show the effects of shear winds, which started two minutes before burst and persisted until burst, blowing into the cavity below the bubble, creating a sail. At burst, film material blew out, apparently from the bubble equator or above, and again within 90° azimuth from one side of the pocket (Figures 16, 17, and 18).

4.3 Model Tests (Figures 19 through 26)

It seemed possible to eliminate the deep unsymmetrical pocket of undeployed material by tailoring the gores to remove much of the excess material between the stress-band area and the top fitting. Such a design would tend to convert the stress band into a stress cap, which would grow from the top in meridional distance with inflation. The development of the stress cap should also move the upper end of the undeployed pocket or pockets outward.

This concept was tested with two balloon models made of 0.55-mil polyethylene with 6-ft-long gores: No. 1, a tapeless cylinder end balloon, and No. 2, a taped, fully tailored natural shape balloon. It was expected that model No. 1 would exhibit a stress band during inflation, and that No. 2 would not.

The balloons were measured before inflation, and comparable static inflation curves (Figures 19 and 24) were plotted, showing material required for a given size of bubble, excess material required for an undeployed pocket, and total material actually available on the basis of the balloon design. The figures helped to strengthen the prediction that the cylinder end design would develop a stress band, and that the fully tailored natural shape would not.

When the cylinder end shape balloon (No. 1) was inflated with helium, it did – in fact – develop a stress band in the area of minimum excess circumferential material (Figures 20, 21, 22, and 23). It was possible to increase the pocket corner gap (Figure 23) by manually restricting the material below the pocket and bubble from deploying, thus duplicating the effect observed in flight photographs (Figures 10, 11, 12, and 15). The taped fully tailored natural shape design balloon (No. 2) was inflated with helium, and failed to show development of a stress band at any stage of inflation (Figures 25 and 26). This balloon deployed uniformly out from the top fitting; the upper end of an undeployed pocket moved slowly outward and meridionally downward while the top of the balloon was being fully deployed.

5. CONCLUSIONS

The analysis of photographs and model test data described above has led to the following tentative conclusions:

1. Development of a circumferential stress band may contribute to balloon failure.

2. Deployment of excess material from an asymmetrical pocket may increase the transverse stresses loading in the stress band, starting at the point where sufficient material is no longer available to reach to the vertical axis of symmetry.

3. Analysis and model tests with a fully tailored natural shape balloon indicate that a stress cap rather than a stress band will develop during ascent. However, a deviation such as a cylinder or taper tangent end section produces a stress band.

4. The type of analysis carried out here allows good preflight prediction of the meridional position of the stress band, based on balloon design data.

5. Similar analysis will provide moderately accurate prediction of the altitude region in which the stress band will threaten the balloon's integrity.

Additional experiments and further analysis are required to confirm the present conclusions, and to specify remedial measures in detail.

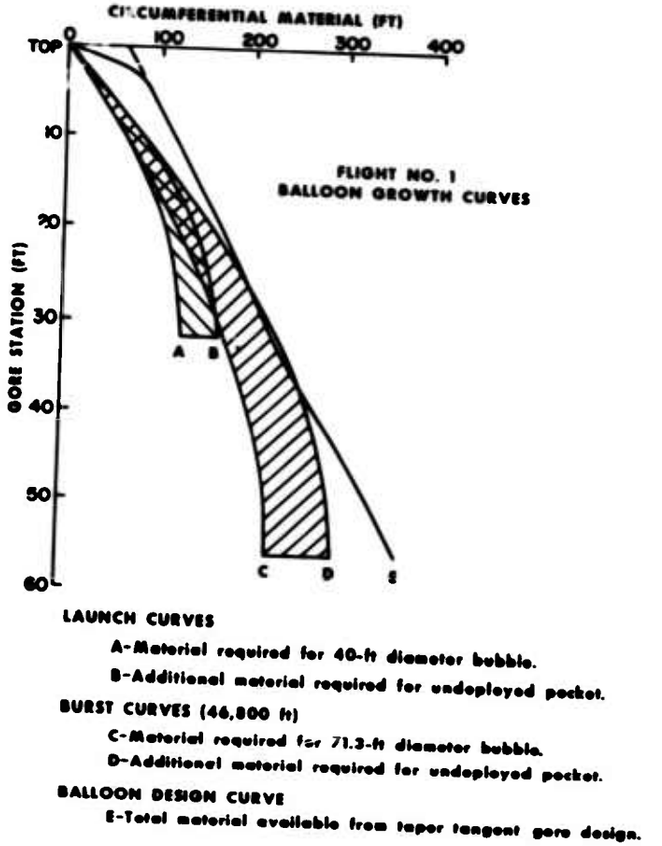

Figure 1. Balloon Growth Curves for Flight No. 1 Comparing the Material Required for Two Extremes of Inflation, Launch and Burst, Against the As-Built Dimensions. The gore station, where minimum excess circumferential material occurs, predicts the location of the circumferential stress band

Figure 2. Side View of Flight No. 1 Before Launch, Showing the Stress Band Slightly Above the Equator, the Depth Penetration of the Undeployed Pocket, and the Pocket Profile

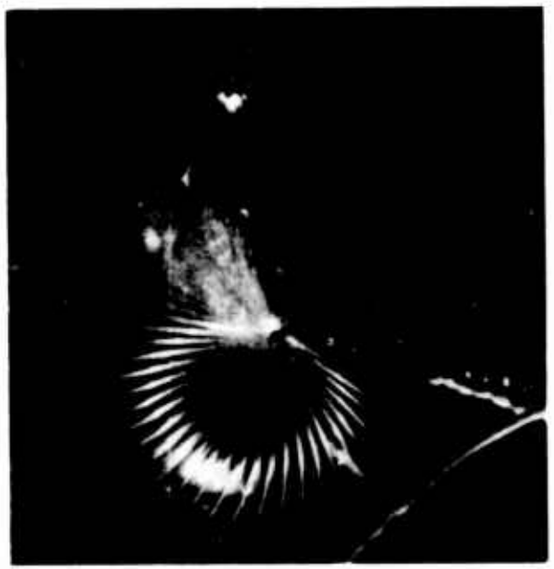

Figure 3. Top View of Flight No. 1 at 33,500 Ft, Showing the Separation of the Undeployed Pocket Corners

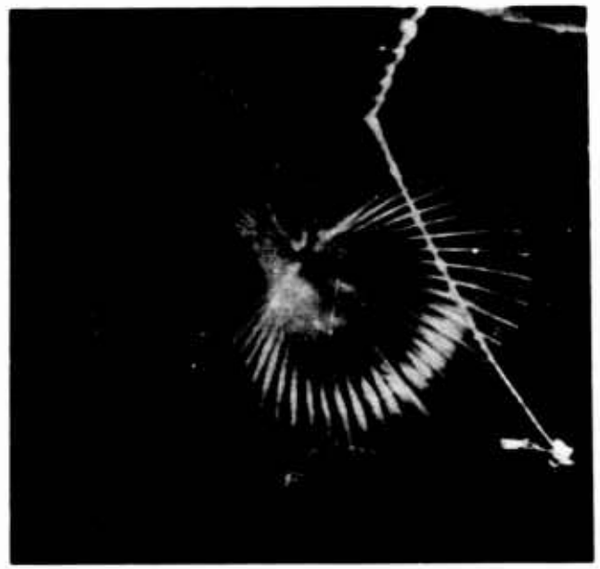

Figure 4. Top View of Flight No. 1 at 40,000 Ft, Showing the Increased Separation of the Undeployed Pocket Corners and Flattening of the Hemisphere Slightly Above the Equator

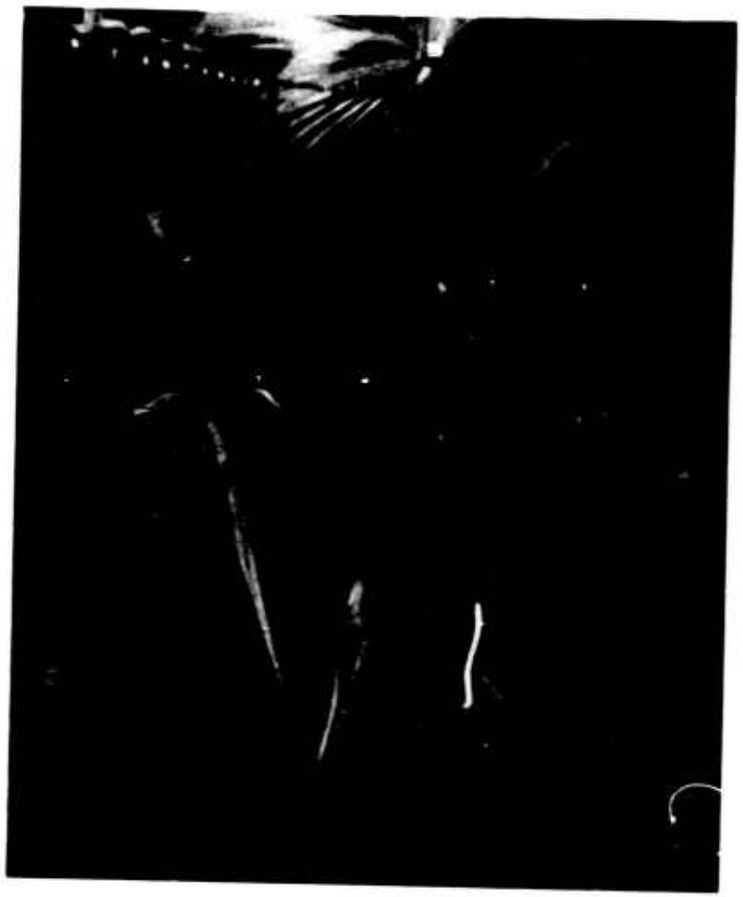

Figure 5. Side View of Flight No. 1 at 45,700 Ft, Showing the Pocket Depth, Pocket Profile, Stress Band, and the Severity of the Band on the Pocket Corners. (For comparison see Figure 2.)

Figure 6. Angle View of Flight No. 1 at 46,800 Ft, 2 to 3 sec Before Burst, Showing Failure Starting in the Circumferential Stress-Band Region While Load Tapes and/or Seams Are Being Displaced Circumferentially by Transverse Loading. Horizontal winds appear to be blowing in the subpressure cavity since it is oriented upwind and the tow balloon is displaced downward.

Figure 7. Angle View of Flight No. 1 at 46,800 Ft, Showing Burst Occurring on Both Sides of the Undeployed Pocket

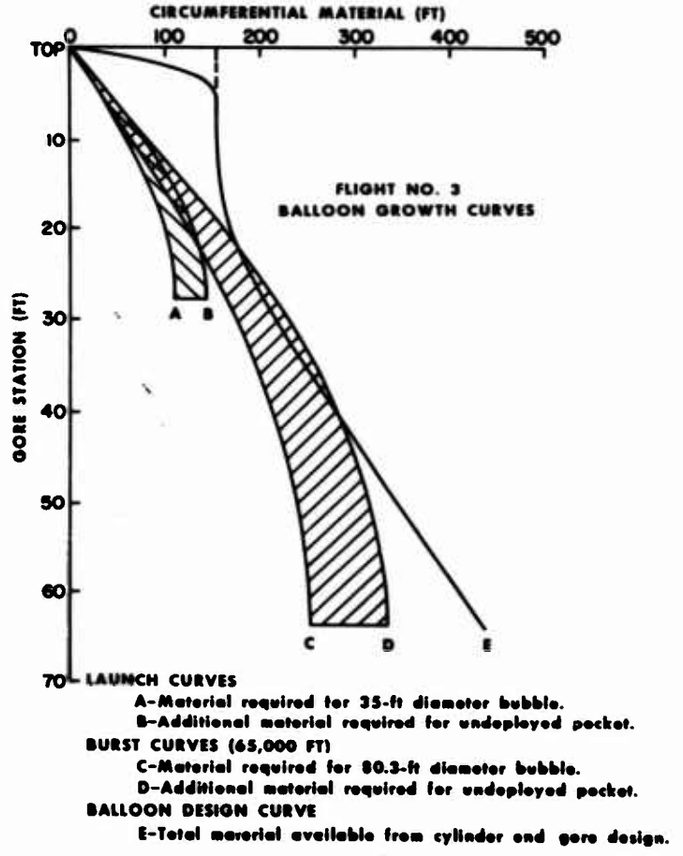

Figure 8. Balloon Growth Curves for Flight No. 3, Comparing the Material Required for Two Extremes of Inflation, Launch and Burst, Against the As-Built Dimensions. The gore station, where minimum excess circumferential material occurs, predicts the the location of the circumferential stress band

Figure 9. Side View of Flight No. 3 Before Launch, Showing the Circumferential Stress Band Centered on the 20-Ft Gore Station Pennants and Approximately 4 Ft Wide

Figure 10. Top View of Flight No. 3 at 7,700 Ft, Showing the First Detectable Separation of the Undeployed Pocket Corners

Figure 11. Top View of Flight No. 3 at 24,000 Ft, Showing an Increased Separation of the Undeployed Pocket Corners and a Circumferential Flattening of the Top Hemisphere

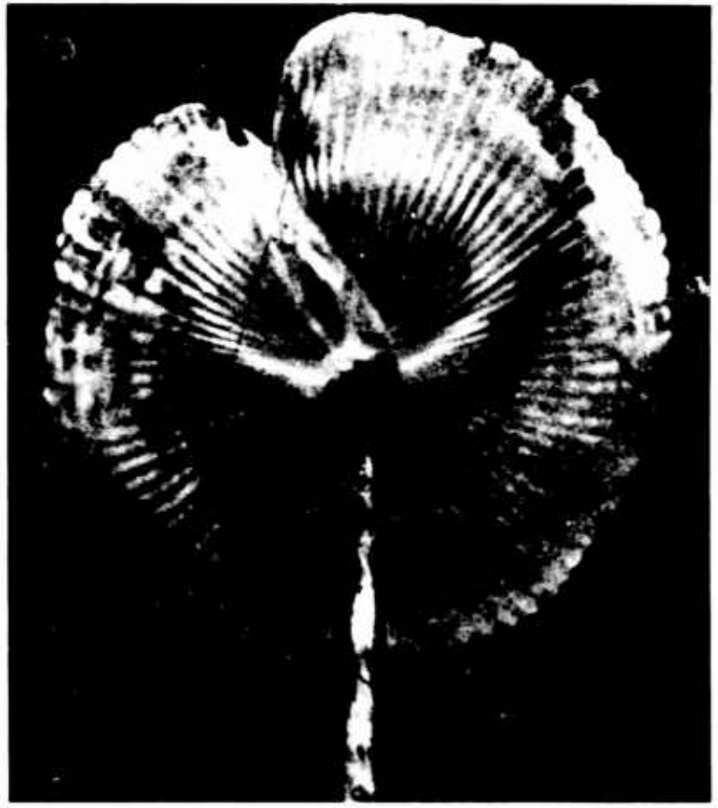

Figure 12. Top View of Flight No. 3 at 31,000 Ft, Showing a Continuously Increasing Separation of the Undeployed Pocket Corners and a More Pronounced Circumferential Flattening of the Top Hemisphere on the 20-Ft Gore Station Pennants

Figure 13. Angle View of Flight No. 3 at 52,400 Ft, Showing the Circumferential Stress Band Spread Between the 20- and 32-Ft Pennants and the Severe Flattening Near the Pocket Corners

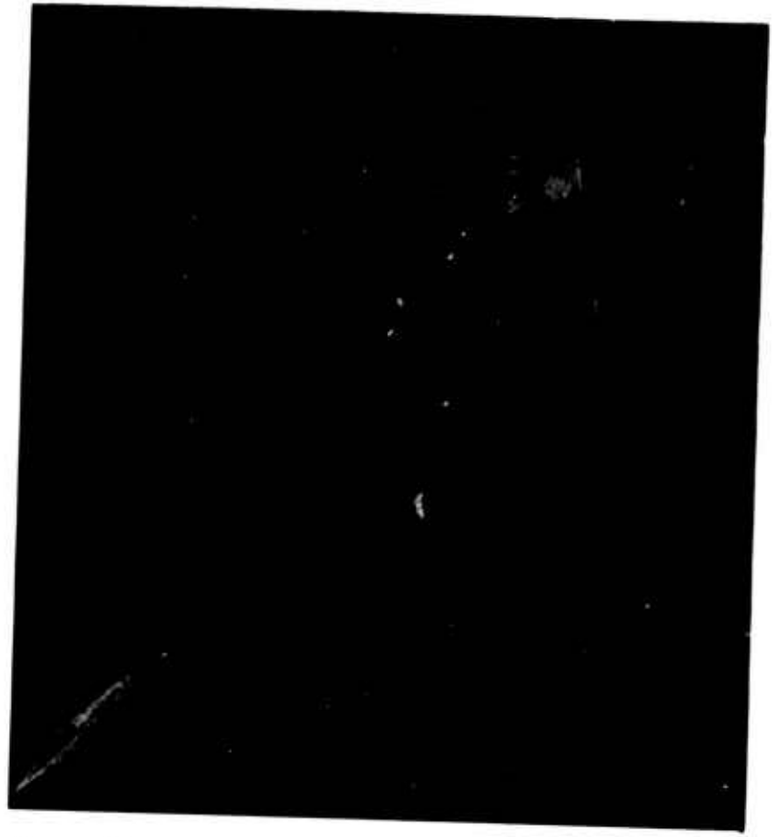

Figure 14. Side View of Flight No. 3 at 54,600 Ft, Showing a Very Pronounced Circumferential Stress Band on the Left-Hand Side of the Envelope and a Very Narrow Sub-Pressure Cavity Compared to Figure 16

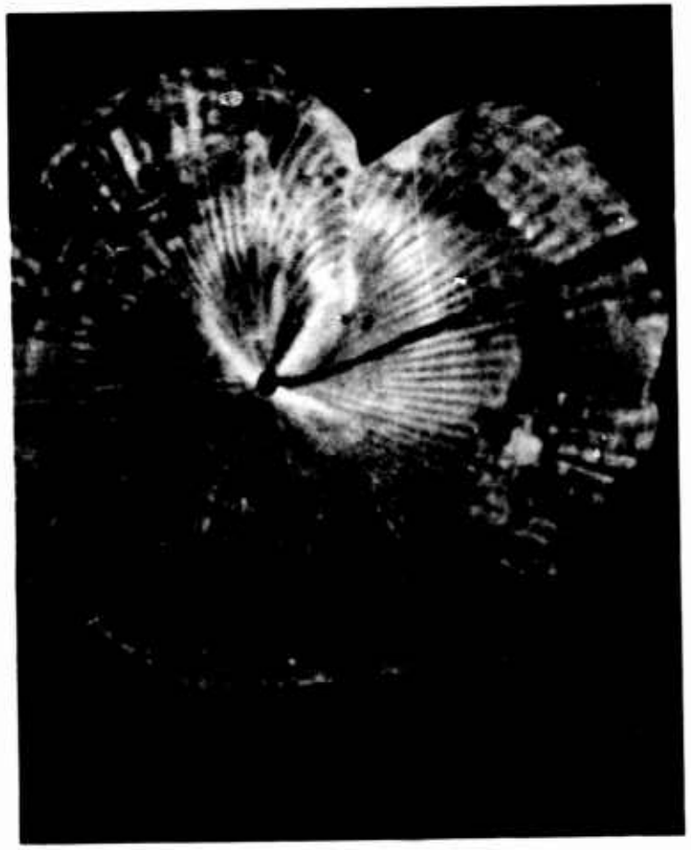

Figure 15. Top View of Flight No. 3 at 57,250 Ft, Clearly Showing the Effects of the Increasing Forces of Deployment on the Undeployed Pocket Corners and Circumferential Stress Band

Figure 16. Up-Camera View of Flight No. 3 at 65,000 Ft, 5 Sec Before Burst, Showing Sailing of the Sub-Pressure Cavity Material From Horizontal Winds. Sailing commenced approximately 2 min before burst

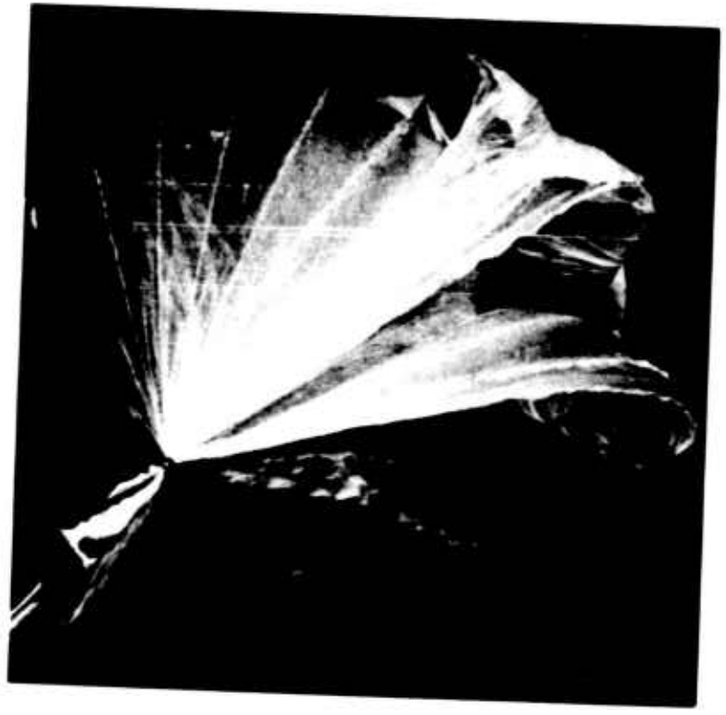

Figure 17. Up-Camera View of Flight No. 3 at 65,000 Ft, 2 to 3 Sec Before Burst, Showing the Back Side of the Subpressure Cavity During Sailing

Figure 18. Up-Camera View of Flight No. 3 at 65,000 Ft, Showing Burst and Polyethylene Blowing Out From the Top Hemisphere Within 90° Azimuth of the Undeployed Pocket on the Right-Hand Side

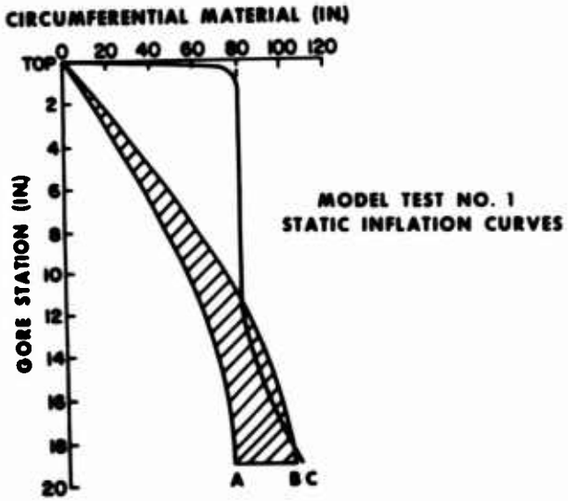

A–Material required for 24-in. diameter bubble.

B–Additional material required for undeployed pocket.

C–Total material available from cylinder and gore design.

Figure 19. Static Inflation Curves for Model Test No. 1, Which Predict a Band Centered on Approximately the 14-In. Gore Station

Figure 20. Front View of Model Test No. 1, Showing the Circumferential Band

Figure 21. Side View of Model Test No. 1, Showing the Circumferential Band Approximately Centered on the 14-In. Gore Station

Figure 22. Rear View of Model Test No. 1, Showing the Circumferential Band

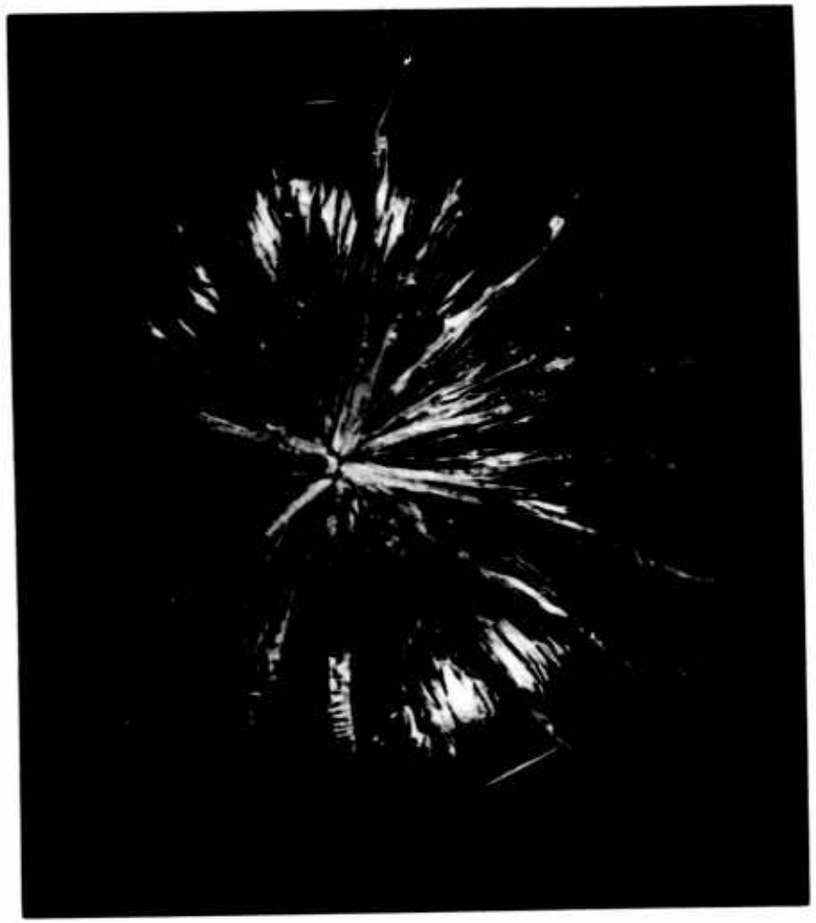

Figure 23. Top View of Model Test No. 1, Showing the Circumferential Band Continuously Around the Envelope

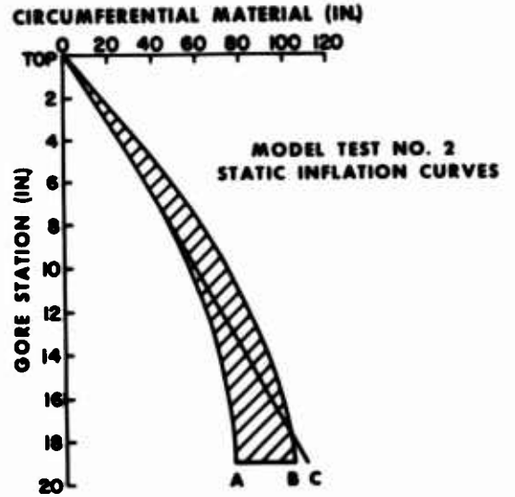

A–Material required for 24-in. diameter bubble.

B–Additional material required for undeployed pocket.

C–Total material available from taped fully tailored natural shape balloon.

Figure 24. Static Inflation Curves for Model Test No. 2, Which Predict No Circumferential Band

Figure 25. Side View of Model Test No. 2, Showing That No Circumferential Band Exists

Figure 26. Top View of Model Test No. 2, Showing That No Circumferential Band Exists

IX. Detonable Gas Explosion: A Unique Application

M.J. Balcerzak
General American Research Division
General American Transportation Corporation
Niles, Illinois

Abstract

Detonable gas explosion is a blast and shock simulation technique utilizing the spherical detonation of a combustible gas mixture initially contained in a balloon to generate shock waves. These resultant shock waves are similar in nature to those produced by conventional high explosives or nuclear explosions. The largest detonable gas explosion produced to date has been the equivalent of 20 tons of TNT. This explosion required a 125-ft diam hemisphere filled with a detonable propane-oxygen gas mixture. Studies are currently under way to use the detonable gas explosion technique as a high-altitude blast generation system. Consideration is also being given to extending the yield of the hemispherical detonable gas explosion to the 500-ton TNT equivalent range. This would require a hemisphere on the order of 365 ft in diam.

1. INTRODUCTION

The Defense Atomic Support Agency is charged by the Department of Defense to maintain a state of test readiness in the event of the abrogation of the Nuclear Test Ban Treaty. In the interim, DASA is developing test techniques by which the various

environments generated by a nuclear detonation (such as nuclear radiation, thermal radiation, blast, and shock, and so forth) may be simulated.

This Chapter briefly describes the results of a program conducted by the General American Transportation Corporation to develop a blast and shock simulation technique using the spherical detonation of a combustible gas mixture initially contained in a balloon to generate shock waves.

To date over 20 tests have been performed with spherical balloons 3 to 110 ft in diam and with hemispheres 17 to 125 ft in diam. Explosions with the equivalence of 20 tons of TNT have been simulated.

By equivalence of a TNT explosion it is meant that, over a particular overpressure range, the pressure signature (pressure-time-distance relations) generated by the detonable gas explosion is the same as the pressure signature produced by the equivalent TNT charge.

The gases used during this program have been various mixtures of methane and oxygen or mixtures of propane and oxygen. The former gases are used to produce explosions above ground level since detonable methane-oxygen gas mixtures are buoyant, while the latter gases can only be used for explosions at ground level.

It is appropriate at this time to mention some of the differences between the balloon requirements for the detonable gas explosion and those for high-altitude lift balloon experiments. During the initial balloon layout and deployment the detonable gas explosion experiments require that the balloon be taken out of its shipping container and laid out in a flat disc shape to facilitate attaching the balloon to the gas inflation tube and to the tether lines. Since the balloon is to be completely filled at ground level, experience has clearly demonstrated that the folding and packing methods used for high-altitude lift balloons (where reefed conditions are required since the balloons are only partially inflated at sea level) are impractical and require prohibitive amounts of labor and handling. For balloons with diameters in excess of 100 ft, normal balloon manufacturing techniques must be modified to incorporate the required balloon folding into the manufacturing process. This eliminates the need for any further refolding when the balloon is received in the field.

Another difference between the two balloon usages is that large volumes of gas are injected into the detonable gas balloons at sea level. For example, 660,000 SCF are injected into a 110-ft-diam spherical balloon. This is in comparison to the 80,000 SCF of helium placed in NASA's 410-ft-diam Voyager balloon. Because of the relatively low gas delivery rates available in present day mobile oxygen equipment, filling times on the order of several hours are required to inject the detonable gases into the balloons. A further complication to the detonable gas experiment is that the fuel gases (that is, propane or methane) must be controlled and injected into the balloon remotely. For the detonable gas explosion experiments the control stations were located so that the shock wave overpressure at any manned control station would be less than 1/2 psi in the event of an accidental explosion.

A third variation is that superpressure balloons are used instead of zero pressure balloons for the detonable gas explosions. If zero-pressure balloons are used they would have to be able to withstand variations in wind environments that develop during the balloon-filling phase. Past experience indicates that zero-pressure balloons are quite vulnerable in winds over 5 mph. Therefore in order to produce a taut balloon in as short a time as possible capable of withstanding winds on the order of 15 mph throughout the filling operation superpressure balloons were used for the 20-ton detonable gas explosions. The use of superpressure ballons was made possible by the incorporation of a ballonet in the balloon. The ballonet is an impermeable membrane which compartmentizes the balloon into two sections, each of which can be filled and emptied independently. The mode of operation is as follows: one side of the balloon is filled very rapidly with air to a superpressure of an inch or less of water; then the detonable gas mixture is injected into the other side of the balloon (first the oxygen and then the fuel gas) at the same flow rate as air is ejected from the air side of the balloon. Thus the balloon remains taut throughout the gas filling operation.

The magnitude of the superpressure in the balloon is determined by the maximum wind loads than the balloon is designed to withstand without deforming. For example a superpressure of less than 1/2 inch of water is required to keep the balloon surface taut in a 30 mph wind.

2. HISTORY OF THE DETONABLE GAS EXPLOSION

During the spring of 1965, spherical balloons with diameters of 3, 5, 10, and 13.5 ft in diam were filled with methane-oxygen gas mixtures and test fired. The 3- and 5-ft diam spherical balloons were made of rubber and are the types used for meteorological soundings. The 10- and 13.5-ft diam spherical balloons were made of clear Mylar film reinforced with a bonded Dacron scrim material. The primary objective of the tests with the 3- and 5-ft diam balloons (see Figure 1) was to determine the detonation limits of methane-oxygen gas mixtures. Whether a particular fuel-oxygen gas mixture detonates or deflagrates can only be determined experimentally. This was done by systematically varying the methane-oxygen mixture ratio and visually observing the reaction. (There is a marked distinction between deflagration and detonation waves. A deflagration wave is a wave propagated by the process of heat transfer and diffusion, whereas a detonation wave is a shock wave which is sustained by the energy of the chemical reaction initiated by the temperature and pressure of the wave. The sensible differences between detonation and deflagration processes are that detonation produces a very bright flash and sharp report whereas deflagration produces an orange tumbling flame and a muffled rumbling sound.)

Figure 1. Five-ft Diameter Balloon During Fill

The tests with the 10- and 13.5-ft-diam balloons (see Figure 2) were performed to verify two major aspects of the detonation phenomenon. The first is the determination of the properties of the gaseous detonation wave. The second is the interaction or coupling phenomenon which occurs when the detonation wave strikes the balloon surface and the air surrounding the balloon, and generates a shock wave.

Analytically, the properties of the detonation wave and the gas behind the detonation front may be determined using an approximate analysis of a one-dimensional plane detonation wave according to S. Penner (1957). From the analysis expressions are obtained for the detonation wave front velocity, the pressure and the particle or flow velocity behind the detonation front, and the energy released by the reaction.

Although this analysis is for a one-dimensional detonation wave, the results may be applied to a spherical or a three-dimensional detonation wave. G.I. Taylor (1950) and Zeldovitch (1942) showed that the hydrodynamic theory makes it possible to consider the existence of spherical detonation waves having the same properties as plane waves. The only difference would be in the pressure and velocity gradients of the gases directly behind the wave.

Experimental verification of the Taylor-Zeldovitch theory is given by Laffitte (1923) and Manson and Ferrie (1953). The latter detonated balloons up to 60 cm (23.6 in.) in diameter.

Figure 2a. Ten-ft Diameter Balloon During Methane Fill

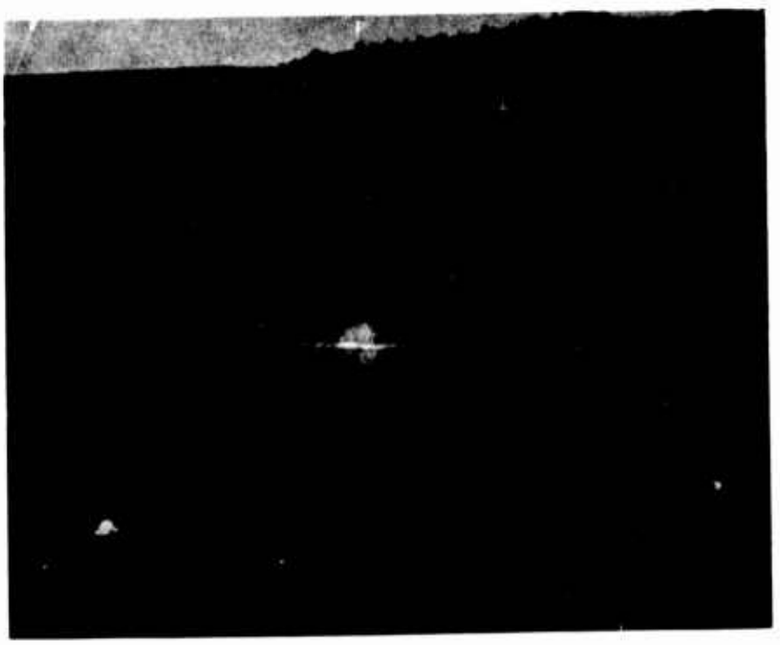

Figure 2b. Detonation of Ten-ft Balloon

At the General American Research Division, a considerable amount of work has been performed in determining the properties of detonation waves using hydrocarbons, such as methane and propane, with oxygen and air. Analytical results for the detonation front velocity and the resultant detonation pressure (see Figures 3 and 4) are presented for various initial oxygen to methane and oxygen to propane mixture ratios. These curves show how the detonation properties are affected by the initial gas mixture mole ratio. The curves also show the mixture mole ratio at which the detonation pressure is maximized.

The one detonation parameter that can be measured directly is the time-averaged detonation wave front velocity. By attaching time-of-arrival circuits (break wires) to the balloon surface, the time interval from detonation ignition until the detonation wave strikes the balloon surface can accurately be determined. Although a small time increment required for the detonation wave to reach steady state conditions after ignition is neglected in this averaging process, the accuracy has been judged to be sufficient for correlation purposes. The agreement between the analytically predicted and the experimentally observed detonation wave front velocity has been found to be quite good (see Figures 3 and 4). This then gives added confidence to the other parameters such as pressure, temperature, particle velocity, and so forth, that were also calculated.

The air blast predictions are more difficult to obtain. Although GARD has computer codes which predict pressure time-distance data for a given detonable gas explosion, heavy reliance is placed on the typical predicted data furnished by the Ballistic Research Laboratories see Keefer (1966), for example for establishing TNT equivalence for the detonable gas explosions. Pressure transducers are placed at various ranges from ground zero along a blast line to obtain pressure-time-distance data for the shock wave generated by the detonable gas explosions. This data is then compared against predicted pressure-time-distance data for TNT to establish TNT equivalence.

Two detonable gas explosions were planned for the month of October 1965 with the principle objective of accurately determining the TNT equivalence of the detonable gas explosions versus balloon diameter. A 32-ft and a 40-ft diam balloon were scheduled to be detonated at the Suffield Experimental Station in western Canada. The tests were to take place at a site and at a height-of-burst at which a previous 1000-lb TNT explosion had occurred. The 32- and 40-ft diam balloons were made of a material consisting of Dacron scrim laminated between two layers of metallized Mylar film. Metallized balloons were used to eliminate any possible buildup of static electricity. Electrical continuity between the inner and outer balloon surfaces was provided by a metal ring assembly in the south polar cap where the gore sections joined. This ring was connected to an earth ground to dissipate any accumulated static charge. The 32-ft balloon filled with methane oxygen was successfully

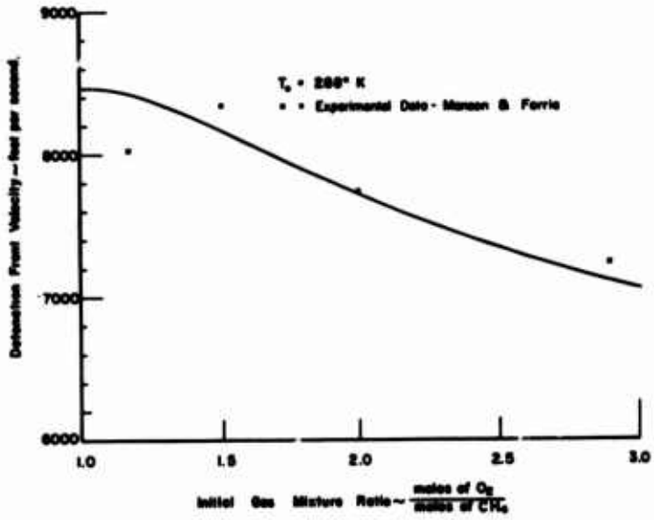

Figure 3a. Detonation Front Velocity vs Initial Gas Mixture Ratio for Oxygen and Methane Mixtures

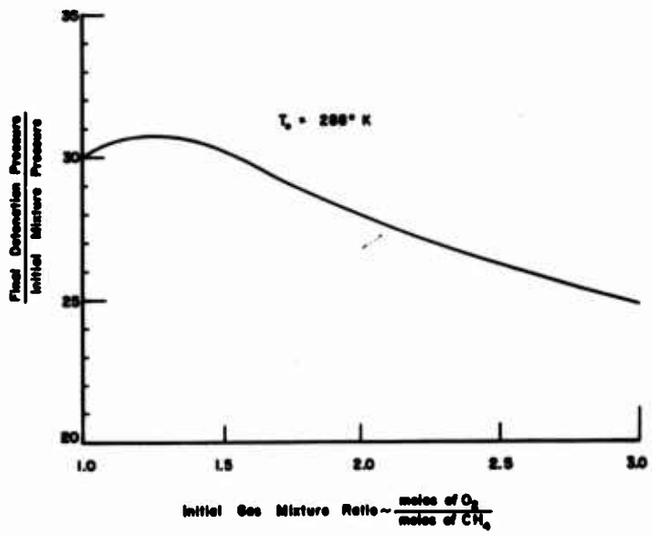

Figure 3b. Detonation Pressure vs Initial Gas Mixture Ratio for Oxygen and Methane Mixtures

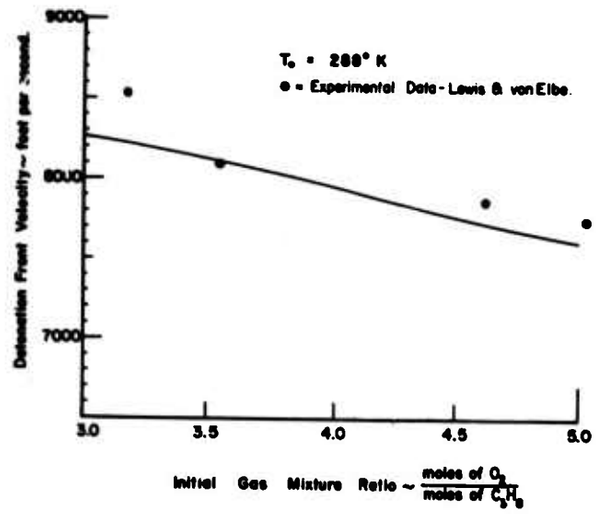

Figure 4a. Detonation Front Velocity vs Initial Gas Mixture Ratio for Oxygen and Propane Mixtures

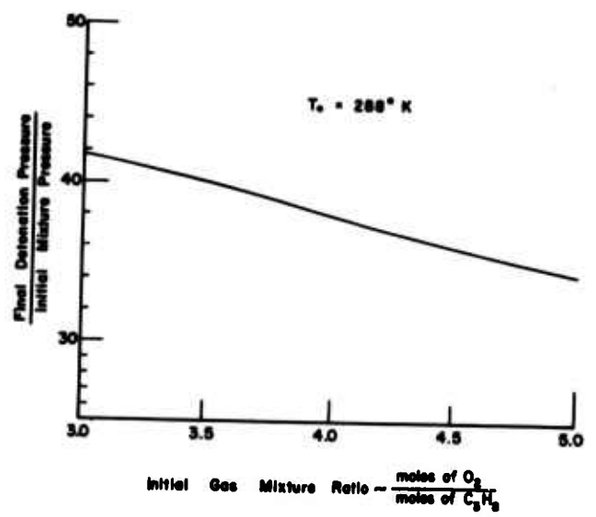

Figure 4b. Final Detonation Pressure Ratio vs Initial Gas Mixture Ratio for Oxygen and Propane Mixtures

detonated (see Figures 5 and 6). Comparison of the detonable gas data with the TNT data indicated that the 32-ft detonable gas explosion was the equivalent of 1000 lb of TNT (see Figure 7).

The test with the 40-ft diam balloon was aborted due to a fatigue failure of the balloon inflation tube.

The results of this test series clearly indicated that balloon handling techniques must assume a more important role in fielding the detonable gas explosion technique.

Up to this point in time, only detonable gas mixtures of methane and oxygen were used. However, with the successful test firing of the 32-ft diam balloon, plans were drawn to test hemispheres filled with propane-oxygen detonable gas mixtures. Because propane is a heavier gas than methane, less volume is required for a given yield explosion. Also, propane is available in bulk liquid which reduces the logistic problem of transporting the fuel gas to the test site. The disadvantage of propane mixtures is that it is nonbuoyant and as such can only be used for ground-level detonable gas explosions.

In the spring of 1966, six 17-ft diam hemispheres (see Figure 8) filled with propane-oxygen detonable gas mixtures were test fired at the GARD Ballistic Test Station located near Colorado Springs, Colorado. The hemisphere material was Dacron scrim laminated between two layers of clear Mylar film. The hemispheres

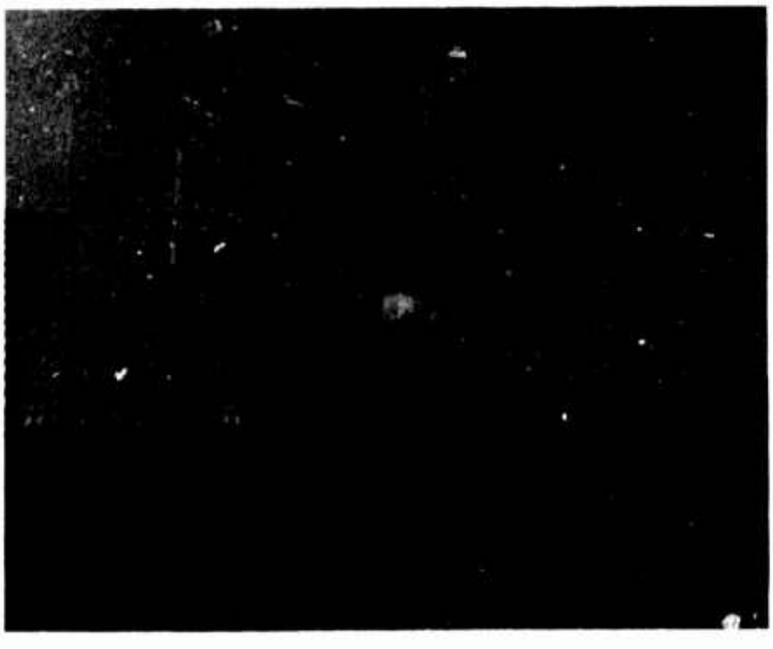

Figure 5. Thirty-two-ft Diameter Balloon After Methane Gas Loading

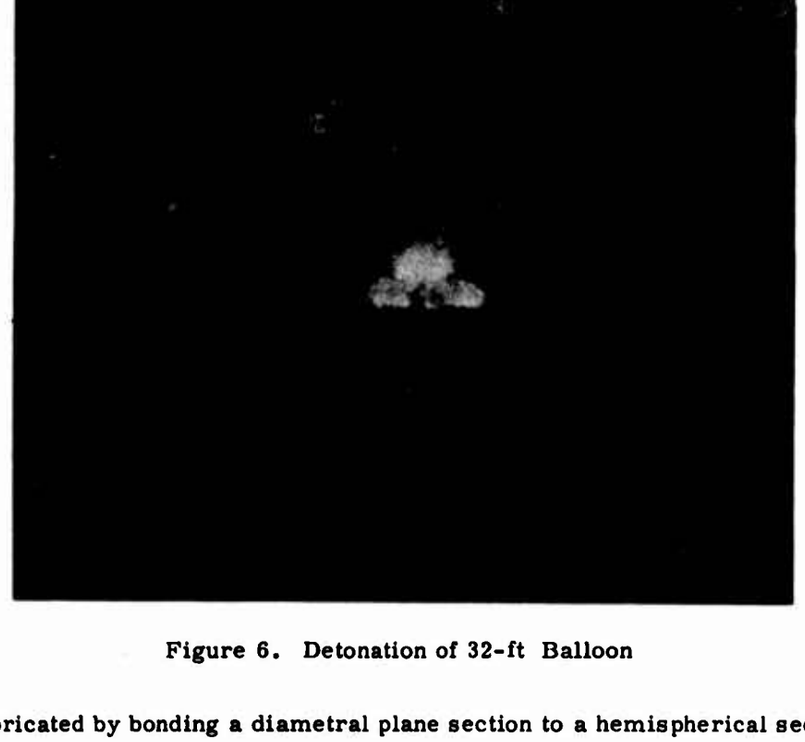

Figure 6. Detonation of 32-ft Balloon

were fabricated by bonding a diametral plane section to a hemispherical section. This made the hemispheres completely gas tight. The objectives of the tests were to determine detonability limits for propane-oxygen mixtures and establish the their TNT equivalence. All the objectives were realized.

It was determined from these preliminary spherical and hemispherical tests that the TNT equivalence of the methane-oxygen and propane-oxygen detonable gas explosion could be satisfactorily scaled with the familiar explosives cube-root scaling law. That is:

$$W = P\left(\frac{R}{R_o}\right)^3$$

where

- W = equivalent TNT charge weight, lb
- P = barometric pressures at test site, atmospheres
- R = actual balloon radius, ft
- R_o = balloon radius for 1 lb TNT equivalent (see Table 1)

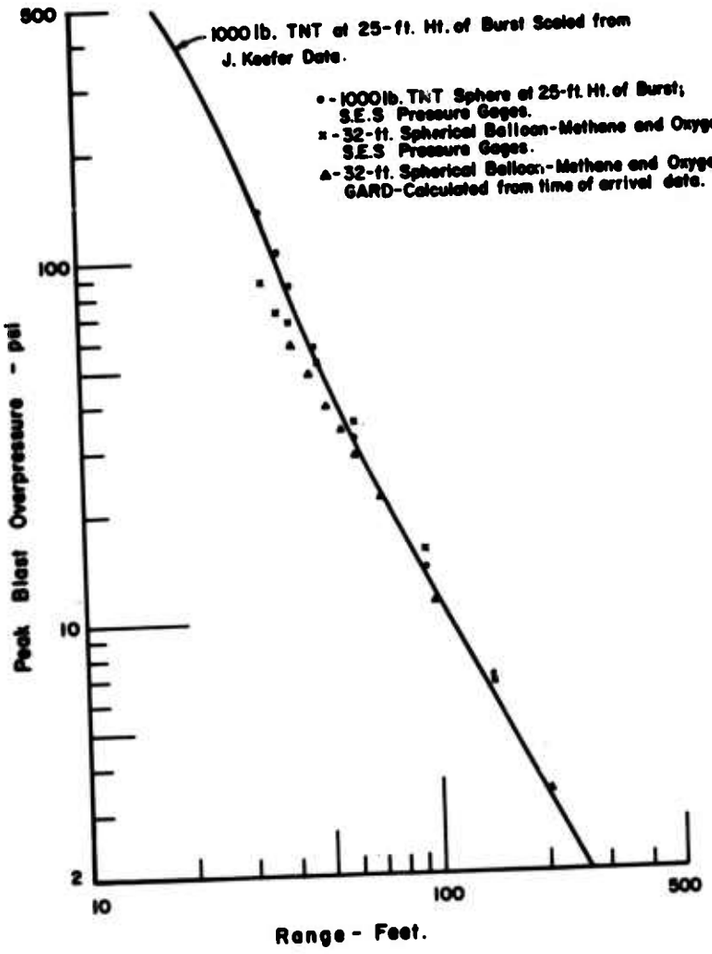

Figure 7. Test Data – Peak Blast Overpressure vs Range. 32-ft diam spherical balloon, 25-ft height-of-burst, methane-oxygen (O_2/CH_4 = 1.5 by volume). Test conducted at Suffield Station, Ralston, Alberta Canada, 19 October 1965

Table 1. Balloon Dimensions for 1 Lb of TNT Equivalent Based on Test Data (Gas Mixture at Standard Temperature and Pressure)

Fuel	Oxygen Fuel Ratio	Hemisphere Radius (Feet)	Spherical Radius (Feet)
C_3H_8	3.5	1.79	1.42
CH_4	1.5	1.99	1.58

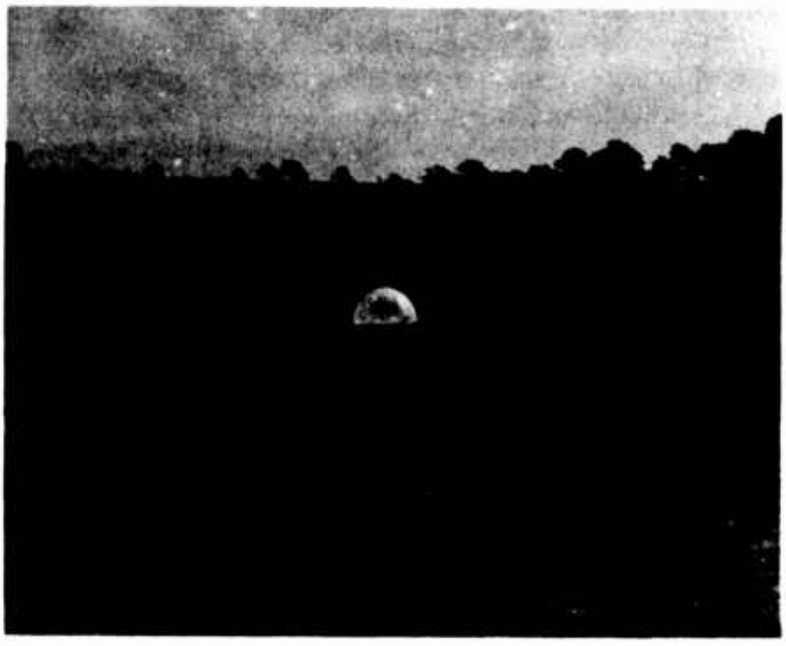

Figure 8a. Seventeen-ft Diameter Hemisphere After Propane Gas Loading

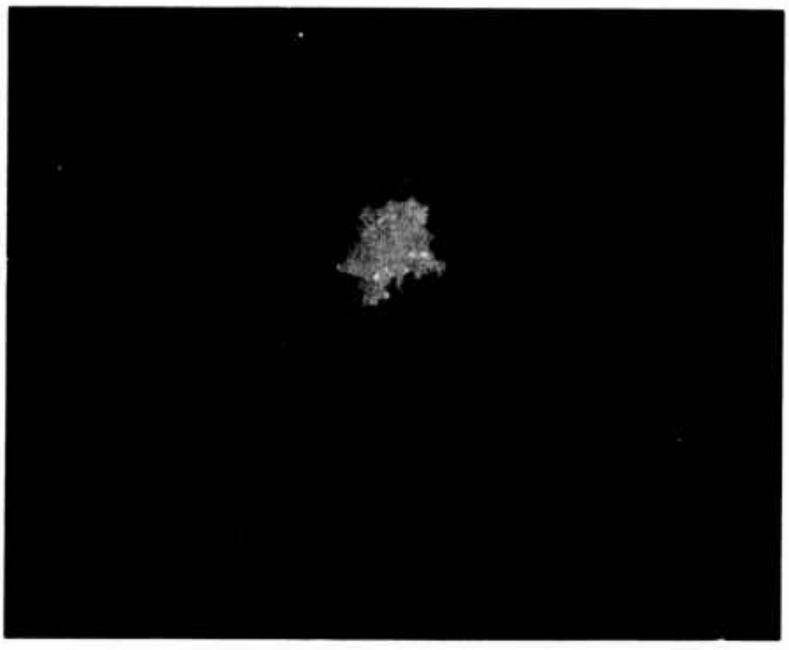

Figure 8b. Detonation of 17-ft Hemisphere

The most recent detonable gas explosion test series was conducted during July 1966 at the Suffield Experimental Station in Canada on Operation DISTANT PLAIN. The test series was to include the explosion of a 110-ft diam sphere tethered with a balloon center at an 85-ft height-of-burst and filled with a methane-oxygen detonable gas mixture, and the explosion of a 125-ft diam hemisphere restrained at ground level and filled with a propane-oxygen detonable gas mixture. Figures 9 through 13 are typical photographs of the operation.

The 110-ft diam sphere was made of clear Mylar laminated between two layers of Dacron scrim. The ballonet is made of clear Mylar reinforced with only one layer of Dacron scrim.

The 125-ft diam hemisphere, ballonet and horizontal diametral plane were all made of clear Mylar bonded to only one layer of Dacron scrim.

To insure electrical conductivity of all important surfaces (that is, the outside balloon surface and inside surfaces surrounding the detonable gas mixture) an aqueous solution of calcium chloride was applied. The Dacron scrim material readily absorbs this solution. Since $CaCl_2$ is hygroscopic, any moisture in the atmosphere surrounding these coated surfaces tends to collect on these surfaces and make them electrical conductive.

Figure 9. Air Inflation of 110-ft Diameter Spherical Balloon

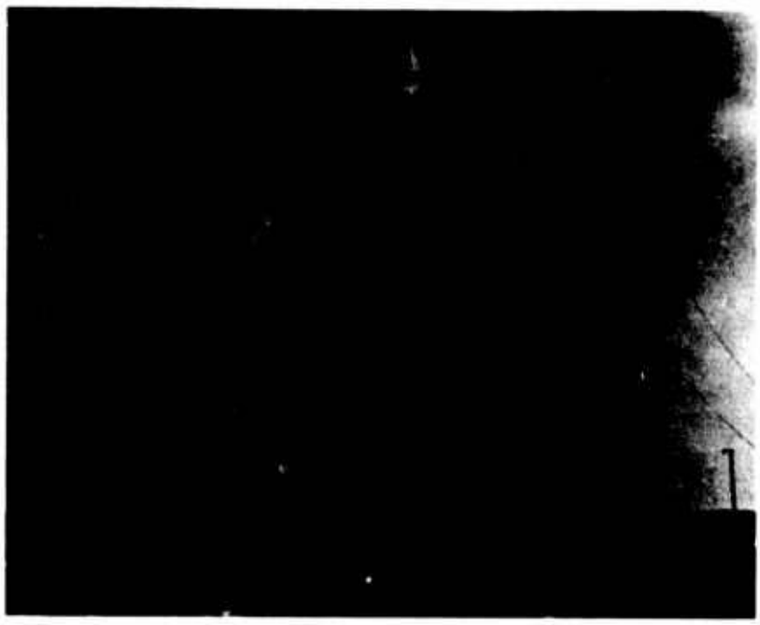

Figure 10. One hundred and ten-ft Balloon Inflated and Shown Position of Ballonet After Approximately 60 Percent of Oxygen Fill

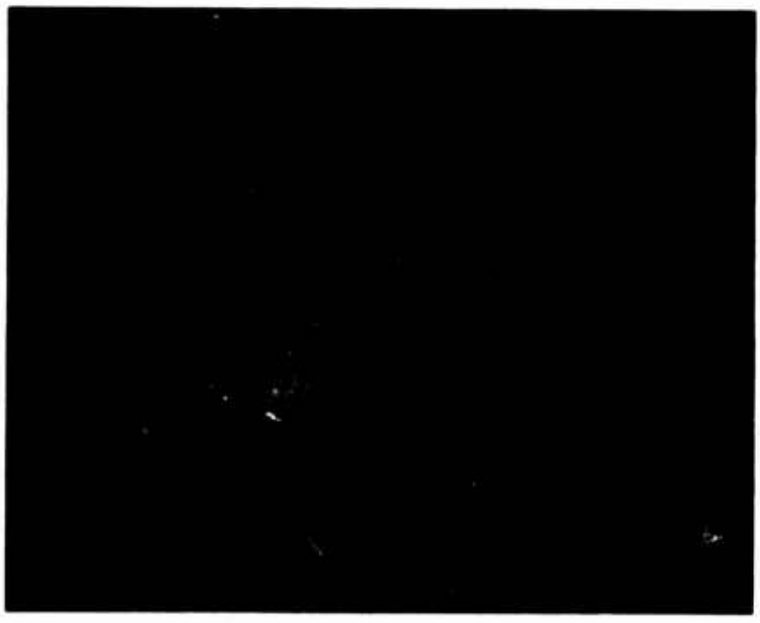

Figure 11. One hundred and twenty-five-ft Diameter Hemisphere During Oxygen Fill and Showing Position Taken by Ballonet

Figure 12. Fully Inflated Hemisphere as Seen From Observation Point Just Before Detonation

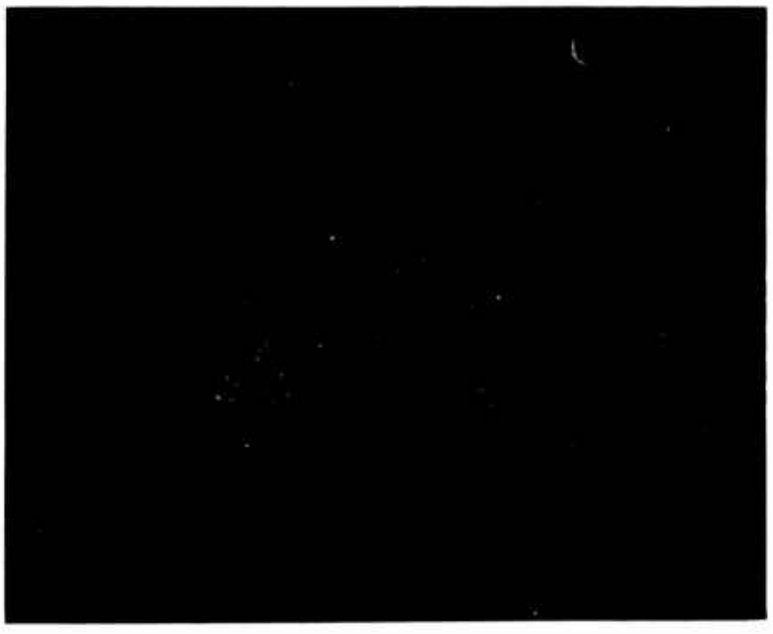

Figure 13. Detonation of 125-ft Hemisphere

The test with the 110-ft diam sphere was prematurely terminated by the failure of the balloon. The failure has since been traced to a design inadequacy at the north polar cap. This can be overcome by a design revision for any future detonable gas explosion.

The detonable gas explosion of the 125-ft diam hemisphere filled with propane-oxygen was completely successful. Preliminary examination of the data has indicated that the detonable gas explosion was the equivalent of a 20-ton hemispherical TNT charge.

3. ADVANTAGES AND DISADVANTAGES OF DETONABLE GAS EXPLOSION

The detonable gas explosion technique offers a number of advantages over conventional high explosives in simulating a blast and shock environment.

a. A well defined shock wave is generated whose properties can be predicted with a high degree of confidence.

b. Little, if any, ejecta is produced by the detonable gas explosion. This provides an ideal test environment when air blast and air-induced ground shock effects are to be investigated.

c. The cost of detonable gas mixtures is low. These cost savings have tended to be negated by the balloon costs during the development of this technique. However, it is anticipated the balloon costs will be proportionally reduced if used with larger scale tests.

d. Air bursts are easier to study with the detonable gas explosion technique than with TNT. Since buoyant detonable gas mixtures can be used, the balloon can be either tethered or free flown to the desired height-of-burst. This, of course, eliminates the need for a supporting tower which produces much undesirable ejecta and causes some shock wave anomalies.

e. The detonable gas explosion technique provides safe working conditions when preparing objects to be tested. The test site can be prepared without the work being done in presence of large charges of high explosives. Only the injection of the fuel gas into the balloon envelope need be done from a remote station after the test site is evacuated.

There are several disadvantages associated with the detonable gas explosion technique.

a. Large balloons are required to simulate high yield explosion. The balloon manufacturers are developing a broader understanding of the unique problems and requirements associated with the detonable gas explosions and they have suggested balloon manufacturing techniques which would facilitate large balloon handling and deployment.

b. Pressure ranges over 500 psi cannot be simulated.

c. When using presently available equipment, the detonable gas filling times could become quite long for high yield explosions. However, gas suppliers are already at work to provide equipment capable of delivering gas at the rate of 300,000 cu ft/hr.

4. FUTURE PROSPECTS FOR THE DETONABLE GAS EXPLOSION

Study programs are currently being sponsored by the Advanced Research Projects Agency and DASA to determine the feasibility of generating reasonable yield detonable gas explosions at high altitudes. The goals of the program are to produce explosions of the order of 10 tons of TNT equivalent at altitudes ranging from sea level to 100,000 ft or wherever detonation ceases.

High yield detonable gas explosions are also being considered. Although only in the preliminary planning stages, 100 to 500-tons TNT equivalent detonable gas explosions now appear feasible. Hemispheres required for 100 and 500 tons TNT equivalent explosion would have to be 215 and 365 ft, respectively, in diameter. Much of the technical experience and background possessed by persons and agencies in the balloon field must be called upon to accomplish explosions of this order.

5. CONCLUSIONS

The detonable gas explosion technique has been demonstrated to be an effective blast and shock simulation test technique. It now joins the arsenal of test techniques available to the experimenter as another means of generating shock waves on a large scale. One need only use his imagination to envision possible experiments for which the detonable gas explosion technique is ideally suited. Height-of-burst explosive tests, full-scale structural response test, warhead vulnerability tests, to mention just a few, can readily be done, and done economically, with this technique.

Acknowledgments

The author wishes to acknowledge the support of the Defense Atomic Support Agency, Washington, D.C., under whose contracts Nos. DA-49-146-XZ-400 and DA-49-146-XZ-422 the work reported herein was performed. The author would also like to express his appreciation to Mr. J. Kelso and Major J. Choromokos of DASA and Mr. M.R. Johnson and Messrs. F. Kurz and S. Lucole of General American Research Division and all the personnel at the Suffield Experimental Station, Ralston, Alberta, Canada, without whose efforts this program would not have been possible.

References

Keefer, J.H. (1966) Air Blast Predictions for Operation DISTANT PLAIN, Ballistics Research Laboratories, Tech. Note 1612.

Laffitte, P. (1923) C. R. Acad. Sc., Paris, 177, 178; Ann. de Phys., 10e ser.

Manson, N. and Ferrie, F. (1953) Fourth Symp. (Int) on Comb., Baltimore, Williams & Wilkins Co., pp. 486-494.

Penner, S. (1957) Chemistry Problems in Jet Propulsion, Pergamon Press, New York.

Taylor, G.I. (1950) Proc. Roy. Soc. (London) A200: 235.

Zeldovitch, J.B. (1942) J. Phys. Exp. et Theor., URSS 112:389.

X. A New Pressure Sensor for High-Altitude Balloons

Dr. Walter C. Wagner
Air Force Cambridge Research Laboratories
Bedford, Massachusetts

We may soon be able to fly balloons up to 180 kft or even higher. This makes it necessary to have an accurate, easy-to-handle pressure sensor on board. The output of such a sensor should be fairly linear with altitude and should have an accuracy of about 1 percent of the indicated pressure (IP). It need cover only the range from 20 mb down to 0.4 mb or lower because aneroid gauges are in most cases adequate above 20 mb.

Many such indirect gauges have been described in the literature, mostly using the heat transfer across an air gap. The more recent ones use thermistors. Our instrument measures the heat transfer across an air gap with thermistors. When the pressure is decreased to the point where the mean free path length L reaches 2 percent of the air gap width D or the dimension of one port of the gap, the heat transfer starts to depend on the pressure with a useful rate. When L is equal to or larger than the gap width, the heat transfer is nearly proportional to the reciprocal of the pressure p. The length of the tubing is chosen long enough so that the heat conduction along the thermisotr wires is small compared with the transfer through the air. The smallest available thermistor bead is the 5 mil bead and its diameter (1.27×10^{-2} cm) is about 2 percent of the mean free path length at 20 mb pressure. As shown in Figure 1, the bead is concentrically suspended inside

a gold tubing. This bead is heated by current. So far it is very similar to many other designs. Our trick is to keep the temperature T_b of the thermistor bead constant. This can be done in two different ways. If a resistance output is desired, one can heat the thermistor with constant current and vary the tube temperature to compensate for the varying transfer coefficient (Figure 2). The resistance of a thermistor glued to the tubing is the output. In case a voltage output is required, the tube temperature is kept constant and the current through the thermistor is controlled to keep the thermistor at constant temperature. The output in this case is the voltage across the thermistor (Figure 3). The heat balance equations are for both cases:

$$i^2 R_b (1 - A\,t_b) = H_1 (t_b - t_h) \quad , \tag{1}$$

$$i_1^2 R_h + H_1 (t_b - t_h) = H_2 (t_h - t_a) \quad . \tag{2}$$

The meaning of the symbols are given below. In the first case (resistance output) we can derive from the heater control circuit the additional equation:

$$i_1 R_h = \alpha (V_1 - i\,R_b\,A\,t_b) \quad . \tag{3}$$

From Eq. (1) we can estimate the requirements for the precision of the fixed parameters to obtain the desired accuracy. If $\alpha = 1000$ or larger and if $V_1 = i R_b$, we can derive from Eqs. (1), (2), and (3) that $t_b \ll t_h$ and we can write approximately:

$$-\frac{\Delta t_h}{t_h} = \frac{2\Delta i}{i} + \frac{\Delta R_b}{R_b} + \frac{\Delta H_1}{H_1} - \Delta(A\,t_b) \tag{4}$$

If the heat would be transferred between bead and tubing by conduction through air only at a pressure of 0.4 mb or lower, the heat transfer H_1 would be proportional to the reciprocal of the pressure (p^{-1}). For an accuracy of 1 percent (IP) the total variation of H_1 due to changes of the parameters must be kept well below 1/2 percent. We can therefore write:

$$\left|\frac{2\Delta i}{i}\right| + \left|\frac{\Delta R_b}{R_b}\right| + \left|\frac{\Delta H_1}{H_1}\right| + \left|\Delta (A\,t_b)\right| \leq 5 \times 10^{-3} \quad . \tag{5}$$

But because the actual heat transfer at a pressure of 10 mb is varying only with about p^{-10} the term on the right side of Eq. (5) should be reduced to 5×10^{-4}. An

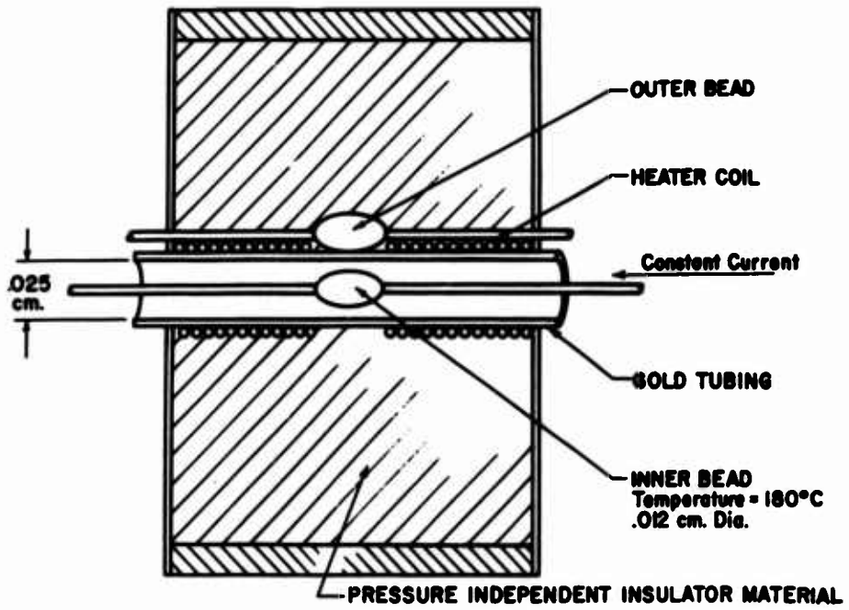

Figure 1. Pressure Sensor

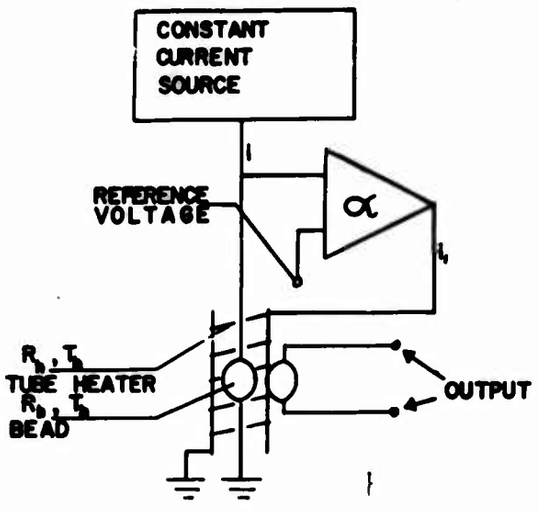

Figure 2. Circuit for Resistance Output

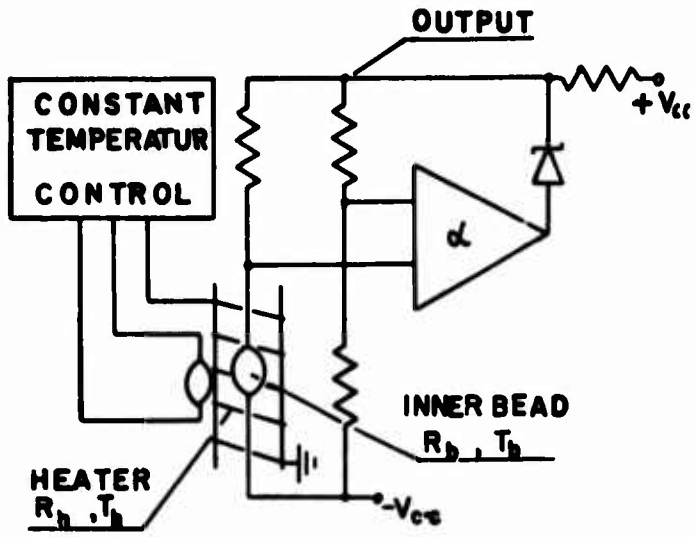

Figure 3. Circuit for Voltage Output

accuracy of 1 percent (IP) will therefore be achieved if each of the following relations are fulfilled:

$$\left|\frac{\Delta i}{i}\right| \leq 10^{-4} \quad , \left|\frac{\Delta R_b}{R_b}\right| \leq 10^{-4} \quad , \left|\frac{\Delta H_1}{H_1}\right| \leq 10^{-4} \quad , \left|\Delta\left(A\, t_b\right)\right| \leq 10^{-4} \quad . \tag{6}$$

The last term of (6) implies that $\Delta V_1 / V_1 \leq 10^{-4}$.

In the following discussion we will consider only the design with the resistance output. The temperature of the tube versus pressure is plotted in Figure 4. The power input into the thermistor for this curve was $4.1 \cdot 10^{-3}$ W. A higher power input would have shifted the curve to the right. The fact that the curve is bending downwards toward the lower pressure region can be explained by the radiative heat exchange between bead and tubing. The curve shows that the temperature difference is a nearly linear function from the logarithmus of the pressure and consequently from the altitude. The resistance output of the gauge is shown in Figure 5. The linearity of this curve may be improved by a parallel resistor to the measuring thermistor.

One can use a logarithmic encoder for a linear output. Figure 6 shows the schematic of an encoder that converts the logarithmus of the resistance to a sequential Morse code signal. It provides an altitude interval per bit that decreases slowly with altitude above 110 kft. To cover the whole pressure range, the gauge is used in combination with a barocoder which provides pressure information over the whole range although the accuracy in the upper altitude range is not sufficient. The sequence of operation is as follows. When the contact pointer of the barocoder had its last contact with the Morse code pattern printed on the rotating drum, the

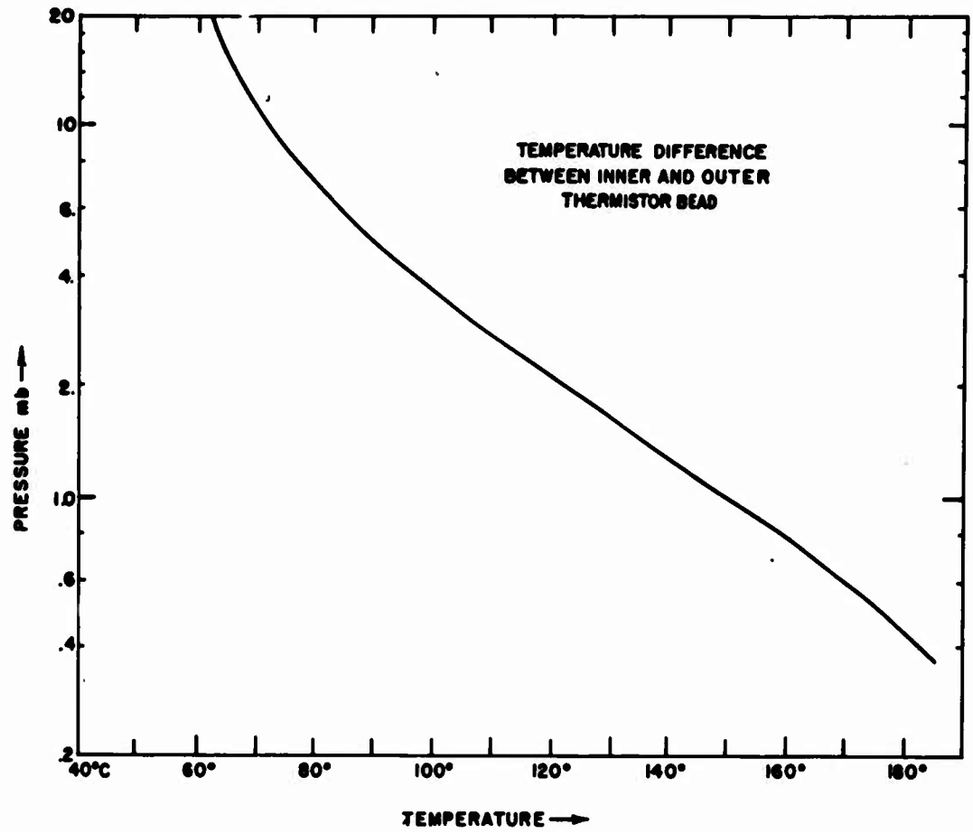

Figure 4. Temperature Difference Between Inner and Outer Thermistor Bead

timer starts the measuring cycle of the thermistor gauge. At first the counter is reset and the A/D converter started. The pressure information is then stored in the counter. Then the timer starts the readout sequence. To each of the counter flip-flops a monostable multivibrator is connected in such a way that its pulse length is either a dot or a dash length depending on the state of the corresponding flip-flop. Each monostable triggers the next one at the end of its pulse and by the combination of all pulses a Morse code is generated that corresponds to the logarithmus of the resistance. The pulses are used to key the relay of the barocoder. In this way we obtain the information alternately from the barocoder and the high-altitude gauge.

The errors of the gauge are mainly drift errors. The main error sources are:

(1) Drift of the characteristics of the inner and outer bead thermistors.

(2) Drift of the main amplifier.

(3) Change of the radiative heat exchange.

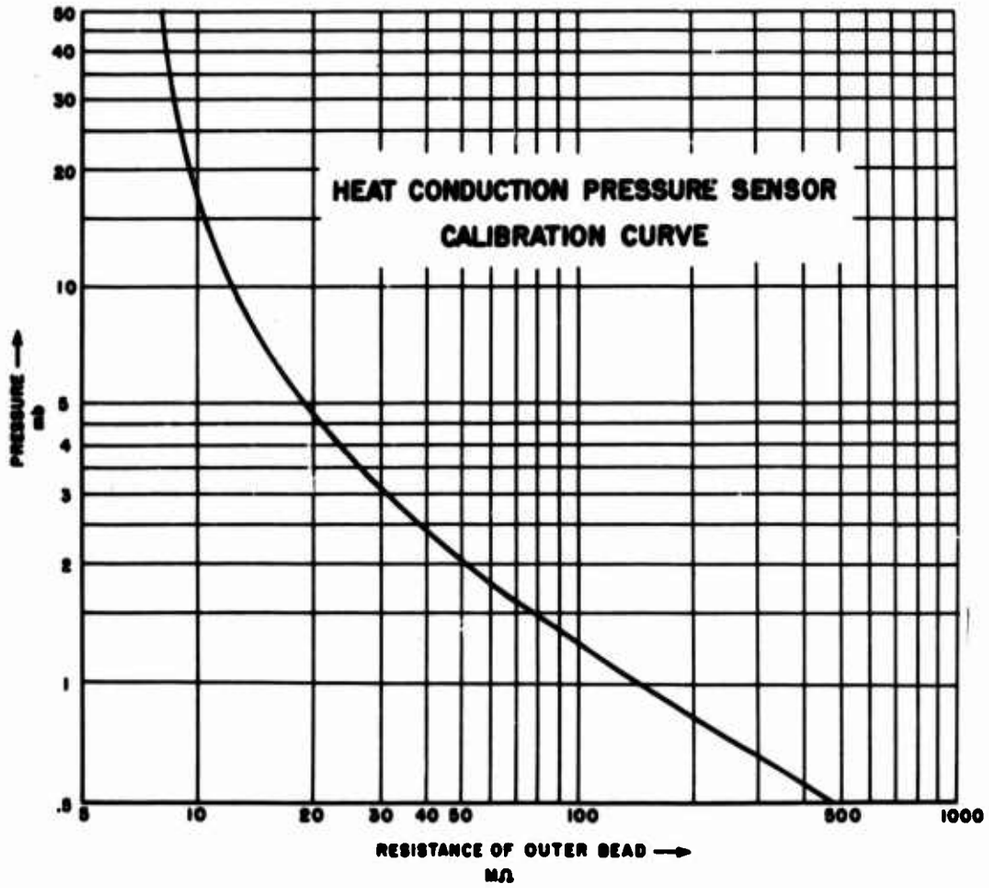

Figure 5. Heat Conduction Pressure Sensor Calibration Curve

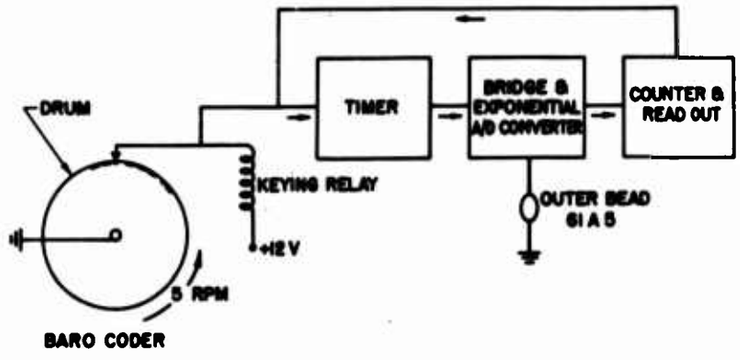

Figure 6. Morse Code Generator

(4) Change of the accommodation coefficient of the tube and the inner bead.
(5) Errors of the A/D converter.
(6) Change of the composition of the air.
(7) Influence of the ambient temperature.

All error sources except (4) and (6) can be held low enough for the required accuracy. We have no practical experience on the effect of outgassing, battery gases, and balloon gases on the composition of the air at higher altitude, but this is not considered a serious problem. The biggest problem is the slow drift of the accommodation coefficient. Some of our latest models have a drift of about 300 ft/day in continuous work, and work will be continued to reduce this drift. Because of the drift problem, no figure of the overall accuracy of the instrument can be given at this time.

Symbols

T_b = Temperature of the inner thermistor (°C)

$\overline{T}_b$ = Mean temperature of the inner thermistor (°C)

t_b = $T_b - \overline{T}_b$ (°C)

R_b = Resistance of the inner thermistor at temperature $\overline{T}_b$ (ohms)

A = $\frac{1}{R_b}\frac{dR_b}{dt_b}$ at the temperature $\overline{T}_b$ (1/°C)

t_h = Temperature difference between tube temperature and $\overline{T}_b$ (°C)

t_a = Temperature difference between temperature of the ambient air and $\overline{T}_b$ (°C)

H_1 = Heat transfer between inner thermistor and tube (watt/°C)

H_2 = Heat transfer between tube and environment (watt/°C)

i = Current through inner thermistor (amperes)

i_1 = Current through heater of tube (amperes)

V_1 = Difference between reference voltage and $i R_b$ (volts)

α = Gain of amplifier

XI. Round Robin Cold Brittleness Tests of Balloon Films

Dr. Ray L. Hauser
Hauser Research & Engineering Company
Boulder, Colorado

1. INTRODUCTION

At the 1965 AFCRL Scientific Balloon Workshop, a number of questions were raised regarding alternative methods for cold brittleness testing. A round-robin test program was suggested to compare the effects of the inclined plane and straight drop impact tests at -80°C. This paper presents the results of the round-robin program, monitored by the author and supported by the National Center for Atmospheric Research.

The inclined plane test is defined in Para. 4.5.5 of MIL-P-4640a (1965). The ball is dropped down a 60° slope which curves into a horizontal chute after a 36-in. descent. The ball then hits a vertical diaphragm of the balloon film under test.

The straight drop impact test has been developed by Winzen Research, Inc. (1964) and is included on their specification for StratoFilm, No. 320. In this case, a similar ball (2-in. diameter, 1-lb) is dropped in free-fall a distance of 27 in. to a horizontal diaphragm of test material.

In both tests, there have been questions regarding the tautness or looseness of the film in the clamps. Some experimenters have provided a slight cup to the film when it is installed at room temperature, so that thermal contraction effects can occur without putting undue stress on the film.

Interpretations of ductile or brittle failure of the films have been based largely upon the definitions given in the military specification (MIL-P-4640a, USAF, 1965). Where a definite star shatter has occurred, there has been no question of brittle failure. When the film breaks are of an intermediate geometry, the inspector's judgment of brittle or ductile failure may be the basis for acceptance.

2. MATERIALS

Film was requested from two manufacturers, and the following materials were received:

Code	Supplier	Thickness	Date or Lot	Roll
A	VisQueen X-124	0.5 mil	KF-29	----
C	VisQueen X-124	0.75 mil	KF-29	----
E	VisQueen X-124	1.0 mil	KF-29	----
G	VisQueen X-124	1.5 mil	KF-29	----
B	StratoFilm	0.5 mil	no record	----
D	StratoFilm	1.0 mil	no record	----
F	StratoFilm	1.5 mil	1343	1358

Samples of materials were coded with letter designations, and swatches 8-in. square were cut from each roll in a predetermined pattern. Ten different agencies or test methods were anticipated for this program, and five replicates of each material were prepared. The test agency/methods were numbered consecutively, and the replicate designations were made with lower case letters a, b, c, d, and e. The cutting pattern of Figure 1 was used for all films. In each case, samples a, b, and c were from the same section across the film, and samples c, d, and e were from the same section in the machine direction of the film.

Samples were mailed to each testing agency with only letter and number designations.

3. TESTING

The military specification inclined plane test is illustrated in Figure 2. This test is performed at -80°C with a ball of diameter 2.0 ± 0.1 in. and of weight 1.0 ± 0.1 lb (a steel ball bearing 1-15/16 in. diameter meets these tolerances). The diaphragm clamp is 5 in. in diameter. Inclined plane tests were performed by VisQueen Corporation, Litton Industries, and Raven Industries.

The drop test is described by the Winzen specification (WRI Specification No. 320, 1964) and it was performed at -80°C in this program. The WRI specification describes a ball of 2-in. diameter and 1-lb weight, with the same tolerances as

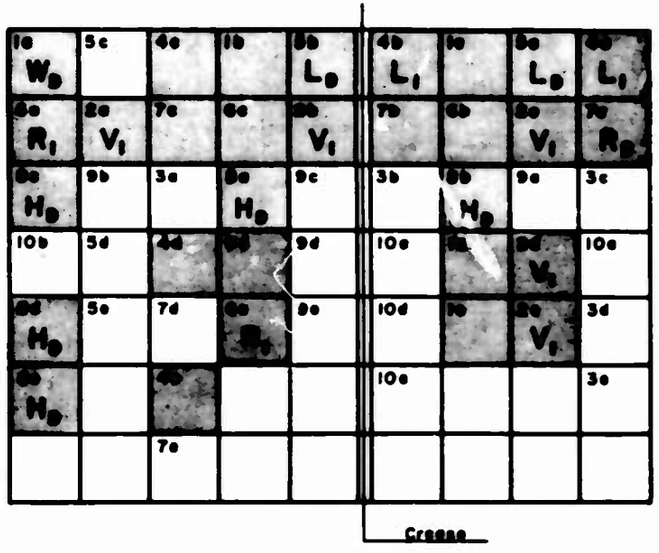

Figure 1. Pattern for Cutting Round-Robin Samples (Brittle failures, among samples tested, shaded areas - Film B, 0.5 mil StratoFilm)

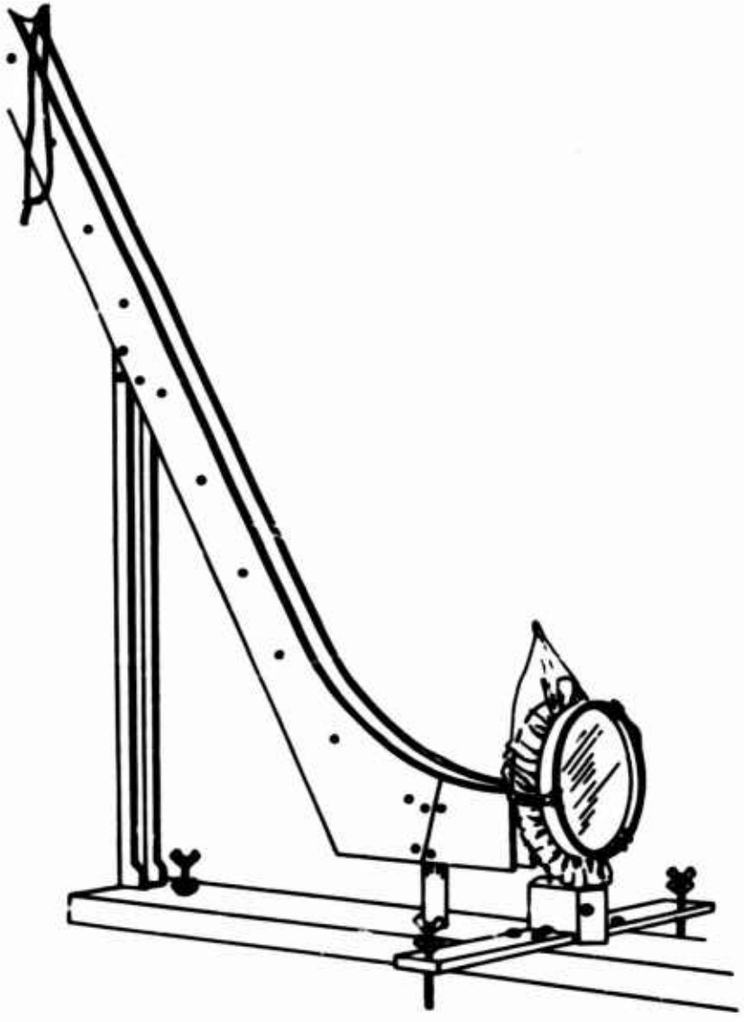

Figure 2. Inclined Plane Ball Tester

the military specification. The 27-in. free-fall was designed to provide approximately the same amount of translational impact energy to the film as the 36-in. inclined plane. Companies with facilities for the drop test were Winzen Research, Raven Industries, Litton Industries, Sea Space Systems, and Hauser Research & Engineering Company.

Companies were asked to test films in terms of their usual procedures for clamping and cupping. These conditions were reported to the monitor prior to distribution of samples. Companies were also asked to report their judgment of brittle or ductile failure, and this was done in most cases.

After testing, a number of samples were prepared for inspection of brittle or ductile failure by participants at the 1966 AFCRL Scientific Balloon Conference.

Mechanical properties of the films at -80°C were tested by the Hauser laboratory for comparison with the dynamic tests. Tensile strength and elongation were measured by methods of National Center for Atmospheric Research (1964).

4. RESULTS

The results obtained from all participants in this program are presented in Table 1. Here the fraction of brittle failures is noted for each agency and test method. In some cases, less than five good tests were obtained. Drop test data from Sea Space Systems and Litton were combined into one column to provide samples of five.

Table 1. Fraction of Brittle Fractures in Round-Robin Tests at -80°C

MATERIAL	Thickness, mils	DROP TESTS 2" Ball, 27" Drop				INCL. PLANE TESTS 2" Ball, 36" Roll		
		Winzen no cup	Rayon 3/8" cup	SeaSpace & Litton	Hauser no cup	Visqueen no cup	Rayon 3/8" cup	Litton no cup
A, Visqueen X-124	0.55	0/5	1/5	4/5	0/5	0/5	0/5	0/5
B, StrataFilm	0.50	1/5	1/5	4/5	5/5	5/5	2/5	2/5
C, Visqueen X-124	0.75	0/3	1/5	3/4	3/5	0/5	0/5	0/5
D, StrataFilm	1.00	0/5	1/5	4/5	1/5	0/5	2/5	0/4
E, Visqueen X-124	1.00	0/4	1/5	4/5	1/5	0/5	0/5	0/5
F, StrataFilm	1.50	1/5	1/5	1/5	4/4	0/5	0/5	0/5
G, Visqueen X-124	1.50	1/5	1/5	3/5	4/4	1/5	2/5	2/5
TOTAL		3/32	7/35	23/36	18/33	6/36	6/36	4/34
		.094	.200	.657	.545	.172	.172	.118

Where results are identified only as ductile or brittle, analysis must be done in terms of fraction defective; this is not as significant, statistically, as would be a quantitative measure of brittleness.

The fraction defective (brittle) results have been treated by the standard analysis of variance techniques to learn significance of differences between test laboratories, test methods, and film variations.

The results from drop tests were quite different among the five laboratories. A comparison of Winzen and Raven results showed a difference in results at the 95 to 99 percent probability level. Even more different results were reported by Sea Space, Litton, and Hauser.

On the other hand, the ski-ball tests were very similar among the three participating laboratories. Their results were equivalent with a 99 percent probability.

The deviation coefficients for interlaboratory tests of cold brittleness were ± 40 percent for drop tests and 38 percent for inclined plane tests. These measures of precision indicate that the present cold brittleness test and inspection methods are not sound bases for acceptance/rejection criteria.

A review has been made of the number of brittle fractures in specimens from various locations in the balloon film – along the crease, in transverse directions, along the machine direction, and so forth. Among the many tests, no evidence of geometric significance was observed.

The intentional cupping of the diaphragms prior to impact gave no significant differences in test results in the inclined plane tests. Cupping and low clamping pressure may have contributed to the smaller number of brittle drop test fractures obtained by Raven and Winzen.

A map measure has been used to measure the total length of tear in each of the specimens on this program. This is suggested as a quantitative measure of brittleness to replace the subjective judgment of brittle or ductile failure. Critiques of the 17 samples which were displayed at the AFCRL conference are presented in Table 2. These samples were mostly marginal in nature, with questioned brittle or ductile failure. Some appeared to have experienced off-center impact. Persons concerned with cold brittleness testing and with specification interpretation were asked to record their judgments whether films were (a) brittle, (b) ductile, (c) questionable and another sample should be substituted, or (d) an improper test and another should be substituted. Respondents were unaware of any concern for quantitative measurement of tear length. These values are included in Table 2 for comparison with the judgments of observers.

All samples that the majority considered to be brittle failures had tear lengths exceeding 9 inches. All but one sample considered to be ductile had tear lengths less than 9 inches. One sample with 16-in. tear length had five ductile votes, three questionable votes, and one brittle vote.

Table 2. Inspection Decisions for Selected Samples From Cold Brittleness Specimens

Specimen	Inspection Decisions				Majority Opinion	Tear Length, inches
	Brittle	Ductile	Questionable, Retest	Improper Test		
B4d	II	⧺	II		Ductile	7.0
A3b	⧺ IIII				Brittle	9.0
D4a			I	⧺ III	No Test	
B4b	I	⧺ II	I		Ductile	7.4
B4c	⧺ IIII				Brittle	18.7
D4b		IIII	II	II	Ductile	6.5
A5d	I	⧺	III		Ductile	16.0
B5c	⧺ IIII				Brittle	45.7
E5c	II	⧺ II			Ductile	8.0
G6b	⧺ III	I			Brittle	19.7
G6c		⧺ IIII			Ductile	5.9
G6a	⧺ IIII				Brittle	12.6
B6a	⧺ I	II	I		Brittle	11.0
B7a	⧺ IIII				Brittle	11.5
A7b	⧺ IIII				Brittle	10.5
D6a	⧺ III				Brittle	12.5
D7b	⧺ IIII				Brittle	22.0

The tear lengths of samples A, B, and G have been measured on specimens from five laboratories. Drop test data were highly nonrandom and showed high deviation coefficients. Tear lengths from inclined plane tests were more nearly random, had lower average values and showed better precision. These data are presented in Table 3.

The criterion of a 9-in. tear length for separation of brittle or ductile behavior appears to have merit in marginal decisions.

The unidirectional mechanical properties of these films are presented in Table 4. Tests were made at -80°C with 4-in. gage length and cross-head speed 0.5 in./min. Ultimate elongations have been considered to have significance and a minimum 40 percent elongation has previously been suggested by the author as an appropriate acceptance criterion. Such a criterion would have rejected samples A and B of this program.

Table 3. Total Tear Length of Five Samples

Film	Drop Test		Incl. Plane Test	
	Length, inches	Precision, percent	Length, inches	Precision, percent
A	68.1	± 44.8	26.8	± 3.8
B	77.9	± 100	46.8	± 28.0
C	67.5	± 55.0	54.0	± 9.2

Table 4. Unidirectional Properties of Round-Robin Films at -80°C

Film	Thickness, mils	Direction	Tensile Strength, lb./in.		Elongation, percent	
			average	dev. coeff.	average	dev. coeff.
A, Visqueen X-124	0.55	machine transverse	5.51 4.99	.070 .124	88 33	.21 .46
B, StrateFilm	0.50	machine transverse	4.00 3.81	.072 .050	47 20	.33 .31
C, Visqueen X-124	0.75	machine transverse	7.27 5.99	.057 .063	150 76	.36 .78
D, StrateFilm	1.0	machine transverse	8.35 8.13	.054 .044	114 71	.31 .86
E, Visqueen X-124	1.0	machine transverse	8.67 7.87	.082 .095	106 89	.38 .68
F, StrateFilm	1.5	machine transverse	11.89 11.55	.038 .010	163 86	.42 .33
G, Visqueen X-124	1.5	machine transverse	12.26 11.92	.027 .063	177 66	.31 .63

5. CONCLUSIONS

The results of these round-robin tests indicate that the drop test is not equivalent to the ski-ball test for evaluation of cold brittleness at -80°C. The drop test is more severe as it is now being practiced by most of the laboratories (see Figure 3 and Table 5).

Cupping of the film diaphragm as much as 3/8-in. at room temperature has no significant effect on the inclined plane brittleness test at -80°C. Cupping may have some effect on the drop test.

These tests have not indicated any significant variability in cold brittleness properties of balloon films in terms of different machine or transverse locations.

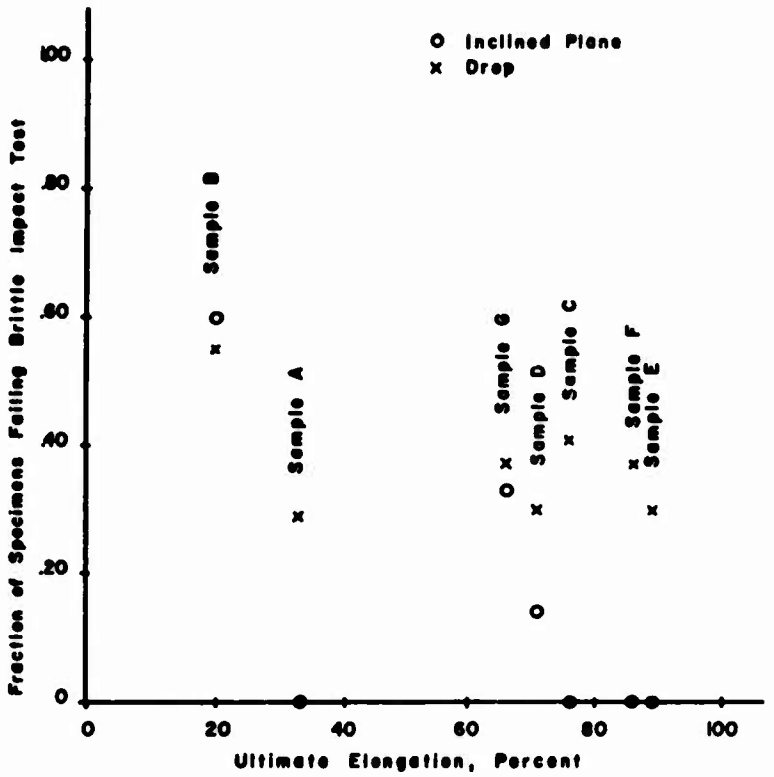

Figure 3. Correlation of Impact Brittleness and Uniaxial Elongation at -80°C

Table 5. Impact Brittleness and Elongation Tests at -80°C

Material	Thickness mils	Fraction Brittle		Ultimate Elongation, percent	
		Drop	Inclined plane	Machine direction	Transverse direction
A, Visqueen X-124	0.55	.333	.000	88	33
B, StrataFilm	0.50	.400	.600	47	20
C, Visqueen X-124	0.75	.333	.000	150	76
D, StrataFilm	1.00	.333	.143	114	71
E, Visqueen X-124	1.00	.333	.000	106	89
F, StrataFilm	1.50	.200	.000	163	86
G, Visqueen X-124	1.50	.333	.333	177	66

The average deviation coefficient for interlaboratory cold brittleness tests indicates a precision of ± 40 percent in this acceptance criterion; this is not a sound basis for acceptance to Specifications MIL-P-4640a or WRI No. 320.

A quantitative measure of cold brittleness has been proposed, and the round-robin test results indicate that a good discrimination for brittleness and ductility might be:

Tear length of four samples, total more than 36 in. – brittle,
Tear length of four samples, total less than 36 in. – ductile.

XII. PAGEOS Fabrication Accuracy and Reliability

S.J. Stenlund and B.D. McLellan
G.T. Schjeldahl Company
Northfield, Minnesota

Abstract

This paper covers the design of the 100-ft-diam PAGEOS Satellite and the Reliability Program used to predict its reliability. This was the first use of a Space Satellite Reliability Program in balloon design and fabrication. The technique for reliability prediction for PAGEOS Inflatable Sphere Assemblies utilizes known theory of probability in evaluating representative random samples of component characteristics. The end result is component, operational phase, and ultimately system reliability prediction including estimation of failure rates. The use of this program in design and building of load-carrying balloons is discussed.

I. MISSION

As a continuation of the NASA effort in support of the National Geodetic Satellite Program, an Echo I type Satellite was launched from Vandenburg AFB on June 23, 1966 into a near-polar orbit at about 2200 miles in altitude. The 100-ft-diam, aluminum-coated, spherical satellite can be observed from the ground as a point source of light while it reflects the incident sunlight. Simultaneous photographs of

this light source taken against the star background by two or more widely separated ground-based cameras will enable geodesists to determine the spatial coordinates of each camera position. An interconnected series of camera positions has been established to cover the entire surface of the earth, thereby permitting geometric determination of each camera position within a single reference system. The use of this satellite for geodetic purposes will continued for a 5-year minimum period during which the necessary photogrammetric observations will be made to provide, for the first time, a purely geometric determination of the shape and size of the earth.

2. DESCRIPTION OF SATELLITE

The PAGEOS satellite is a spherical shell of 1/2-mil Mylar coated with vapor-deposited aluminum approximately 2000 Å thick, giving a resistance of less than 1 ohm per square. The aluminum film serves to reflect most of the incident sunlight and protect the plastic film from the degrading ultraviolet radiation.

The aluminized material was initially processed in long flat sheets (10,000 ft long by 54 in. wide). This material was then treated and inspected before being cut into 84 gores required for the sphere. The gores, 45 in. wide at the center and 157 ft long, were then butted together and sealed with a 1-in. wide tape made from the same material, but coated with a thin layer of thermosetting adhesive specially selected for characteristics suited for space use.

Polar caps were sealed over the gore tips to provide structural integrity at the terminating gore points. Since the gores were insulated from each other by the plastic film dielectric along the seams, the polar cap was electrically connected to each gore by a ring of conductive paint.

To ready the sphere for flight, an inflation system* was added, and after the final seal was made, the sphere folded into a small canister. Upon completion the package was sent to Vandenburg AFB, mounted on a Thor Agena vehicle, and rocketed into space. When the canister was in orbit it separated, leaving the sphere free to inflate to its full (100-ft diam) size.

3. FABRICATION ACCURACY

The PAGEOS satellite is the most accurately fabricated, large inflatable ever built. During the full-scale inflation test, measurements showed that the polar and equatorial diameters were less than ± 1/2 percent from the design. Measuring the

*A mixture of subliming powders, namely benzoic acid and antraquinone.

100-ft-diam sphere accurately was an engineering challenge. The polar diameter was easily measured directly by fastening a measuring tape at the top, or north pole of the sphere, and allowing it to hang through the duct at the bottom of the sphere. The equatorial diameter was measured at 8 different points with a system of theodolites and a computer program. As measurements were taken, the information was put into a desk computer at the test site, and diameter measurements made available within a few minutes after the theodolite readings. The accuracy of this sytem was believed to be within 2 in. for a 100-ft length measurement. Figure 1, a picture of Echo I, should be compared with Figure 2, which shows PAGEOS at approximately the same skin stress (4000 psi). Comparisons of the reflected images, the smoothness of the seals, and the flatness of the gores, show the results of the much improved fabrication techniques used on PAGEOS. A closer view, Figure 3, shows the meaning of fabrication accuracy with an apparent optical illusion. This picture is actually a reflection taken by the photographer standing in the lower center portion of the picture. Careful examination of the upper right-hand corner of the picture shows a seal which is just visible under proper lighting conditions taken at this range. This picture clearly shows the superior optical reflective qualities of the spherical surface.

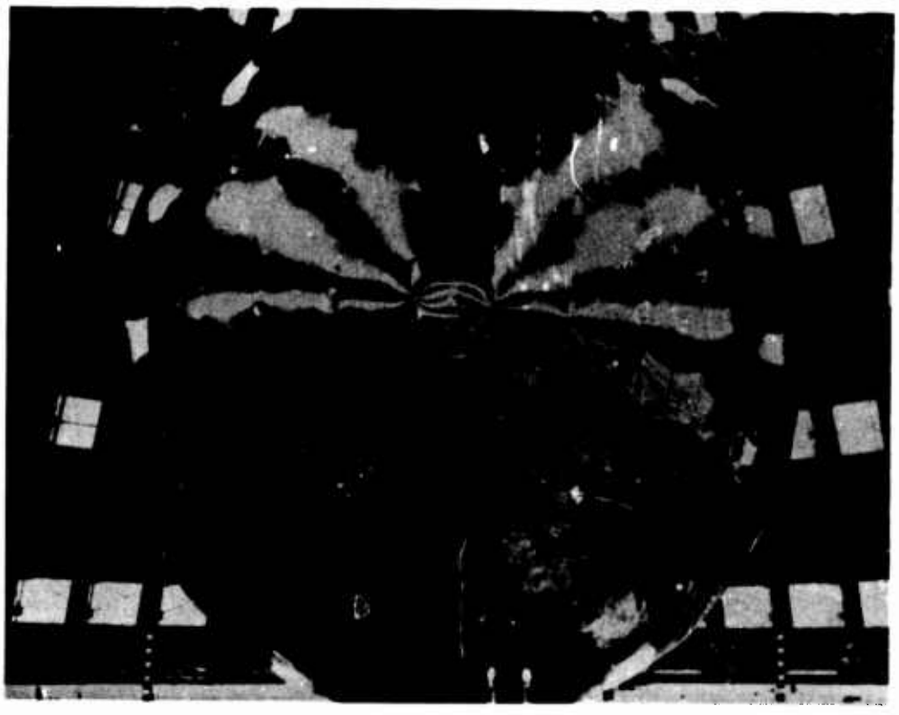

Figure 1. Echo I Static Inflation

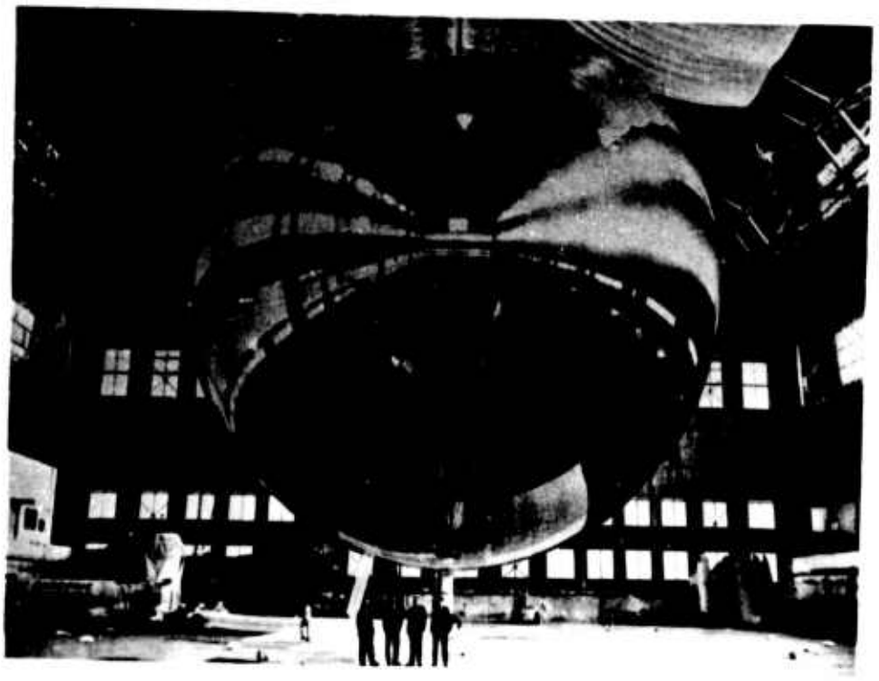

Figure 2. PAGEOS Static Inflation

Figure 3. Reflected Images

This high degree of accuracy was attained by using an accurate gore pattern, by maintaining seal tolerances, and by lowering the sealing temperature. Continual and vigorous inspection during all stages of fabrication insured the proper use and control of tools and procedures.

For the 157-ft long gore pattern, the length tolerance established was ±1/4 in., while the width tolerance was ± 0.030 in. at the midpoint, reduced to ± 0.015 in. near the tip. The center line was held straight within ± 0.060 in. These tolerances were measured and verified with conventional engineering tools such as a theodolite, a calibrated steel measuring tape, and vernier calipers.

In butt-joining the gores, the maximum allowable gap was 0.030 in. and the maximum allowable overlap was 0.040 in. Frequent measurements during fabrication showed that these tolerances were rarely exceeded indicating the capability of sealing techniques to maintain such tolerances.

Mylar has a tendency to shrink and distort when heat is applied. To minimize this effect, it was found necessary to reduce the normal sealing temperature from 390 to 340°F. The result was the distortion-free seals shown in Figure 2.

The gore-cutting template was accurately laid out and then periodically re-measured to insure continued accuracy. Random measurements were made daily and checked against the last periodic measurement to insure no changes beyond tolerance limits were taking place. During sealing each of the seals was inspected with go-no go gages and optical comparitors. The temperature of the sealing irons was continuously monitored.

To verify the design before orbiting a sphere, a static inflation test was planned of a full-scale sphere to determine polar and equatorial diameters, structural integrity of the sphere, materials and construction, seam creep over a period of time, and to evaluate workmanship and effectiveness of inspection.

The static inflation sphere required two modifications, attachment points (tie-down patches), and ducts, or openings, in the sphere wall. The tie-down patches were to hold the sphere in place and the ducts to add or discharge air. Both were necessary because the sphere was to be flown 10 feet off the hangar deck as a tethered, hot-air balloon to facilitate accurate measurements of the diameter.

To insure that the modifications would not degrade the performance of the sphere during the static test, each was thoroughly tested. Figure 4 shows the tie-down patch being tested with a dead weight of 60 lb. Further loading caused it to fail under a load of 430 lb. Since the maximum operating load expected was 50 lb, the results of the test were very encouraging.

The duct installations were tested by constructing spherical segments and pressurizing them. Figure 5 shows a spherical segment with an unmodified polar cap of the design to be used in the final sphere. This was the control segment for the

Figure 4. Testing the Tiedown Attachment

modified spherical segments. Figure 6 shows a polar cap modified in its center with an inflation duct for adding air to the bottom of the sphere and for discharging air from the top. The opening was reinforced so that loads were transmitted across it.

Figure 7 shows a side duct segment used for discharging air. This opening differed from the polar ducts since less reinforcing and reinforcing tapes were available away from the poles. Test data were satisfactory, as failure levels were verified to be well above the maximum to be encountered during the static inflation test. The results of these tests gave us confidence in the reliability of design for the static inflation test sphere.

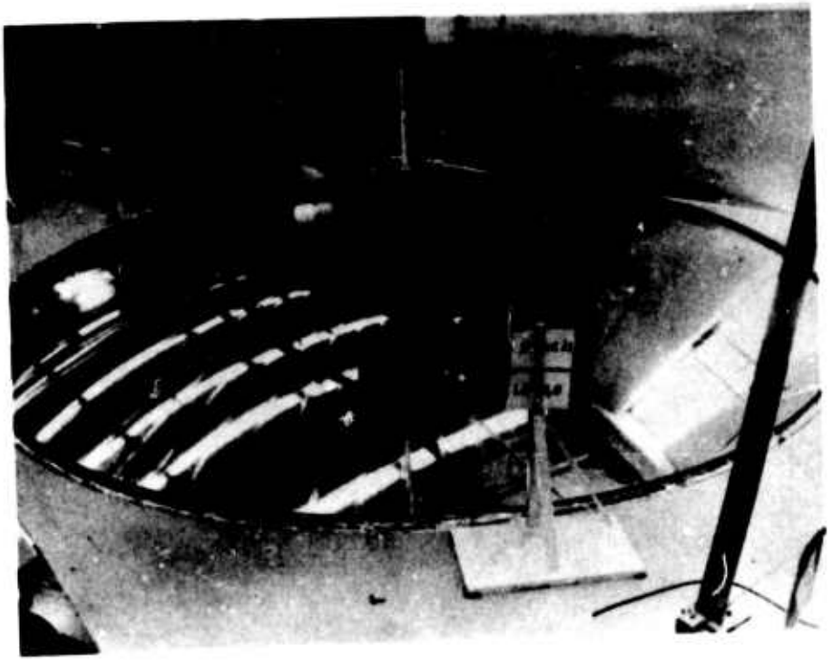

Figure 5. Polar Cap

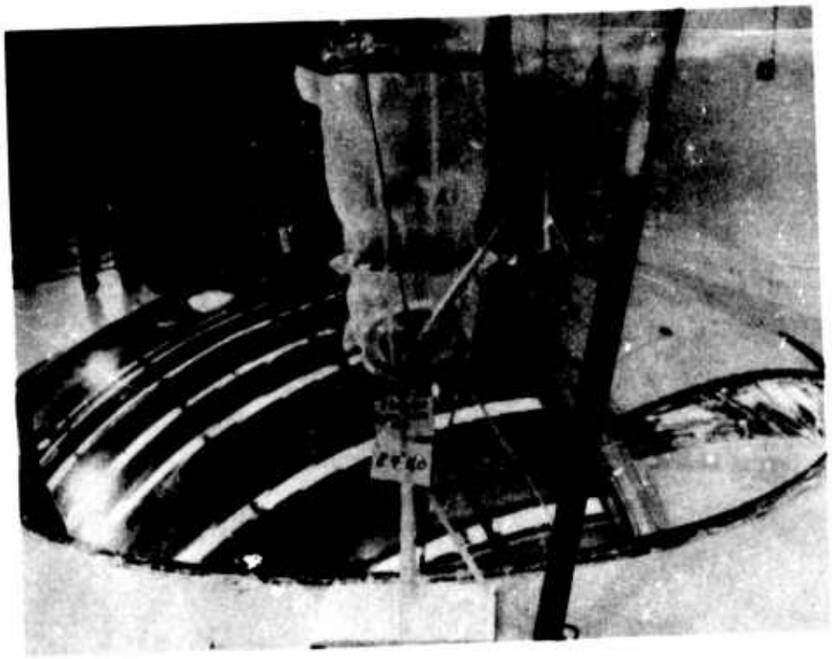

Figure 6. North Polar Cap with Duct

Figure 7. Exhaust Duct

The final design test was the actual inflation of the full-scale sphere. This was conducted in an air ship hangar at Lakehurst Naval Air Station, Lakehurst, New Jersey. The results of this test showed that the key objectives had been met, but that blocking, the adhesion of the material to itself, was present. As a result, special emphasis was placed on solving the problem. It was found that chemically treating the Mylar side of the material with a solution of Freon TF and Valclene No. 1 virtually eliminated blocking. Testing, manufacturing, and inspection procedures were modified to reduce the potential for blocking to take place. A final redundant change, to further prevent blocking, consisted of dusting the inflatant powder over the entire inner surface of the sphere since it served as a lubricant and release agent. Although these changes were overlapping, they were felt necessary since blocking would surely cause catastrophic failure of the sphere when inflated in space.

A successful simulated deployment test of the full-scale sphere in a 60-ft-diam vacuum chamber showed the results of these changes. A few minor changes were required in other parts of the system, but the last high hurdle had been passed, and fabrication of the flight spheres was ready to begin. After holding a design review and considering every design aspect as required by the NPC documents, fabrication began.

During the manufacture of the flight spheres routine material tests were conducted to assure quality and reliability of the sphere. For each sphere built there were 750 tensile strength tests, 350 tensile impact tests, 170 thermal shock tests, 170 thermal flex tests, 170 seam creep tests, and 175 reflectance tests. These nearly 1800 tests measured the variable characteristics of the material. In addition, 530 adhesion tests, 530 hot-wheel-blocking tests, 170 seam-peel tests, and 500 aluminum-adhesion tests were conducted, making a total of nearly 3,500 individual tests on each sphere. The results of this test effort were used in estimating failure rates. Reliability prediction for components and the system were based on these estimated failure rates.

Meanwhile, special emphasis was placed on minimizing handling and workmanship defects by manufacturing. Only 9 material defects (due to handling) in over 31,000 sq ft of material and not one single seal defect in over 2 miles of seal were detected in the flight sphere. The final reliability prediction for the flight article sphere was 0.9602. The reliability goal had been established at 0.96 early in the program.

How were these tests accomplished? During the early stages of the program we were required to plan the quality program and submit it for approval. The plan included the approach that was to be used throughout the program to implement, staff, and maintain the program; and the requirements to be met during all phases of engineering design, development, fabrication, processing, assembly inspection, testing, checkout, packaging, shipping, and storage. The contract required conformance to the NASA Documents NPC 200-2 and 250-1.

What was management's role in reliability? The program management motivated those working on the job so that they had an intense desire to avoid failure. The people were well trained in their jobs and their morale was kept high by keeping them informed on how well the work they had done was performing downstream. Test results were made known, pictures and movies were shown, and program management showed high interest in the work as it progressed.

4. RELIABILITY APPLIED TO BALLOONING

How can the PAGEOS experience benefit balloon programs? A technique for reliability evaluation and prediction has been developed. The tools for doing the job were found. The mathematical approach developed is applicable to balloon programs where full-scale item testing (reliability demonstration testing) is not practical. The technique developed can be modified to suit individual programs. It would not be practical to use a high reliability balloon with a payload and launch system of marginal reliability. Nor is it wise to use a balloon of marginal reliability

with an expensive and important payload as is sometimes done. Nor can the users of balloons assume that reliable components in a system are compatible. Reliability must be designed into the balloon system. To do this the RFQ should include as much information as possible relating to the specific mission such as launch condition, flight durations, and environment. A quality and reliability program should be set up for each balloon program, even if a very simple one. It will evaluate on its own merits all of the aspects associated with the flight and will predict the failure modes of the mission.

The conclusions can be summarized as follows:

1. The PAGEOS program reduced fabrication and inspection arts to a science.
2. Large spheres can be accurately built and measured to an accuracy of ± 1/2 percent using state-of-the-art equipment and methods.
3. A reliability prediction can be made without large-scale testing of the whole unit either in a huge environmental system or in space.
4. Reliability techniques developed during the program have application in other balloon systems.

XIII. Balloon Materials

D.R. Williams and Jean R. Nelson
Winzen Research Inc.
Minneapolis, Minnesota

1. PERFORMANCE (D.R. WILLIAMS)

This AFCRL sponsored balloon symposium provides a very convenient time mark to review a year's developments in our efforts to provide balloon vehicles which are more reliable and yet carry heavier loads and go to greater altitudes.

Since our report on StratoFilm balloon flight results at this symposium last year, with few exceptions our customers and friends have continued to provide us with flight data information. We now have reports on 339 flights of balloons made from Stratofilm. Last year we reported on 114 – this year our compilation covers 225 more.

Of this number 204 were successful in balloon performance for an overall percentage success this past year of 90.7 percent. Using our batting average – base on balls concept and eliminating ground aborts and other failures which were not indicative of the balloon's flying ability, that is, to get a payload to ceiling and hold it there as long as desired, we find a success record of 94.4 percent.

Analysis of failures now seems to indicate random results. The most interesting achievement we feel was the record of 32 successes in 32 flights made by our friendly competitors in flights at Ft. Churchill this past summer for ONR with

Winzen balloons. To make it even more significant, 18 of these were with 10.6-million-cu-ft balloons, 3 were 1/2-mil 6-million-cu-ft with cap, and 2 were 7-mil 5.25 million-cu-ft. Thus, of the 32 flown, 23 were over 5-million-cu-ft.

Looking at the past year as a whole again, there were 34 10.6-million-cu-ft balloons flown with 29 successful. Of the 5 failures, 1 was a ground abort at NCAR and the other 4 were an unfortunate series flown by Raven about a year ago. The first of these 4 did not lift the payload off the ground and the other 3 failed at 47,000 ft, 49,000 ft, and 56,000 ft. We feel that since these balloons were random production from the summer of 1965, the failures most probably are attributed to either or both of the following reasons: (1) too rapid ascent or, (2) severe wind shears.

Since the failures are so few we can again discuss them all. A 5.25-million-cu-ft,0.7-mil balloon failed at Palestine about a year ago at 61,000 ft – reason unknown. In November of 1965, Goodfellow Air Force Base had a 1.5-mil, 5.25-million-cu-ft balloon fail at ceiling at 120,000 ft. They suspect a trapped duct resulting somehow from the extreme cold at launch. A third 5.25-million-cu-ft balloon failed at Mildura, Australia last February at 31,000 ft. This was 1.5-mil. Strangely enough there were two failures with 2.94-million-cu-ft balloons, and they were both 1.5-mil. One was at Goodfellow Air Force Base and one at Palestine in September and October of 1965.

In the 1.6-million-cu-ft category, out of 30 balloons one failed at Mildura in March 1965 at 89,000 ft.

Analyzing the effect of film thickness, out of these 10 balloon failures in flight, 5 were 1.5-mil, 2 were 0.7-mil, and 3 were 0.5-mil.

With such few failures it seems quite difficult to attempt to generalize on the reasons for failure. It would seem that our preoccupation with failures a couple of years ago is pretty much a thing of the past. One wonders now if we are designing with greater margins of safety than necessary to get maximum use of the material.

I would like to point out that a few years ago many people would only buy or use a so-called proven balloon (for example, the 2.94, or the 128 TT). For two years we have been designing new balloons according to our design formulas and the new designs perform every bit as good as the so-called proven designs.

We had hoped to be able to discuss some new balloon materials with you at this symposium but our time-table of development has slipped and we are not prepared to do so. Perhaps next year we will have information on new materials which will open further avenues of advancement in ballooning.

2. PERFORMANCE AND PROPERTIES (JEAN R. NELSON)

Winzen StratoFilm was initially developed to combat the rash of polyethylene balloon ascent failures at or near the tropopause. After two years of operations experience, notably in India and Panama, with flights through extremely cold tropopause temperatures as low as -83°C, we have concluded that the primary objective of increasing film resistance to cold brittleness failures has been significantly improved. During this period other temperature characteristics have been evaluated and this discussion covers two areas of investigation. First, the effect of different temperature environment on StratoFilm altitude performance, and second a comparison of stratosphere temperatures inside small cubes covered with production StratoFilm, StratoFilm "K", and StratoFilm "W".

During the 1965 Ft. Churchill balloon program, sponsored by the Office of Naval Research, it was noted that a number of flights were not ascending to full theoretical altitude. This performance was a matter of concern and an investigation was immediately initiated to determine the source of the problem. After ruling out mechanical problems such as balloon damage as a cause of the decreased altitude, the stratosphere environment was examined for its effect on balloon performance. It was found that two factors could result in an apparent or actual altitude deficiency in the Arctic atmosphere operation.

First an apparent altitude deficiency would result due to the elevated temperature profile of the Arctic stratosphere. The balloon, operating on Archimedes principle, floats in the atmosphere in accordance with the density of the displaced air, whereas the altitude measuring barotransmitter provides only pressure altitude area. Thus when a barotransmitter is calibrated in thousands of feet or millibars of the 1962 Standard Atmosphere Model, it will give a lower reading in the higher temperature Arctic environment; that is, the correct density altitude is attained at a lower pressure altitude.

The second factor is more significant in that the high temperature affects the actual density altitude achieved in some instances when the balloon does not reach its full design inflation. According to work done by the University of Minnesota and Dr. John Gergen, and using actual temperaturements by rocketsonde and balloon-borne sensors at Ft. Churchill, an analysis of flights 1030W-15C and 1016W-14C during the 1965 program was made.

In most instances, particularly in the stratosphere, the lifting gas in a balloon is not at ambient air temperature. The lifting gas temperature during a stabilized condition is a function of the balloon fabric temperature, since the gas is assumed to be transparent to both short-wave and long-wave radiation. On flight 1030W-15C the airborne weight was 1196 lb including the 10.6-million-cu-ft balloon

and the free lift was 229 lb. Assuming that there was no loss of helium after initial inflation and that air and helium temperatures were equal, the weight of helium was

$$Wg = \frac{F + G}{\frac{Ma}{Mg} - 1} = \frac{1425}{\frac{28,96}{4} - 1} = 228 \text{ lb} \quad .$$

Solving for the free lift at 3-mb altitude

$$F = Wg\left(\frac{\rho a}{\rho g} - 1\right) - G = 228\left(\frac{2.7489 \times 10^{-4}}{4.2704 \times 10^{-5}} - 1\right) - 1196 \quad ,$$

F = 44 lb at 3 mb compared to F at inflation of 229 lb.
Computed data showed agreement that the lift went to zero at the actual ceiling altitude of 2.25 mb instead of 1.78 mb theoretical altitude. The conclusion was that the balloon ran out of free lift before achieving full inflation.

A corollary to this problem was the effect of cloud cover on balloon altitude. Shielding the balloon from earth infrared radiation cooled the helium and initiated a descent to lower, cooler air temperature where the density balance for float was reinstated.

It was found that under the worst temperature profile conditions it was necessary to carry approximately 25 percent free lift on a large balloon. Since this cannot be accomplished by overinflation at launch due to aerodynamic damage during ascent, it is necessary to carry the excess free lift in the form of ascent ballast. Additional ballast to replace loss of lift due to cloud system effects on the worst cloud condition and longest flight was computed to be 7 percent.

Turning to the second area of investigation of temperature effects, a flight was conducted by Winzen Research Inc. to compare temperature characteristics of StratoFilm 340, StratoFilm "K" and Stratofilm "W", which are polyolefin, polyurethane, and nylon materials. This flight, No. 1043W, was conducted with a Model SF 85.4-070-NS-01, 243,000 cu ft, natural shape taped balloon. The gross airborne weight was 664 lb including the 109-lb balloon. Free lift at launch was 57 lb (2 lb over preselected figure).

One of the flight objectives was to check the empirical relationship derived by the University of Minnesota in their work for the Office of Naval Research to anticipate the free lift requirements for a desired ascent rate. The equation is

$$F.L. = \frac{C_1 (L+4)^{3/4} G^{1/4} v^{3/4}}{T^{1/2}} + C_2 \left(\frac{P}{TG}\right)^{1/3} v^2$$

F. L. = Relative Free Lift
C_1 = 7.4×10^{-4} const.
C_2 = 6.5×10^{-7} const.
L = Lapse rate (°C/1000 ft)
G = Gross Airborne Wt (lbs)
v = Ascent Rate (ft/min)
T = Ambient Air Temperature (°K)
P = Pressure (mb) .

Based on the preflight Weather Bureau data and a desired ascent rate of 600 ft/min, the relative free lift was determined from anticipated conditions to be:

Free Lift = (0.08305) (664) = 55 lb.

Actual in-flight ascent rate data taken at 34,000 ft agrees with the preselected relative free lift. Solving the foregoing equation for v (using inputs for 34,000 ft) yields:

$$\text{F. L.} = \frac{7.4 \times 10^{-4}(4 - 1.24)^{3/4}(664)^{1/4}v^{3/4}}{(235.5)^{1/2}} + 6.5 \times 10^{-7}$$

$$\left(\frac{250.6}{660 \times 235.5}\right)^{1/3} v^2 = 0.0858$$

$$5.24 \times 10^{-4}\, v^{3/4} + 0.76 \times 10^{-7}\, v^2 = 0.0858 , \text{ or } v = 570 \text{ ft/min.}$$

The formula has also been checked on subsequent flights with good agreement.

Another objective of flight 1043W was to determine film temperature characteristics of StratoFilm 340, "K" and "W" films. Frames of balsa wood in 10-in. cubes were covered with the films of interest, and a Yellow Springs precision beam thermistor mounted in the center of each. These cubes were mounted on a 12-ft wooden boom to place them outside the convective stream from the parachute and gondola. An unshielded thermistor to measure ambient air temperature was mounted upright on the end of the boom. An unshielded thermistor was suspended from the apex fitting approximately 20 ft below the top to measure helium temperature inside the balloon. Each thermistor was calibrated with its bridge circuit and the temperature indicators periodically photographed in the photo panel assembly. Sampling was approximately once per minute. The panel incorporated an Acutron Clock for real time reference and a Wallace and Tiernan Gauge for altitude reference. Altitude was also telemetered from the Winzen RBA-6 barotransmitter.

The cubes covered with film were equipped with a small flapper appendix and filled with dry helium to prevent the inclusion of water vapor from affecting the results.

The one-hour float at ceiling before ballasting was apparently not sufficient to allow stabilization of the helium temperature as desired. The convective heating of the helium from the balloon film has a much longer time constant than was anticipated. It is therefore apparent that during transient conditions the balloon is primarily responsive to changes in air temperature fields rather than to helium temperature changes from film heating or cooling. The helium temperature is responsive to adiabatic expansion or compression. This is particularly apparent in the small models where there was overboard venting and the volume so small that free convective heating of the helium by the film has a very short time constant leading to temperatures above balloon helium and free air temperature. If the flight had been allowed to proceed at float for a longer period of time, the helium temperature of the balloon should have approached that of the StratoFilm 340 model.

All temperature data was tabulated in 1-min intervals and each plotted curve on 100432 graph was from a running average of 5 readings for smoothing purposes. It is assumed that in-phase cycles of free air and helium temperatures were actual temperature field variations and they affected ascent rates. Out-of-phase cycles of free air and film temperatures, however, probably were shadow effects from the boom and/or parachute during system rotation.

It was concluded that there was no significant difference in stabilized radiation temperature characteristics between StratoFilm 340, polyurethane, and nylon films. Further such tests will be conducted to confirm or alter this conclusion under various atmospheric conditions.

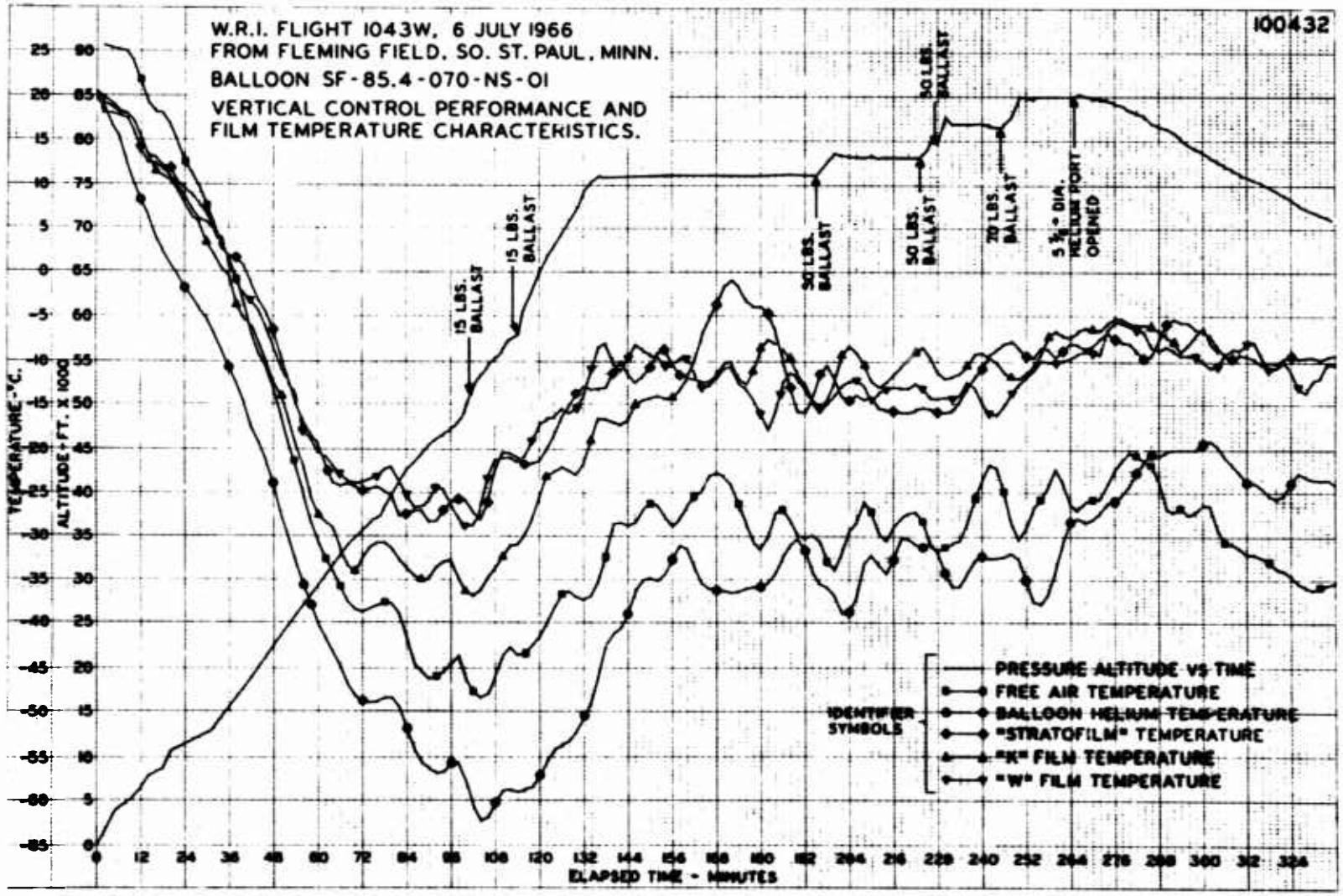
W.R.I. FLIGHT 1043W, 6 JULY 1966
FROM FLEMING FIELD, SO. ST. PAUL, MINN.
BALLOON SF-85.4-070-NS-01
VERTICAL CONTROL PERFORMANCE AND
FILM TEMPERATURE CHARACTERISTICS.
100432
15 LBS. BALLAST
15 LBS. BALLAST
50 LBS. BALLAST
50 LBS. BALLAST
50 LBS. BALLAST
20 LBS. BALLAST
5 ½" DIA. RELEASE PORT OPENED
TEMPERATURE - °C.
ALTITUDE - FT. X 1000
ELAPSED TIME - MINUTES
IDENTIFIER SYMBOLS
PRESSURE ALTITUDE VS TIME
FREE AIR TEMPERATURE
BALLOON HELIUM TEMPERATURE
"STRATOFILM" TEMPERATURE
"K" FILM TEMPERATURE
"W" FILM TEMPERATURE

XIV. Balloon-Borne Instrumentation

Chester G.R. Czepyha, Lt Col, USAF
Air Force Cambridge Research Laboratories
Bedford, Massachusetts

Abstract

A few of the more important recent developments within AFCRL in the field of balloon instrumentation for command and control and safety of flight will be presented. Included will be a discussion of recent flight results of both the UHF communications relay on a balloon carrier in the Holloman Air Force Base area and the prototype VHF-HF omnidirectional balloon locating system carried aboard long duration/distance flights from Chico, California. A further area of significant interest will be a discussion of lightweight and economical radar reflectors for attachment to balloons to insure a sufficient target cross-sectional area for adequate radar balloon tracking at all times.

1. INTRODUCTION

I would like to present, briefly, a few of the more important recent developments within AFCRL in the field of balloon instrumentation, and to mention a few of the plans for future development. Since the allocated time is rather short, I propose to limit my coverage to two principle areas in which significant progress and interest have generated, plus a third general status area as a catch-all.

Specifically, I will present information on the recent use of the UHF radio communications relay on a balloon carrier, and the location of balloons by means of onboard VHF-HF equipment.

2. VHF-HF OMNIDIRECTIONAL BALLOON LOCATING SYSTEM

The VHF-HF omnidirectional balloon locating system, which utilizes the signals generated by standard FAA navigational VOR stations located throughout the United States, was described in some detail during the 1965 AFCRL Scientific Balloon Workshop. The operational prototype system, Figure 1, was delivered by Zenith Radio Corporation earlier this year and has been flown on seven flights from the AFCRL Balloon Launch Site at Chico, California, during the period 11 March 1966 through the present. As delivered by Zenith, the prototype units provide a selectable 15- to 120-min readout cycle with a choice of either 3, 4, 5, or 6 channels per cycle. Twelve of 80 available frequencies in the range of 108.00 to 117.90 MHz may be selected for scanning on any particular flight. The HF telemetry output provides a Morse code signal identifying the preselected channel and the associated bearing information. A complete readout requires 38 seconds per

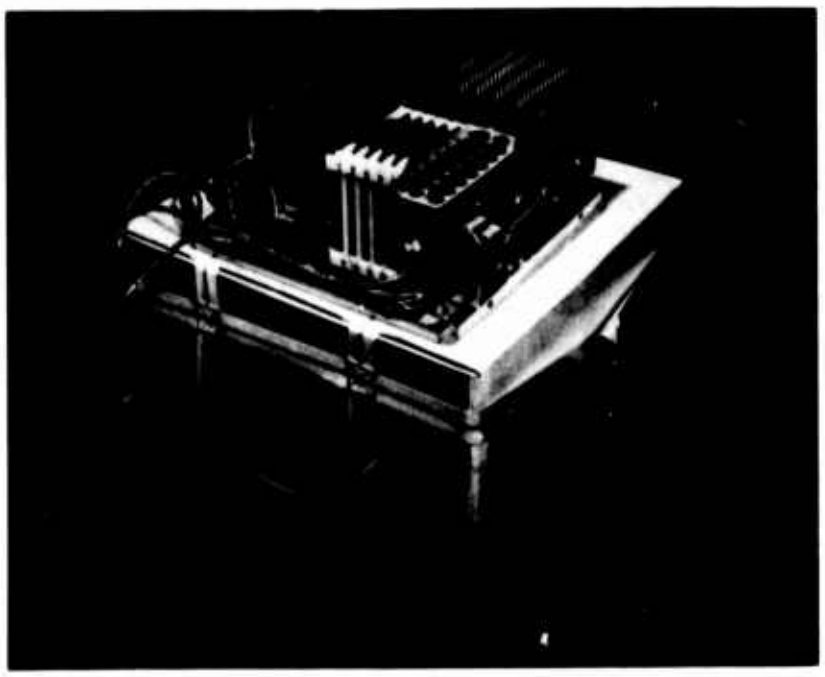

Figure 1. VHF-HF Omnidirectional Balloon Locating System

channel, 25 seconds for station lock-on and stabilization plus 13 seconds for information transmission. Weight of this full system is 66 lb, with 39 lb being the VOR detection and coding system itself, and the balance being support equipment. In addition, power adequate to support the length of the mission must be added. The unit requires +28 VDC for the positioning portion and -12 VDC for the data transmitter and command receiver units, 2.2 amps operating and 180 ma standby.

The first two of the seven previously mentioned flights, C66-5 and C66-9, were long duration, 105,000-ft altitude tests flown specifically for flight acceptance of the prototype units. The first trajectory as shown in Figure 2 ran from the launch site at Chico, California, through Nevada and Utah to Southeast Colorado, while the second ran from Chico, through Nevada, Utah, Wyoming, and South Dakota to Northeast Nebraska. Of the roughly 100 fixes obtained during these two flights, approximately 83 percent fell within the desired 5 nautical miles accuracy, an additional 9 percent were within 10 miles, and the balance were essentially unplottable because of parallel lines of position and weak signal areas. It is important to realize that these essentially unplottable fixes are a recognizable transient and short-time effect condition. As the balloon continues along its flight path, new stations become available, lines of position become more favorable, and the normal fix accuracies will become evident. All fixes were plotted by using special tables of latitude and longitude crossings versus VOR station signals which were developed by AFCRL specifically for this purpose. The remaining five flights were in support of routine operations, but also served to familiarize station personnel with the system operating procedures.

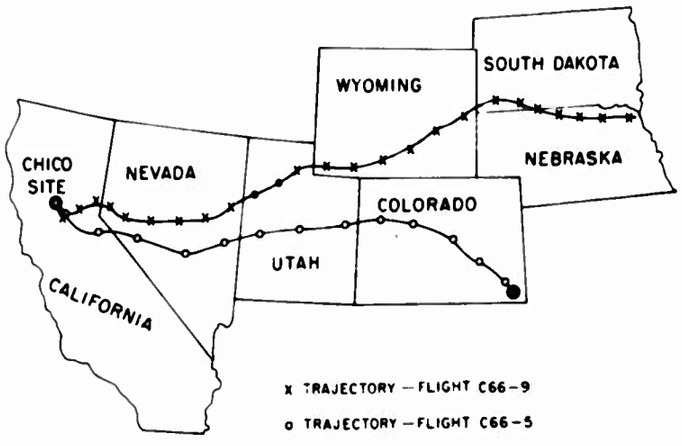

Figure 2. Balloon Locating System Flight Tests C66-5 and C66-9

A summary of flight data indicates that the system can be programmed w. ' three frequencies to give 5-mile accuracy when the flight is to remain within 400 miles of the launch area. As the flight area increases, additional frequencies must be programmed, up to the point where 10 to 12 frequencies will adequately cover the entire United States with the same accuracy. This same flight data has been used to formulate design criteria for the development of an operational system of smaller size, lighter weight, reduced power consumption, and a faster data acquisition and telemetry readout.

3. THE UHF COMMUNICATIONS RELAY

The UHF communications relay, Figure 3, was developed for AFCRL by Sylvania Electronic Systems. When included as part of the balloon-borne instrumentation package, it will extend UHF two-way communications to far beyond the normal ground/ground line-of-sight distances. Actual horizontal range radius, of course, will increase with altitude of the balloon carrier. At a nominal 80,000-ft balloon-float altitude, the extended line-of-sight distance is approximately 340 nautical miles. This means a maximum ground/ground communications distance of 680 miles if one assumes the balloon carrier located at the midpoint between ground stations. With this unit, aircraft and/or surface recovery units will have a reliable communications link with the balloon control center in order to properly coordinate the necessary actions and events that occur during a balloon mission.

The UHF relay has both the receiver and the transmitter included in a single package. An added feature allows external modulation inputs and transmitter keying capabilities in order to allow the transmitter to be fed from a separate receiver if desired. A power switch on the front panel disables the receiver when an external receiver is used. When in normal operation, the relay transmitter is turned off internally unless a signal is received. Any received signal keys the transmitter. When the received signal disappears a delay circuit keeps the transmitter operating for a fraction of a second. This feature makes it possible for a ground operator to determine whether the repeater is in range and operating by listening to the "tail" of the repeater when he momentarily keys his ground transmitter. The standby feature was included to conserve battery power. Input power required is 3 amps at 28 VDC during a transmission, and 200 ma during standby. Power output is 20 watts pep, or 6.8 watts average with 85 percent modulation. Total weight, less batteries for power, is 11.5 lb.

One successful limited flight has been accomplished with the AFCRL equipment to date. This was a piggy-back experiment; and so, unfortunately, relay testing played a secondary role to the accomplishment of the primary flight objectives.

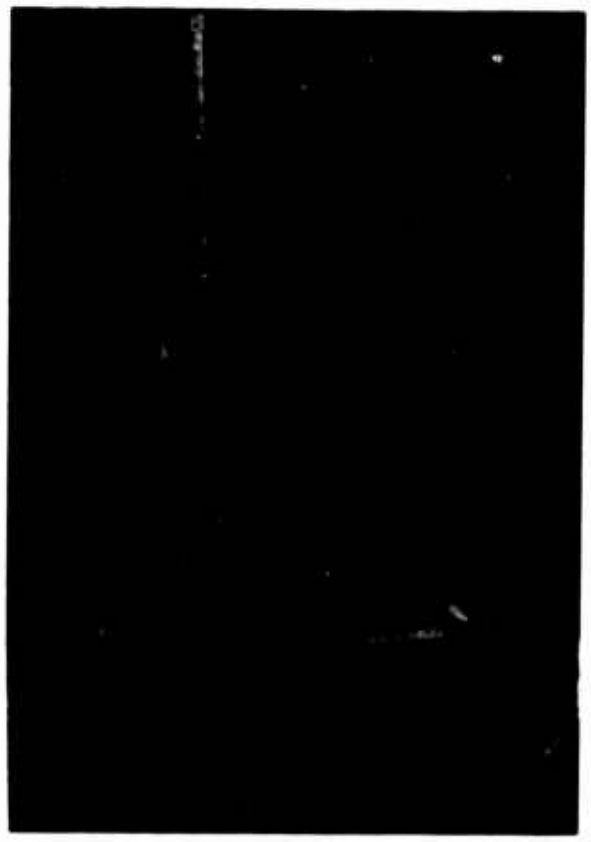

Figure 3. UHF Communications Relay

This test, balloon flight No. H66-69 from Holloman AFB, New Mexico, was a short-duration flight to 59,400 ft altitude, with total flight duration of 56 min to float, 8 min at float, and 18 min descent on the recovery parachute. Communications links for voice existed between mobile vehicles with relatively low power URC-54 portable transceiver equipment, Figure 4, at both Holloman and Artesia, New Mexico, the Command Center at Holloman, and a Range Support Monitoring Station of the U.S. Army Electronic Proving Ground at Fort Huachuca, Arizona, Figure 5, all through the balloon-borne radio relay. Ground transmissions were on 316.9 MHz, balloon-relay transmissions were on 261.7 MHz. Fort Huachuca is located 230 nautical miles WSW of Holloman. Artesia is located 80 nautical miles East of Holloman. Both Fort Huachuca and Artesia are separated from Holloman by mountain ranges of approximately 10,000-ft elevations. Sufficient time existed on this flight to verify adequate communication via all links as the flight system was ascending to float, at float, and during the initial portion of the equipment's descent on the recovery parachute. Communications were perfectly clear at all times for maximum range while the flight system was above 35,000 ft.

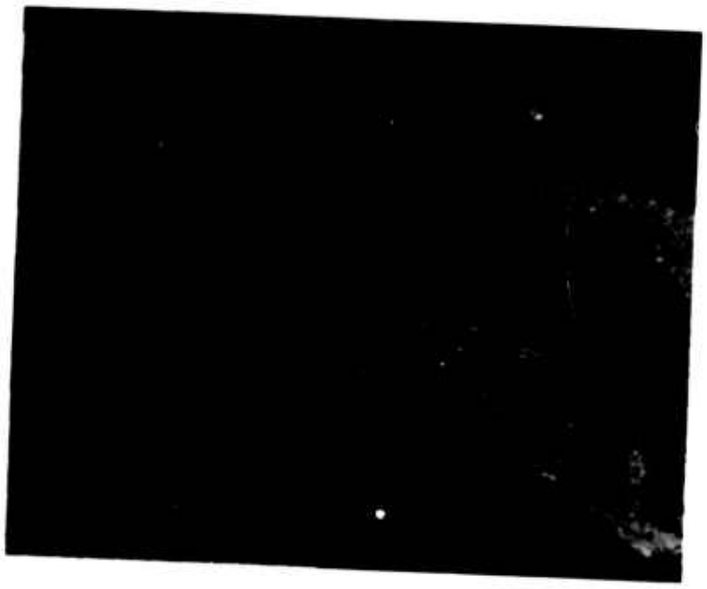

Figure 4. URC-54 Portable Transceiver Equipment

Figure 5. UHF Communications Relay Flight Test H66-69

Earlier tests of similar equipment were conducted by Rome Air Development Center during the period 5 November through 7 December 1965. These tests involved aircraft, drones, and balloons as the relay carrier vehicles, and covered aircraft altitudes of 18,000 ft, drone altitudes of 52,000 ft, and balloon altitudes of 80,000 ft. The results definitely showed the feasibility of using the system with various carriers to meet the specific requirements.

The applications of this equipment, of course, go much beyond the present balloon command and control usage. Our own applications need suffer no longer from lack of communications between control center and recovery ground units, nor between tracking aircraft and either ground recovery vehicles or the control center. Wartime applications could provide ground commanders at all echelons with the clear longer range communications so essential for coordinated campaigns of any magnitude.

4. GENERAL

I will mention a few other smaller but nevertheless important recent advances in instrumentation equipment. Further information concerning these will be available from any of the instrumentation personnel.

(a) One area of research is directed towards the study and development of more efficient balloon-borne antennas for use on high-altitude scientific balloons for the purposes of better control and tracking. The desired result will be a non-deployable, structurally simple antenna design having a controlled directional radiation pattern towards the horizon which is not affected by the balloon-borne scientific payloads. This work has been proceeding since February of this year under an Aerospace Research, Inc., development contract. What appears most promising is a dipole made of two flat sheets of 1-in. mesh screening, Figure 6, with a center balun interface 28-ft long and 5.7-ft wide. This would be suspended below the skirt of the recovery parachute, rolled compactly as a window shade until the parachute is fully extended for launch, then extended to its full length prior to balloon release.

(b) A second area of interest is the development of an FM wireless balloon control subsystem to control various functions at the apex of a balloon. This will augment the standard AFCRL command and control equipment and will allow command switching information to pass to the upper portion of extremely large balloons without the installation of special external wiring along the surface of the balloon as is now required. This work is proceeding on schedule since April under a development contract with the Aerospace Research, Inc., and the first units are expected for flight during the last quarter of CY-66.

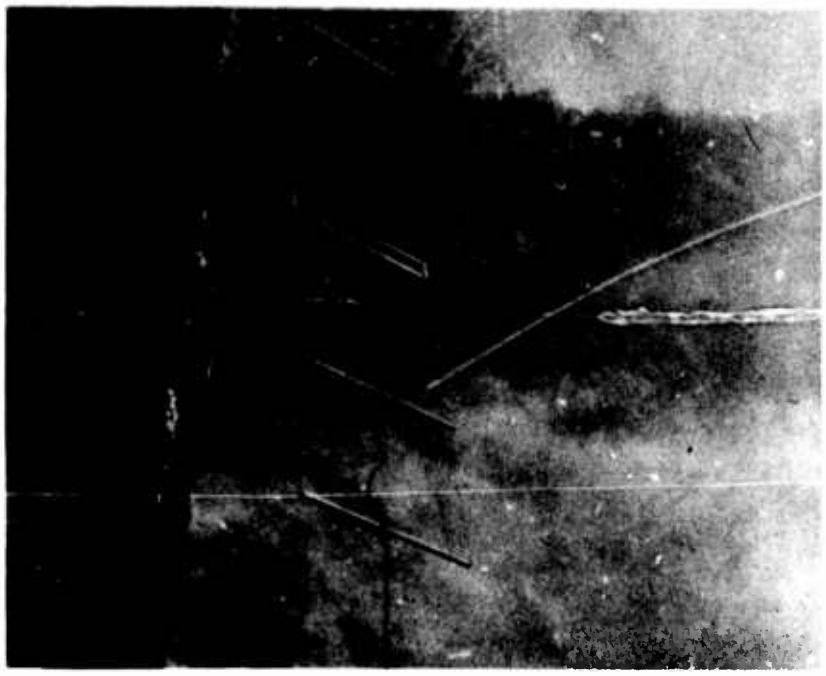

Figure 6. HF Dipole Screen Antenna

(c) An in-house effort has been directed towards the development of a reversible control unit in which it is possible to reprogram timer durations during flight via radio command. This unit has been flight tested satisfactorily and is in general use at this time for those flights where the potential reprogramming requirement exists.

(d) An area of strong interest recently has been that of insuring reliable radar tracking of balloons, both during flight and after separation of payload and balloon. Considerable in-house effort has been directed to the study and test of several forms of radar reflectors and a suitable method of attachment of these reflectors to the balloon in order to assure sufficient target area from all radar-viewing profiles. One system involved the in-line encasement of dipoles along several 16- to 20-ft lengths of tape (Figure 7) which would then be attached to the balloon apex. These dipoles would be randomly cut to bracket known radar frequencies in the area. A second system involved lengths of ordinary aluminum foil attached to the balloon as in Figure 8. Although both of these methods gave increased radar signals, the most promising was a third system which was an accordion-folded reflector of polyethylene-encased standard household aluminum foil, as indicated in Figure 9. When fully extended, this becomes a 10-ft length of spiraling corner reflectors. This has been attached to the sides of balloons in flight tests, but the best and safest mounting positions are at the base of the balloon.

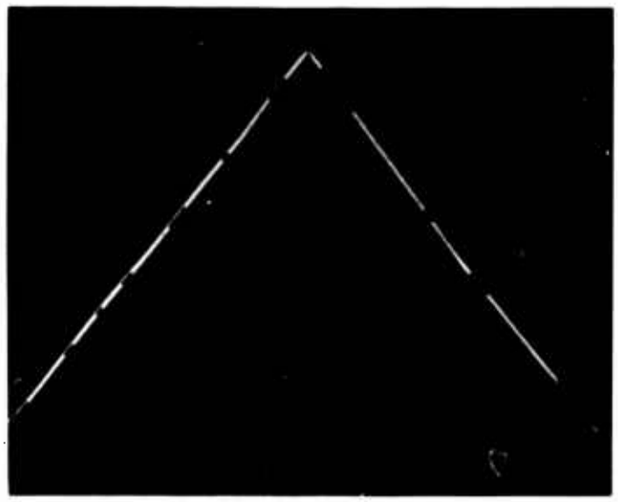

Figure 7. Dipole Radar Reflector

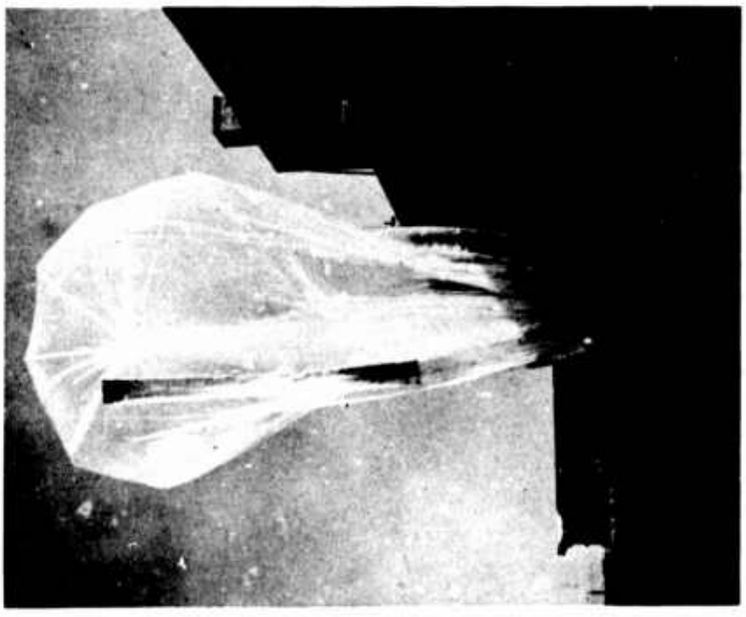

Figure 8. Flat Aluminum Foil Radar Reflector

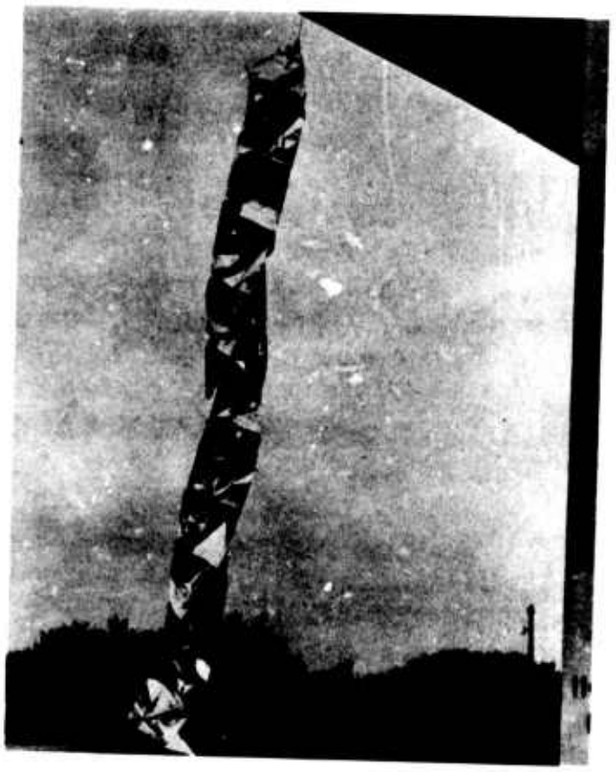

Figure 9. Accordion-Folded Aluminum Foil Radar Reflector

Reports from ground radar operating personnel indicate that the return from this system approximates that from a large airplane. Lightweight, economical, and easy to fabricate in the field for the attachment to all balloons, this system will insure sufficient target cross-sectional area for adequate radar tracking.

XV. Problems Encountered in the Development of the Stratoscope II Flight System

G.C. Ellerton, Jr., and J.P. Jackson
Vitro Laboratories
Silver Spring, Maryland

Abstract

The balloon development phase of the Stratoscope II Program began in the Fall of 1960. At that time, the design of the telescope was, for all practical purposes, complete and fabrication was in progress. Flight system requirements were established with certain limitations imposed by the instrument design. It was immediately obvious that Stratoscope II requirements were pushing the state-of-the-art in ballooning and that some pioneering in the development of heavy-load high-altitude techniques would be necessary. The principle problems encountered during the balloon development phase were related to and grew out of the sensitivity of the Stratoscope II telescope to ground handling, launching and recovery shocks; the requirement for a night flight; the unprecedented weight of the payload; the need for a reasonable standby time when the system was flight ready; and, the need for a single all-year-round launching site. Problems were approached and solved during a period of analysis, design, fabrication, laboratory and actual full-scale field tests culminating in a fully instrumented scientific flight in March of 1963. Since that time, the flight system has been under continuous review and modification to improve its reliability.

1. INTRODUCTION

In 1960, Princeton University, under the sponsorship of the Office of Naval Research, National Science Foundation and National Aeronautics and Space Administration, issued a Request for Quotations on the management of the Stratoscope Flight Program. It was the intention of Princeton and the sponsors to employ an engineering management firm to handle the development of a flight system capable of lofting the Stratoscope II telescope to 80,000 ft and to manage the flight operations.

Vitro Laboratories was successful in winning the contract and we commenced our assignment in September 1960. The job involved, among other things, a survey of the balloon development situation to determine whether or not we could handle the heavy load to the 80,000-ft ceiling with state-of-the-art hardware. The assignment also required that we investigate various methods of launch and recovery including a study of possible operations from land as well as on the sea. It became immediately obvious that no balloon system was readily available on the shelf to do the Stratoscope job and this led us into direct contact with the balloon manufacturers in our investigation of the state of development of balloon fabrics.

Our problems commenced immediately in 1960 and some still remain as a challenge. In the short space available, I hope to present some of the more interesting problems encountered in developing the Stratoscope II flight system and operational techniques.

2. PROBLEM SOURCES

There were five major sources of problems stemming from a set of conditions associated uniquely with the Stratoscope II Program as listed in Figure 1. Each of these problem sources is discussed briefly here with the specific problems and their solutions covered later in this paper.

(1) Sensitivity of Stratoscope II Telescope to Ground Handling, Launching, and Recovery Shocks

Princeton University specified that the telescope should receive no greater than a one-third Δ-g acceleration during ground handling and launch. It was a further design goal that the telescope be subjected to no greater than a 2-g shock on landing.

It was also a requirement that the launching and handling system place no horizontal loads on the telescope structure. To minimize turn-around time between flights, it was desirable to have the telescope land with as little damage as practicable; and, therefore, the landing shock limitation of 2-g was considered reasonable.

1. SENSITIVITY OF STRATOSCOPE II TO HANDLING
   - HANDLING AND LAUNCHING VEHICLE
   - STATIC LAUNCH SYSTEM
   - CONTROLLED DESCENT
   - IMPACT SHOCK ABSORPTION
   - AUTOMATIC BALLAST JETTISON
   - TELESCOPE IMPACT ORIENTATION
2. REQUIREMENT FOR NIGHT FLIGHT
   - LAUNCH TIMING
   - CAREFULLY CONTROLLED ASCENT
   - NIGHT TRACKING
   - LATE AFTERNOON BAD WEATHER
3. UNPRECEDENTED WEIGHT OF PAYLOAD
   - BALLOON DESIGN
   - BALLAST LIMITATION
   - HIGH STRENGTH MATERIALS
4. NEED FOR SHORT STANDBY TIME
   - HIGH WIND SPEED CAPABILITY
5. ALL YEAR-ROUND LAUNCH SITE
   - PROXIMITY OF GULF OF MEXICO – WATER IMMERSION, CLOUDS

Figure 1. Stratoscope II Flight System Development Engineering Problems

(2) Requirement for Night Flight

The Stratoscope II telescope was designed for night observations only. The astronomers desired the maximum observing time; and, therefore, it was essential to plan the launch and ascent phase of the flight system to allow arrival of the telescope at altitude as close to sunset as possible. This requirement, coupled with the necessity to limit overall system weight wherever possible (for example, sunset ballast), posed problems associated with careful timing of the launch and careful controlling of the ascent phase to accomplish sunset on the balloon just prior to reaching ceiling. The night flight added problems associated with night tracking and control and it forced the balloon preparation, inflation, and launch phases into the bad weather portion of the day.

(3) Unprecedented Weight of Payload

At the inception of the Stratoscope II Program, the anticipated payload was heavier than any which had been carried to high altitudes on a plastic balloon. This heavy weight of payload had its effect on increasing the weight of the entire system to the unprecedented gross lift of 16,000 lb. These heavy loads resulted in great stresses on both balloon material and balloon rigging including ancillary equipment such as winches, cables, release mechanisms, and so forth. Equipment to handle these heavy loads was not readily available and much of it had to be developed for this program.

(4) Need for Short Standby Time After System is Flight Ready

The large layout of personnel and equipment needed for a Stratoscope II flight meant high standby costs. Also, the requirement for precooling the telescope's

primary mirror was anticipated to involve a significant technical effort continuously during the days waiting for adequate launch weather. Therefore, it was necessary to develop a system which could be launched as soon after being flight-ready as practicable. This meant the possibility of launching in surface winds higher than had ever before been considered safe for a static launch.

(5) The Need of Single All-Year-Round Launching Site

Dr. Schwarzschild desired to fly the Stratoscope II without restrictions as to time of year. This necessitated search for a launching site that could be used throughout the year. The final location of this site presented its own set of problems associated with the proximity to the Gulf of Mexico.

3. PROBLEMS RESULTING FROM SENSITIVITY OF STRATOSCOPE II TELESCOPE TO GROUND HANDLING, LAUNCHING, AND RECOVERY SHOCKS

3.1 Handling and Launching Vehicle

The delicate nature of the telescope and its unique physical configuration posed problems in handling and launching. The handling problem was solved with a conventional cargo-type trailer modified to hold the telescope upright while being moved from the Stratoport (telescope shelter) to the launch site and to retain it in this position until launch. As insurance against jolts resulting from sudden loss of air in tires, the trailer is equipped with three axles and six tires.

To protect against damage at launch, the telescope is supported on two-hinged tripods. Just prior to balloon release, locking pins securing the tripods to the trailer floor are removed permitting the supports to hinge outward if the telescope sways on take-off. This has happened occasionally in actual take-off situations with no ill effects.

The combination transportation and launching vehicle is shown in Figure 2 with the telescope secured in the launching configuration.

Salient features of the launching vehicle include:

Tripods
Hold-down anchors at each end of the beams
Hold-down cables
Canvas chute to hold suspension rigging.

The vehicle was designed to double as a recovery trailer. After launch, all launching appurtenance can be unbolted and removed in a short time to make the trailer available for recovery operations after impact.

3.2 Static Launch System

The fragileness of the Stratoscope II telescope dictated a static type of launch. Dr. Schwarzschild realized at the very beginning of the program the telescope could

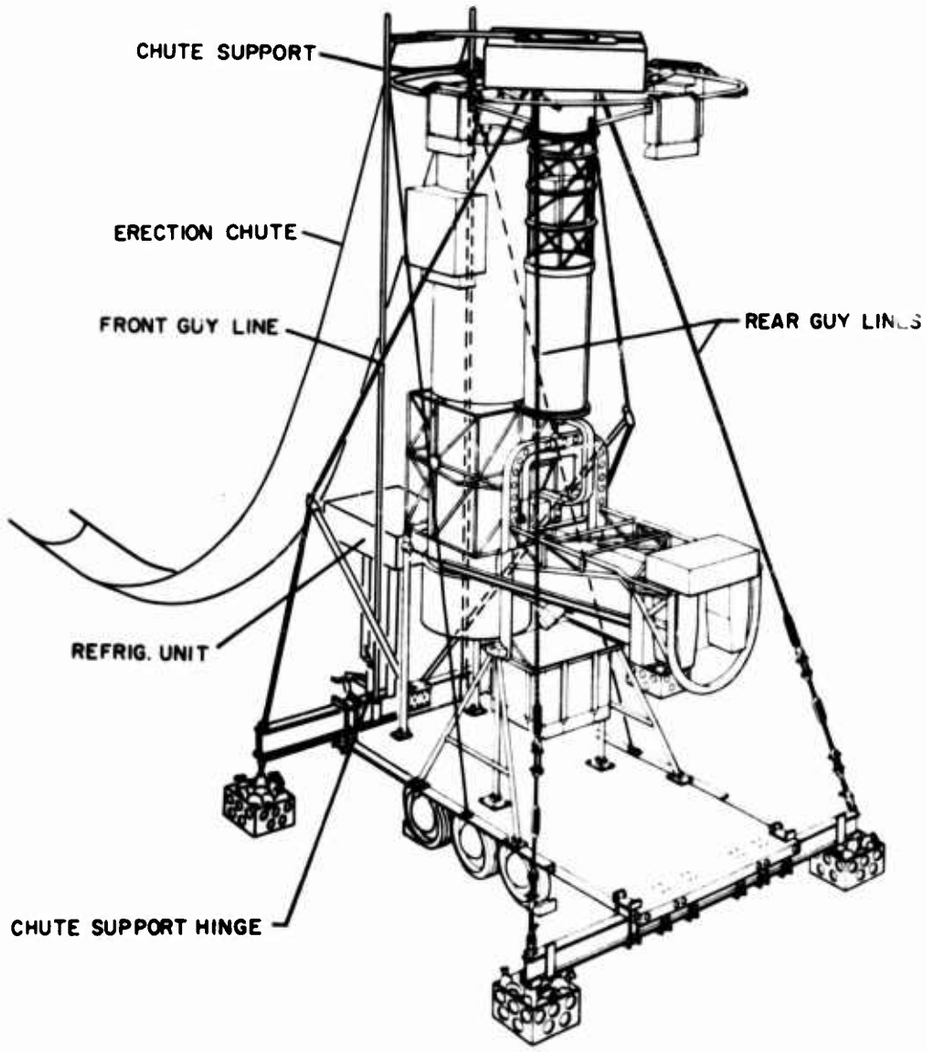

Figure 2. Stratoscope II Telescope on Launching Vehicle

not stand the accelerations to be expected from the normal dynamic launch method. This requirement for a static launch was in opposition to our desire to provide a system which could be launched in relatively high winds.

After a number of discussions with the various balloon companies, Air Force personnel at AFCRL and representatives of the Office of Naval Research, it was decided to develop a static launch system using a mainstay to hold the balloon until launch. The tandem balloon design patented by Otto Winzen and Verner Suomi in 1959, appeared to be a good starting point for our development since it offered an attachment point for the mainstay.

Early in the program, we agreed on an upper surface wind limit of 20 mph for launching and 15 mph for inflation. The concept of launching the system statically in winds up to 20 mph required sleeving of the main balloon to prevent sailing during system erection and while retaining the system in the launch configuration before release. The 15 mph upper wind limit associated with the inflation also presented a problem of what to do with the uninflated portion of the launch balloon in the early stages of inflation. Consequently, the launch balloon was also shrouded with a sleeve fabricated for easy removal as the launch balloon inflation progressed. To hold the entire system in a 20 mph ground wind when inflation was completed required that we keep the aerodynamic drag to a minimum. Therefore, the launch balloon was designed to be as completely inflated as practicable while still on the ground. Thus, the launch balloon presented a fairly reasonable aerodynamic shape to the surface winds with a minimum of undeployed material which could possibly sail.

Figure 3 shows the Stratoscope II system in the launch configuration. The mainstay is used to tether the system during inflation and erection. Prior to actual release, the mainstay is used to pull the entire system up-wind about 10°. This technique puts sufficient tension in the mainstay to insure that it springs well clear of the payload. This angle also insures that in winds up to 20 mph there will be sufficient tension on the balloon train and at the top of the telescope to reduce shock loads to tolerate limits at time of mainstay release.

The length of the mainstay has also been chosen to provide this equitable distribution of tension between the mainstay and the balloon train below the center fitting. After release of the mainstay, the flight system moves to an erect position vertically over the payload. At this moment, the hold-down cables are released.

3.3 Controlled Descent

The weight of the telescope and its requirement for careful handling suggested some type of descent from altitude which would insure minimum damage on impact. Parachute descent as a primary means of recovery was ruled out early in our considerations. To attain the descent velocity we desired would require an extremely large parachute canopy area. Furthermore, the parachute descent from ceiling altitude provided very limited control over the selection of an impact point. It was decided to attack this problem by using a valve-down technique in conjunction with helicopters to assist in the actual impact. The concept involved valving the balloon to approximately 5,000 ft above the ground at which point helicopters or a large single helicopter would take the system in tow. It was intended that the helicopters be used to cancel out the horizontal velocity due to wind and hold the balloon system over a desirable landing point while it was valved vertically to impact.

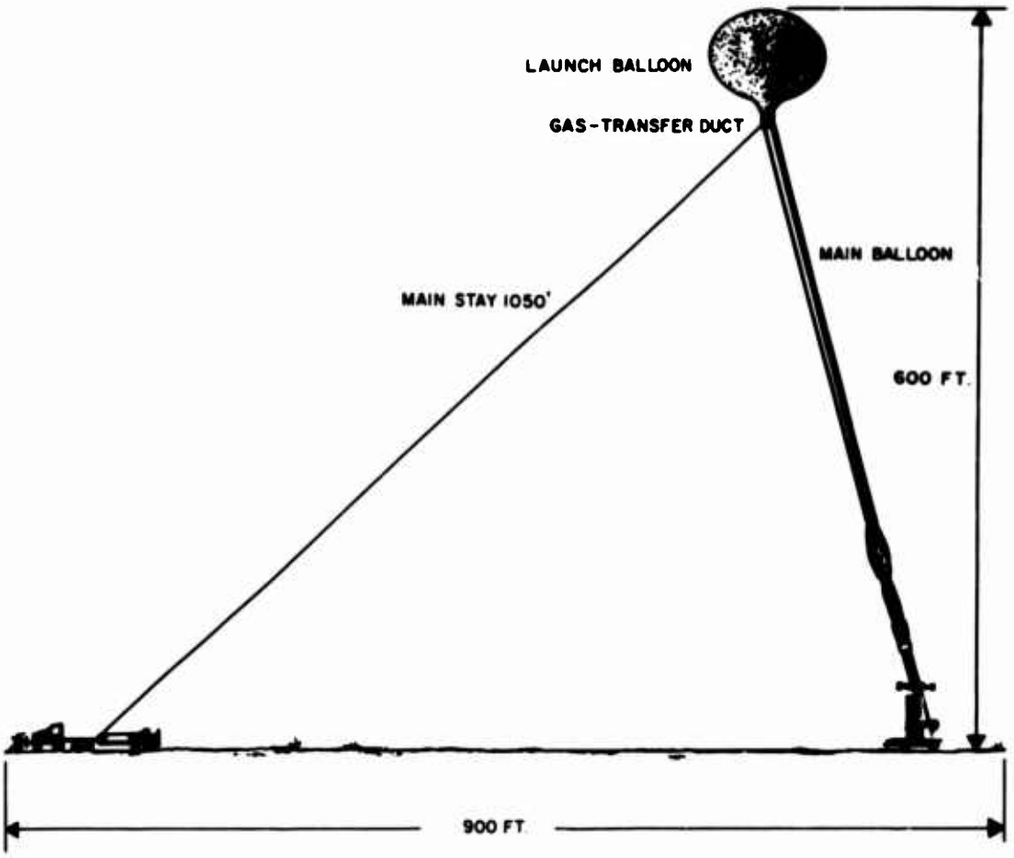

Figure 3. Stratoscope II Launch Configuration

A helicopter attachment and towing system was developed and given preliminary tests with both large and small helicopters. Although this system still appears feasible from a technical point of view, the nonavailability of large helicopters forced us to abandon it. After eliminating the helicopter-assist recovery program, it was decided to valve the balloon from ceiling altitude to impact as the primary means of recovery. This procedure requires the valve to be opened until the balloon acquires a descent velocity of approximately 300 ft/min above the tropopause. Upon penetration of the tropopause, the balloon acquires a velocity of about 750 ft/min. The goal is to achieve a descent rate of about 600 ft/min at impact. This method of recovery provides very little control over the impact point but it does permit us to control the descent sufficiently to avoid large metropolitan or other undesirable landing areas.

Our control consists of selecting the proper duration for valve opening and controlling the descent velocity with valves and ballast. To prevent a rebound of

the system after impact, we have installed switches on the bottom of the crash pad to initiate the opening of the top of the launch balloon. Thus, on impact, the gas is jettisoned quickly from the launch balloon and lift is lost immediately.

3.4 Impact Shock Absorption

Another problem associated with the delicate structure of the telescope involved the design of a suitable shock absorption system. In a paper presented at the Scientific Balloon Symposium in September 1964, Mr. J.P. Jackson of Vitro, provided a detailed outline of our efforts in approaching this problem. In brief, we investigated many methods for cushioning the impact of the telescope and finally chose the one now in use. This consists of a crash pad of Armstrong Armalite attached to a honeycomb flooring which in turn is secured firmly to the structure of the telescope azimuth frame. The crash pad is designed for optimum efficiency when the impact velocity is 600 ft/min. The vertical deceleration on impact at the descent velocity has been observed to be between 2 and 3 G's.

Figure 4 depicts the Stratoscope II crash pad attached to its floor. Although we proposed it for Princeton's consideration, it has been decided not to provide shock-absorbing devices to protect the telescope when it falls over after landing. Our experience shows that the inertia ring to which the ballast hoppers are attached provides a certain measure of shock absorption for the instrument when it topples after vertical impact.

3.5 Automatic Ballast Jettison

To further assist in limiting impact shock, it was decided to make every effort to eliminate all ballast prior to actual impact with the ground. This is normally accomplished by radio command from the primary control station. We wanted to provide for dumping of ballast in the event of descent by parachute when we no longer have radio command. We, therefore, designed a switch circuit which automatically opens the ballast valves whenever the payload and its parachutes separate from the balloon. When the payload and parachutes separate from the balloon, power from the instrument package, which remains with the balloon, is removed from a relay on the telescope. When the relay loses power, its contacts close to connect all ballast valves to an auxiliary battery carried on the inertia ring of the telescope.

3.6 Telescope Impact Orientation

The unique configuration of the Stratoscope II telescope presented several landing orientations which could be severely damaging. Since we had no control over the rotation of the balloon system during descent and since we had to assume there would be some horizontal velocity on impact, we investigated means for

orienting the telescope prior to impact. The solution to this problem was the development and fabrication of a side-arm orientation system. This system comprised three major parts: the decoupling swivel; the direction sensing unit, and the thrust fan. The basic element of the direction sensing unit is a magnetic compass modified to provide photocell tracking of the north point of the compass card. When the proper wind angle is sent in by radio command from a control station, a reference direction is established.

A swivel connects the upper part of the telescope suspension lines to the parachute rigging. When the system is activated by command below 30,000 feet, the swivel is unlocked permitting the telescope to rotate freely with respect to the balloon. At this time an electric motor drive propeller drives the telescope around to the most favorable landing orientation. This orientation is established before launch and is normally with the telescope's side-arm trailing at impact. In still air, the side arm will complete its orienting cycle in about four minutes from its maximum displacement position of 180°. Wind angle is set by radio command on the basis of the latest meteorological information available at the impact site. This setting can be checked at any time by radio command to the balloon which initiates the telemetry sequence to transmit the data to the ground station on the balloon beacon frequency.

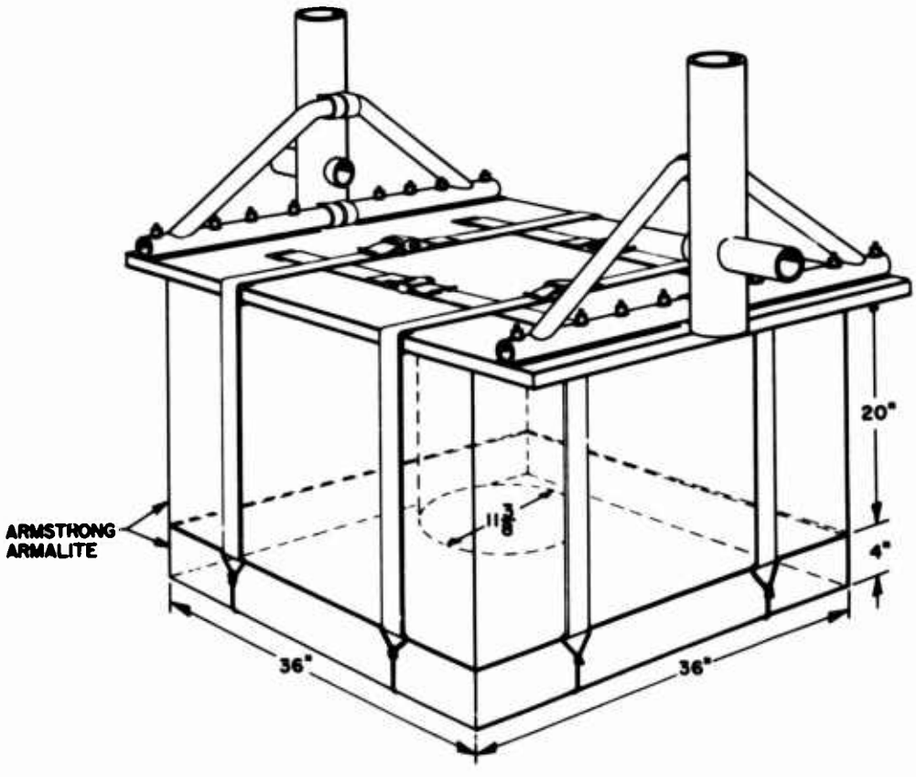

Figure 4. Stratoscope II Crash Pad

The orientation system is automatically activated at 30,000 ft when descending on parachutes.

4. PROBLEMS RESULTING FROM REQUIREMENT FOR A NIGHT FLIGHT

4.1 Launch Timing

Timing of the Stratoscope II launch is influenced by two major factors. One is the requirement for the telescope to be at altitude as nearly after sunset on the balloon balloon as practicable in order to provide the maximum observing time for the astronomers. The other factor is related to overall system weight. To conserve weight, we have eliminated sunset ballast by programming the ascent to have the sun set on the balloon just prior to arrival at ceiling. This requires careful timing of launch if we are to achieve sunset on the balloon just prior to arrival at ceiling and also provide a rapid ascent. If we select an early launch time with a slower ascent rate, we incur the difficulties associated with a longer trajectory. If we select a later launch time, we will have the sun setting on the balloon early in the ascent which would delay arrival of the balloon at ceiling and thus shorten the observing time available to astronomers. Therefore, a relatively narrow launch window is available. The practical attainment of a launch within this window is accomplished by careful programming of all launch preparation activities to decrease the probability of a delay at the critical time. The demand for a precise launching time also presents the problem of insuring a predetermined ascent rate. This has been accomplished using actual flight data along with a computer program to assist in determining the quantity of ascent ballast needed and the points where it should be dropped. These problems associated with a narrow launch window are relatively straightforward in their solution. However, they are mentioned here since many people have asked why we have selected the seemingly poor time of day for launching the Stratoscope II. It has been suggested we launch the system early in the day to avoid unfavorable conditions. I think I have explained that the resulting longer trajectory would be a disadvantage in that the telescope ground station telemetry is limited to about 200 miles. It has also been suggested that the system be released after sunset on the ground to avoid carrying sunset ballast but this would have the obvious disadvantage of shortening the astronomical observing to an unacceptable degree.

4.2 Carefully Controlled Ascent Program

In the preceding section, I mentioned the problem of carefully controlling the ascent phase of the Stratoscope system. After launch of the balloon within the rela-

tively narrow window, it is necessary to insure that the balloon does not reach ceiling before sunset but that it does undergo sunset during ascent. As a result of thermodynamic analysis of the balloon ascent phase and actual flight data, we had adopted a program of ballasting which seems to produce very satisfactory results. Five minutes after the balloon is launched, we drop 300 lb of ballast to counter the adiabatic bounce. When the balloon is at the calculated tropopause, we drop another 300 lb to overcome the slow-down effect of tropopause penetration. At sunset on the balloon, which is programmed to occur when the balloon is at about 65,000 ft, we drop the remaining ascent ballast of about 300 lb.

4.3 Night Tracking

The fact that the balloon requires tracking and controlling during the night presented only minor engineering problems. The problem of insuring positive control through the entire trajectory has been met by employing several airborne and ground tracking and control stations. A twin-engine aircraft is used as the primary tracking and control station with three vehicles prepositioned along the anticipated flight line as back-up stations.

4.4 Late Afternoon Bad Weather

In the foregoing sections I have explained the narrow launch window available and where it occurs during the launching day. This period in the afternoon is about the worst part of the day for balloon operations. This part of the day seems to abound in all sorts of meteorological disadvantages such as increased thunderstorm activity, maximum surface-wind velocity at the time of inflation and increased probability of cloud cover. We approached the problem of high winds by designing a system which can be inflated in 15 mph and launched in 20 mph winds. The physical configuration of the balloon system discussed in earlier sections of this paper alleviated, to a certain extent, the problem of late afternoon surface winds. To decrease the hazard from late afternoon thunderstorms and showers, the system has been designed to be under protective covering as long as possible. Up until the time erection commences, the main balloon and other parts of the balloon system below it are housed in their shipping boxes under water-repellent covers. In the event we are caught in a thunderstorm or rain squall after inflation starts, we may have to abort and lose the launch balloon but the remainder of the system is protected. The telescope is exposed a minimum amount of time since it is retained in the Stratoport until just prior to being required on the launch pad. The problem of increased late afternoon cloud cover is still a serious one but is alleviated somewhat by the relaxation of cloud-cover rules by the FAA when launching from Palestine, Texas.

5. PROBLEMS RESULTING FROM THE UNPRECEDENTED WEIGHT OF THE PAYLOAD

5.1 Balloon Design

At the outset of the program it was realized that the gross lift of this system would far exceed that of any previous high-altitude plastic balloon. Although polyethylene balloons of a size that would contain the required helium had been successfully flown to high altitudes, this material had not been proven in the really heavy load area. Therefore, a search for other balloon fabrics was initiated. Of all the various materials investigated, the G.T. Schjeldahl Company's laminate of mylar film and dacron scrim seemed to hold the most promise. This material has proven itself capable of handling the heavy Stratoscope II loads with high reliability. Problems encountered in the balloon development phase were never associated with a failure of the material itself. Problems encountered were associated more with the manner in which the material was secured in the balloon fittings and in the operational techniques of inflation. Some of the interesting problems encountered in the development phase of the balloon design are discussed in the following:

5.1.1 END FITTINGS

It was discovered early in the program that conventional fittings would not utilize the full strength capable of the scrim/mylar fabric. A redesign of the fittings to eliminate weak points was accomplished after a flight attempt failed because of material tearing away at the top fitting. A technique for attaching the balloon fabric to a hoop at each end of the balloon proved very successful. The hoop to which the material was attached was in turn held in a top or bottom fitting of more conventional design. Figure 5 is a sketch of the loop-seal method of securing balloon fabric to the end fittings. Tests to check the capability of this attachment procedure indicated very little loss of fabric strength at the end fittings.

5.1.2 SEALING OF SCRIM MATERIAL

The sealing of scrim material presented a problem in that it was difficult to prevent passage of helium around and through the actual scrim fibers when the scrim material was lapped at the joints. This problem was solved by butting the gore edges together with a plain no-scrim mylar tape secured to the smooth side of the balloon material for gas seal. On the outside of the seal where the gore edges butted together a scrim/mylar tape was secured to provide the strength bond between gores. This bi-tape seal technique solved the problem of helium leakage.

5.1.3 MULTIPLE INFLATION TUBES

The heavy weight of the payload and the associated balloon system meant a large volume of helium for initial inflation. To reduce the inflation time the balloon was

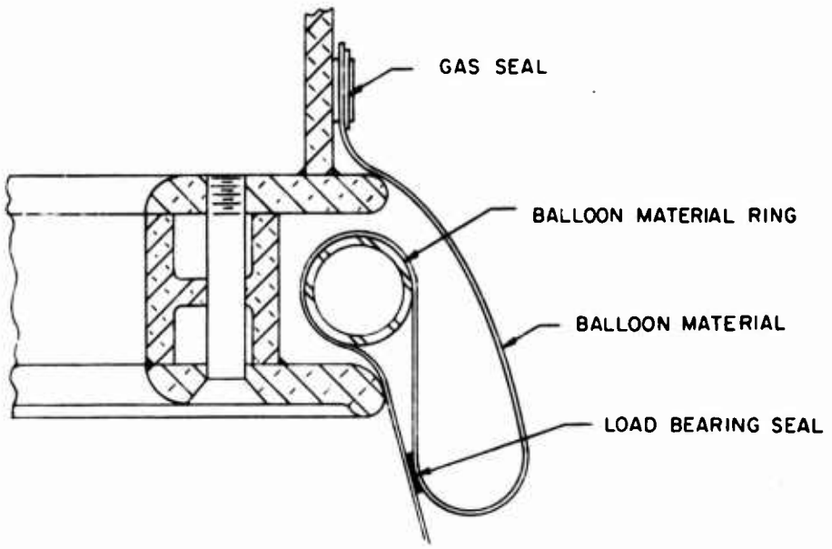

Figure 5. Loop-Seal End Fitting

designed with four inflation tubes. These inflation tubes were designed to pass helium from the high-pressure hoses to the balloon at the maximum rate available from the helium tanks.

5.2 Ballast Limitation

As the program progressed, the weight of the telescope increased. To keep the overall system weight to a practical minimum, we made every attempt to limit the ballast requirements. After the balloon system design was firm, the telescope increased further in its weight and this limited even more the quantity of ballast that could be carried. The problem was one of minimizing the need for ballast. The elimination of sunset ballast by launching just before sunset has been discussed in previous sections of this paper. The quantity of ballast for optimum control of the balloon system during the latter phases of its descent was estimated to be about 2500 lb at the beginning of the program. This weight of ballast was considered minimum for useful control of the balloon in selecting a desirable impact area. However, to further reduce the weight of ballast carried, it was decided to allow the balloon to descend continuously from ceiling to ground without pausing at some intermediate altitude for selection of a landing site. The present operational technique is to valve enough helium to attain an initial descent rate of 300 ft/min which increases to approximately 750 ft/min upon penetration of the tropopause without further valving. The ballast is used to adjust the final impact descent rate to

600 ft/min. This simpler procedure allowed us to eliminate a large portion of the ballast. The total ballast now used in the system is 2400 lb with the programmed use as follows: 900 lb for ascent; and 1500 lb for maintaining and controlling descent.

5.3 High Strength Materials

The heavy weight of the payload dictated high strength materials in the suspension system and the rigging used in restraining the balloon prior to launch. This high strength requirement tended to result in heavy rigging components thus increasing the overall gross weight of the system. Careful stress analysis of all portions of the system was conducted to eliminate excess weight due to over-design.

To insure safety of personnel and equipment, it was necessary to conduct a careful and thorough testing program of all equipments subjected to heavy strains. This included payload, suspension rigging, auxiliary stay, mainstay, and the various numerous fittings and release devices employed in the system. To keep the weight of the mainstay to manageable proportions, it has been found necessary to use a relatively light weight cable. As far as safety is concerned, the mainstay is operating well below its breaking load but the sudden release of tension at launch causes birdcaging which prevents its reuse as a mainstay.

6. PROBLEM RESULTING FROM NEED FOR A SHORT STANDBY TIME

As indicated earlier in this paper, a short standby time after Stratoscope II is ready for flight is desirable for both economic and technical reasons. Technically, it is desirable that the telescope system be flown within a reasonable time after reaching a full state of readiness to minimize problems resulting from deterioration in electrical and optical systems. In view of the large numbers of personnel required and expensive equipment needed in the operation, it is desirable to limit this costly day-to-day expense. The only factor contributing to a delay in launching after flight readiness other than equipment and technical problems is the weather. The problem confronting us as the result of attempting to minimize standby time stemmed principally from adverse surface winds and cloud cover. The facet of this problem which we could attack from a system design point of view was related to high velocity surface winds.

6.1 High Velocity Wind Problem

To limit the standby time we felt we should design a system which would minimize the time spent in waiting for very low surface winds. This problem was solved as indicated in previous discussions by using a tandem system with the "cast-iron"

launch balloon concept. The phrase "cast-iron" implies the launch balloon when inflated can withstand relatively high surface winds which would normally preclude a static launch. The remainder of the flight system, including the main balloon, is placed in a tight sleeve to present a good aerodynamic configuration to limit drag forces in high surface winds. This general balloon design permits us to restrain the balloon system in winds up to 20 mph and to launch statically in this type of wind condition without undue hazard to the delicate payload.

7. PROBLEMS RESULTING FROM AN ALL-YEAR-ROUND LAUNCH SITE

Dr. Schwarzschild's desire to have a launch site useable the year round presented the program with the general problem of finding such a location in the United States. We solved this problem with the help of the U.S. Weather Bureau which made a statistical weather study of the entire country. In addition to the data analysis accomplished by the Weather Bureau, we made a visual airplane survey in the region surrounding the area recommended by the Weather Bureau. Our first selection of launch site was Hope, Arkansas, and several flight operations were conducted from this location. This site was not acceptable to the FAA for a permanent balloon operations base because of the density of commercial air traffic. When NCAR was ready to proceed with the establishment of a permanent scientific balloon flight station, they conferred with the FAA to obtain a position in this general vicinity that would be satisfactory from both balloon operations and commercial aircraft safety considerations. As a result of these discussions, Palestine, Texas, was selected as the NCAR Scientific Balloon Flight Station and as the all-year-round operations site for Stratoscope II. The general problem presented by this launching site is associated with the proximity of the Gulf of Mexico. The Gulf of Mexico is a prolific source of clouds under certain weather circulation conditions which occur frequently in this area. The Gulf is also a hazard to the safety of the telescope in the event of a change in the balloon trajectory which might carry it out over the water. We have no solution for clouds resulting from Gulf moisture. We have minimized the danger to descent of the Stratoscope II in the Gulf by: (1) Careful analysis of anticipated trajectories before launch and avoiding launching on those days when trajectories are uncomfortably close to the Coast; and, (2) establishing back-up balloon control stations which can terminate the flight in the event the trajectory changes toward the Gulf.

XVI. In-Flight Deployment of Long-Train Instrumentation Packages From High-Altitude Balloons

R. J. Reddy, Major, USAF
Air Force Cambridge Research Laboratories
Bedford, Massachusetts

Abstract

In 1957 and 1958, techniques were developed for the precise positioning and in-flight deployment of several 50-lb instrumentation canisters along a 3500-ft-long balloon-borne train. Hardware and techniques developed during this earlier program have been expanded and refined to permit the placement of much larger canisters in a similar manner. This proven system and its component parts have high potential in a variety of applications where an elongated train of accurately positioned instruments or devices is desired.

1. INTRODUCTION

In 1957 a need existed for launching balloons carrying sensing instruments placed at various known distances along an extended train. These instruments were designed to measure gradient pressures and temperatures during atmospheric blast experiments.

Early attempts to launch lengthy balloon-borne trains in other than calm or zero wind conditions presented many problems. In some cases the instruments on

150 to 250-ft long trains were damaged during launch. These problems were primarily solved through the design of a compact launch configuration (see Gilpatrick and and Fruge, 1958) that permitted train deployment during the balloon ascent (Figures 1 and 2).

Figure 1. Launch Configuration

Figure 2. Flight Configuration

Since 1957 several flight configurations have been developed under projects known as VHA, VHB, and "C" Launch (Table 1). Payloads ranged from 760 lb to 4500 lb and consisted of 6 to 7 instrumentation canisters placed along trains between 2350 and 3500 ft in length. The individual canisters ranged in weight from 50 lb to 325 lb.

Table 1. Balloon Instrumentation Trains

	Balloon	Float Altitude (ft)	Payload (lb)	Train Length	Canisters		
					Size	Weight (lb)	Number
VHA	800×10^3 cu ft 2.0 Mil Poly	85,000	760	3500 ft 500-Reel	43" L. 10-1/4 O.D.	50	5 + 1*
VHB	5.27×10^6 cu ft 1.0 Mil Poly	115,000	1200	2350 ft 350-Reel	6' L. 8-1/2 O.D.	90	5 + 1
"C" Launch	1.15×10^6 cu ft GT-12	65,000	4500	2600 ft 1500-Reel	5-1/2-7' L. 11" O.D.	300-325	6 + 1

*The additional canister is located below the reel at launch and does not deploy from within the tube.

Essential elements of each train deployment system are:

(1) The deployment tube assembly used to deploy the instrumentation canisters.

(2) A fluid brake-type reel used to lower the deployed canisters further from the balloon.

(3) The line connecting the canisters which provides us with the desired canister positioning.

2. DEPLOYMENT TUBE ASSEMBLY

The deployment tube assembly consists of a long fiberglass tube contained within a parachute. The tube acts as a casing into which the canisters and their connecting lines are compactly stored at launch. The 19-ft-long VHA tube was fabricated of wound fiberglass and weighed 27 lb. Today's 38-ft-long "C" launch tube is of fiberglass-covered aluminum honeycomb construction and weighs approximately 280 lb. It is split longitudinally for access during loading.

After launch, at between 1500 and 2000 ft above the ground, tube cutaway is commanded. The released tube parachutes to earth and the canisters are withdrawn in turn by the ascending balloon. Proper tube parachute design became a paramount consideration.

To insure a desirable tube orientation and a minimum of lateral displacement during canister withdrawal, the parachute descent rate and stability had to be consistent with the design load limitations of the canister train. The connecting line between the canisters is particularly vulnerable to failure. It was essential that shock loads on the system be kept at a minimum during canister deployment. In the VHA and VHB programs a guide personnel-type parachute satisfied these deployment requirements. In the "C" launch program the much heavier canister and deployment system demanded a higher drag parachute design which included minimum oscillation and good recovery characteristics. A 48-ft diameter, full-guide, surface-ribbed canopy appeared to meet these requirements.

Early tests of the "C" launch deployment system using this parachute showed an unsatisfactory opening time. In one of 3 tests the tube parachute failed to open during the deployment sequence. Once inflated, however, the 48-ft parachute demonstrated good stability and drag characteristics. If a more rapid and positive parachute opening could be assured, this parachute remained highly desirable.

Several devices were designed and fabricated to aid or to produce a more rapid parachute opening. These included (1) a ballistically powered forced opening device developed by the Stencel Corporation; (2) an inflatable torus designed and fabricated by Raven Industries; (3) a mechanical opening device designed by AFCRL; and (4) a scaled-down 32-ft-diam parachute of the same design as the original 48-footer. This smaller parachute would open more rapidly and would provide closer to the ideal ratio between canopy diameter and shroud line length. This latter characteristic, of course, would provide improved stability. In addition to parachute system redesign, the canister harness was beefed up and the connecting line terminal loops protected by leather inserts. These modifications were necessary to withstand the higher deployment shock loads possible with the smaller parachute. Both the Stencel forced-opening system and the 32-ft parachute performed satisfactorily during tests conducted last May (1965). The Stencel system spread the 48-ft canopy in approximately 1/2-sec and the 6 instrumentation canisters were deployed in 23 sec. The 32-ft unassisted parachute opened in 2 sec and the 1100-ft train was deployed successfully in approximately 20 sec. An envelope of shock loads recorded during canister deployment indicated an initial 10 g upward acceleration of the load bar at tube release. During deployment of the canisters this shock envelope decreased from 6 g's to 2 g's in magnitude. These loads were all well within system design limitations.

3. THE FLUID BRAKE REEL

The fluid brake reel was initially employed in the VHA program and was designed to lower a 600-lb load a distance of 500 ft below an ascending balloon. The final design incorporated a series of brake disks working against a braking fluid. This fluid – a General Electric product, trade-named Viscasil – was selected because of its good qualities of slight change in viscosity over a wide temperature range, good oxidative stability, unusual chemical inertness and resistance to breakdown under mechanical shearing. The VHA reel weighed 43 lb and measured 22-in. in height, 14-in. in width, and 12-in. in depth. Use of 725-stoke Viscasil with this reel permitted full deployment of the 600-lb load a distance of 500 ft in 4 min. The load was deployed essentially with little initial or terminal shock. Today's "C" launch reel utilizes the identical principal and a similar design. It measures nearly 2-1/2 times the width, twice the depth, and a few inches higher than the VHA reel. It weighs 330 lb and has successfully lowered 2800 lb 1500 ft in 7 min using 1000-stoke Viscasil.

The number and size of brake plates for a particular design requirement can be readily calculated mathematically (Wagner and Doherty, 1958). Variations in drum capacity and initial fluid viscosity permit use of the fluid brake reel for a variety of payload, train length, and deployment time requirements (see Figures 3 and 4).

4. THE TRAIN CONNECTING LINE

The third and last item I should like to discuss is the train connecting line. The method of deployment requires connecting line that possesses excellent shock absorption and predictable stretch characteristics. In all three deployment programs we have successfully used coreless nylon braid manufactured in accordance with MIL-C-7515. This, or similar type line, is recommended for like applications.

Tests conducted at AFCRL locations and at the South Weymouth Naval Air Station blimp hangar provided some static, dynamic, and creep stretch characteristics for both 5000-lb (MIL-C-7515 Type X) and 10,000-lb (Type XII) coreless nylon braid. Generalized results of these tests are shown in Table 2. Elongation of the line as loads were applied was termed static stretch. Additional elongation as a function of time was termed creep. Elongation which could be attributed to shock loading was termed dynamic stretch.

As can be seen from Table 2, the greatest percentage line elongation resulted from the application of load statically. Limited measurements of temperature and humidity effects on creep showed insignificant change over the ranges recorded.

Table 2. Nylon Stretch

Type	Elongation Percent
1. Static	7 - 12
2. Dynamic	1 - 2
3. Creep	.2 per day (for 8 days)

A relative humidity change from 35 to 65 percent added less than 1/2 percent elongation during some limited static tests.

Temperature variations between 40°F and 60°F recorded during these same tests showed no effect on stretch.

Precutting the connecting line to compensate for static load permits positioning of instruments to within 3 percent error.

Precise positioning can be obtained after deployment by either electrical or optical means.

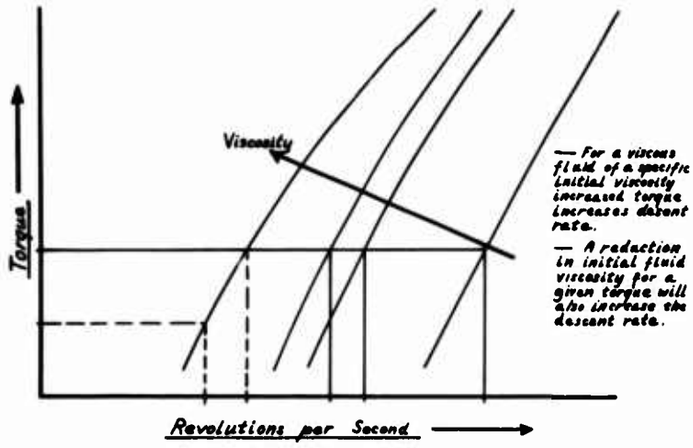

Figure 3. Fluid Brake Calibration Curve for a Particular Reel

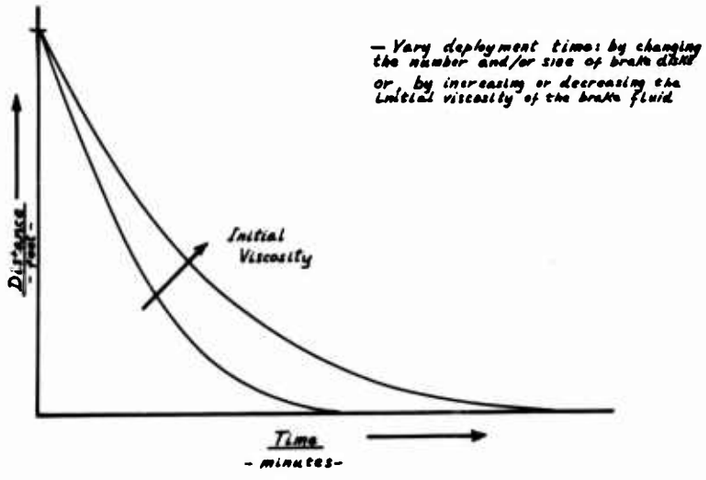

Figure 4. Fluid Brake Calibration Curve for a Given Load and Deployment Distance

Precutting the connecting line to compensate for static load will permit positioning of instruments to within 3 percent error. Precise positioning can be obtained after deployment by either electrical or optical means. To avoid line failure at the terminal loops through abrasions incurred during the dynamic deployment, it is recommended that all terminal loops be lined with a soft leather.

5. CONCLUSIONS

The three test programs (VHA, VHB, and "C" Launch) have led to the development of a unique in-flight method for deploying instrument canisters on long trains beneath balloon carriers. These trains have varied between 2350 and 3500-ft in length with 5 to 6 canisters of from 50 to 325 lb each suspended at intervals along the train.

These proven systems and their component parts have high potential in a variety of applications where an elongated train of accurately positioned instruments or devices is desired.

References

Gilpatrick, A.E., Maj., and Fruge, R.C., Capt. (1958) Equipment and Techniques for In-flight Deployment of Long Train Instrumentation Packages from High-Altitude Balloons, AFCRC-TR-58-258, ASTIA Document No. AD160 750.

Wagner, W.C. and Doherty, F.X. (1958) Device for Lowering Loads from High-Altitude Balloons, AFCRC-TR-58-240, ASTIA Document No. AD152 583.

XVII. Midlatitude Stratospheric Humidity Regime to 30 km

N. Sissenwine, D.D. Grantham, and H.A. Salmela
Air Force Cambridge Research Laboratories
Bedford, Massachusetts

Abstract

The results of monthly soundings of humidity up to 25 to 30 km over a year utilizing a highly sophisticated alpha-radiation hygrometer and associated balloon sounding equipment are described. The stratosphere was never found to be near saturation as has been suggested by some investigators, nor was it as dry and completely devoid of variability as is indicated by the most accepted circulation theory. A small minor increase in humidity above the tropopause to altitudes of about 25 km was usually noted. Variability in this region of the lower stratosphere approached a factor of 10. Spasmodic transfer of water vapor upward through the tropopause is suggested and speculation related thereto provided.

1. INTRODUCTION

Starting more than 20 years ago British scientists (Dobson, et al, 1945; Brewer, 1949; Brewer, 1955; Helliwell, et al. 1956, 1957, 1960) reporting upon initial aircraft investigation of humidity in the lower stratosphere presented evidence that the tropopause acts as a cap to water vapor, which enters the atmosphere

from the earth's surface preventing it from penetrating into the stratosphere. This finding was presented in conjunction with a circulation theory, which indicated that tropospheric air passes into the stratosphere only over equatorial regions from where it moves northward. It sinks back into the troposphere at higher latitudes, closing the cycle.

Tropical tropospheric air, which is wetter than all other surface level air, following this route into the stratosphere would have to pass through the very cold tropopause of the tropics where the water vapor density would be forced down to a level lower than elsewhere due to condensation. As this air departs upward from this level, the mixing ratio (the weight of water in a given weight of dry air) must remain constant if there is no source of nor condensation of water vapor. It follows that water vapor density, the absolute humidity, must become monotonically lower as density falls off with altitude. Frost and dew point have a 1:1 relationship with absolute humidity and thus would have a parallel decrease. Chemical production of water in the stratosphere could reverse this trend, but there has been no substantial evidence of this although some speculation exists (Hesstvedt, 1964, 1965; Rangarajan, 1963; Dobrovol-skiy, 1964; Suvorov, 1964). In fact in some very early United States experimental work in which relatively crude frost point devices were carried to 30 km by balloon (Barrett, 1950), thin saturated layers were observed.

Measurement of water vapor at cold temperatures is extremely difficult, and doing this without contaminating the air sampled complicates this problem even further. Thus the British findings were considered quite authoritative for many years and have not been completely contradicted to date, although evidence to be presented herein and by others (Murcray, 1966; Pybus, 1966; Brown and Pybus, 1964) indicates a modification may be in order. Many slightly earlier investigations in England, Japan, and the United States, summarized by Gutnick (1962), indicated much higher humidities at 15 to 30 km. Some parallel investigations (Mastenbrook, 1963, 1965a, 1965b, Williamson and Houghton, 1965) are providing evidence more in keeping with the British theory.

There are basic scientific reasons for substantiating or contradicting the British theory of a dry nonvarying stratosphere. For meteorology, presence of nonuniformly mixed water vapor at these altitudes could lead to local modifications of a circulation pattern, such as proposed by the British, since it could account for absorption of solar energy in the infrared spectrum. The resulting differential heating would lead to pressure gradient changes, and these to changes in the wind field. From an astronomical viewpoint, the water vapor in the stratosphere must be known when observations of the atmospheric constituents of other planets are made from balloons in the earth's stratosphere. There are also engineering reasons for looking into this matter. In the development of aerospace systems an unexpected amount of water vapor could affect the performance of infrared devices when used

in the stratosphere, and on horizon sensing instrumentation used for spacecraft (Gutnick, 1960).

Two years ago, on the same platform, we (Grantham, et al., 1965) described a program being supported by AFCRL's Laboratory Director through special funding to help shed light on this quandary which had been aptly described by my associate (Gutnick, 1961) in a widely acclaimed paper, "How Dry the Sky?". Ballinger, et al. (1965) described the instrumentation to be utilized on these investigations at the 1964 Balloon Symposium. Details are well documented in the 1964 proceedings. I will just briefly review this background.

The program involved flights of two frost-point soundings a month for one year from the surface to 27 km (about 85 to 90 kft) from Chico, California. Balloons of 500,000 cu ft with controlled valving and ballasting for obtaining desired vertical velocity were employed. A total payload of 450 lb included the alpha-radiation hygrometer which, when sealed with a recorder and dry ice in a stainless steel desiccated container, weighed 75 lb. The sensor package was lowered 2000 ft from the load bar on a hydraulic reel shortly after launch to separate it from water vapor which may be emitted from the surface of the balloon and associated equipment. Rates of ascent and descent were made commensurate with the time lag of the instrumentation. Though uncontaminated conditions were expected on ascent, due to the 2000-ft separation, the sounding system design included special consideration of battery and chemical coolant life in order to insure operation through descent. As a further precaution against contamination we required balloons be packaged dry, instead of with cornstarch, which is usually used as a lubricant.

In this connection I will divert from the main theme of my paper. Following successful flights of our first two soundings in January 1965, we were plagued by a series of bursts during ascent. Speculating that the lack of lubrication on the film while unfolding at cold temperatures was the cause, we established a routine for dusting balloons with teflon powder before flight, a messy procedure. Our success rate improved phenomenally. However, we did have a balloon failure with teflon later in the program, and there is still question in the minds of our balloon engineers and operators as to the real reason for this improvement. The dusting process led to discovery of some flaws in the balloons, which were repaired. Those interested in the pros and cons of lubricating and type of lubrication should discuss this with members of AFCRL's Balloon Research Branch.

Now returning to the instrumentation, the alpha-radiation hygrometer is an automatic frost-point instrument (Ballinger, et al., 1964, 1965) in which temperature of polonium surface is controlled by a servomechanism which strives to maintain a stable deposit of frost on it. The polonium emits alpha radiation which is monitored by a Geiger-Mueller detector. The frost point is recorded by a miniature thermistor embedded in the polonium. The accuracy of the sensor in this instrumentation varies

with true frost point, atmospheric pressure, and time allowed for the sampled air to reach equilibrium with the sensor. Poorest performance, 2 to 3 °C errors in frost point, are found near 100 mb when the frost point is between -80 and -90°C. At the top of the soundings the sensor error will be only a fraction of a degree, but the recorder limits readings to about 1°C.

2. FINDINGS

As already indicated we had some balloon problems which detracted from our two flights per month goal. Some malfunctioning of equipment due to damage incurred in recovery also hurt this average and caused us to extend over into 1966. All in all we launched 24 flights and obtained 16 soundings which provided useful data. Of the 8 failures, 3 can be totally attributed to instruments, 3 to balloon failure, and 2 to both instrument and balloon malfunction. Seven balloons did burst on ascent, but useful data were obtained on many of these.

Figure 1 depicts the first sounding. Despite the extensive precautions to prevent contamination it appeared we had failed. In the stratosphere, on ascent, frost points were running around -75°C. Frost points were colder by 10° or more during descent. This amounts to a factor of 5 in the amount of water vapor density at these temperatures. This early finding caused us to study carefully the configuration of our sounding system as shown in Figure 2. The geometry of the sensor in the stainless steel container which will be lowered 2000 ft from this hydraulic reel still has one shortcoming. Air passing over the can could sweep molecules of water vapor off its surface and then be sucked into the sensor intake which protrudes directly beneath it. Though the can is stainless steel, a relatively dry surface, the top had to be constructed of heavy-gage aluminum. It was quite apparent that our ascent data could not be considered as truly representative of the stratosphere with this defect. The remedy was to bend the tube 90° and lengthen it slightly to get it out of the boundary layer. The tube was in itself a possible source of contamination (Ballinger, et al., 1965) and had to be kept as short as possible.

Several flights later we were able to prove the effectiveness of the configuration (see Figure 3). In this case the air encountered in ascent was actually drier than that encountered in descent in the stratosphere and upper troposphere. During the several hours of flight the balloon had moved a considerable distance and was sampling a different air mass, but we had two good soundings.

Figure 4 shows the monthly summary of all data found acceptable. Frost points are averaged through the pressure levels indicated. This picture appears to depict an annual cycle for layers higher in altitude than 100 mb (50 to 55,000 ft). A maximum is reached in the late winter and a mirimum in the summer. However, it

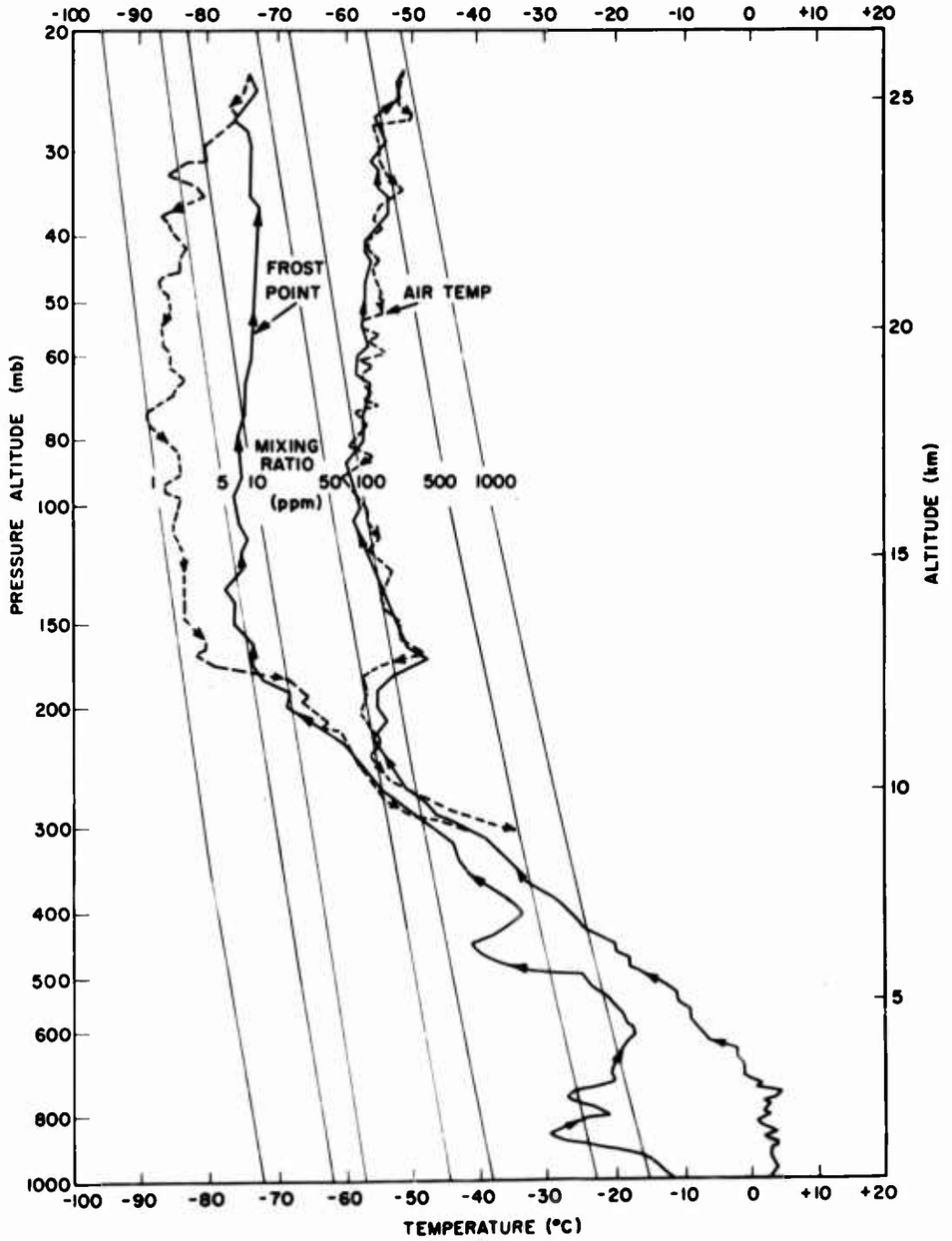

Figure 1. LDF Flight No. 1V

would be hard to argue the significance of such a systematic variation with this limited sample. During the month of April 1965 the range of the 6 separate profiles is nearly as great as that of the curves depicting the annual cycle. However, such an annual cycle is in fair agreement with a theoretical study by Roney (1965) on stratospheric ozone and water vapor in the stratosphere but we would not care to argue the extent and the exact pattern, if any. A harmonic analysis of these data is now being made, and statistical significance will be determined.

Earlier, I mentioned the British findings without assigning any quantities. The humidity that can best be attached to the nonvarying dry British stratosphere is 2 ppm by weight, to meteorologists more recognizable as a mixing ratio of 0.002 g/kg. The values we obtained near the 100 to 150 mb layer, which is the maximum altitude of the British aircraft data, are in good agreement with this nominal value. Our data ranged from 1 to 10 ppm at this level. However, as you will note from the scale on the far right, though the annual cycle appears to be damping out with altitude, the proportion of water vapor appears to be increasing, attaining some 10 to 40 ppm near the top of the soundings. This increase is sufficient so that the frost point increases from about -81°C at 18 km to about -79°C at 25 km. This trend caused us concern for the reliability of our data. If continued upward the partial pressure of the water vapor would, at some altitude, exceed total atmospheric pressure. This is not physically possible.

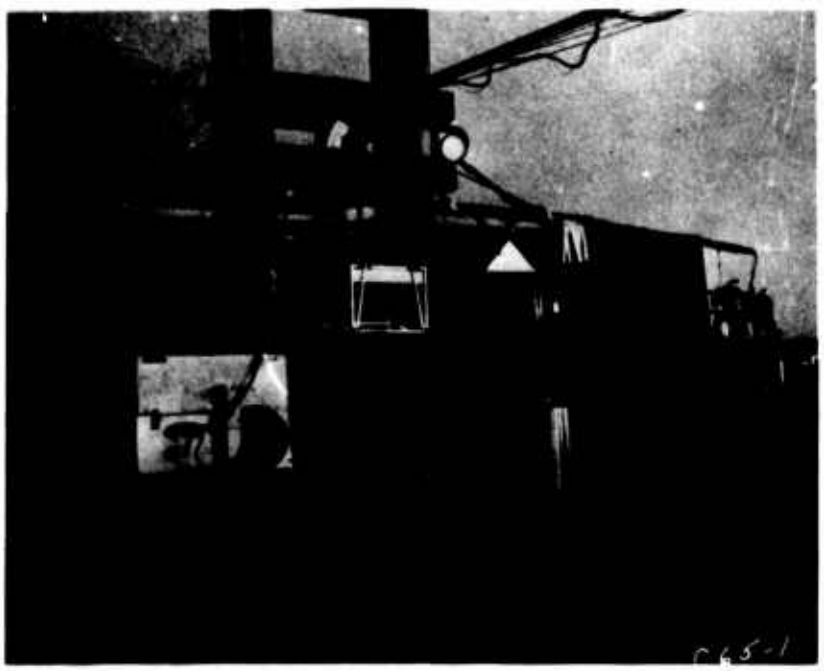

Figure 2. Instrumentation Package

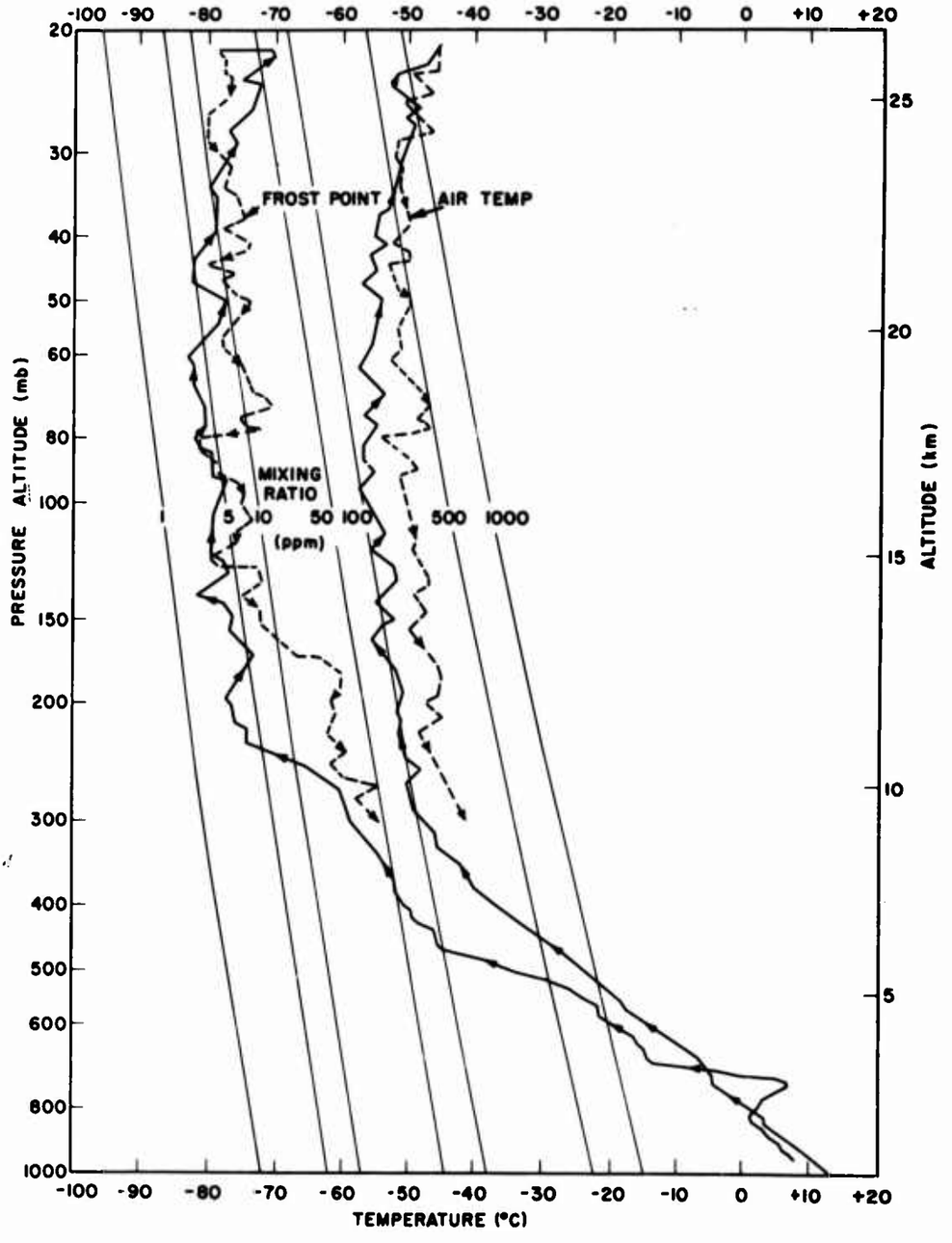

Figure 3. LDF Flight No. 6V

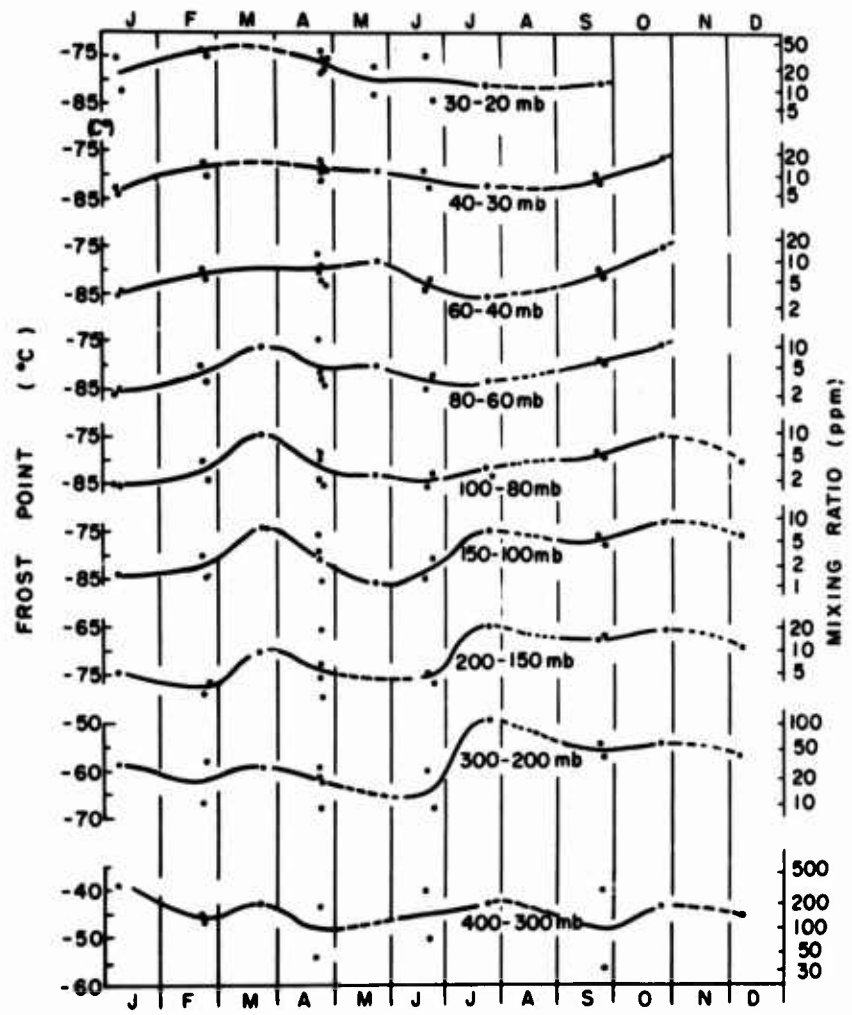

Figure 4. Mean Humidity With Selected Layers by Month

For this reason we arranged for a special balloon to carry our equipment to higher altitudes. This sounding (Figure 5) reached a pressure of 8 to 9 mb, about 32 km, as compared to the usual 25 km. The lower 25 km of this sounding differs little from any one of the earlier soundings. Once above the tropopause, frost point increases from a -84°C minimum to a maximum of -75°C at 23 mb, about 25.5 km. However, above this point a trend is established toward lower frost point. At 9 mb it dips to -82°C, lowering the mixing ratio to 27 ppm, still 10 times that at the base of the stratosphere.

A convincing factor in this high-altitude sounding that provides confidence in the presence of a slightly more moist layer at 25 km than immediately above or below this level is that it is seen in both ascent and descent. There are some differences due to time and space, since about 187 min elapsed between ascent and

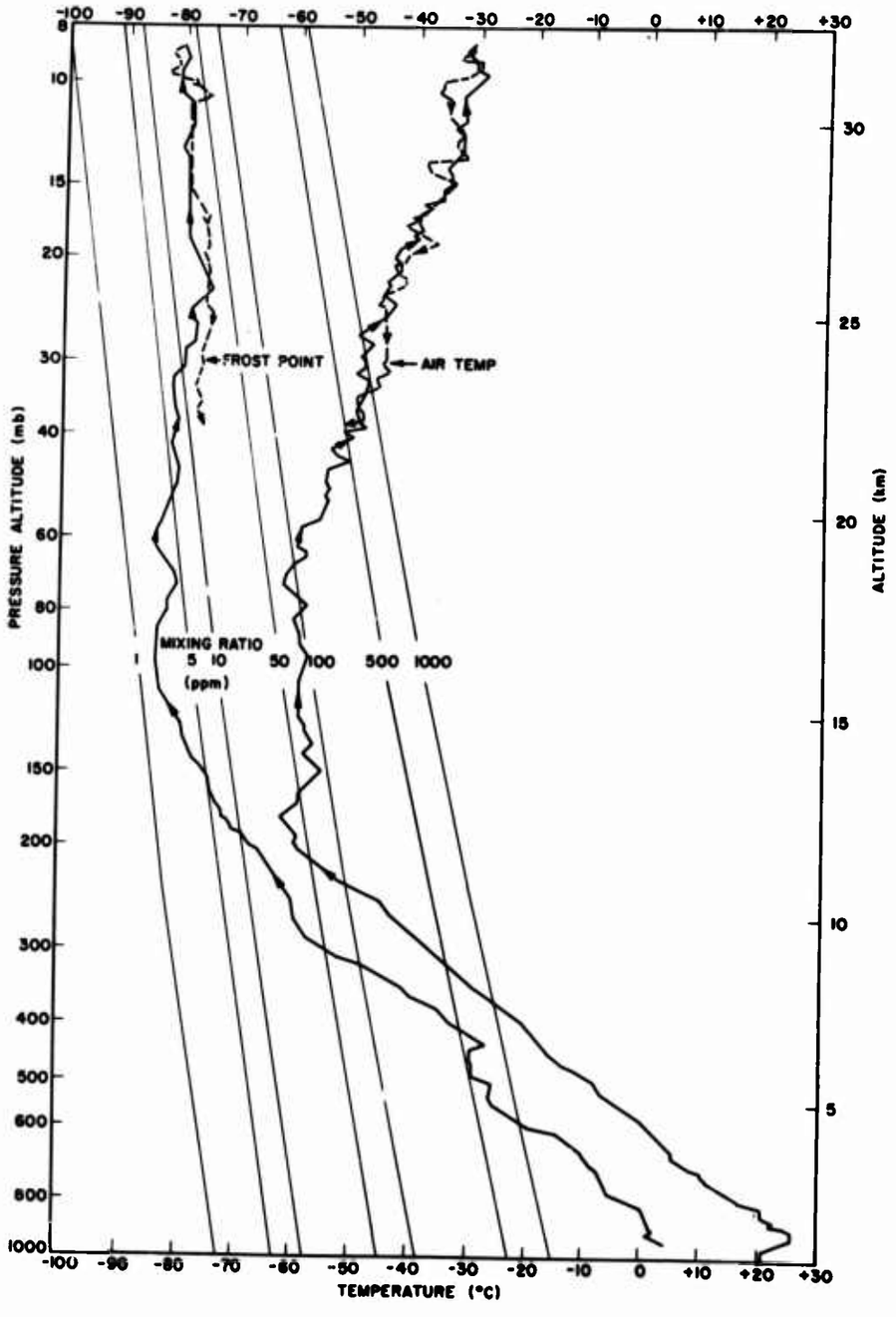

Figure 5. LDF Flight No. 22V

descent through the 25-mb level. If contamination were thought to be the reason for the maximum in humidity on ascent, however, it would be difficult to argue that this is the cause of the maximum on descent, since the system had dried out at higher altitudes as evidenced by the lower humidities with higher temperatures. Also, the air sampled in descent is less likely to have had any contact with the boundary layer air of the balloon system than on ascent. The fact that the sensor had the range to reach much colder in frost point both above and below this layer argues for confidence in the instrumentation. Figure 6 is presented as further support for the tendency of a humidity maximum at 25 km, at least over midlatitudes. (This is also the altitude of nacreous clouds. Such clouds generally form to the leeward of mountains during periods of strong upper air flow across the range.) This sounding was obtained at Holloman AFB in New Mexico during investigations (Ballinger, et al., 1965b) of frost-point sounding-system contamination. The alpha-radiation frost-point hygrometer was flown on the load bar in these studies (rather than at 2000 ft beneath it as in Chico) and usually showed much less contamination than in the flight pictured in this figure. Presumably this is because of the drier surface and troposphere conditions of the New Mexico desert. However, both ascent and descent of this Holloman flight also showed the tendency for the slight increase in moisture at 25 mb.

How does this fit into a picture which includes the water vapor distribution at even higher altitudes? The only information on water vapor in a layer at high altitudes in which we can place great confidence is that noctilucent cloud particles formed at the 80 km mesopause include water (Soberman, 1963; Michaels, 1965). Such clouds are not found at tropical and midlatitudes where temperatures are seldom colder than -100°C (Cole and Kantor, 1963) at this level. They are only seen at higher latitudes in the summer where extremely cold temperatures are usual at the mesopause. During one experiment (Anon., 1963), at which such clouds were physically sampled, the temperature observed was -143°C. During another sampling, when the clouds had dissipated, a temperature of -120°C was measured. Assuming a pressure of 10^{-2} mb (COESA, 1966), if the mixing ratio at 30 km at the top of our highest sounding, 27 ppm (Figure 5), were considered to hold uniformly up to 80 km, the frost point would be -115°C, not quite cold enough. The frost point in this sounding had fallen 7°C in the top 6.5 km, however, a gradient of about 1°C/km. At this rate 48 km are required to drop the frost point from -82°C to -130°C, a nominal value for noctilucent clouds suggested by the experimental data just mentioned. Since these clouds are found about 50 km above the top of this sounding, the trend in humidities in the 25 to 32 km altitude region provided by the Chico sounding appears to support the values of humidity which must be present at altitudes of noctilucent clouds.

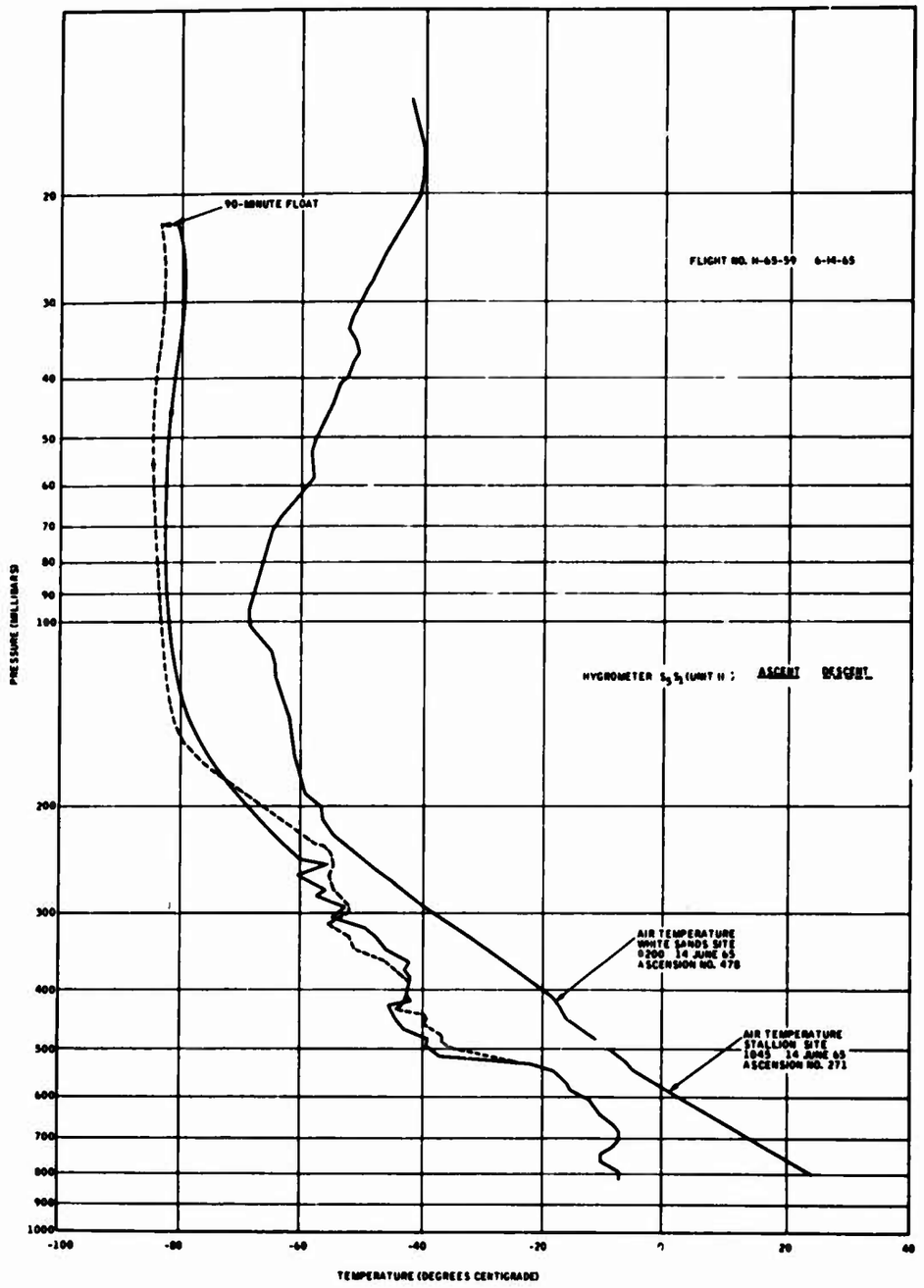

Figure 6. Flight No. 3 From Holloman, New Mexico, Contamination Study

We are now left with the problem of explaining the relatively moist layers at 20 to 25 km. Mixing ratios in this layer are five times those at the base of the stratosphere and can only be considered credible if evidence for a source for such a "spiking" of the layers just above the troposphere can be presented. The British and other investigators (Mastenbrook, 1965) had noted a near saturated layer in the upper troposphere and a sharp drying out in water vapor content upon passing upward through the tropopause. We corroborate these findings. In Figure 7 the average change in depression in frost point below free air temperature during penetration of the tropopause for this series of soundings is shown. The drop in frost point from -61°C at the tropopause to -79°C in 3 km, drops the water content by a factor of 15. The tropopause certainly seems to be acting as a barrier.

However, there are exceptions which if not present would have made these average rates of decrease even more dramatic. On Figure 8 in the graph at the left, you will note a sharp temperature tropopause (the solid line). With it there is a very sharp decrease in the frost point (the dashed curve). At the right of Figure 8, for another weather situation the tropopause is not well defined (solid curve). The parallel frost point decreases were far less drastic, as is indicated by the dashed curve. With varying intensity of the tropopause inversion on a day-to-day basis, especially when there are overlapping or leafing of tropical and polar tropopauses, as is usual at midlatitudes, it does not appear unlikely that there will be occasional transfer of moister tropopause air into the stratosphere in midlatitudes. For example, over the Gulf of Alaska where such leafing action could be forced by well-developed cyclones regularly entering the Aleutian low (the tropopause is known to rise and fall as cyclones pass), the tropopause temperature remains between -50 and -55°C (Ratner, 1957, 1958) throughout the year. This air is about 25°C warmer than in equatorial regions and can contain nearly 100 times more vapor. Small amounts of this saturated tropospheric air being mixed upward could add considerably to the water vapor of higher level warmer air, even if this higher altitude air had entered the stratosphere over the route suggested in my opening statements. Extensive cloudiness through a deep layer well above the tropopause over Anchorage, Alaska, was noted by an Air Weather Service forecaster (Ehrlich, 1966). Though a very well-defined polar tropopause was present at 25,000 ft, jet aircraft were unable to top all cloudiness after climbing to 39,000 ft. This happened during a transition season and was associated with passage of a not unusually strong extra-tropical cyclone.

Passage of water vapor into the stratosphere during leafing of multiple tropopauses at midlatitude and higher is one, but not necessarily exclusive, source. Another possibility is vaporization of the ice crystals of convective clouds penetrating into the stratosphere over continental midlatitudes in the warmer half of the year. These have been observed to attain altitudes of 22 km by aircraft and radar (Grantham

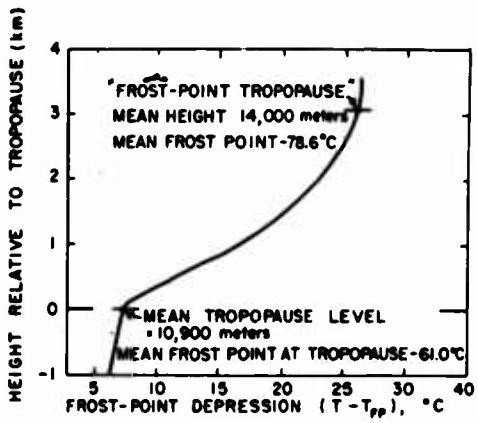

Figure 7. Mean Frost-Point Spread in Vicinity of the Tropopause Level

and Kantor, 1966; Long, 1966) with greater frequency than has heretofore been considered likely. They must evaporate to dissipate and thus also add vapor to the air. Crutcher (1963) also summarized much evidence of clouds in the stratosphere in an address on problems of supersonic aircraft and quoted remarks of a 100,000-ft parachutist who observed thin layers of clouds at this high altitude.

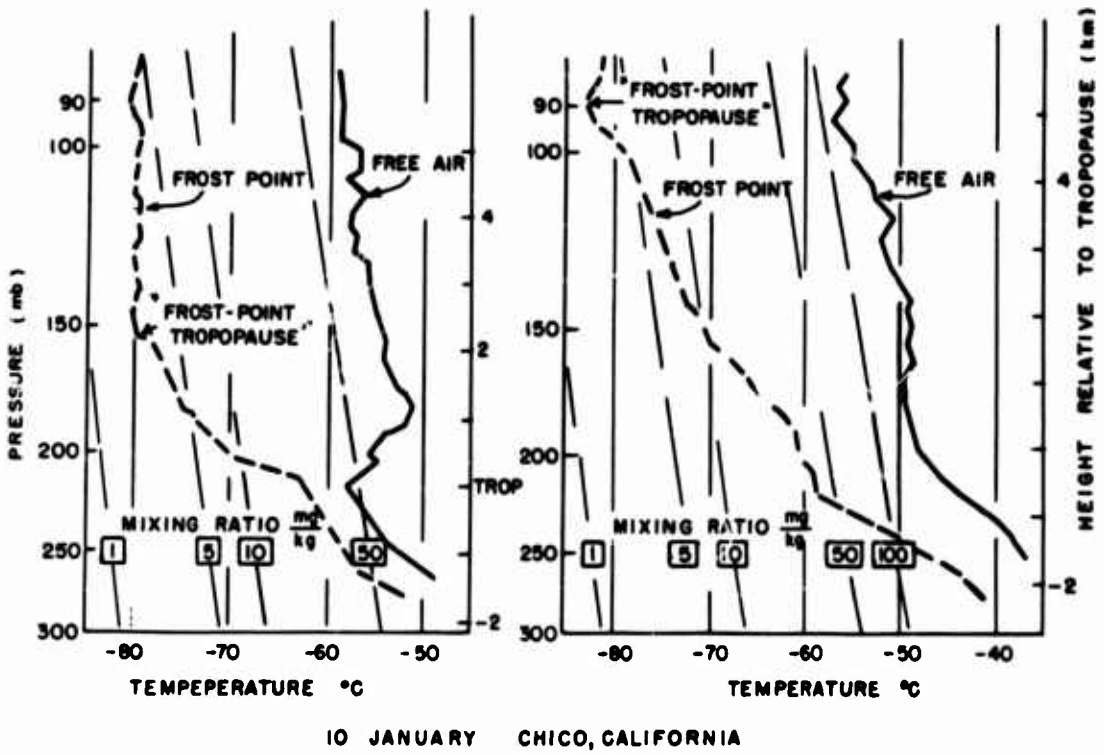

Figure 8. Frost-Point Profiles in the Vicinity of the Tropopause

3. CONCLUSIONS

In conclusion I would like to present a graphical summary of this one-year effort at Chico (Figure 9). The center curve is the average of the 16 Chico soundings. The dashed portion is a result of only one sounding. The curve reveals a stratospheric humidity minimum just above the tropopause, 15 to 20 km, a maximum near 25 km, and a gradual decrease upward. This rate of decrease provides reasonable agreement with the data on noctilucent clouds. The midaltitude maximum requires a physical explanation, a water source to make it plausible. Two mechanisms have been suggested.

The curve on the left is representative of the frost points that one could expect if the mixing ratio remained constant at 2 ppm, the value suggested and still considered valid by British investigators. This curve would provide a frost point of -125°C at the altitudes of noctilucent clouds, which is in reasonable agreement with the experimental data of -120°C no cloud, -143°C cloud present, presented

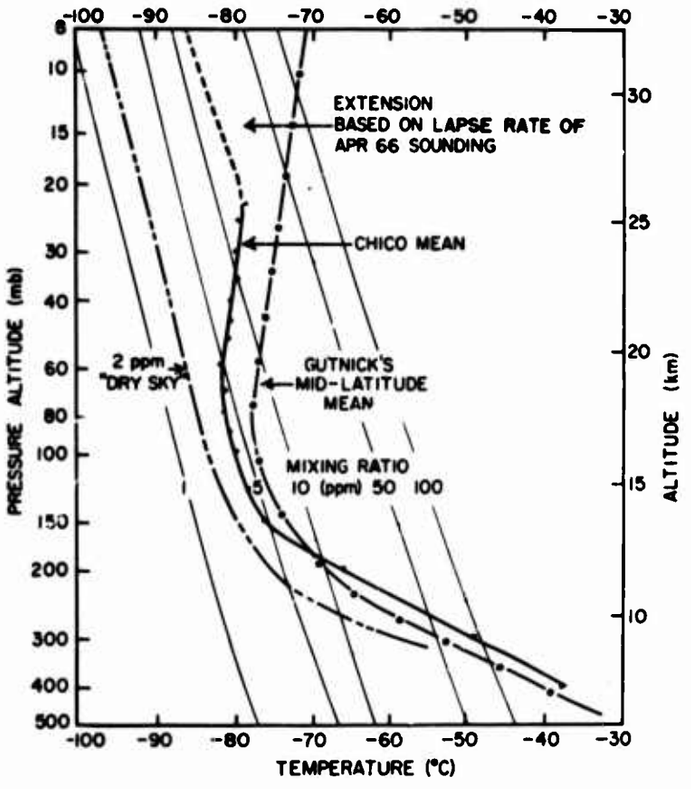

Figure 9. Comparison of Frost-Point Profiles

above. The curve on the right, prepared in 1962 (Gutnick, 1962) shows the mean conditions observed to that time after screening out data thought to be erroneous through subjective examination. This water content profile could not be reasonably extrapolated upward since it would require noctilucent clouds over most of the earth and result in a partial pressure of water vapor which exceeds the total pressure of the atmosphere.

Finally, the processes that introduced water vapor into the stratosphere are sporadic so that there is random variability of nearly ten-fold in the lower stratosphere. Systematic variability, such as associated with seasons, also appears to be present but much more evidence is required to prove it. None of the Chico data support speculation that the stratosphere is sometimes nearly saturated.

Acknowledgments

This experimental program would not have been possible without the efforts of M/Sgt John E. Bowers, Instrument Technician. Special thanks are also due to Messrs. S. Rohrbough and J. Ballinger, of Honeywell, Inc., for design of the sensor and aid during initial flights. The balloon systems were designed by AFCRL's Balloon Research Branch. Messrs. T. Kelly and L. Grass are to be commended for operation of these systems exactly as predicted. Mr. T. Danaher and Capt. D. Cunningham deserve credit for the field support of this program. Capt. Clarence Duff and his Weather Detachment were very helpful in providing weather support. This research was supported by the Air Force In-House Laboratory Independent Research Fund.

References

Anonymous (1963) Lowest measured temperature in the earth's atmosphere recorded in U.S.-Sweden experiments, BAMS 44:806.

Ballinger, J.G., Kirvida, L., Fricke, M.P., and Crowley, J.E. (1964) Automatic Frost Point Hygrometer for Stratospheric Water-Vapor Measurements, Final Report, Vol. 1, Contract No. AF19(604)-8418, Honeywell, Inc., Minneapolis, Minnesota.

Ballinger, J.G., Koehler, L.E., Fricke, M.P., and Murphy, R.D. (1965a) Toward Improved Measurements of Stratospheric Humidity With Balloon Borne Frost Point Hygrometers, Proceedings 1964 AFCRL Scientific Balloon Symposium, Air Force Surveys in Geophysics, No. 167, AFCRL.

Ballinger, J.G., Koehler, L.E., Murphy, R.D. (1965b) Contamination Effects in Stratospheric Humidity Measurements, Final Report, Contract No. AF19(628)-3857, Honeywell, Inc., St. Paul, Minnesota.

Barrett, E.W., Herndon, E.A., and Carter, H.J. (1950) Some measurements of the distribution of water vapor in the stratosphere, Tellus 2(No.4):302-311.

Brewer, A.W. (1949) Evidence for a world circulation provided by the measurement of helium and water vapor distribution in the stratosphere, Quart. J. Roy. Met. Soc. 75:351-363.

Brewer, A.W. (1955) Ozone concentration measurements from an aircraft in N. Norway, Meteorological Research Committee, London, MRP 946.

Brown, J.A., Jr., and Pybus, E.J. (1964) Stratospheric water vapor soundings at McMurdo Sound in Antarctica – Dec 1960, Feb 61, J. Aerospace Sci. 21:597-602.

Cole, A.E., and Kantor, A.J. (1963) Air Force Interim Supplemental Atmospheres to 90 Kilometers, AFCRL-63-936, 29 p.

COESA (1966) U.S. Standard Atmopshere Supplements, 1966, in publication, GPO, Washington, D.C.

Crutcher, H.L. (1963) Climatology of the Upper Air as Related to the Design and Operation of Supersonic Aircraft, presented at Sixth Annual Symposium of Society of Experimental Test Pilots, Available U.S. GPO, Washington, D.C.

References

Dobrovol-skiy, S.P. (1964) The nature of noctilucent clouds, Priroda 3:87-89.

Dobson, G.M.B., Brewer, A.W., and Cwilong, B.M. (1945) Meteorology of the Lower Stratosphere, Bakerman Lecture.

Ehrlich, A. (1966) Personal conversation with N. Sissenwine.

Grantham, D.D., Kantor, A.J. (1966) Horizontal and vertical distributions of radar echoes, presented at the American Meteorol. Soc. Meeting, 17-20 October 1966, Oklahoma City, Okla.

Grantham, D.D., Sissenwine, N., and Salmela, H.A. (1965) AFCRL Stratospheric Humidity Program, AFCRL-65-486, pp. 261-272.

Gutnick, M. (1960) An Estimate of Precipitable Water Along High Altitude Ray Paths, Air Force Surveys in Geophysics, No. 120, AFCRL.

Gutnick, M. (1961) How dry the sky?, J. Gephys. Res. 66(No. 9):2867-2871.

Gutnick, M. (1962) Mean Annual Mid-Latitude Moisture Profiles to 31 Km, Air Force Surveys in Geophysics No. 147, AFCRL.

Helliwell, N.C. (1960) Airborne Measurements of the Latitudinal Variations of Frost Point, Temperature and Wind, Sci. Paper I, Air Military Meteorological Office, London.

Helliwell, N.C. and Mackenzie, J.K. (1957) Observations of Humidity, Temperature and Wind at Idris, 23rd May - 2nd June, 1956, MRP 1024, Meteorological Research Committee, London.

Helliwell, N.C., Mackenzie, J.K., and Kerley, M.J. (1956) Further Observations of Humidity up to 50,000 ft Made From an Aircraft of the Meteorological Research Flight 1955, MRP 877, Great Britain Meteorological Research Committee.

Hesstvedt, E. (1965) On the special distribution of some hydrogen components in the mesosphere and lower thermosphere, Tellus 17(No. 3):341-349.

Hesstvedt, E. (1964) On the water vapor content in the high atmosphere, Geofysiske Pubikasjoner, Geophysica Norvegica, XXV, 18 p.

Long, M.J. (1966) A preliminary climatology of thunderstorm penetrations of the tropopause in the United States, JAM 5:467-473.

Mastenbrook, H.J. (1963) The status of water vapor observations above 20 km and implications as to the general circulation, Paper delivered at the Upper Atmosphere Meteorological Symposium, August 21, 1963, Berkeley, California.

Mastenbrook, H.J. (1965a) Frost-Point Hygrometer Measurements in the Stratosphere and the Problem of Moisture Contamination, Humidity and Moisture, Vol. 2, Reinhold Publishing Corp., pp. 480-485.

Mastenbrook, H.J. (1965b) The Vertical Distribution of Water Vapor over Kwajalein Atoll, Marshall Islands, NRL Report 6364, 11 p.

Michaels, D.W. (1965) Noctilucent Cloud Research, Foreign Science Bulletin 6, Library of Congress, pp. 51-55.

Murcray, D.G., Murcray, F.H., and Williams, W.J. (1966) Further data concerning the distribution of water vapor in the stratosphere, Quart. J. Roy. Met. Soc. 92:159-161.

Pybus, E.J. (1966) Private communication with attached graphs of frost-point vs altitude for Grand Turk Island, Bahamas; McMurdo Sound, Antarctica; Palestine, Texas.

References

Rangarajan, S. (1963) Secondary source water vapor in the upper atmosphere, Nature N4872: 1099-1101.

Ratner, B. (1957, 1958) Upper-Air Climatology of the United States, Parts 1 and 2, U.S. Weather Bureau Tech. Paper No. 32.

Roney, P.L. (1965) On the influence of water vapor on the distribution of stratospheric ozone, J. Atmos. Terres. Phys. 27(No.11, 12):1177-1188.

Soberman, R.K. (1963) Noctilucent clouds, Sci. American, June, pp. 51-59.

Suvorov, N.P. (1964) The origin of noctilucent clouds, Priroda 12:114.

Williamson, E.J., Houghton, J.T. (1965) Radiometric measurements of emission from stratospheric water vapour, Quart. J. Roy. Met. Soc. 91(No. 1):330-338.

XVIII. Beginning Studies of Balloons at Off-Design Conditions

Justin H. Smalley
Boulder, Colorado
National Center for Atmospheric Research

1. INTRODUCTION

This paper concerns some initial studies of balloons at off-design condition. The phrase "initial studies" is used advisedly. A balloon is complex and oddly shaped. The analysis is a very difficult problem and will occupy investigators for some time. By "off-design conditions" is meant carrying a payload other than the design payload or floating at an altitude other than the design altitude. A theoretical examination has been made of the shape taken and the stresses developed by (1) balloons carrying payloads both greater and less than the design value, and (2) balloons carrying the design payload at altitudes below the design altitude. This later condition is comparable to a balloon rising to its float altitude.

In this paper consideration has been confined to rotationally symmetric balloons made of nonextensible material. The studies have been performed by numerical methods with a computer. In some respects it is a form of numerical experimentation.

2. BALLOON STYLES

Several styles of balloons have been considered and are illustrated in Figure 1. The solid line shows the shape that the balloon achieves at float altitude. When the gores are cut to this shape with no excess material anywhere, then this style is known as a fully tailored balloon. The fully tailored balloon is one extreme of design. The other extreme of design, or style, is where there is excess material everywhere except at the maximum radius. Such a balloon could also take on the shape indicated by the solid line. If the end fittings at the top and the bottom were released and the material expanded outward as far as it could go, however, a plain tube of material would result. The outer dashed lines indicate the cylindrical shape. This is known as the cylinder balloon. Historically it was contemplation of the shape resulting from the use of a tube of material that led to the concept of the natural-shape balloon. It is apparent that if there is excess material everywhere, there can be no circumferential stress. Between the two extremes just described

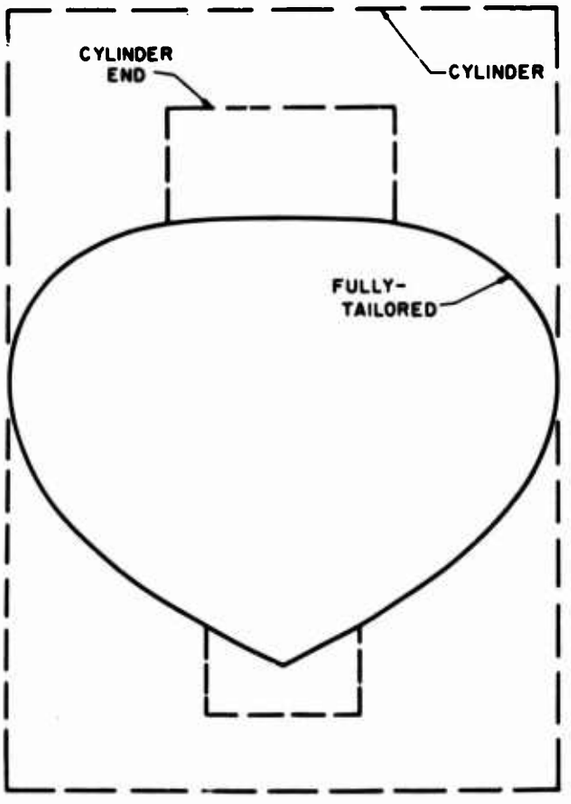

Figure 1. Styles of Balloons

lie several other possible styles. Illustrated in Figure 1 is a balloon with cylinder ends. Between the ends, the balloon is fully tailored. For cylinder-end balloons the gore pattern is cut with rectangular end sections and then the excess material is gathered in the end fittings. We will not consider the effects of the end fittings or the effects of seams or tapes. We will however consider the effects of the cylinder-end sections.

3. DEFINITIONS

The pressure inside a balloon increases from bottom to top. If we fix the position of the zero-pressure level and fix the circumferential stress variation, then the only independent variable remaining is the weight of the gas barrier. The nondimensional form of the gas barrier weight is given by Σ (Figure 2). With the zero-pressure level and the circumferential stress fixed, Σ uniquely defines the shape of the balloon. The shape Σ is determined at the design condition; that is, where the balloon is carrying its design payload at its design altitude. Length units other than λ are sometimes used. It is often more graphic or more meaningful to do so. The use of λ, however, simplifies initial calculations. A subscript "d" is used to represent design conditions.

$\Sigma = kw/b\lambda$

Σ = NON-DIMENSIONAL FILM WEIGHT

w = FILM WEIGHT
(WEIGHT/UNIT AREA)

b = UNIT BUOYANCY OR UNIT LIFT
(LIFT FORCE / UNIT VOLUME)

$\lambda = \sqrt[3]{P/b}$
(LENGTH)

P = PAYLOAD WEIGHT

$k = \sqrt[3]{2\pi}$

Figure 2. Definitions

4. OFF-DESIGN LOADS

With that as an introduction, let us start experimenting with a particular balloon. We have chosen a balloon with cylinder end sections, a Σ value of 0.2 and with all the payload at the bottom. Now, let us assume that somehow we can stand beside the balloon as it floats quietly in the air. Let us also imagine that we have a supply of lifting gas and payload weight. Figure 3 shows what happens as additional payload is added. If a small amount of payload is added, the balloon will start to descend and as it moves downward the zero-pressure level will rise. If nothing more is done the balloon may eventually reach the ground. If, however, payload is added slowly and at the same time gas to offset the payload is added such that the zero-pressure level remains at the bottom of the balloon, our experiments

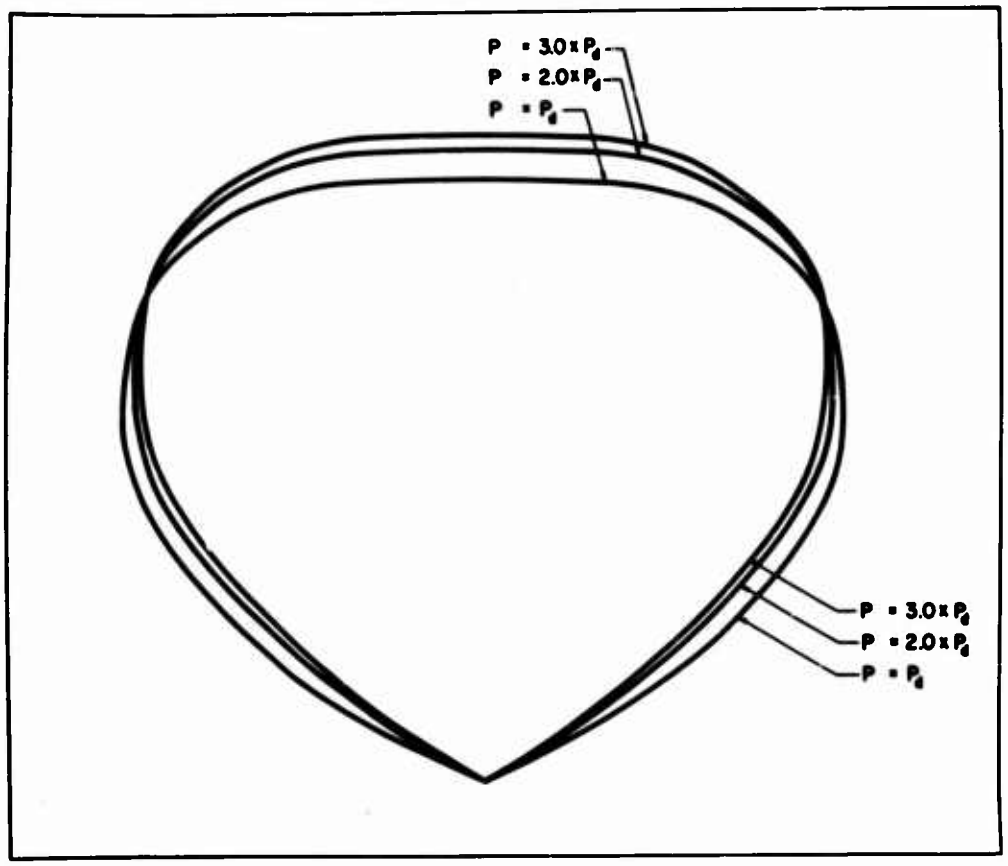

Figure 3. Shapes Taken by Balloon as Payload is Increased

on the computer show that the balloon will seek a new float altitude which is lower than the design value. At the same time it will take on new shapes as indicated by the curves. Shapes are shown for twice the design payload and three times the design payload. While these shapes in themselves are not of great significance, it should be noted that any point on the shape curve moves inward as the balloon is loaded. This means that for payloads greater than the design payload circumferential stresses do not appear. This is an assumption that has been made for some time, and the numerical calculations confirm it.

Now let us slowly remove the excess payload and valve-off the excess gas until design condition is again achieved. In fact, let us continue to slowly remove payload and slowly valve gas, keeping the zero-pressure level still at the bottom of the balloon. Figure 4 shows the shape the balloon takes under these conditions. Remember, for both Figures 3 and 4, the balloon is floating at equilibrium – there is just enough gas to lift itself and the payload. The maximum radius portion of

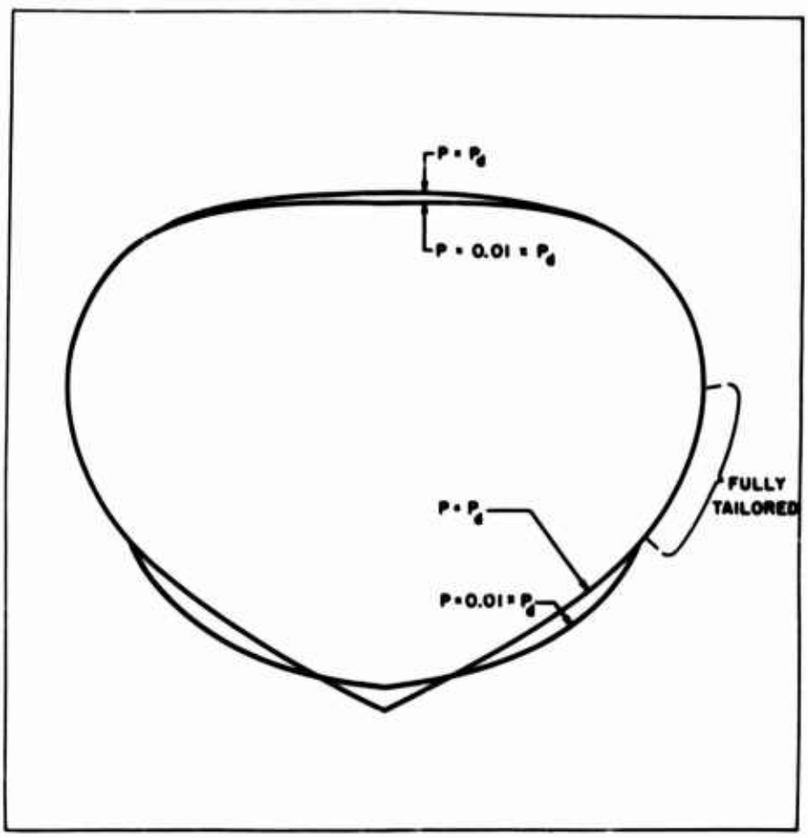

Figure 4. Shapes Taken by Balloon as Payload is Decreased.

the balloon is fully tailored. This section cannot expand, so it maintains its original shape. The top and bottom have cylinder ends and here we see their effect. At the bottom the effect is particularly noticeable. One of the curves is the shape for a payload one hundredth of the design value. The excess material in the lower end section permits the shape to expand. There is also a small amount of expansion of the curve in the top end section and flattening at the top. Our experiments on the computer show that the balloon rises as the payload is decreased. In this particular design circumferential stresses develop only in the fully tailored portion. There may be some designs where circumferential stresses would also appear in the cylinder end sections.

The stresses developed are shown in Figure 5. This figure shows the variation of stress from the bottom of the balloon to the top of the balloon (along a meridian). The stress is given in percent of the stress experienced when carrying the design payload. Under this condition there is 100 percent stress, as indicated by the

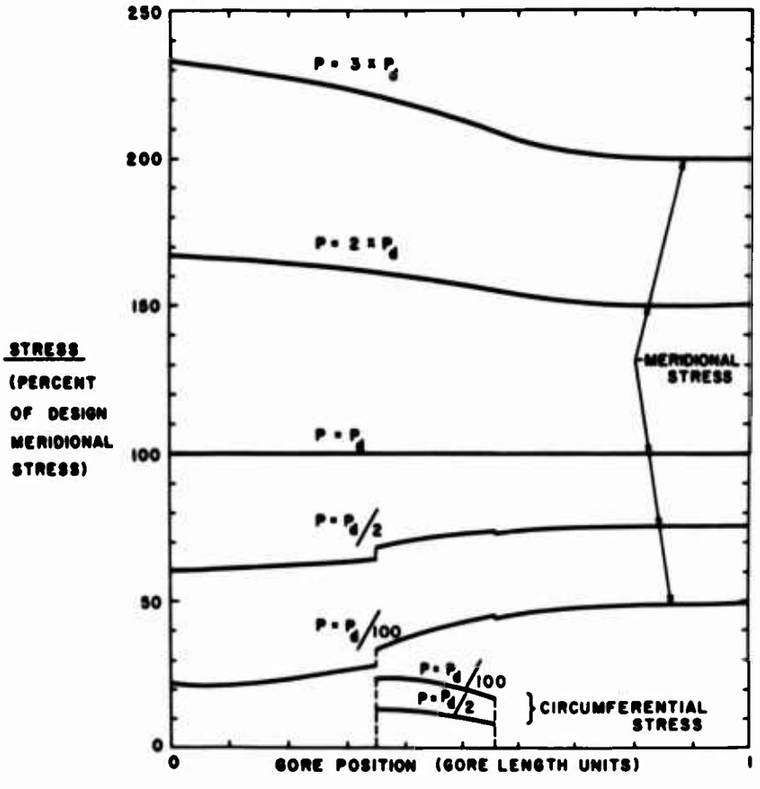

Figure 5. Change in Stress With Change in Payload

$P = P_d$ line. When the payload is doubled the stress rises to between 160 and 170 percent of the design value. When the payload is tripled the meridional stress is now over 200 percent of the design value. There certainly is danger of overloading a balloon. In the same figure two curves show the effect of reducing the payload below the design value. If the payload is one-half the design value, the meridional stress at the bottom is about 60 percent of the design value and at the top is about 75 percent of the design value. With only one hundredth the payload, the stresses are in the 20 to 50 percent range. The important point here is that in the fully tailored portion of the balloon there is a discontinuity in meridional stress and circumferential stress is present. At design condition there is no circumferential stress, but as the payload is reduced circumferential stresses develop as shown by the curves at the bottom of Figure 5. There is an important observation to be made here. In the usual balloon design the seam strength and transverse strength of the material are normally not less than the design meridional stress. Since the maximum circumferential stress is only about 20 percent of the design meridional stress, it is concluded that this particular balloon design does not have a minimum permissible payload.

Figure 6 shows the variation in volume with variation in payload. With just sufficient gas to float the balloon and the payload at equilibrium and to maintain the zero-pressure level at the bottom of the balloon, the maximum volume is approximately 102 percent of the design volume. The volume with three times the design payload is about 95 percent of the design volume.

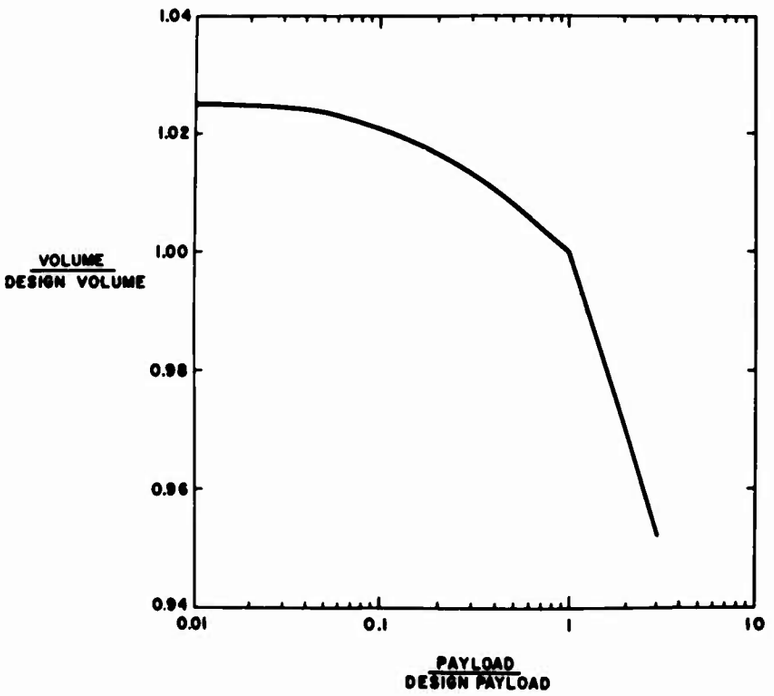

Figure 6. Change in Volume With Change in Payload

5. LOCATION OF CENTER OF GRAVITY AND CENTER OF BUOYANCY

During the calculation of balloon shapes a question occurred: Where is the center of gravity and the center of buoyancy? Figure 7 shows these for natural shape balloons. The weight parameter Σ varies from zero to one. The dashed lines show the center of buoyancy and the center of gravity for a cylinder style balloon. Here we see that for all values of Σ, the center of gravity remains below the center of buoyancy. Remember that only a perfect balloon is being considered. Also the payload is not considered. Something very interesting develops when the fully tailored balloon is analyzed. For Σ equal to zero, the center of

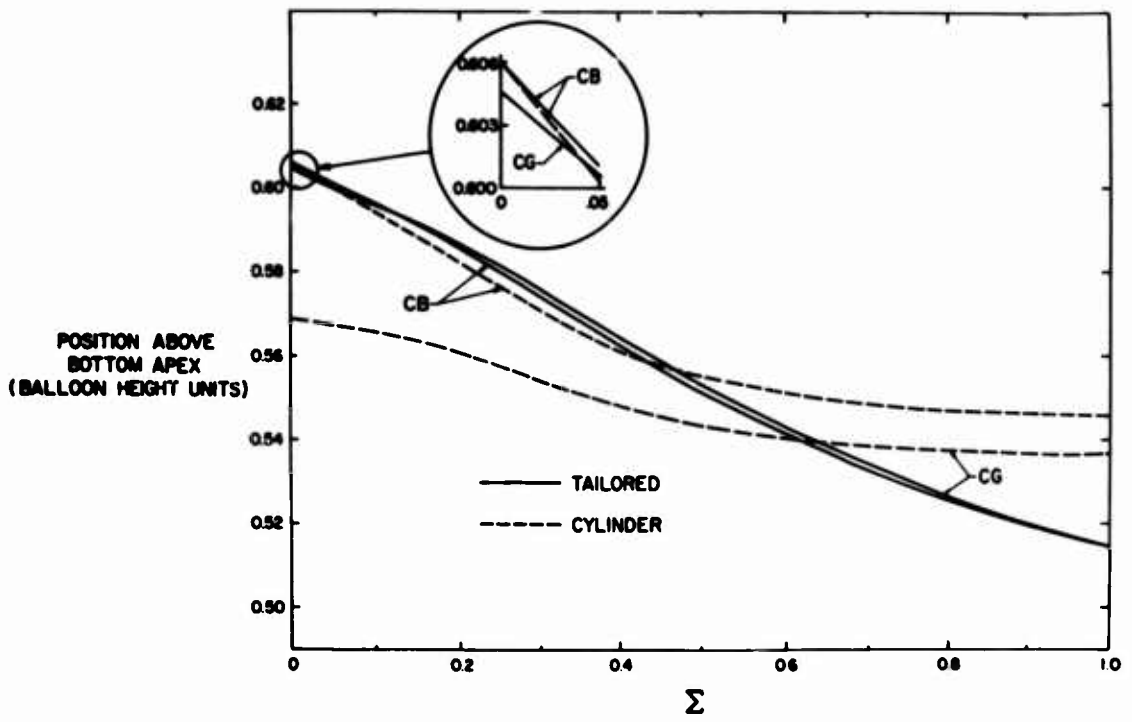

Figure 7. Position of the CB and the CG in a Natural-Shape Balloon

gravity is just below the center of buoyancy. For a Σ of 0.2 and greater, the center of gravity is actually slightly above the center of buoyancy. As Σ increases to one and beyond, the balloon becomes more and more symmetrical – top and bottom – and the CG and CB approach each other at a location of one-half the height of the balloon.

6. OFF-DESIGN ALTITUDES

Returning now to the balloon at off-design conditions, consider a balloon as it is launched and slowly rises to its float altitude. This time we shall consider a fully tailored balloon without any excess material and a Σ value of 0.2. Figure 8 shows the variation of shape as the balloon floats at different altitudes between the surface and its design altitude. In this case the payload is constant at the design value. This study has not considered the effects of the rate of rise. They would be small. Neither has the study considered the effect of free lift, but it could be easily included. For all of these shapes the payload is located at the bottom apex. By using multiples of the design buoyancy the results are generalized but numerical values can be attached to them. If the balloon took on the fully inflated shape at

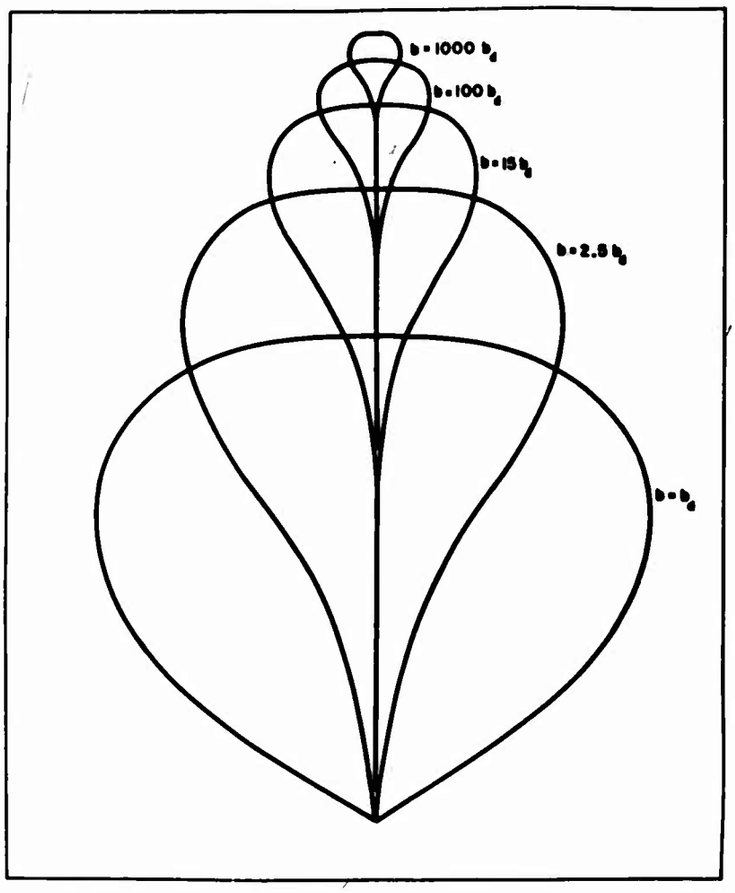

Figure 8. Shape of a Balloon Below its Design Altitude (Σ = 0.2)

140,000 ft, then for a sea-level launch the unit buoyancy would be one-thousand times the buoyancy at 140,000 ft and the shape would be as indicated by the top envelope. If instead the design altitude was about 107,000 ft, then at launch the unit lift would be one-hundred times the value at float and the shape would be as indicated by the second envelope. At 107,000 feet the shape would still be as show by the largest envelope. Recall that we have been dealing with the rotationally symmetric balloon only. However, it is certainly apparent that these curves bear a resemblance to what is seen in a balloon rising to its float altitude.

The computer gives not only the shape of the balloon but the stresses as well. Figure 9 shows the meridional stress in the balloon from the bottom to the top of the balloon. Again the stress is given in terms of the design value experienced at float altitude. This value is, of course, 100 percent and is not seen in the figure. It is easier to think of these results as if the balloon were descending from its float

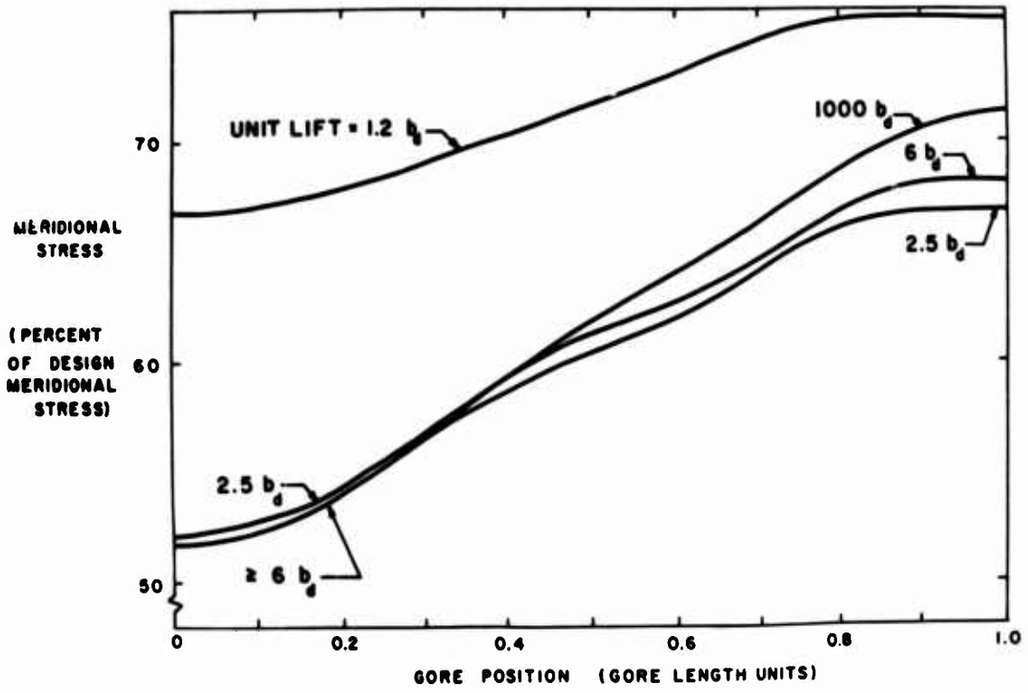

Figure 9. Meridional Stress in a Balloon Below Altitude

altitude. If the balloon were designed for 100,000 ft and descended, for example, from that altitude down to about 95,000 ft ($b = 1.2\ b_d$) the meridional stresses would have dropped to about the 70 percent level. At the bottom of the balloon the meridional stress continues to decrease until we reach an altitude, in this case of about 60,000 ft ($b = 6\ b_d$). Here the apex angle at the bottom of the balloon is essentially zero and the stress no longer changes. The meridional stress at the top of the balloon decreases until an altitude is reached of about 80,000 ft ($b = 2.5\ b_d$). At lower altitudes the meridional stress at the top of the balloon rises slightly. Even when the unit buoyancy is much greater than the design value the meridional stress at the top of the balloon reaches a maximum value of about 72 percent of the design value. At this point, a conclusion can be made but it must be done with "tongue in cheek". The conclusion is that, based on stress considerations, the float condition is the worst condition for the balloon. Such things as temperature, material deployment, and winds have not been considered.

From the standpoint of maximum stresses these calculations may not be particularly realistic. However, some information derived from the same calculations is realistic and will be of particular use to designers of tandem balloon systems. The height of the zero-pressure level above the bottom of the balloon is shown in

Figure 10. With a lift ratio of one, the zero-pressure level is at the bottom. As the lift ratio increases the zero-pressure level rises rapidly. An increasing lift ratio corresponds to a descending balloon. The zero-pressure level in a cylinder balloon is higher than in a comparable fully tailored balloon, but then of course for

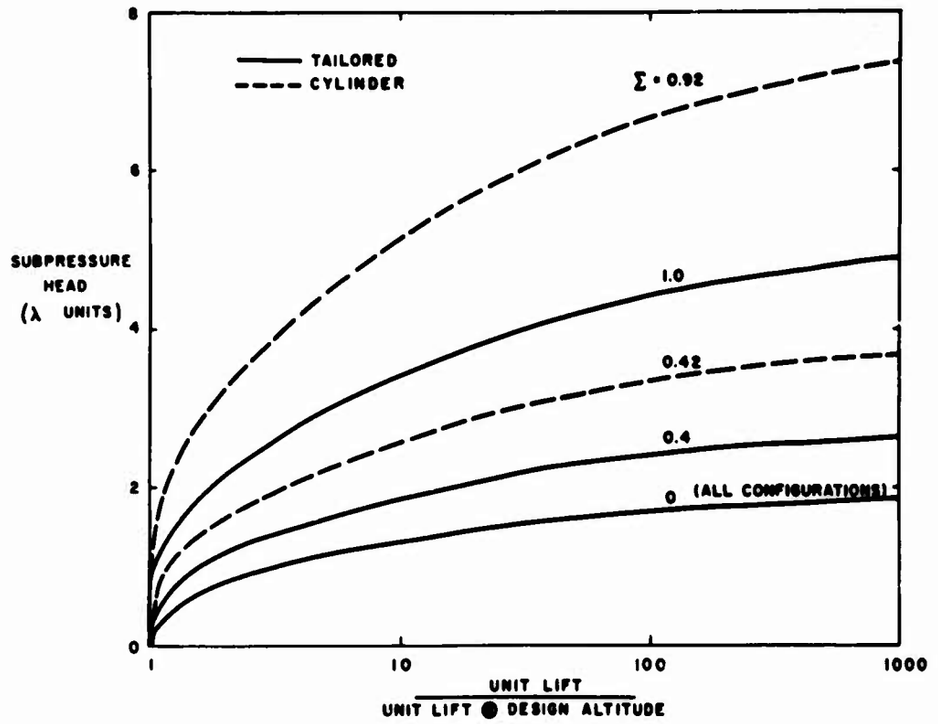

Figure 10. Subpressure Head in a Balloon Below its Design Altitude

a given Σ, the balloon is bigger. If we change from λ units to gore-length units, in effect we take out the size of the balloon. This change in units is shown in Figure 11. Only two curves are shown. When $\Sigma = 0$, the style of balloon is immaterial and the subpressure level varies as shown by the solid line. The dashed line is for a very heavy cylinder balloon with $\Sigma = 0.92$. All zero-pressure balloon designs with Σ approximately 0.9 or less lie between these two curves. For many practical purposes a single curve may be used for any balloon.

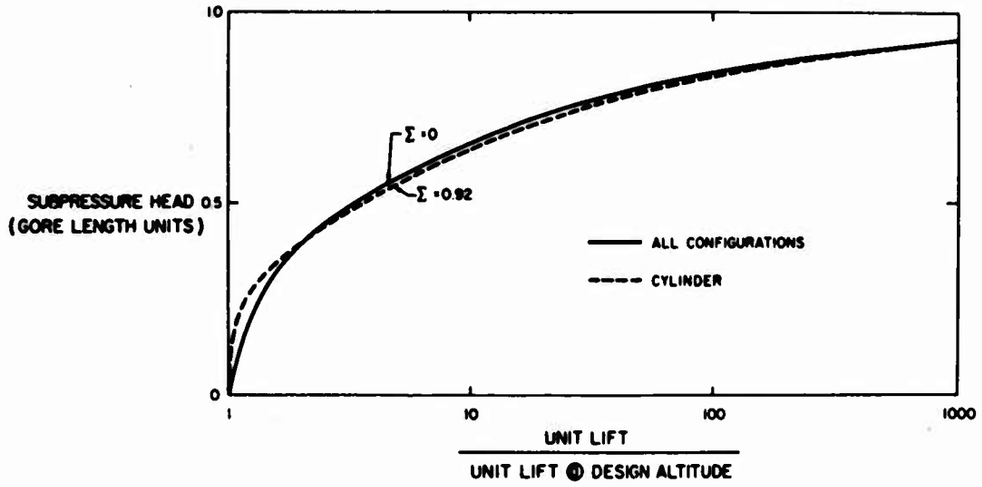

Figure 11. Subpressure Head in a Balloon Below its Design Altitude

7. SUMMARY

It has been shown how the stresses and volume vary for a particular balloon as the payload is changed from essentially no payload to a payload three times the design value. For overloaded balloons there is no circumferential stress. Circumferential stress develops in the fully tailored portion of subloaded balloons. However, it is only on the order of one-quarter the design stresses of present-day materials and seaming methods. This should not prove to be of serious magnitude. We have found a variation of the zero-pressure level in a balloon as it rises to its float altitude, at least for the rotationally symmetric, static case. In the static case, stresses in the rising balloon do not exceed the stresses in the balloon at float.

XIX. Fifty Millibar Balloon Trajectories

Iver A. Lund
Air Force Cambridge Research Laboratories
Bedford, Massachusetts

Abstract

Twice daily 50-mb grid-point height data were used to objectively estimate trajectories of superpressure balloons. The computed trajectories were regarded to be sufficiently representative of actual trajectories and streamlines to conclude that a useful climatology of 50-mb balloon trajectories could be derived from grid-point height data of the type generated by the Third Weather Wing.

1. INTRODUCTION

Large superpressure balloons (payloads of 50 to 100 lb) are being constructed so they will drift for at least one month without deviating more than a few hundred feet from a constant density surface. Such surfaces lie quite close to constant pressure surfaces for which wind fields can more easily be specified from standard upper air data. These balloons often carry costly data-gathering instruments. Scientists need to know the paths the balloons are likely to follow in order to select launch sites and recovery areas. A typical altitude of interest is the 50-mb surface,

about 67,500 ft. An insufficient number of superpressure balloons have been flown at 50 mb to obtain a trajectory climatology from actual flights. This paper presents evidence that balloon trajectories computed from 50-mb height data can be used to develop the needed climatology.

Many different methods for estimating trajectories and trajectory dispersion are described by Angell (1961) and authors referenced in his article. More recent papers on the subject include articles by Lally (1965), Nolan (1965), Charney (1965), and Angell and Hass (1966).

2. DATA

Twice daily (00Z and 12Z) 50-mb height data at 1977 grid points for the three-year period 3 January 1962 (00Z) through 2 January 1965 (12Z) were used for this study. The data were made serially complete by assuming any missing map was the same as the map twelve hours earlier. If two successive maps were missing the first was assumed to be identical to the preceding map and the second was assumed to be identical to the succeeding map. Only twice during the three-year period were more than two successive maps missing. On these two occasions maps were missing for 2-1/2 days and 5-1/2 days, respectively. The last available map was substituted during the first half of the period and the remaining half of the period of missing data was filled in with the first available succeeding map. The dates and hours when maps were missing and for which maps were substituted in their place are shown in Table 1. (None of the trajectories presented in this paper involved more than one missing map.)

3. 50-mb HEIGHT ANALYSIS

The 50-mb height values were obtained from the Global Weather Central, Hq 3rd Weather Wing, Offutt AFB, Nebraska. This section is derived from their descriptions of the computer programs used to generate the height values.

The upper air analysis program used at the Global Weather Central (GWC) is based on the procedures developed by Gilchrist and Cressman (1954), Bergthórssen and Döös (1955), and Döös and Eaton (1957). This program produces a grid-point analysis by successive modifications of a first-guess field. The GWC program differs from those referenced above in the method of obtaining the first-guess fields and in some details of the correction procedure.

The analysis program uses raobs, pibals, and aircraft reports to derive the 50-mb heights. The first-guess field is developed systematically from the lowest level to the desired level, in this case the 50-mb level. In general, a temperature

Table 1. Missing 50-mb Maps. Values in parentheses show which maps were substituted to make the data serially complete

Hour	Day	Mo	Yr	Hour	Day	Mo	Yr	Hour	Day	Mo	Yr
00(12)	02(01)	03	62	00(12)	15(14)	09	62	00(00)	08(06)	10	63
12(00)	06(06)	03	62	12(00)	16(16)	09	62	12(00)	08(06)	10	63
00(12)	07(07)	03	62	00(12)	28(27)	09	62	00(00)	09(06)	10	63
00(12)	24(23)	04	62	00(12)	13(12)	10	62	12(00)	09(12)	10	63
00(12)	07(06)	05	62	12(00)	14(14)	10	62	00(00)	10(12)	10	63
12(00)	09(09)	05	62	00(12)	15(15)	10	62	12(00)	10(12)	10	63
00(00)	10(09)	05	62	12(00)	18(18)	10	62	00(00)	11(12)	10	63
12(00)	10(09)	05	62	00(12)	19(19)	10	62	12(00)	11(12)	10	63
00(00)	11(12)	05	62	12(00)	28(28)	10	62	00(12)	18(17)	11	63
12(00)	11(12)	05	62	00(12)	18(17)	11	62	12(00)	22(22)	12	63
12(00)	01(01)	06	62	00(12)	31(30)	12	62	12(00)	30(30)	12	63
00(12)	10(09)	06	62	12(00)	10(10)	01	63	00(12)	04(03)	02	64
00(12)	09(08)	07	62	12(00)	23(23)	01	63	12(00)	15(15)	03	64
12(00)	13(13)	07	62	00(12)	11(10)	03	63	00(12)	16(16)	03	64
00(12)	15(14)	07	62	00(12)	19(18)	03	63	00(12)	25(24)	03	64
00(12)	21(20)	07	62	00(12)	23(22)	05	63	12(00)	29(29)	03	64
12(00)	21(22)	07	62	12(00)	23(23)	06	63	12(00)	10(10)	09	64
12(00)	24(24)	07	62	12(00)	03(03)	08	63	12(00)	03(03)	10	64
12(00)	26(26)	08	62	00(12)	05(04)	08	63	12(00)	16(16)	10	64
00(12)	27(27)	08	62	12(00)	06(06)	10	63	12(00)	24(24)	11	64
12(00)	01(01)	09	62	00(00)	07(06)	10	63	12(00)	25(25)	11	64
00(12)	03(02)	09	62	12(00)	07(06)	10	63				

analysis is performed first for a given level, then this temperature analysis is used with the height and temperature analysis at the level immediately below to produce an extrapolated height field at the level being worked on. This is then blended with the first-guess offered by extrapolation from the surface, a prognostic chart, or regression equations from a lower level, to produce the first-guess for the height analysis. The temperature first-guess for the next higher level is then modified by a fraction of the difference between analysis and first-guess temperature at the level last analyzed. The cycle is then repeated.

Since the GWC 50-mb analysis involves the use of extrapolation equations from surface analysis, prognostic charts from the JNWP mesh model, prognostic charts from the GWC 6-level program, regression equations developed by the United States Navy, error checks, analysis equations, smoothing procedures, and methods to boost the vorticity after smoothing, it would require a book to explain, in detail, the derivation of the grid-point height values. The purpose of this section of the paper is to stress the fact that the 50-mb heights used in this study were not simply plotted values of the observations as they are reported, but rather they are obtained by methods developed in extensive theoretical and empirical studies.

4. WIND COMPUTATIONS

The wind fields were generated from 50-mb height values with a computer program obtained from the Global Weather Central. This program computed the geostrophic wind components with respect to the GWC grid and then corrected the wind speeds for curvature of the contours. The correction factor was determined using a slightly modified form of the method of Endlich (1961).

5. TRAJECTORY COMPUTATIONS

The wind components with respect to the grid were converted from units of knots to grid interval units per three hours and then the balloon trajectories were computed in three-hour time steps assuming a linear change in the wind field during the twelve-hour period between observations.

Each balloon trajectory was started at the midpoint between three hourly maps. The trajectories were computed from winds interpolated in space, after Thomasell and Welsh (1962) and others, to the balloon position.

The U component at the balloon position (α) is

$$U_\alpha = U_{j+1,i+1} + X(U_{j+1,i} - U_{j+1,i+1}) + Y(U_{j,i+1} - U_{j+1,i+1})$$
$$+ XY(U_{j+1,i+1} + U_{j,i} - U_{j,i+1} - U_{j+1,i})$$

where the grid points and the balloon position are as shown below.

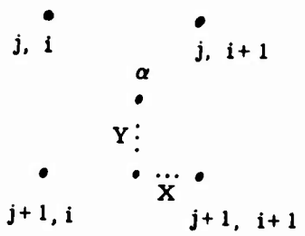

The interpolation of the V component is of similar form.

6. TRAJECTORY EXAMPLES

6.1 Flight 1

The first trajectory was computed to simulate a launch from near Bermuda on 1 June 1962. The simulated launch point matched the location of a superpressure balloon which had been released from Bermuda on 31 May 1962.* The actual balloon drifted at approximately 68,500 ft for a period of 19 days. The simulated flight was extended for 15 days. A comparison between the observed and computed trajectories is shown in Figure 1. The agreement is not good since the computed trajectory is north of the actual trajectory and the balloon travelled faster than the computed speeds. A streamline map of the winds reported between 2 and 3 June showed winds from the southeast in the vicinity of the balloon, but these observations must have been in error since the balloon floated with northeast winds. The computer program appeared to have operated properly.

The computer program was restarted at the reported position of the balloon on 3 June 1962 and a new trajectory was computed. This trajectory is also shown in Figure 1. This time the agreement between the observed and computed trajectories was good for the first four days, but between 8 and 9 June the computed trajectory headed much too far south. The streamline map showed divergence over Mexico and the possibility of the balloon proceeding westward or taking a turn to the south.

*This balloon was launched by the Aerospace Instrumentation Laboratory of AFCRL.

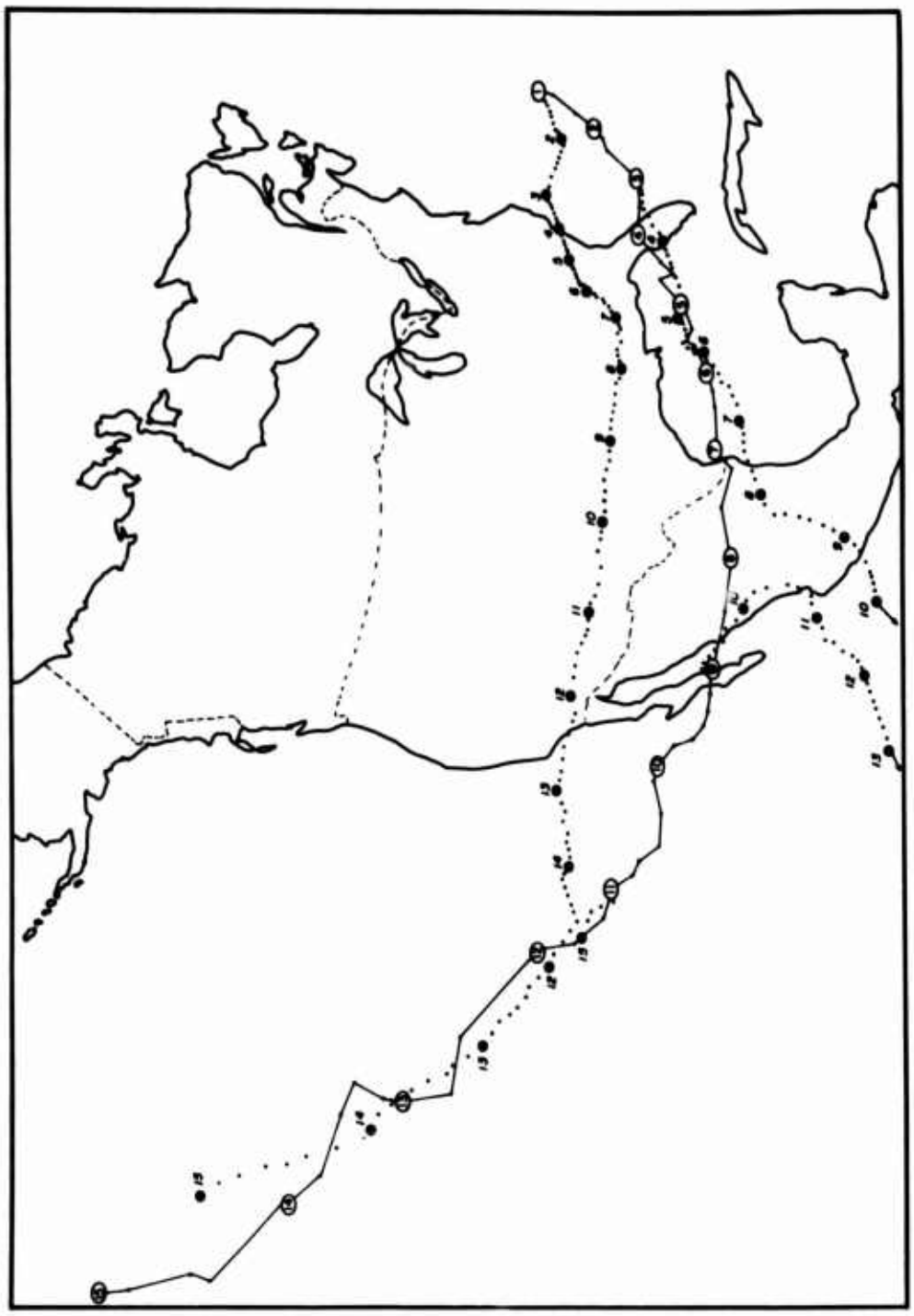

Figure 1. Observed (solid line) and Computed (dotted lines) Trajectories of a Superpressure Balloon Floating at About 68,500 Ft From 1 June to 15 June 1962. Circled numbers show the observed positions and circled X's show the computed positions at 00Z of each day

The computer program was restarted from the reported balloon positions on 6, 9, and 11 June. The trajectory after 6 June closely resembled the trajectory following restarting on 3 June. The 9 and 11 June trajectories are shown in Figure 1. There was no agreement between the actual track of the balloon and the computed trajectory after 9 June. After 11 June the agreement might be described as fair.

6.2 Flight 2

The procedure followed for Flight 1 was used for Flight 2, which was also flown from Bermuda. This flight was launched on 10 June 1962* and the balloon remained at approximately 66,000 ft for a period of 30 days. Again the trajectory was computed for 15 days, this time starting at the reported position of the balloon on 11 June 1962. The actual and computed trajectories are shown in Figure 2. The agreement was remarkably good between the computed and observed positions.

By the 16th of June the computed position was lagging the observed position by about 18 hours, so the computer program was restarted at the balloon position on 16 June. The computed and observed positions are shown in Figure 3. Again the agreement was considered to be very good.

6.3 Twelve Simulated Flights on 2 June 1962

The winds at 50 mb over the United States are generally westerly in winter and easterly in summer. The easterly circulation is just becoming established in early June, and some rather interesting patterns appear in the streamlines. One such pattern is shown in Figure 4. It is the streamline map for 2 June 1962.

Twelve simulated flights were launched on this date to estimate where the balloons are likely to float under such ill-defined conditions. Figure 5 shows the twelve trajectories. The positions 3, 6, 9, 12, and 15 days after launch are connected by a heavy solid line. A substantial amount of clustering is evident.

6.4 Twelve Simulated Flights on 29 June 1962

The streamline map for 29 June 1962, shown in Figure 6, depicts easterly winds over the entire United States. The wind speeds are slightly higher in the south than in the north. Twelve simulated flights were launched on this date to estimate balloon trajectories under conditions of more nearly uniform winds. Figure 7 shows the twelve trajectories.

---

*This balloon was launched by the Aerospace Instrumentation Laboratory of the AFCRL.

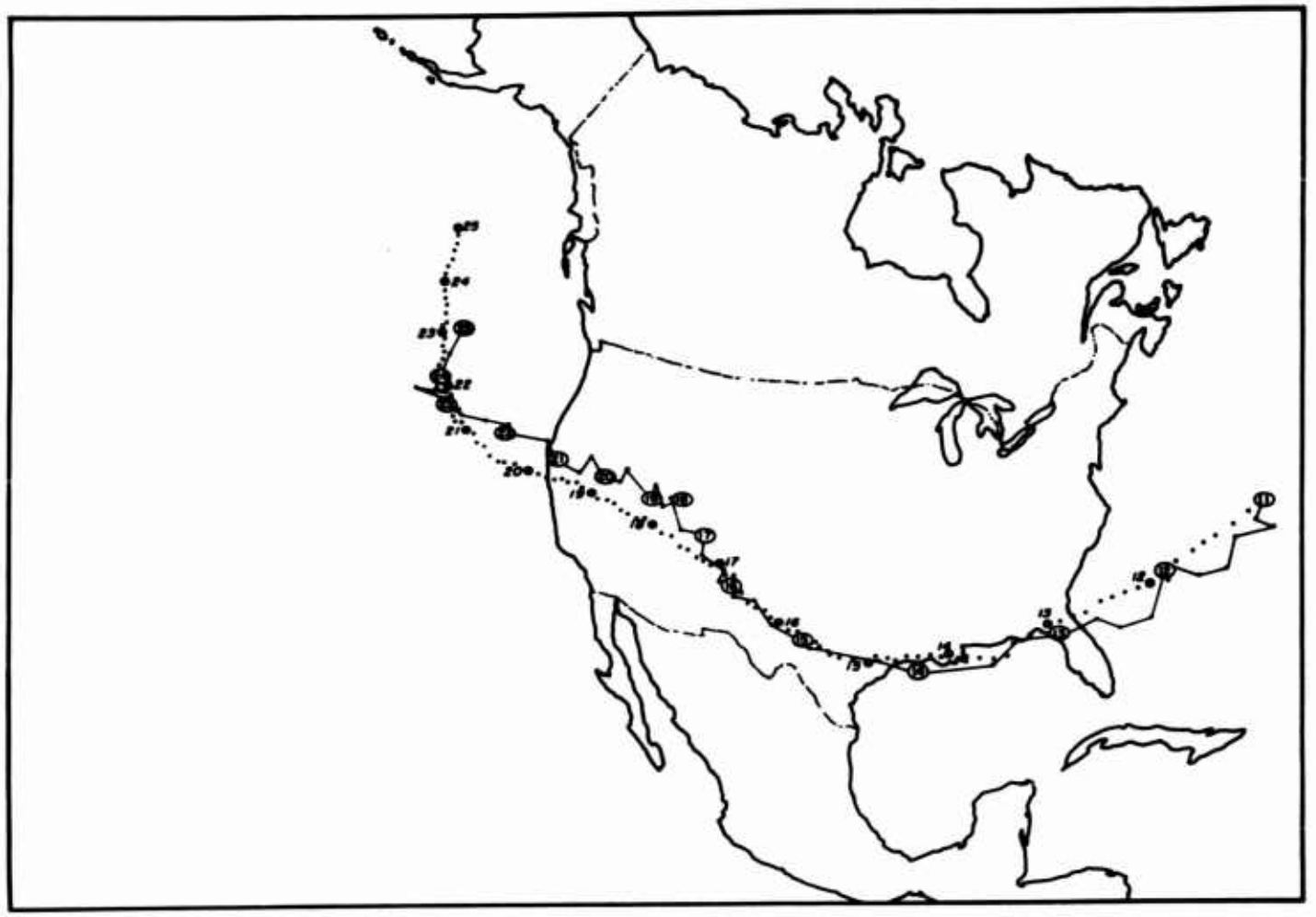

Figure 2. Observed (solid line) and Computed (dotted line) Trajectories of a Superpressure Balloon Observed at About 66,000 Ft From 11 June to 25 June 1962. Circled numbers show the observed positions and circled X's show the computed positions at 00Z of each day

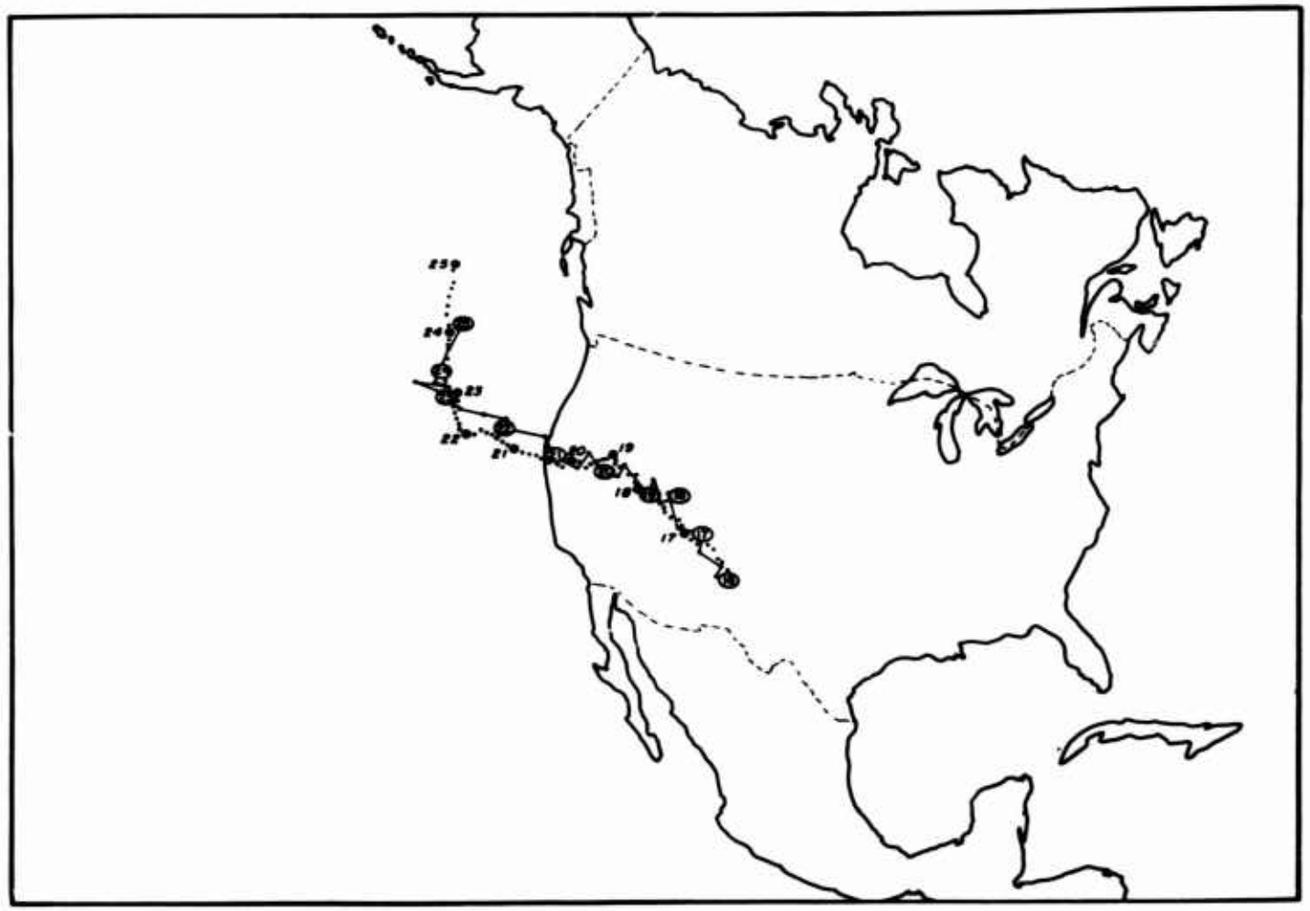

Figure 3. Observed (solid line) and Computed (dotted line) Trajectories of a Superpressure Balloon Floating at About 66,000 Ft From 16 June to 25 June 1962. Circled numbers show the observed positions and circled X's show the computed positions at 00Z of each day

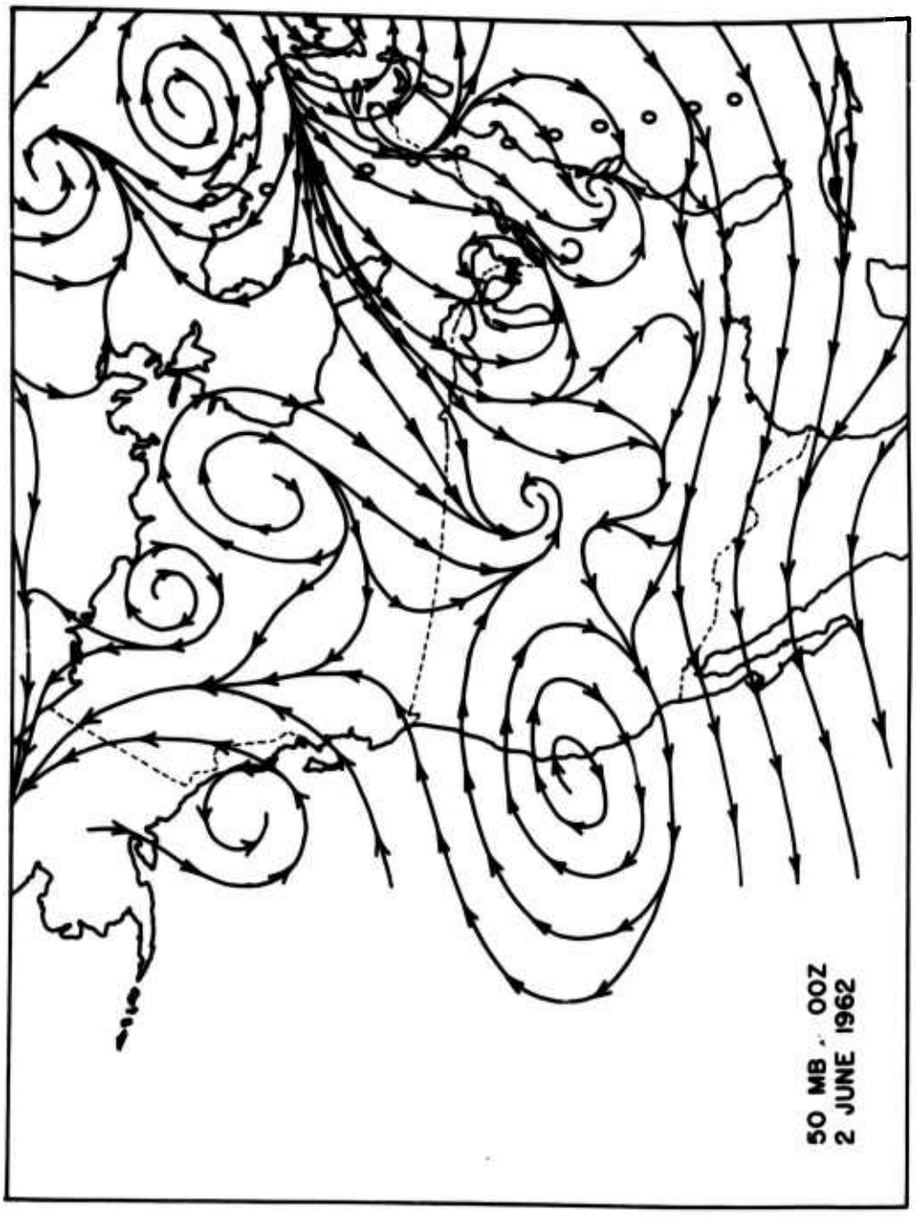

Figure 4. Streamlines at 50-mb Drawn for Winds Reported on 2 June 1962. The twelve zeros mark the positions from which simulated balloon flights were launched

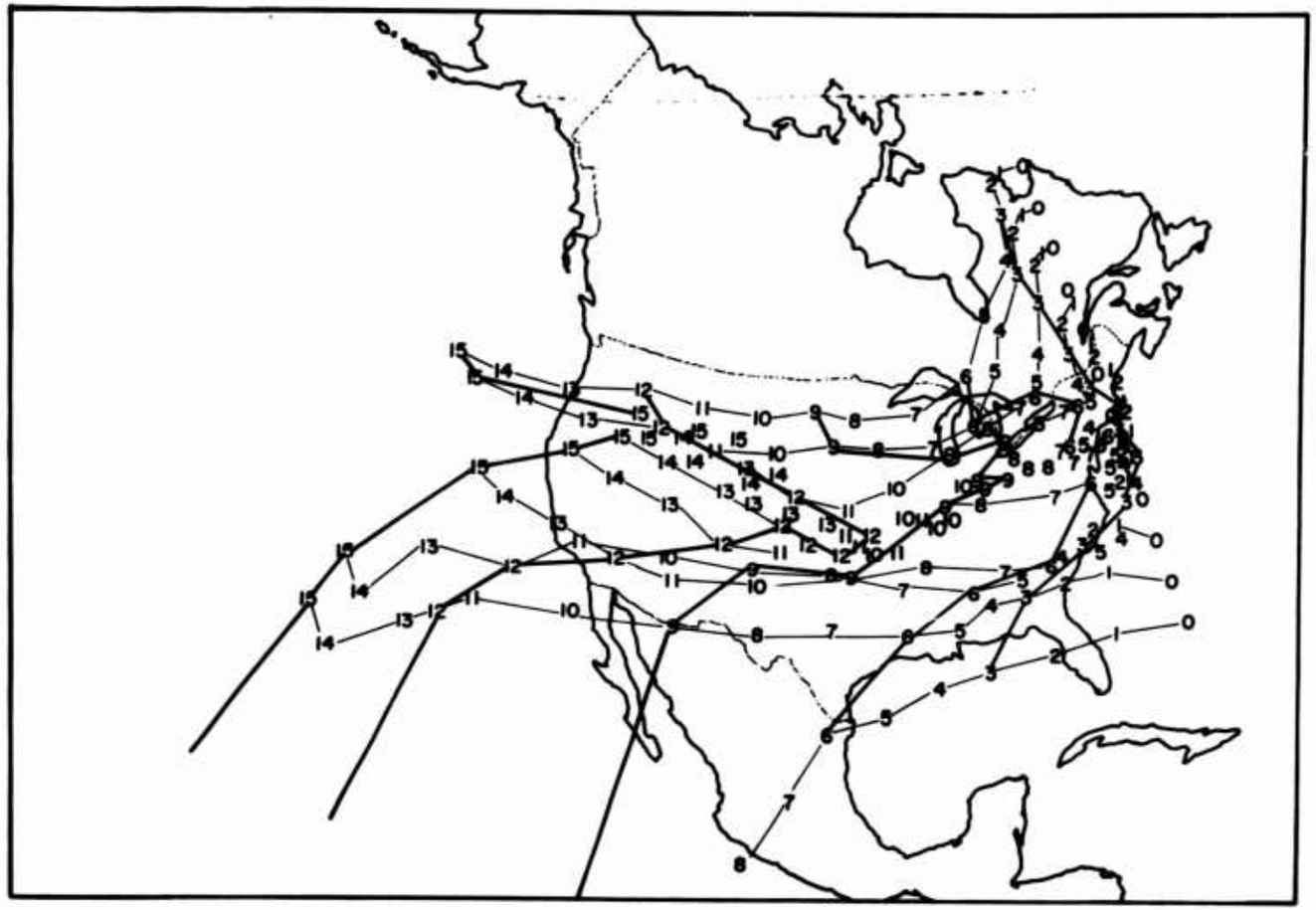

Figure 5. Twelve Simulated Balloon Flights Launched on 2 June 1962. The numbers show the positions of the balloons after each day's travel. The positions after 3, 6, 9, 12, and 15 days are connected by heavy lines

Figure 6. Streamlines at 50 mb Drawn for Winds Reported on 29 June 1962. The twelve zeros mark the positions from which simulated balloon flights were launched

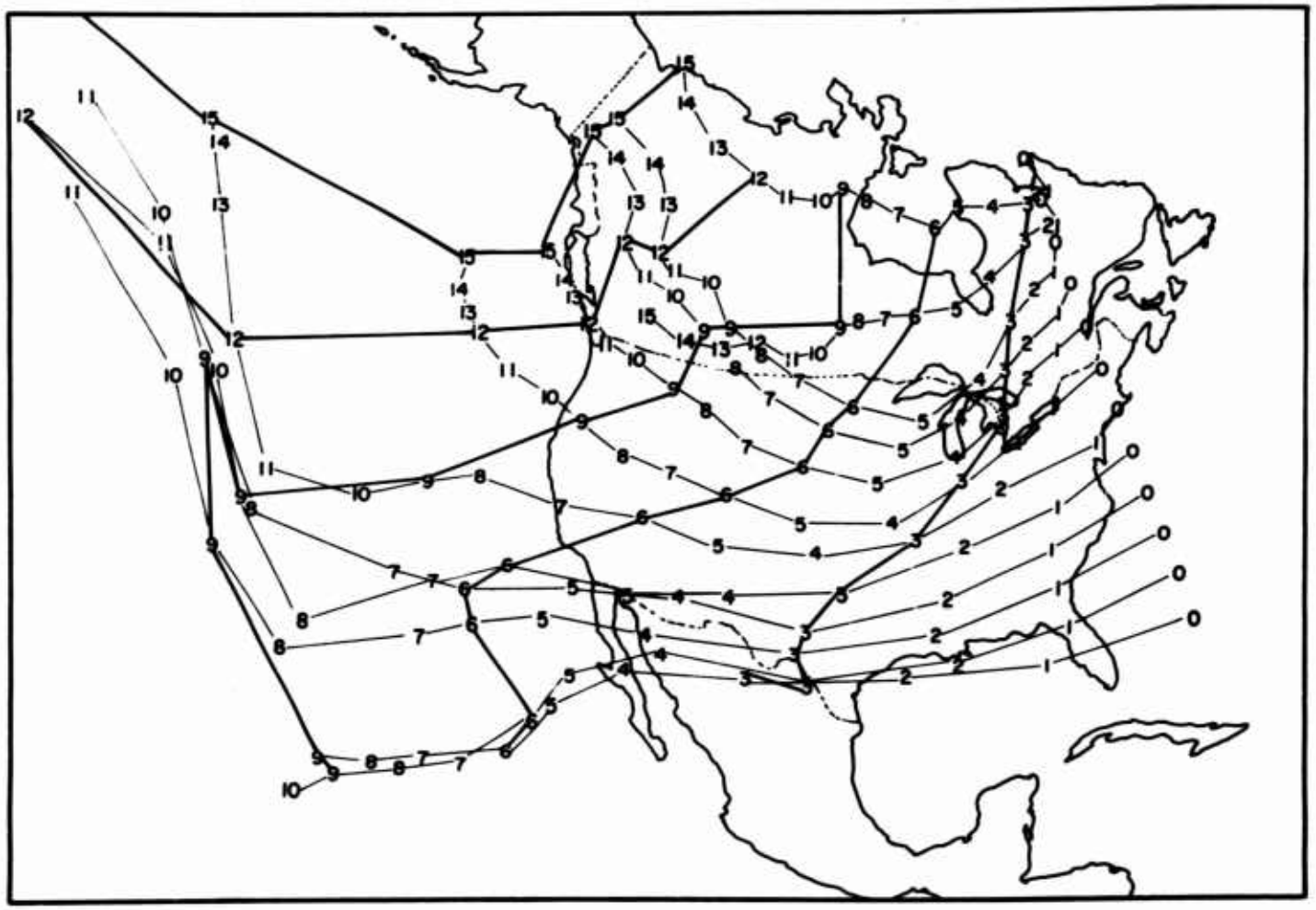

Figure 7. Twelve Simulated Balloon Flights Launched on 29 June 1962. The numbers show the positions of the balloons after each day's travel. The positions after 3, 6, 9, 12, and 15 days are connected by heavy lines

7. TRAJECTORY DISTRIBUTIONS IN JUNE

Simulated 15-day trajectories were computed for launches from Bermuda on every third day of June (1 June, 4 June, . . . , 28 June), for three years (1962, 1963, 1964). The positions of the simulated balloons on the 3rd and 9th days after launch are shown in Figure 8. Also shown on the figure are the median latitude and longitude positions.

Figure 9 shows the positions of the simulated balloons on the 6th and 12th days after launch. Also shown on the figure are the median latitude and longitude positions.

Figure 10 shows positions of the 30 simulated balloons after each of the 15 days of flight. The large numbers mark median latitude and longitude balloon positions. The trajectories are for two actual flights launched in June 1962.

8. CONCLUSIONS

A sample collection of computed trajectories based on 50-mb height analysis derived at SAC is sufficiently representative of actual trajectories and streamlines to warrant generating a provisional trajectory climatology for use in planning superpressure balloon flights at approximately 67,500 ft. Prognostic 50-mb charts with accuracy comparable to present-day analysis would greatly improve estimates of balloon trajectories, but they would not always insure good predictions since there are areas of divergence and convergence where trajectories are highly unpredictable. Winds at 50-mb are frequencly light and variable, adding to the problem of estimating trajectories at this level (Nolan and Smith, 1964).

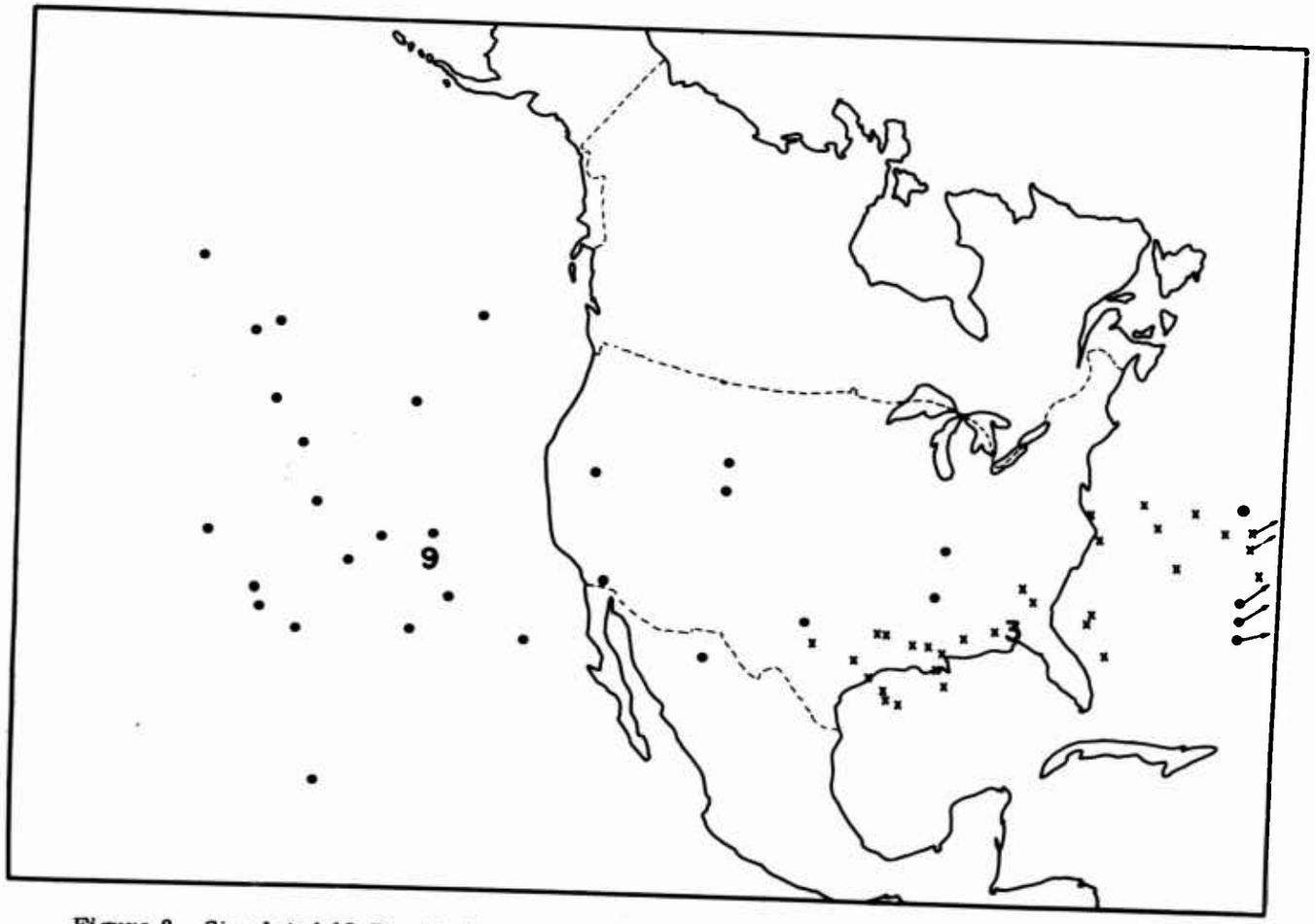

Figure 8. Simulated 15-Day Trajectories for Balloons Released from Bermuda in June. The X's mark balloons positions three days after release; the dots mark positions nine days after release. The numbers 3 and 9 mark median latitude and longitude positions

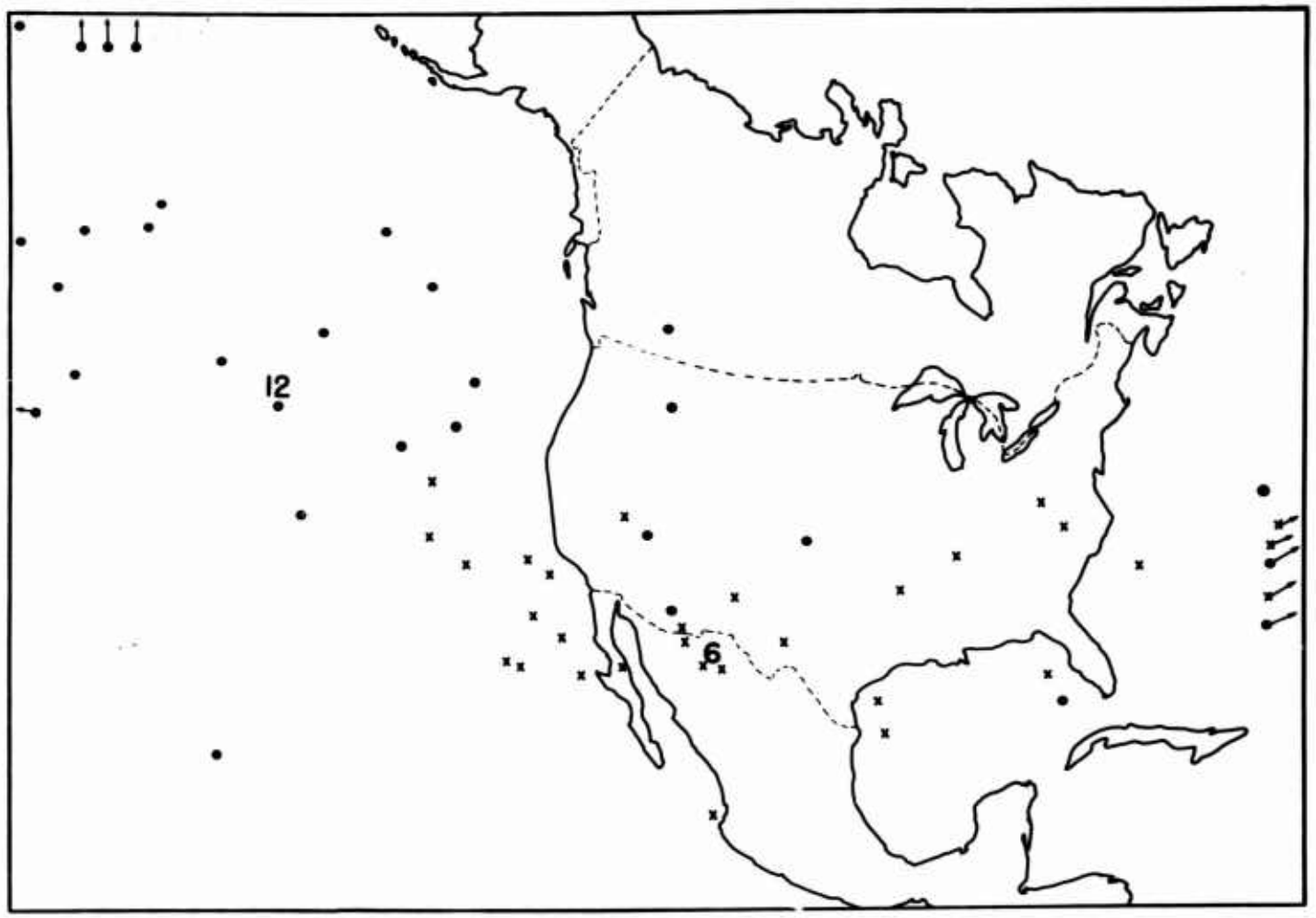

Figure 9. Simulated 15-Day Trajectories for Balloons Released From Bermuda in June. The X's mark balloons positions six days after release; the dots mark positions twelve days after release. The numbers 6 and 12 mark the median latitude and longitude positions

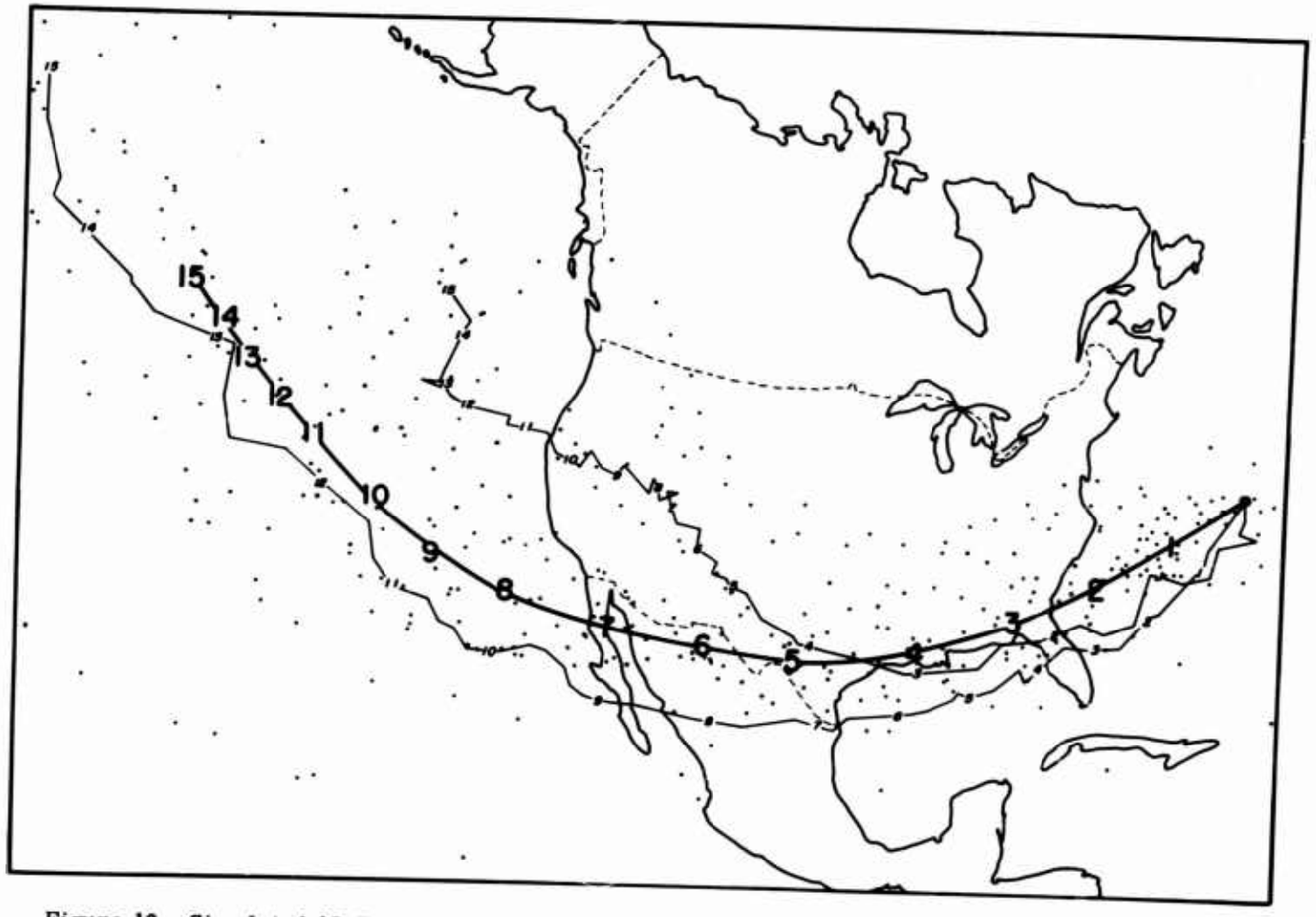

Figure 10. Simulated 15-Day Trajectories for 30 Balloons Released From Bermuda in June. The dots mark positions of balloons after each of 15 days of flight. The large numbers from 1 through 15 mark median latitude and longitude positions. The trajectories are for two actual flights launched in June 1962

Acknowledgments

The author is grateful to Tech Sgt Ralland A. Smith and Mr. Joseph Hess, AFCRL; Mr. Arthur Clayman, General Computing Services, Inc.; Mr. John A. Fusco, Analysis and Computer Systems, Inc.; and personnel of Hq Third Weather Wing for preparing and processing the data. The labors of Mr. Eugene A. Bertoni, AFCRL, in supervising and checking all of the computer operations and preparing the figures, and the valuable advice of Mr. Irving I. Gringorten are especially appreciated.

References

Angell, J.K. (1961) Use of constant-level balloons in meteorology, Adv. in Geophys. 8: 137-219.

Angell, J.K. and Hass, W.A. (1966) Effect of clustering upon a 500-mb horizontal Monthly Weather Review 94:151-165.

Bergthórsson, P. and Döös, B.R. (1955) Numerical weather map analysis, Tellus 7:329-340.

Charney, J.G. (1965) The feasibility of a global observation system, unpublished draft of the report by the Panel on International Meteorological Programs of the Committee on Atmospheric Sciences, 155 pp.

Dóös, B.R. and Eaton, M.A. (1957) Upper-air analysis over ocean areas, Tellus 9:184-194.

Endlich, R.M. (1961) Computation and uses of gradient winds, Monthly Weather Review 89:187-191.

Gilchrist, B., and Cressman, G.P. (1954) An experiment in objective analysis, Tellus 6:309-318.

Lally, V.E. (1965) Superpressure balloon flights from Japan, Air Force Surveys in Geophysics No. 167, pp. 205-211.

Nolan, G.F. (1965) The constancy of the winds in the lower stratosphere and constant-level balloon flight planning, Air Force Surveys in Geophysics No. 166, 23 p.

Nolan, G.F. and Smith, R.A. (1964) High-Altitude Minimum-Wind Fields and Balloon Applications, Environmental Research Papers No. 64, 19 pp.

Thomasell, A. and Welsh, J.C. (1962) The Objective Analysis of Sealevel Pressure and Surface Temperature, Dew Point, and Wind, The Travelers Research Center, Inc., Hartford, Tech. Rpt 7044-36.

XX. The Balloon Borne Optical Beacon: A Useful Geodetic System for Purposes of Densification

Jack A. Cook, Major, USAF, and Michael S. Tavenner, Major, USAF
Air Force Cambridge Research Laboratories
Bedford, Massachusetts

Geodesy, one of the oldest sciences, may be defined simply as that science concerned with the precise positioning of points on the surface of the earth and the determination of the exact size and shape of the earth. In the past the practical aspect of the precise positioning of points was primarily used in the compilation of maps while the determination of the size and shape of the earth was regarded as a purely scientific role. However, modern requirements of the "missile age" requires both the practical and scientific applications be combined to provide answers to operational problems. This paper is concerned only with that portion of geodesy dealing with the precise positioning of points on the earth's surface.

In the past, short distances on land masses have been measured by the surveyor's transit, but now it is necessary to go in jumps of several thousand miles to tie the many separate land masses to a common system. A program designed to accomplish this initial world framework of triangulation which began in 1962 with the launch of the ANNA 1B satellite (Sheldon and Eckhardt, 1964; Williams, 1965) was further expanded with the GEOS-A launch in 1965 (Huber, Gleiber, and Weiss, 1966), and will be continually updated until the operational requirements are satisfied. These satellites are active satellites; that is, they contain optical beacons, transponders, and other electronic components. To make use of the optical beacons

a basic method developed in recent years has been to extend triangulation methods off the earth's surface and use satellites in space as reference points with which to triangulate. Optical methods have been pursued as they offer the possibility of a high degree of accuracy for a modest effort.

Satellites with flashing lights have been orbited and photographed against stellar backgrounds. The star positions are reasonably well known from astronomical observations over the years and the flash points of the satellite can be measured on a photographic plate in relation to these star positions. One observation gives an x and y plate position, while a second observing station can fix the satellite's position uniquely in space. A third station can be carried as an unknown, and with multiple observations its position can be determined. This method of triangulation produces accuracies of 1 part in 500,000 in triangles with bases separated from 1500 to 2000 km, or simply translated into station coordinates an uncertainty of from 1 to 3 meters. But as the bases of the triangles become shorter, this uncertainty increases if the same satellite altitudes are used. Ideal geometry for maximum accuracy requires an equilateral triangle composed of the two ground stations and the satellite. It is obvious, therefore, that as the baselines shorten, as they will have to do in the densification of the primary global network, the satellite will no longer be useful and some alternate vehicle will be required. Two alternate vehicles immediately come to mind, the airplane and the balloon.

In 1962, a B-57 aircraft equipped with a flashing (stroboscopic) light was flown at night at altitudes as high as 35,000 ft between ground camera sites located in the Florida area (Tavenner and Swenson, 1963). Results obtained from this test indicated that this method of azimuth determination is entirely feasible from an operational standpoint but a prime factor was the altitude limitations of the aircraft. From experience gained in this test, a light-weight (5 lb) optical beacon was designed for AFCRL through contractual efforts (EG&G, Inc.) for the specific purpose of being carried aloft by a high-altitude balloon. In 1965 with the combined cooperative efforts of the 1381st GSS (MAC) and the AFCRL balloon branches both at Bedford and at Holloman AFB, a balloon-borne optical beacon test was conducted.

The objectives of this test were as follows:

1. Evaluate the performance of the optical beacon at altitude.
2. Feasibility of balloon-borne optical-beacon geodetic surveying.

In order to perform geodetic stellar triangulation, three technical problems had to be considered. These are:

(1) recording flash images along with star images on a photographic plate,

(2) recording the time of exposure of the star background,

(3) recording the time of exposure of the beacon flash.

The method used in this test to solve these technical problems was that of allowing a high-altitude research balloon to carry aloft a flashing light which is

photographed by a one-meter focal-length camera (PC-1000). The flash image points are recorded on a photographic plate against a background of star images. By recording the time of the opening and closing of the camera shutter, one obtains a coordinate system in which to measure. This timing data need not be at the exact time of flash, since a translation in time constitutes a direct rotation of the coordinate system and can be easily computed, provided the event and exposure times are accurately known. The time accuracies depend on the measurement accuracy required. For measurements with accuracies of the order of less than one second of arc, star positions need only be known to ± 10 ms. Also, to maintain measurement accuracies when considering nominal wind velocities, approaching theoretical aims of 1 part in 10^6 or approximately 10 cm at 100 km ranges, the timing requirement for the optical beacon's flashes had to be known to ± 10 ms. With the accuracy requirements determined, the electronic package designed to record the time of each flash was fabricated at AFCRL, support by three PC-1000 camera teams obtained from the 1381st GSS(MAS), and balloon flight dates obtained from AFCRL Det #1, Holloman AFB.

The field evaluation was conducted in early June 1966 with the first flight flown on the night of 6 June. Cameras were positioned at Walker AFB, New Mexico; White Sands Missile Center, New Mexico; and Stallion Range Camp located on the northwest corner of the White Sands Missile Test Range. This placement formed a triangle with two sides of 205-km length and one side 155-km length. Due to the forecast winds for launch, Artesia, New Mexico was selected as the launch site with the balloon programmed to reach float altitude (100,000 ft) over Artesia and then float in a westerly direction, passing through the center of the established triangle.

The ground preparations for this flight were quite simple. All timing signals were recorded with reference to WWV. The necessary corrections to correct this time to UT-2 were made later in the reduction phase. The beacon's repetition rate was selected prior to launch, nominally 1 flash per 10 sec, with the only control capability being of turning the beacon on or off by means of a commanded switch closure. Flash time was observed by a photo diode placed next to the flash tube (thus avoiding spurious flash signals from internal electronic noise). This photo diode signal would then key a transmitter for approximately 1 sec. This signal would be recorded at the ground site through a receiver onto one channel of a stereo tape recorder. On the other channel of this recorder the time signal from WWV was continuously recorded. During the data-reduction phase, the tape is played back through an oscillograph and the flash time is directly scaled against WWV. In concept, this method of timing is perfectly feasible. In practice, satisfactory results were obtained with minor and irritating difficulties. Two problems were apparent: (1) Noise on the HF frequencies used (6771 kHz and 4875 kHz) in the

receivers, and noise generated by the tape recorder; (2) the transmitter was keyed by a mechanical relay and the bounce of the contacts caused a double pulse at the beginning of the tone. This double pulse, plus a slow apparent rise time (approximately 7 ms) of the signal, made it difficult to precisely define the start of the signal. However, in spite of these difficulties, the time tapes are reducible to an accuracy better than 5 ms.

A key question that was required to be answered was the procedure to be employed by the camera teams for aiming their cameras at the optical beacon. Original ideas on this subject included the following thoughts:

(1) Each camera team would independently observe the beacon through binoculars and preset the camera.

(2) Information received at balloon operations from radar trackers located on the range or from a direction-finding station receiving signals from the radiosonde would be used to establish the ground position of the balloon. "Look-Angles" for each camera site would be computed and then transmitted via telephone to the various stations.

(3) The balloon would be tracked by means of theodolite. This information along with the known altitude of the balloon provided enough data to position the balloon and look angles were then computed and transmitted as stated above by Williams (1965).

All three of these methods were attempted and upon evaluation of the results of each, the following method is considered the most reliable.

Each station should be provided with a tracking theodolite. Both camera and theodolite are accurately aligned in azimuth, placing both in the same reference system. Once the balloon reaches float altitude the horizontal movement of the balloon is only a few degrees per minute. Tracking of the balloon therefore presents no problem and the increased magnification of the theodolite greatly enhances the operators ability for continually tracking the beacon at extended ranges. Just prior to selected event times, azimuth and elevation of the balloon can be taken from the theodolite and set into the camera. The PC-1000's 10° field of view can readily accommodate small inaccuracies in position. Periodically, azimuth and elevation can be transmitted to the command post where either multiple or single-station fixing can be done, thus providing a rapid method of positioning the balloon's flight path.

From the flight flown on the night of 6 June 1966, the amount of useful geodetic data collected consists of three 2-station ties, and four 3-station ties covering a time period of just 1 hr and 30 min. The balloon had been observed and photographs taken for a period of approximately 3 hr, but since the balloon's flight path was in very close proximity to a full moon the early photographic plates were fogged beyond use.

Examination of the useful photograph plates indicate an average of 22 recorded flash images per plate from each camera site. One observed effect was an apparent irregular image spacing on the photographic plates, as well as a variation of flash-image size and density. An initial assessment of plate 102-M-BT3-10-07 June 66 taken at 1012Z from the Stallion site of the balloon located at a distance of 198 km and an altitude of 98,500 ft and with "look angles" of 135° azimuth and 6.5° elevation revealed the following information:

(a) The cross station velocity component of the balloon approximated 7 meters/sec.

(b) The irregular spacing of the image of 0.075 mm showed a pendulum effect with an excursion approaching 40 ft or an angular movement of 2-1/2° from perpendicular.

(c) The change in image densities verified the above estimate when the beam patterns of the beacon were examined. A swing of the above magnitude would produce a change in light intensity due to changing the beam pattern by a factor of 50 percent, which would decrease the image size and density by a distinct factor.

(d) Based on design studies, the optical beacon was to produce an exposure of 0.008 meter candle seconds (that required to expose an image on a 103F spectroscopic plate) when using a PC-1000 camera of 200-mm aperture lens at a distance of 185 km. The photographic plate (102-M-BT3-10-7 June 66) was of special interest as it was on the threshold of recording images at 198 km under conditions of good visibility. Most images were detectable while perhaps 30 percent were undetectable by methods other than a statistical grain count. As a result of these considerations, it was felt that the flash lamp met its design criteria.

Based on the results of these tests, the following conclusions can be reached:

1. The optical beacon performed exceedingly well and met all design requirements as to weight, flash rate, environmental and optical parameters.

2. Prior to rigid geometric solution and error analysis, preliminary results indicate that a geodetic surveying system using the balloon-borne optical beacon for intermediate distances would be feasible.

Along with the evaluation of the feasibility of using this system primarily for geodetic surveying, other observed effects of this test became apparent. These are listed as follows:

a) An optical beacon when placed aboard a research balloon provides a precise method of measuring wind shifts and wind characteristics at high altitudes.

b) A method for cheap but accurate tracking and positioning of balloon flights becomes available, thus giving the launch facility a better 24-hr launch capability. Deviations from programmed flight profiles can be quickly detected through use of tracking theodolites and rapid data analysis.

c) A method is available at the command post for the rapid post-mission analysis of precise positioning of experimental payloads.

d) Velocity vector measurements by 2-station ties can be recovered rapidly through data analysis.

Now that the initial feasibility tests are completed and it is felt that this system can become a useful geodetic surveying tool, what remains to be done to produce the final operational product? The interfacing of the optical beacons with its necessary electronic package was at best a breadboard model. Work is presently continuing to incorporate a highly reliable electronic package into the optical beacon, keeping in mind the weight restrictions placed on the payload. The balloons used at Holloman AFB for these tests can hardly be classified as an operational system capable of being launched in remote areas by a two or three man crew. This is exactly what is needed, a balloon matched to the necessary payload capable of being launched on a world-wide basis. This balloon would be required to carry a payload of approximately 20 lb to an altitude greater than 80,000 ft. A recovery of the payload system is also a requirement for this system. And finally, more accurate and complete high altitude (above 80,000 ft) meteorological forecast data must be made readily available.

References

Huber, D.N., Gleiber, W.L., and Weiss, C. (1966) Geodetic Positioning with the PC-1000 Camera System, Aeronautical Chart and Information Center.

Sheldon, L.L. and Eckhardt, D.H. (1964) Geodetic Positioning From Simultaneous Optical Observations of the ANNA 1-B Satellite, AFCRL Rpt 64-562.

Tavenner, M.S. and Swenson, P.B. (1963) Operational Concepts of Photogrammetric Determinations of Azimuths Over Intermediate Distances, Journal of the Surveying and Mapping Division, Proc. Am. Soc. Civ. Engr.

Williams, O.W. (1965) ANNA Satellite Yields Photogrammetric Parameters, AFCRL Rpt 65-379.

XXI. Ballute Retardation Device for Meteorological Rocketsondes

John B. Wright
Air Force Cambridge Research Laboratories
Bedford, Massachusetts

John J. Graham, Jr.
Goodyear Aerospace
Akron, Ohio

Abstract

The basic aerodynamic and structural aspects of the BALLUTE* (BALLoon-parachUTE) are discussed, and some current applications are cited. Under an Air Force Cambridge Research Laboratories contract, Goodyear Aerospace developed the BALLUTE into configurations suitable as substitutes for conventional silk parachutes used to retard falling rocketsondes. The evolution of these BALLUTEs is described in this paper. Test data from flights of the Arcasonde and Loki-Dartsonde BALLUTE systems are used to show performance with respect to descent rate, stability, telemetry reception, weight, and volume. By extrapolation of current flight performance envelopes, a preview of the BALLUTE potential in meteorological sounding technology is described.

*TM, Goodyear Aerospace Corporation, Akron, Ohio.

1. INTRODUCTION

Meteorological use of parachutes began with simple paper devices placed in the train of balloonsonde systems. These chutes prevented human injury from falling radiosondes after balloons burst at the end of the sounding periods. When rocket-sounding systems extended the search for atmospheric knowledge above balloon levels, the parachute became necessary to allow a reasonably slow and controlled descent during the sensing phase of the radiosonde after ejection at rocket apogee (200,000 ft). Horizontal motion during descent of the parachute-sonde combination, like the ascending balloon-sonde, is interpreted as wind motion.

Parachutes currently used in standard Arcasonde and Loki-dartsonde sounding systems represent state-of-the-art design from the middle 1950's. Generally made of silk, the parachutes have hemispherical or elliptical shapes, radar reflective properties, and appearances much like personnel or cargo chutes.

Application of conventional parachutes for descent retardation from altitudes of 200,000 to 100,000 ft has proved to be less than optimum. Parachute attitude or stability nominally is attained by controlled air flow through the canopy. This flow is established through the selection of cloth porosity. As altitude increases, effective fabric porosity decreases and at the highest altitudes considered, little effective porosity is present (Heinrich and Haak, 1962).

During continuing operational missions, it has been noted that temperature recordings from rocketsondes have intense and periodic signal dropouts that could have been caused by periodic sonde motion. Substitution of a camera for the sonde produced motion pictures of a parachute (Murrow and Whillock, 1964). These pictures show pitching-mode oscillations of as much as ±45 deg at the highest altitudes, motions that diminish as the sonde descends. A parachute with little or no porosity may be stable at an angle of attack other than zero. In such a case, a gliding motion may be inferred improperly to be caused by wind.

To eliminate these undesirable features, several methods are being evaluated by the Aerospace Instrumentation Laboratory of AFCRL. Several experimenters have shown that geometric porosity (cutting of holes in parachute canopies made of lightweight, nonporous thin films) stabilizes the descending system. Another approach to the problems of retarding and stabilizing a radiosonde and sensing winds is being sponsored by AFCRL. Goodyear Aerospace Corporation (GAC) is engaged in developing its BALLUTE into a retardation system for packaging into the volume available in the Arcas and Loki-dart rocketsondes. The program goal is to design a radar reflective BALLUTE that will (1) provide a slow system descent rate with a maximum value of 300 fps at 180,000 ft, a rate about equal to current parachute fall rates; (2) have no more than a 3° coning angle; (3) be competitive in cost with standard parachutes; and (4) be 98 percent reliable.

2. EVOLUTION OF BALLUTE CONCEPT

Goodyear Aerospace began development of the BALLUTE about eight years ago when space requirements demanded deceleration, stabilization, and recovery of payloads from high altitudes and supersonic velocities. The then known parachute configurations were unable to perform adequately in this space environment. In recent years, however, new parachute designs employing geometric porosity and tailored canopies are exhibiting promising performance. Such concepts as Goodyear Aerospace's Parasonic parachute and Mr. Murrow's (NASA-Langley) work with the disk-gap-band and cross-form are breaking the Mach number and density barriers.

In an early Goodyear Aerospace-sponsored approach to the problem, drag was attained towing a pressurized sphere behind the recoverable article.

Although this approach supplied required drag forces, the sphere was violently unstable in subsonic and transonic velocity regimes. To stabilize the sphere, an inflated torus called a burble fence was added to act as a vortex generator and to ensure flow separation at a constant station around the BALLUTE.

The burble fence gradually progressed from an original 3 percent of the basic BALLUTE diameter to from 10 to 25 percent for current applications. Canned gas pressurization of the BALLUTE gave way to ram-air inflation as detailed analysis and wind tunnel testing proceeded.

Concurrent with evolution of BALLUTE geometry, the isotensoid theory of pressure membrane design for BALLUTE applications was developed (Houtz, 1962). This design permits maximum use of the film or fabric by causing membrane stresses to be nearly equal in all directions over the total BALLUTE surface.

BALLUTEs of various configurations are being used on such programs as Gemini, Air Launched, Air Recoverable Rocket (ALARR), and the Prime lifting reentry vehicle being developed by Martin Co.

The high degree of stability and drag efficiency made the BALLUTE a promising candidate for rocketsonde missions.

3. ANATOMY OF A BALLUTE

A BALLUTE, like the parachute, requires a dynamic environment. Aerodynamic pressures from the passage of the device through the air must first inflate the BALLUTE or parachute to its operational shape. This inflated shape determines the effectiveness of the devices as stabilizer and decelerator.

The BALLUTE, unlike the parachute, has a relatively small inflation inlet that takes longer to inflate (4 to 6 sec in the case of the Arcasonde BALLUTE) than the

parachute. Conversely, in the event of a gust or wind shear, inflation air cannot be rapidly expelled, permitting the BALLUTE to maintain its geometric and, therefore, its aerodynamic characteristics. For this reason, the BALLUTE may be considered aerodynamically as a rigid body (see Figures 1 and 2).

The basic principle underlying the operation of the BALLUTE is that the ram-air inlet oriented into the airflow allows pressurization of the body to a level equal to the sum of the dynamic and ambient pressures of the flow. This internal pressure acting normal to the membrane is always greater than a combination of the external ambient pressure and the dynamic forces that act externally and obliquely on the membrane.

Figure 3 shows the distribution of pressure on the BALLUTE in subsonic flow as determined by wind tunnel tests. The magnitude of the forces is depicted as percentage of the free-stream dynamic pressure.

Figure 4 presents only the axial components of the external forces or those that affect drag.

In the forward area of the burble, negative pressures created by accelerated flow result in a thrust component.

The major portion of the drag results from negative base pressure rather than direct frontal loads. The center of pressure is therefore further aft than might be expected; this enhances stability.

Figure 5 shows the differential or cumulative pressures across the membrane. These pressures represent the energy level that must be reacted by tension in the BALLUTE film.

Early in Rocketsonde development the toroidal type burble fence proved inadequate to provide the ±3° stability requirement, resulting in the evolution of the hexagonal burble fence.

Figure 6 is a schematic representation of the flow lines around the BALLUTE. Initially, the flow is three-dimensional but, as it passes over the burble fence segments, becomes two-dimensional.

Adjacent sheets of air induce small-scale perturbations along the line of intersection at six symmetrically located points in the transverse plane of the BALLUTE. This additional wake control provides the required ±3° stability.

4. METEOROLOGICAL ROCKETSONDE MISSION

4.1 General

Currently at Goodyear Aerospace, development of a BALLUTE system for two separate rocketsondes is underway, the Arcasonde and the Loki-dartsonde.

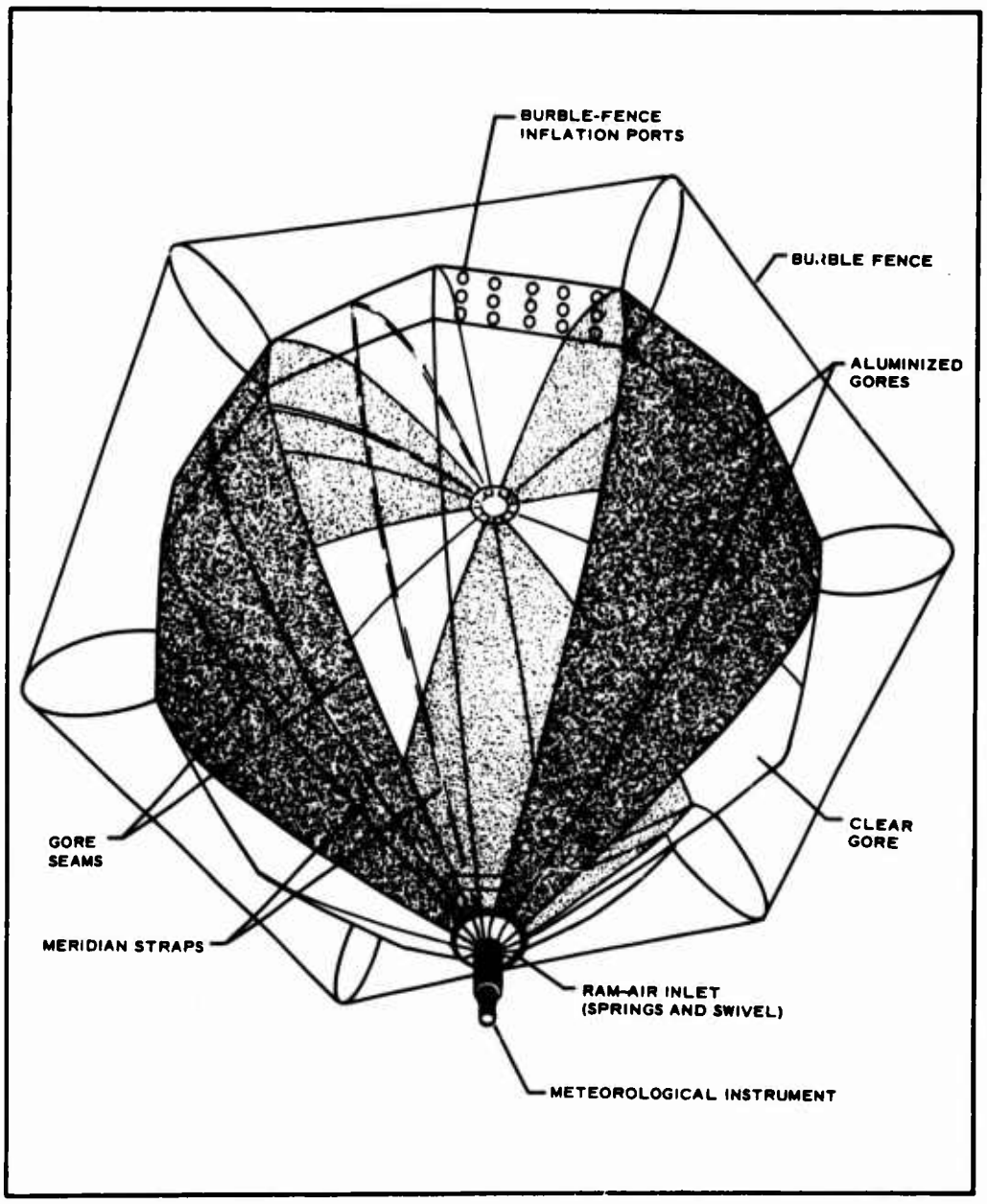

Figure 1. BALLUTE Component Schematic

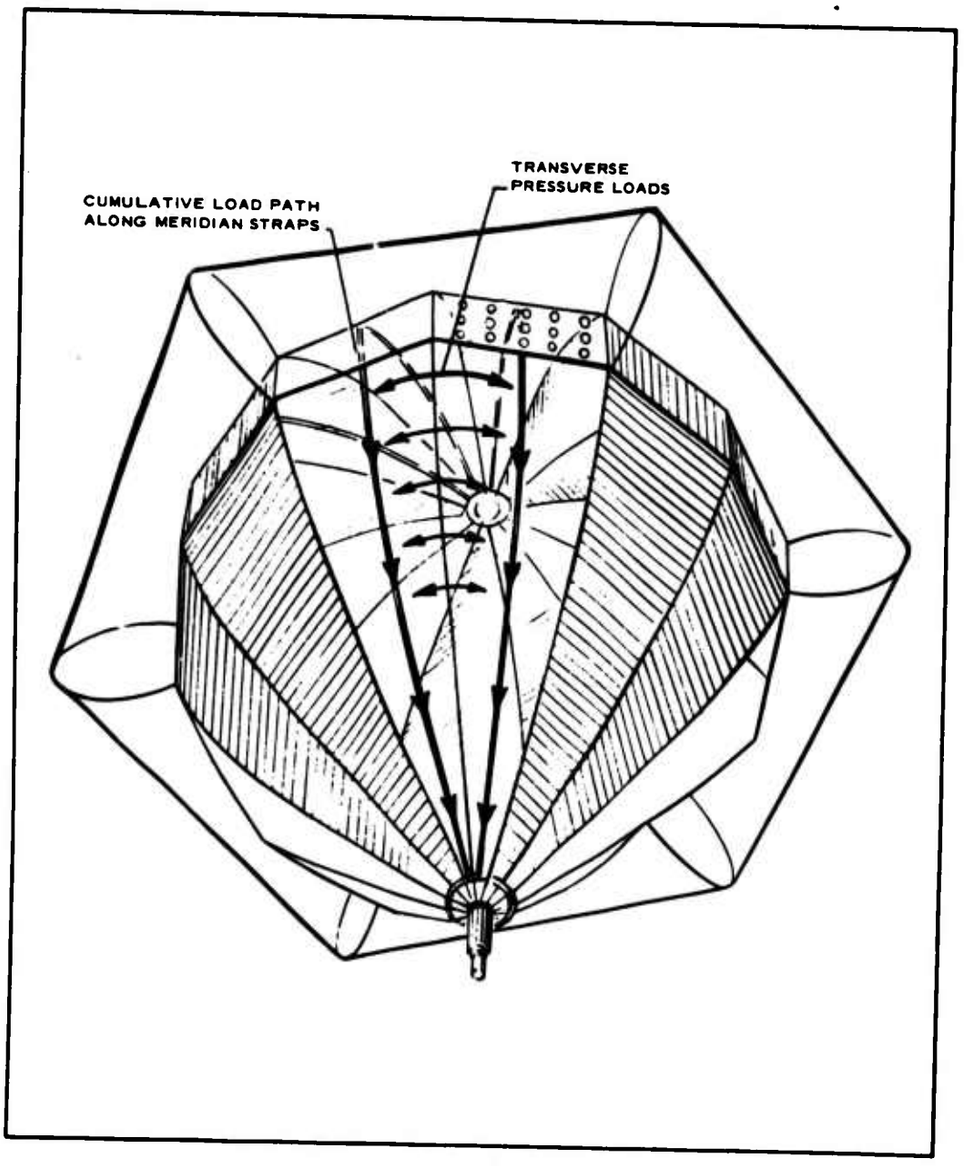

Figure 2. Schematic of BALLUTE Membrane Stresses

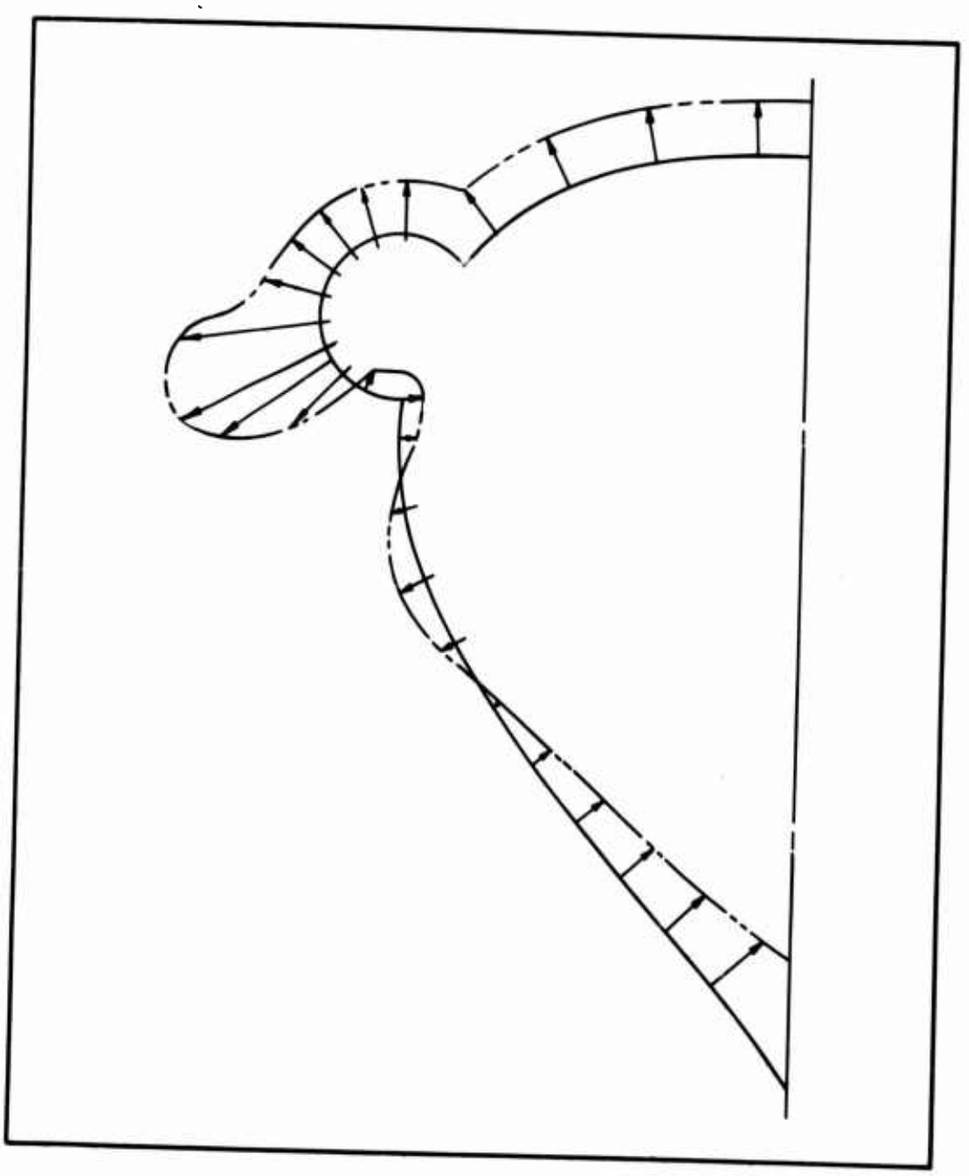

Figure 3. BALLUTE Subsonic Pressure Distribution

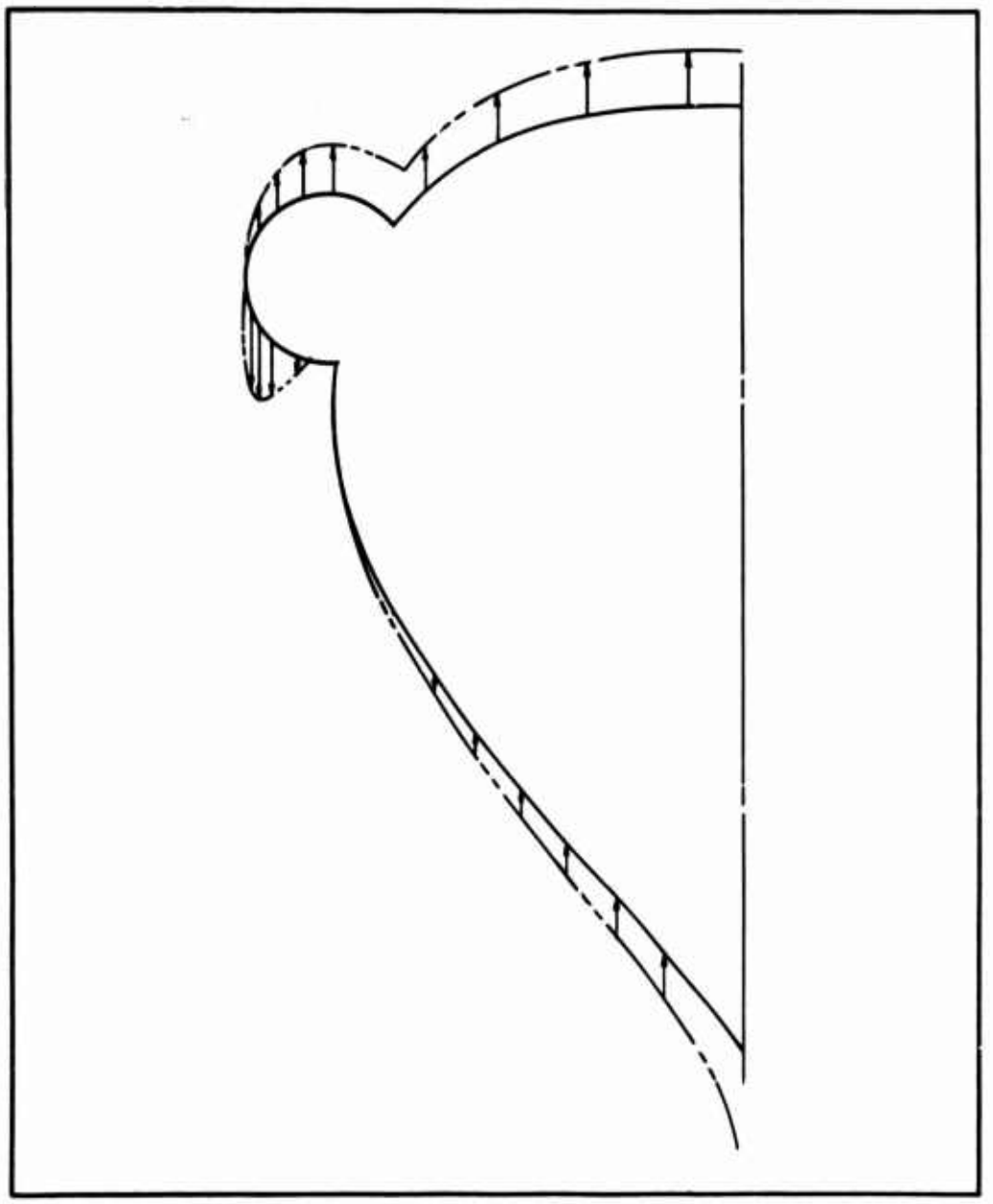

Figure 4. BALLUTE Drag Force Distribution

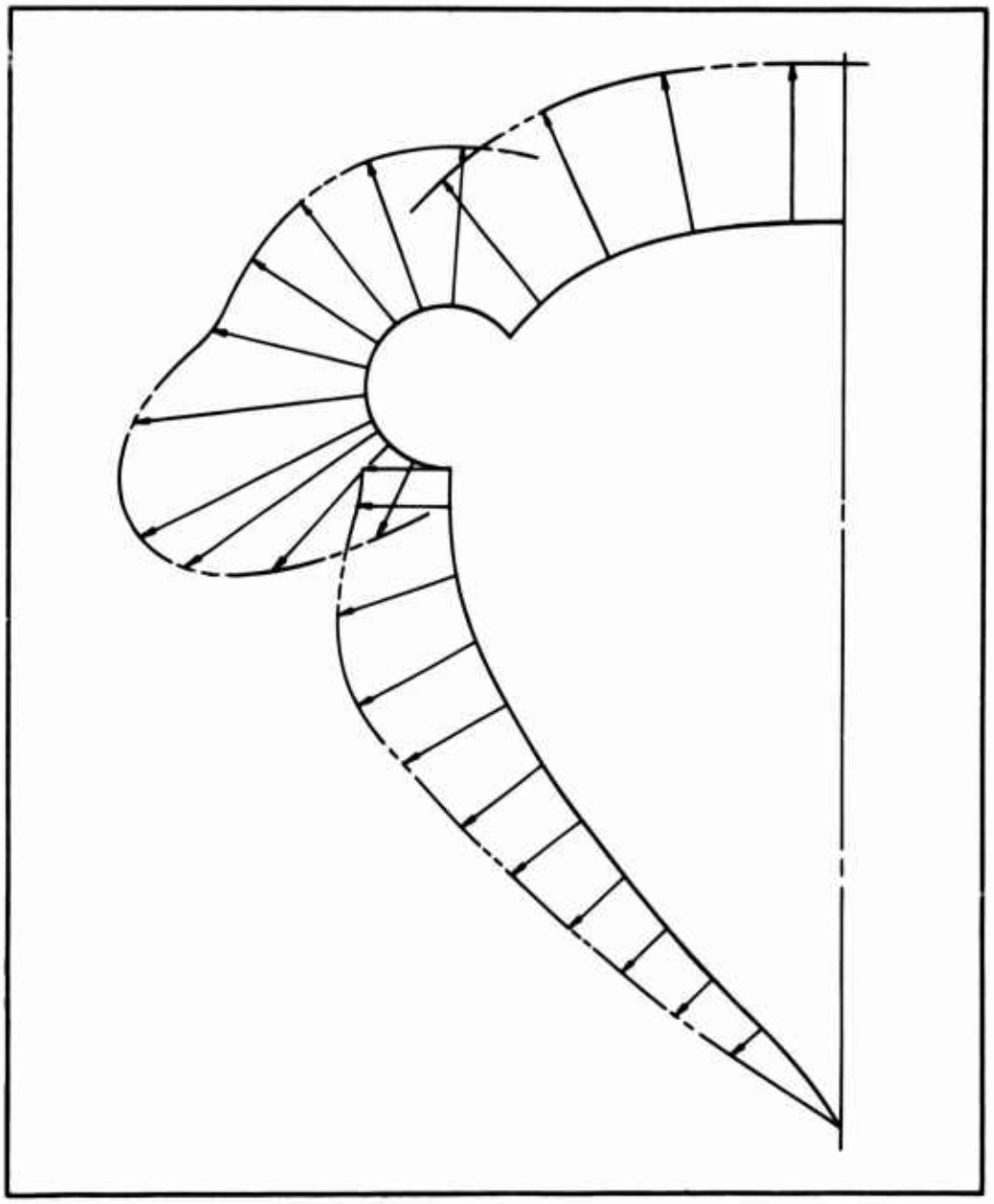

Figure 5. BALLUTE Membrane Differential Pressures

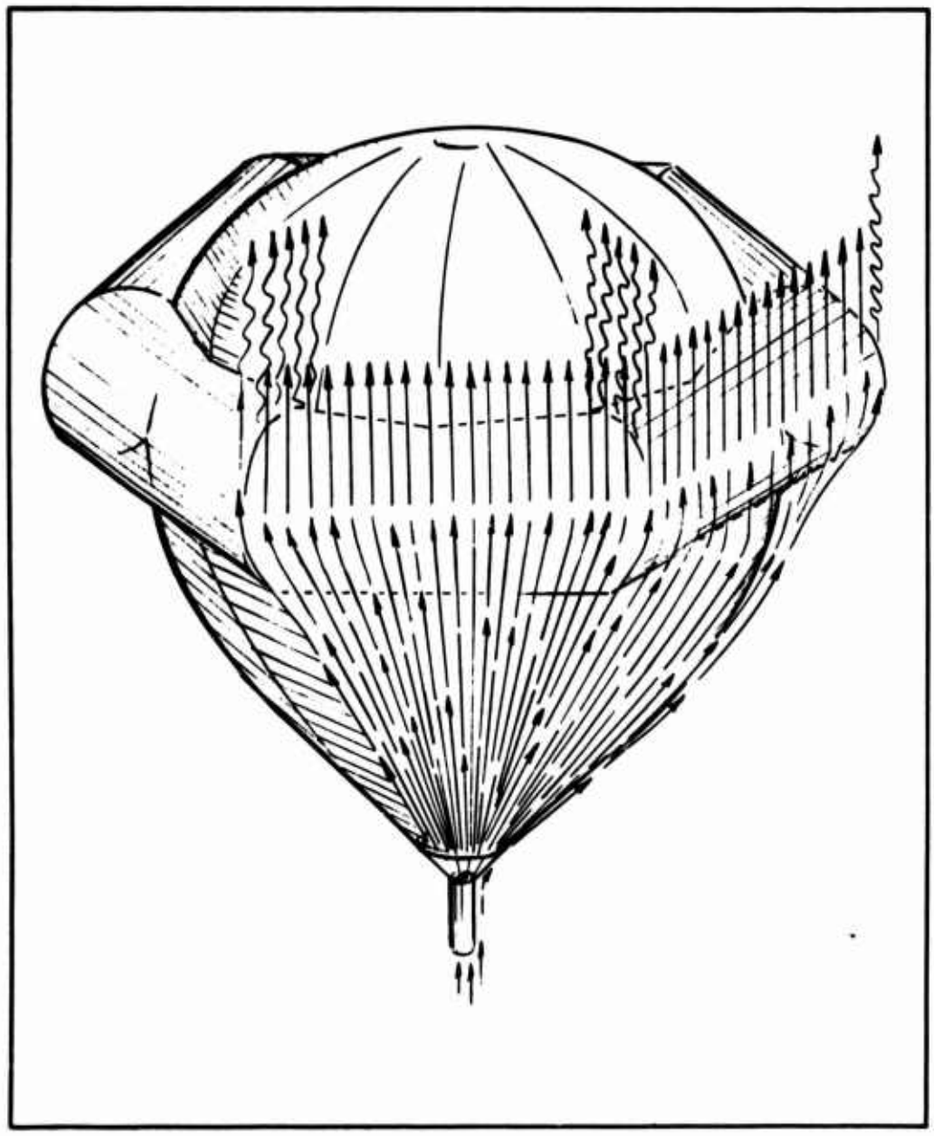

Figure 6. Flow Field Around BALLUTE

The mission of both systems is the same; to measure temperature and winds from apogee to 80,000 ft. Ambient temperature is monitored by a thermistor-modulated circuit with output transmitted to a ground station. Winds are measured as lateral excursions of the de cending system recorded by skin-tracking radar. Figures 7 through 10 show operational schematics of Arcasonde and Dartsonde systems.

To permit proper acquisition of these data, descent flight must be controlled rigorously through proper design. Data accuracy is directly proportionate to the ability of the parachute or BALLUTE to provide necessary deceleration and stabilization.

4.2 Descent Rate

Generally, the slower the fall rate of the system the more precise will be temperature and wind data within such practical limits as battery life and the length of time ground-tracking equipment is required. Because temperature is measured by a thermistor forward of the sonde proper, descent velocity should be sufficiently slow to ensure that induced aerodynamic heating is negligible or reasonably small. Slow descent is required for accuracy in measuring winds (Leviton and Lally, 1958). Accuracy of measurement by tracking a falling object decreases inversely with vertical velocity.

Without reviewing the method used to establish an acceptable fall rate for the two sonde systems in question, it can be stated that both systems currently require maximum velocity of 300 fps at 180,000 ft or a ballistic coefficient value of W/C_DA = 0.05. Slower fall rates are of course desirable.

4.3 Stability

Aerodynamic stability of the sonde-decelerator configuration can be defined as the degree to which the axis of the system remains aligned with the flight path. The goal established for the current GAC effort is ±3°. Small coning or angles of attack to insure lack of glide are required so that the horizontal motion of the system is due only to the horizontal winds.

An additional reason for desiring small angles of oscillation is concerned with the telemetry of the sonde. As the temperature is being sensed, the signal must be amplified and transmitted to the ground. The transmitted signal emanates from a vertically oriented dipole antenna.

The radiation pattern around the antenna is strongest in the horizontal plane with a null along the vertical axis. When the sonde approaches a position directly above the ground station, the reduced signal strength results in a "signal dropout" or "spike" and the temperature trace and temperature data are lost.

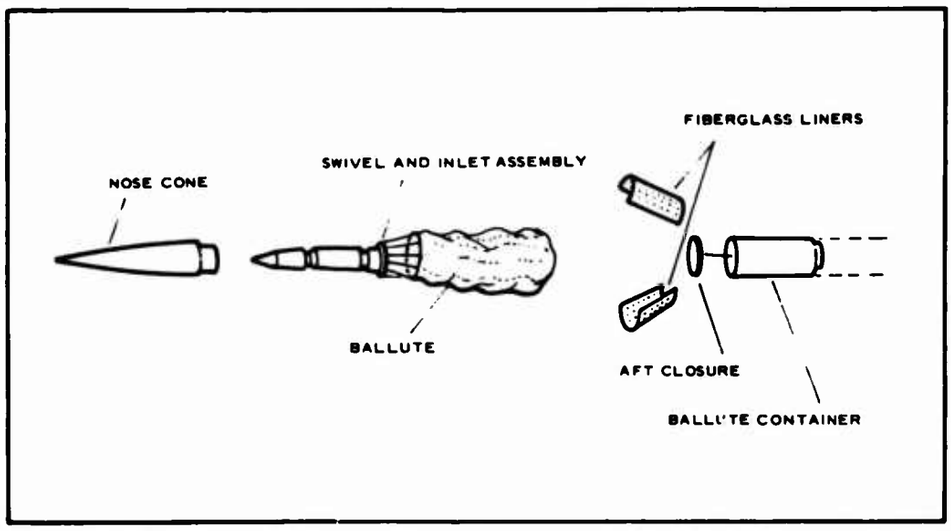

Figure 7. Arcasonde BALLUTE Deployment Schematic

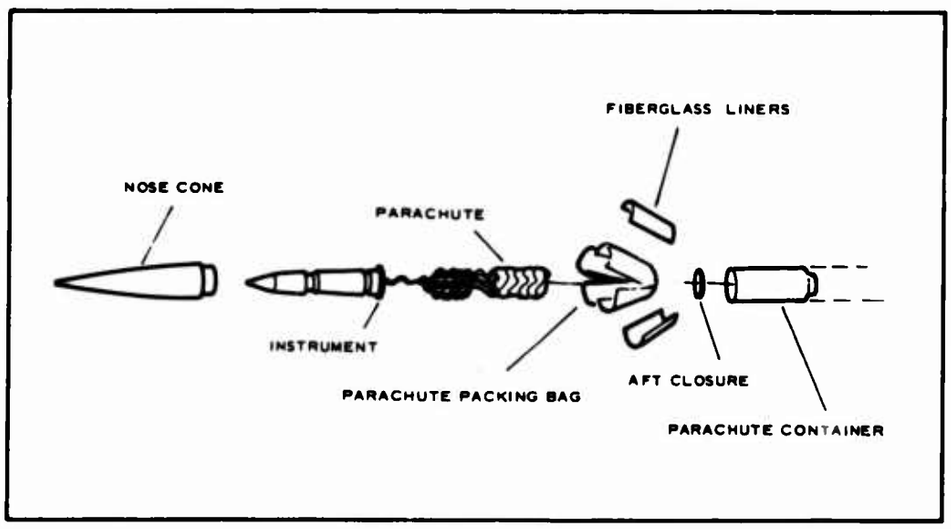

Figure 8. Arcasonde Parachute Deployment Schematic

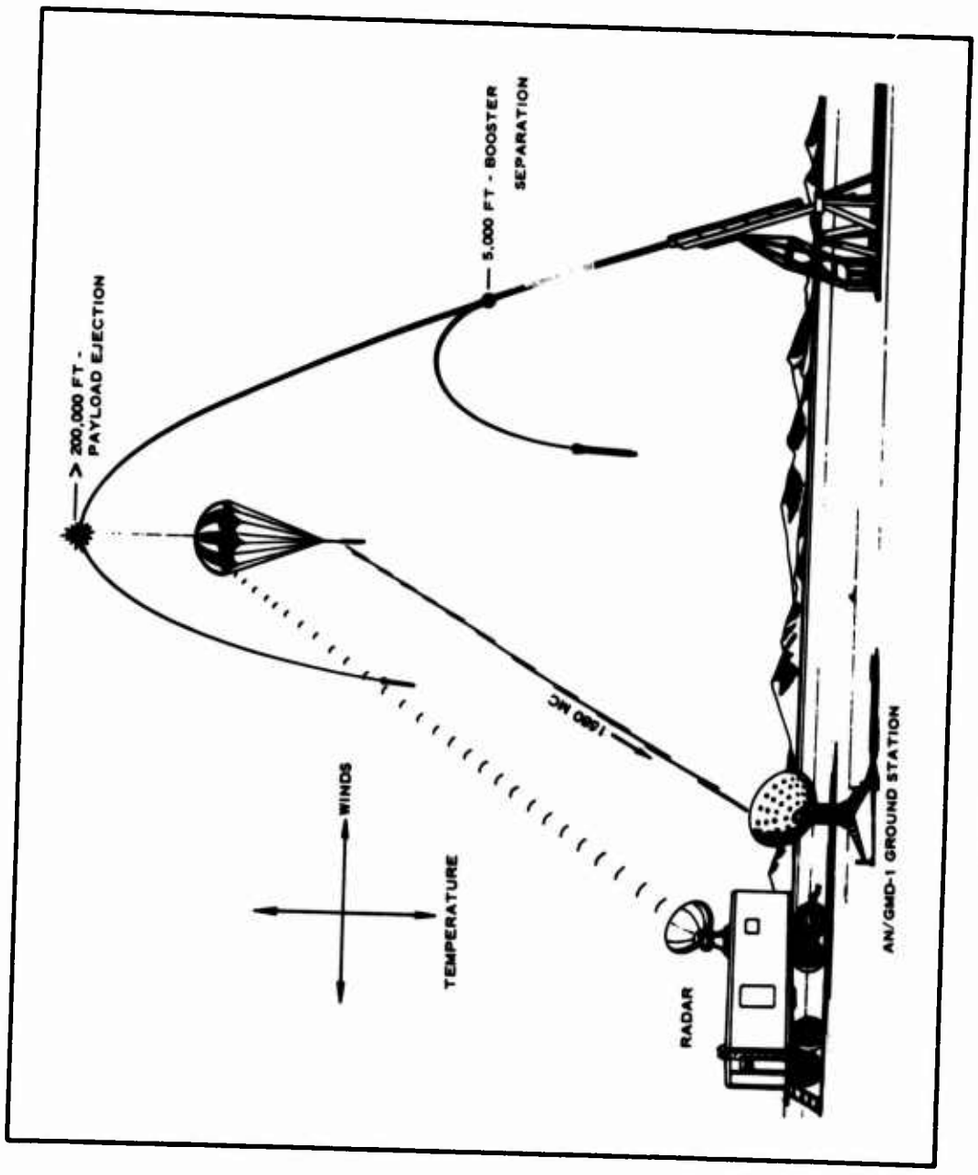

Figure 9. Dartsonde Trajectory Schematic

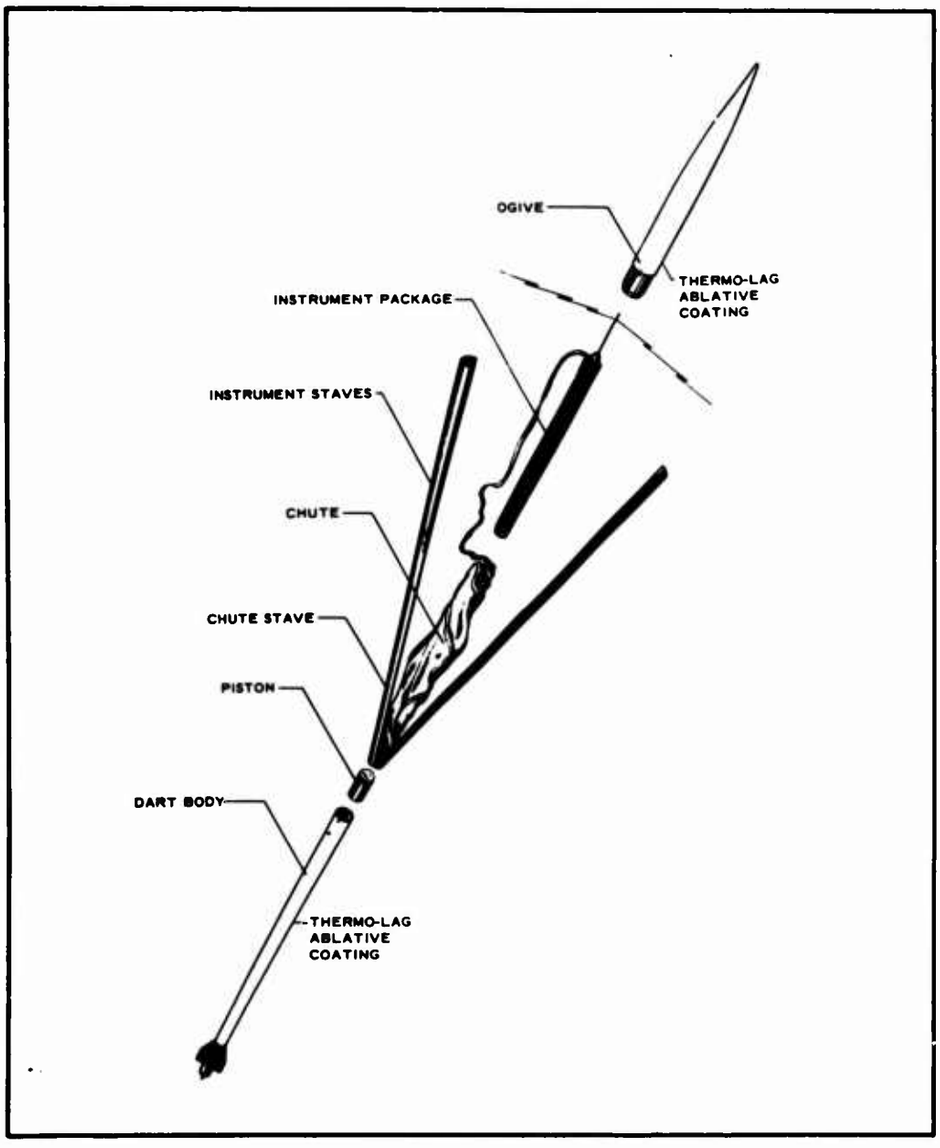

Figure 10. Dartsonde Parachute Deployment Schematic

Antenna pattern is critical in an oscillating sonde when the null may be aligned with the ground station once each cycle. Signal dropout, a continuing problem with the current parachute systems, constitutes another primary reason for the BALLUTE development program. In the case of a transponder sonde, periodic loss of signal may also result in loss of range.

A third point of concern might be stated here. If the system is oscillating or coning through wide angles, velocity of the thermistor through the air is no longer the vertical velocity of the system, but some higher and variable velocity along a helical or oscillatory path. The result is an increase of aerodynamic heating and inconsistency of the flow field around the thermistor.

5. ARCASONDE BALLUTE

The most recent BALLUTE configuration tested on the Arcasonde system has a 14-ft diameter with a 10-percent burble fence, as shown in Figure 11. The body of the BALLUTE is constructed of 12 gores of 1/2-mil Mylar. The seams are butt and tape constructed. Six gores are aluminized to provide the necessary radar trackability. The burble fence also is made of 1/2-mil Mylar and is attached by lap seams and tape. Meridian straps that transmit drag load to the instrument are flat woven nylon lacing stock attached to the center of each gore with 1/2-mil Mylar tape. The inlet assembly consists of 12 beryllium-copper leaf springs mounted on a swivel plate (see Figure 12).

6. DARTSONDE BALLUTE

The basic geometry of the Dartsonde BALLUTE is a scaled-down version of the Arcasonde configuration. A full-scale unit in free flight is shown in Figures 13 and 14. Because of its smaller size, this BALLUTE can be made with 6 gores instead of 12. The packaging of the Dartsonde BALLUTE shown in Figure 10 differs from the Arcasonde assembly in that it is inverted in the canister and is attached to the instrument with a single riser line. The single-line suspension system permits oscillation of the instrument even though the BALLUTE is stable. However, signals of the same quality as the Arcasonde system have been received in flight tests. The inlet in this case is erected by 3 music wire springs. Specifications for both BALLUTEs are presented in Table 1.

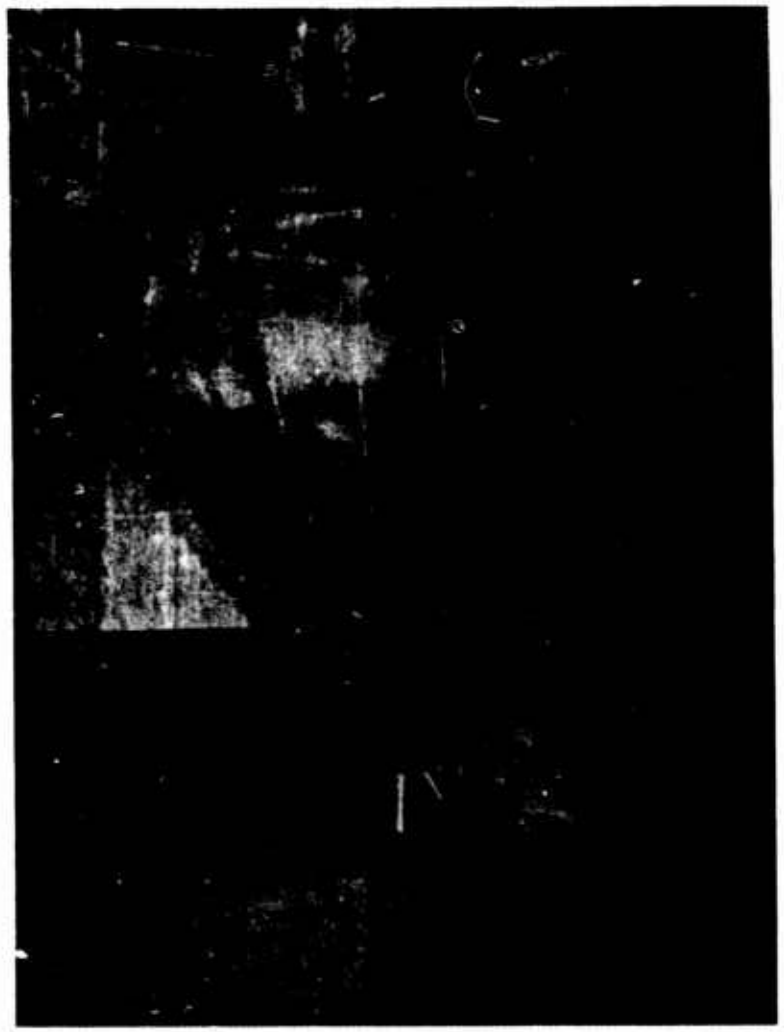

Figure 11. Inflated Arcasonde BALLUTE

Figure 12. Meridian Strap Inlet Detail

Figure 13. Dartsonde BALLUTE

Figure 14. Dartsonde BALLUTE During Inflation

Table 1. Comparison of Dartsonde and Arcasonde Specifications

Specification	Dartsonde	Arcasonde
Type BALLUTE	6 gores - 80 deg angle	12 gores - 80 deg angle
Fence type	6 sides	6 sides
Material type	Mylar-clear-alum	Mylar-clear-alum
Material gage	0.00025 in.	0.00050 in.
Suspension system	15 lb straps (6)	(12) 50 in. straps
Inlet assembly	3 springs - each 5.65 in.	12 springs - 11.2 diam
Swivel assembly	5/32-in. pin in Mg housing	Mounted on needle bearings
Canister assembly	Teflon and fiberglass liners	Perforated
BALLUTE weight	0.286 lb	1.89 lb
Swivel assembly weight	0.026 lb	0.84 lb
Total weight	0.312 lb	2.73 lb
BALLUTE diameter	6 ft	14 ft
BALLUTE volume	69.12 cu ft	878.03 cu ft
Inlet area	130 sq ft	110 sq in.
Frontal area	33 sq ft	169.7 sq ft
Packing density	31.11 pcf	25.7 pcf

7. BALLUTE PERFORMANCE IN ROCKETSONDE FLIGHTS

7.1 General

During Phase I of the BALLUTE development program, the initial design of the Arcasonde BALLUTE was established and many of the problems associated with packaging, deployment, structural integrity, and aerodynamic shape were resolved. For example, more than 200 drop tests of various BALLUTE configurations were conducted in the Goodyear Aerospace airdock in Akron to determine empirically a shape combining high-drag efficiency and aerodynamic stability. A swivel assembly was incorporated at the BALLUTE-instrument interface to negate the untoward effects of the spinning instrument on BALLUTE inflation.

Unlike a parachute, a BALLUTE is an impermeable pressure vessel with the only opening at the relatively small ram-air inlet. To prevent bursting of the BALLUTE at deployment from expansion of air trapped within the packaged BALLUTE, a perforated canister was developed to permit bleed-off of this residual air during

the two-minute ascent to apogee (see Figure 15). Structural integrity of such components as meridian straps, seam attachment points, and reinforcement of high-stress areas was verified functionally in a series of drop tests from a helicopter at the Goodyear Aerospace Wingfoot Lake facility in Akron.

Phase I of the Arcasonde-BALLUTE development was completed with three successful flight tests of the final design at Cape Kennedy last year. However, while the units demonstrated small coning angles, their fall rate was escessively large.

The scope of the second phase of the program now in progress is twofold: to increase the size of the Arcasonde BALLUTE, which had not provided as slow a descent as the parachute and to adapt the system to the Loki-dartsonde system. At this point, 11 Arcasonde and 7 Dartsonde missions have been fired at Cape Kennedy.

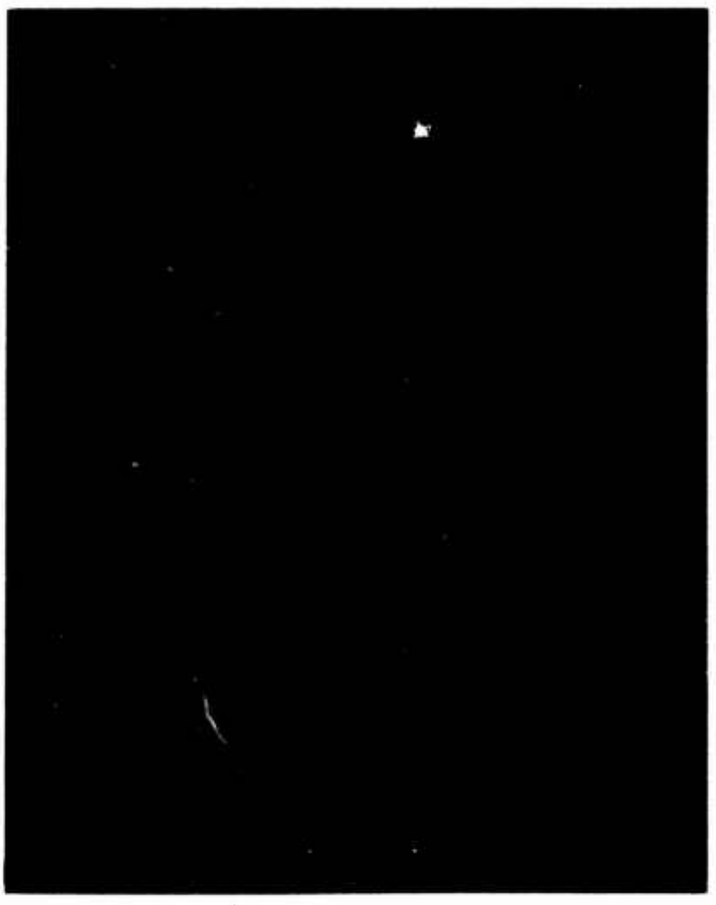

Figure 15. Packaged Arcasonde BALLUTE

The Dartsonde program has been highly successful as evidenced by the preliminary analysis of flight data. Of 7 Dartsonde firings, 1 dart failed to separate from the Loki booster and one premature separation occurred. The remaining five 6-ft diam, 1/4-mil Mylar BALLUTEs were successful, yielding excellent temperature data and lower descent rates than required. Ballistic coefficients of 0.04 were attained for several units. Figure 16 illustrates one such flight.

In the Arcasonde test program, 1/4-mil Mylar BALLUTEs, 14- and 16-ft in diameter and with various minor modifications, completely or partially failed at deployment. Return to 1/2-mil film for the Arcasonde configuration has resulted in successful missions in the three systems flown thus far. The current unit is 14 ft in diameter and has a ballistic coefficient of 0.06 as compared with the target of 0.05.

Results of two Arcasonde flights one hour apart from Cape Kennedy may be reviewed for proper evaluation of the BALLUTE. Tests 5554 used a BALLUTE and Test 6097 a Gentex parachute; both tests utilized Arcasonde 1A payloads. Figures 17 and 18 are reproductions of the temperature records from the two flights.

7.2 Temperature Data

The first and most obvious comparison that can be made is the absence of signal dropout or spikes in the BALLUTE trace. The consistency of the signal strength from the BALLUTE-stabilized instrument is construed as a clear indication of aerodynamic stability.

The dotted lines in Figures 17 and 18 indicate the fairing of the data performed by the ground station operator. The presence of more real temperature data in Test 5554 facilitates and enhances the accuracy of this smoothing operation.

It appears that the removal of signal dropout may well have some important secondary effects. Instrument performance will be better evaluated and diagnostic analysis of the minor or suboscillations perhaps can be made. Similarly, a meteorologist, provided with a statistically appropriate quantity of test records, may by comparison reevaluate the validity of some temperature variations currently being smoothed out.

Figures 19 and 20 depict velocity versus altitude profiles of Tests 5554 and 6097. Velocities have been computed as the finite difference in altitude for 30-sec intervals. The time-altitude data are derived from the radar track as recorded on a plotting board. The equilibrium velocity curve inserted for comparison is based on the standard atmosphere. Raw unsmoothed radar data for these flights are being reviewed at University of Dayton Research Institute to establish appropriate smoothing techniques for a more precise evaluation of BALLUTE performance and optimum wind determination. Descent rate of the parachute is slightly slower than that of the BALLUTE.

Pending completion of the smoothing program for wind determination, a portion of typical raw flight data is shown in Figure 21. The data show the flight path through a wind direction change.

Figure 22 shows horizontal excursions of the sondes in Tests 6097 and 5554 with the corresponding times and altitudes indicated. The temperatures recorded in the two flights as transmitted to the Meteorological Rocket Network are compared in Figure 23.

8. PLANNED IMPROVEMENTS FOR ROCKETSONDE BALLUTES

Because of its pressure-stabilized constructions, the BALLUTE is capable of numerous variations in size, shape, and relationship of its various components. In the current development program each modified configuration tested reveals new possibilities for investigation. This is true whether the test is successful or not. Promising areas are discussed in this section.

The universal consideration in any proposed configuration is of course the greatest performance for the least weight. In the earlier discussion of the distribution of forces acting as the BALLUTE, it was evident that the greater deceleration forces results from negative pressure on the after surface of the BALLUTE. By increasing the relative size of the burble fence, the base area of the BALLUTE may be increased with less additional material than if the whole BALLUTE were simply made larger. Both the Arcasonde and Dartsonde BALLUTEs have burble fence heights that are equal to 10 percent of the diameter of the body of the BALLUTE. BALLUTEs with 18-percent and 25-percent burble fences have been made and tested in the GAC Akron airdock (see Figures 24 and 25).

A second approach to improving BALLUTE efficiency has been to use the pressure drag on the forward area better without sacrificing stability. Because pressure drag is to a great degree a function of angle of the surface with respect to the airflow, the obvious indicated modification is to make the apex of the BALLUTE more obtuse. Figure 26 shows a BALLUTE that combines both these modifications.

For advantages in weight and production costs, experiments have been conducted to minimize the number of gores in the BALLUTE. The current Arcasonde BALLUTE consists of 12 basic gores and 12 burble fence gores. Available film width is a consideration in the larger BALLUTEs. The Dartsonde BALLUTE on the other hand has 6 basic gores and 6 burble fence gores.

To improve the Dartsonde configuration further, a square BALLUTE was designed and is shown in free flight in Figure 27. This configuration, with 8 pieces of film, has exhibited excellent aerodynamic characteristics.

Another modification of the square BALLUTE with an extremely blunt forward section is shown in Figure 28. These types of modifications to the BALLUTE design promise increased performance efficiency as well as cost and weight reduction.

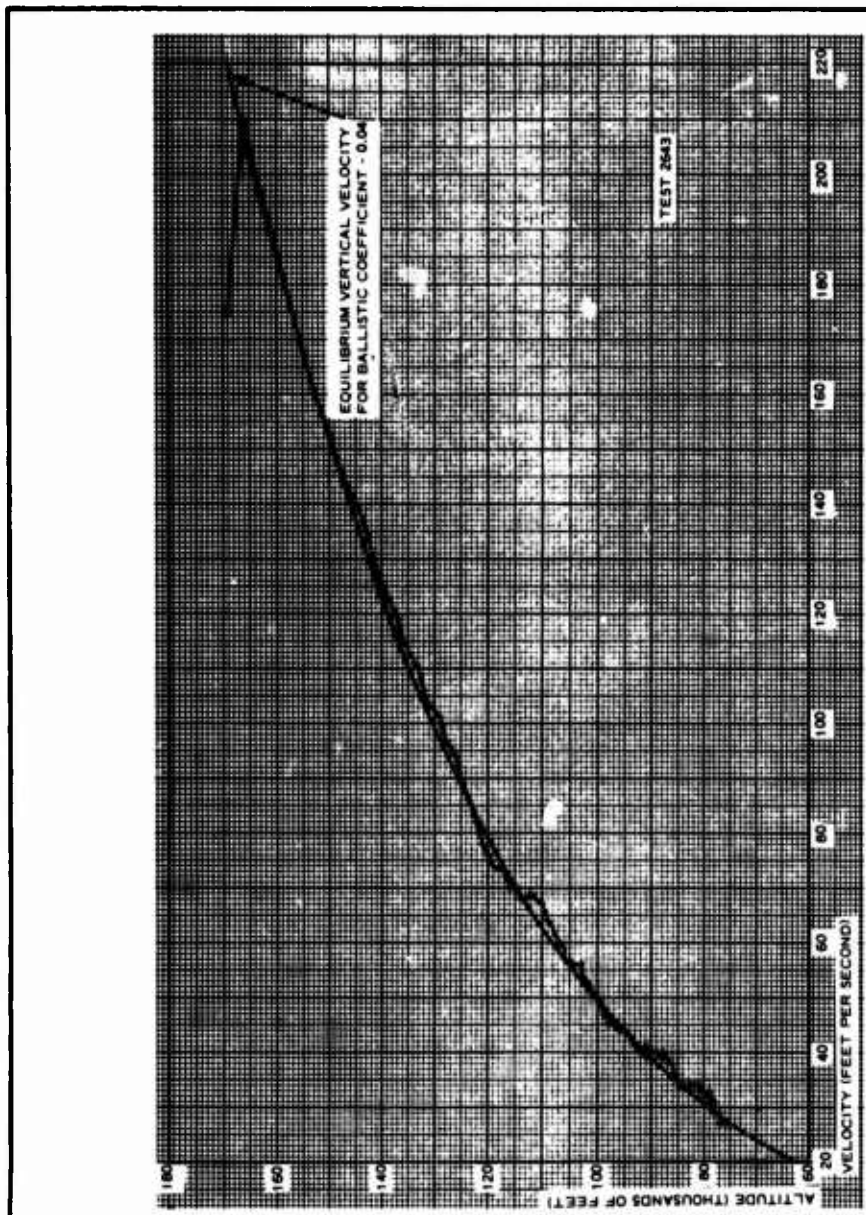

Figure 16. Smoothed Velocity-Altitude Profile, Test 2643 Dartsonde

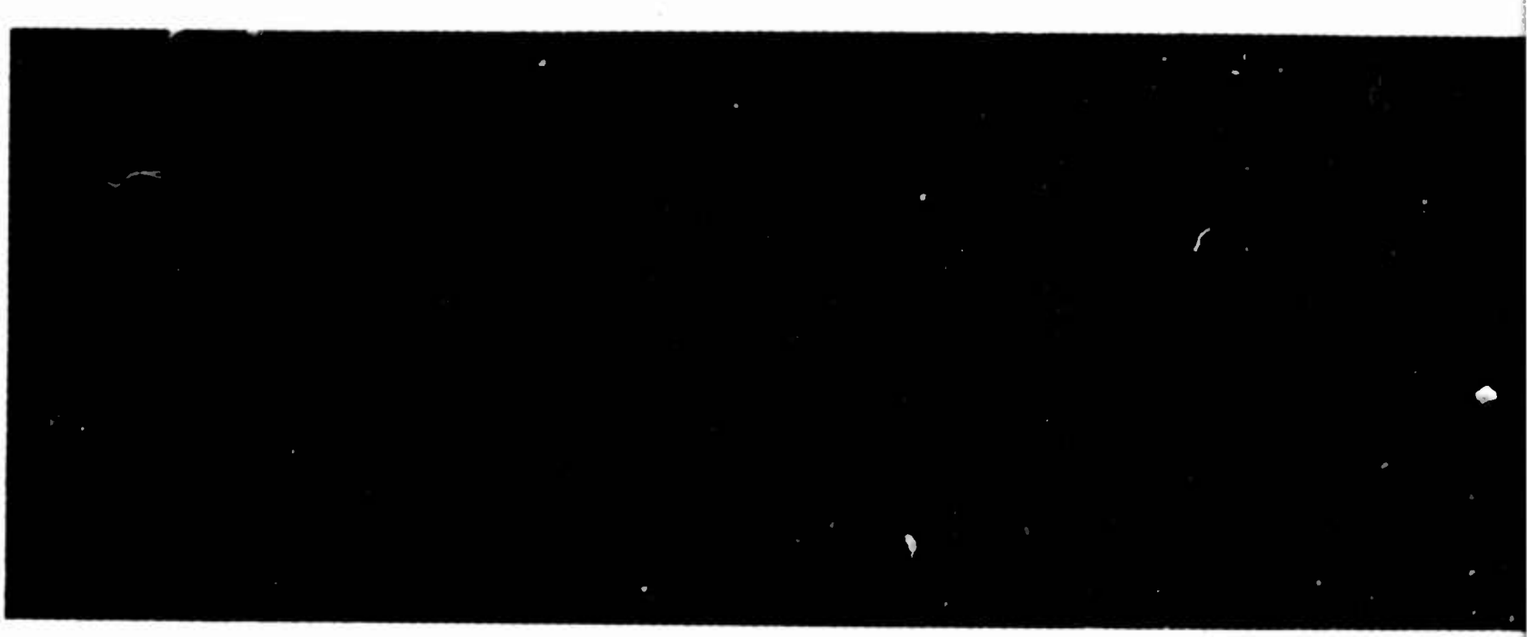

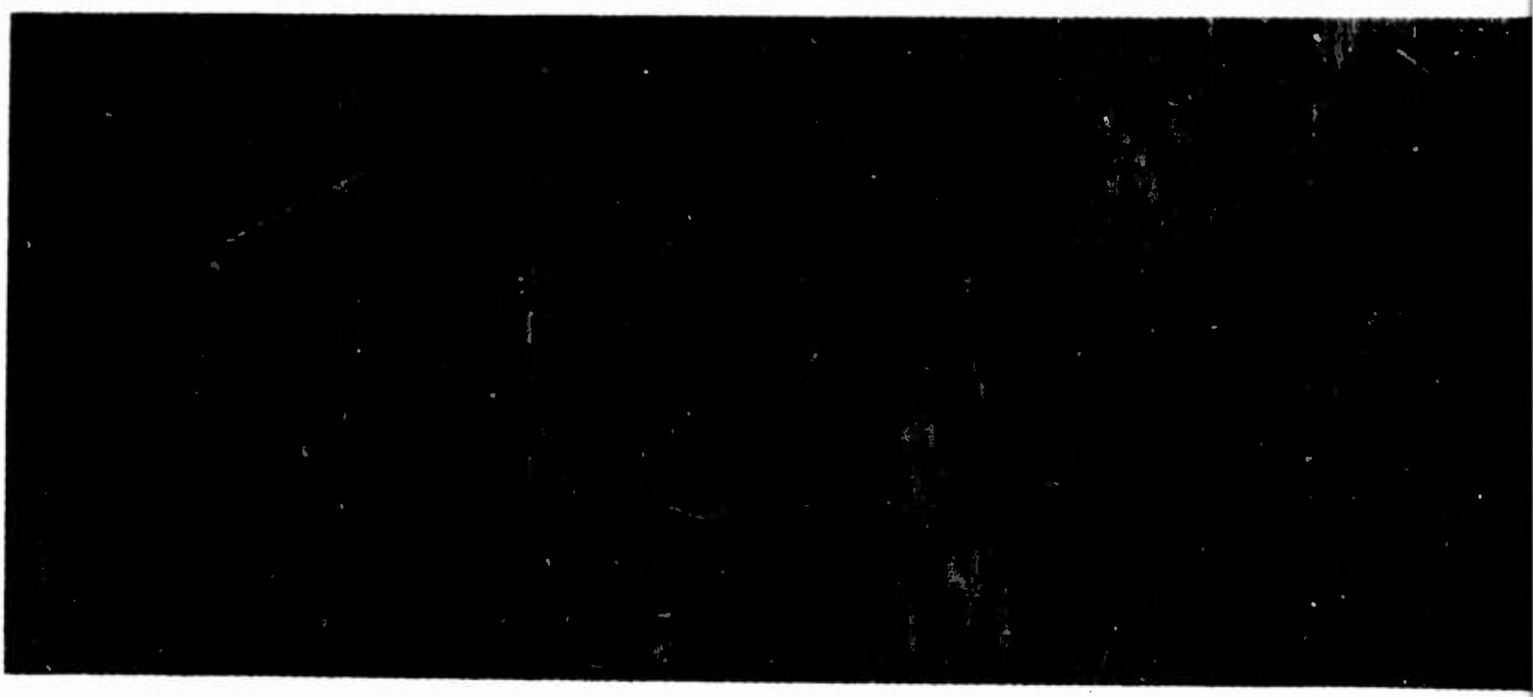

Figure 17. Temperature Tracing, Parachute

Figure 18. Temperature Tracing, BALLUTE

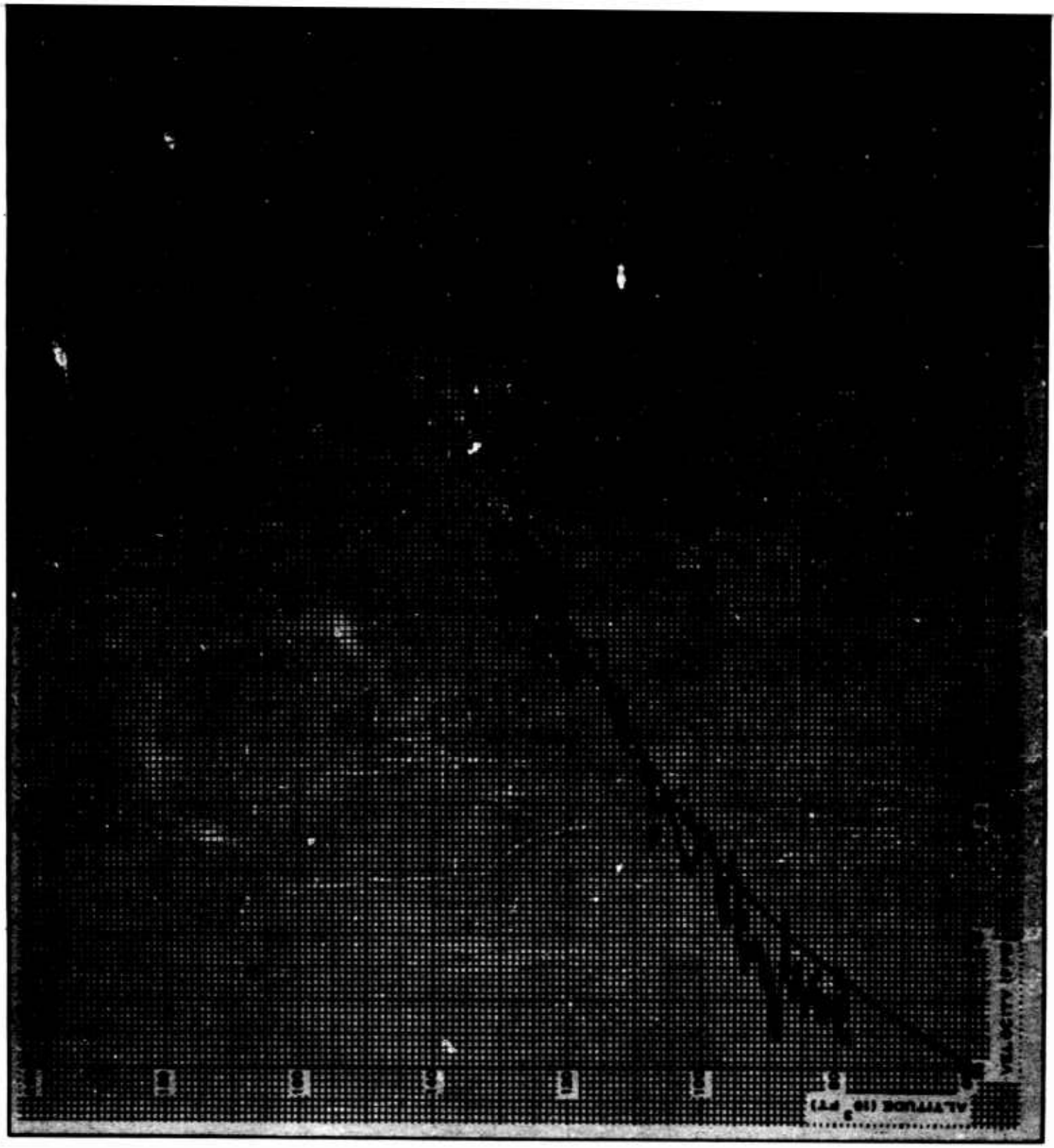
ALTITUDE (10^3 FT)

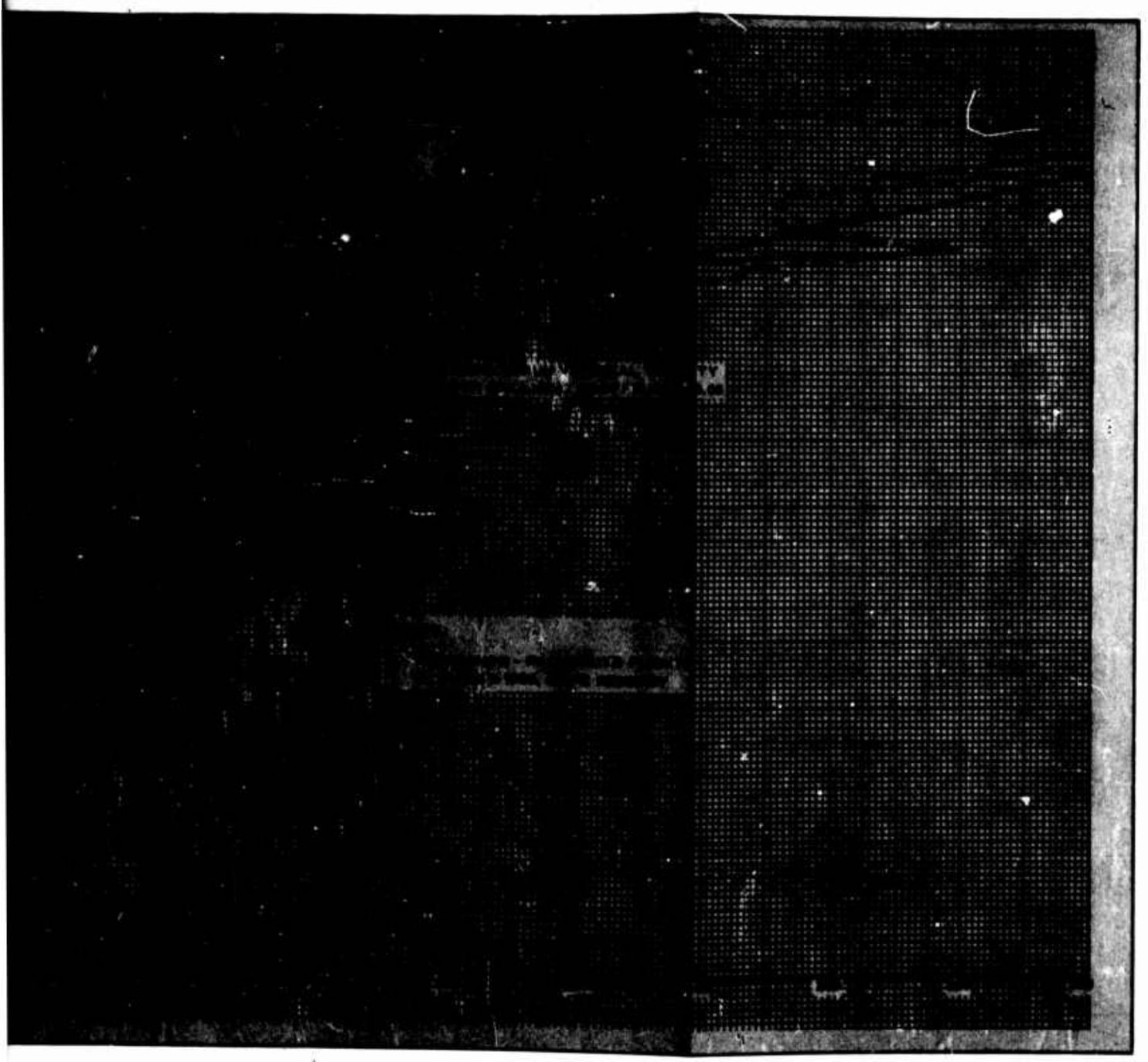

Figure 19. Descent Rate, Parachute

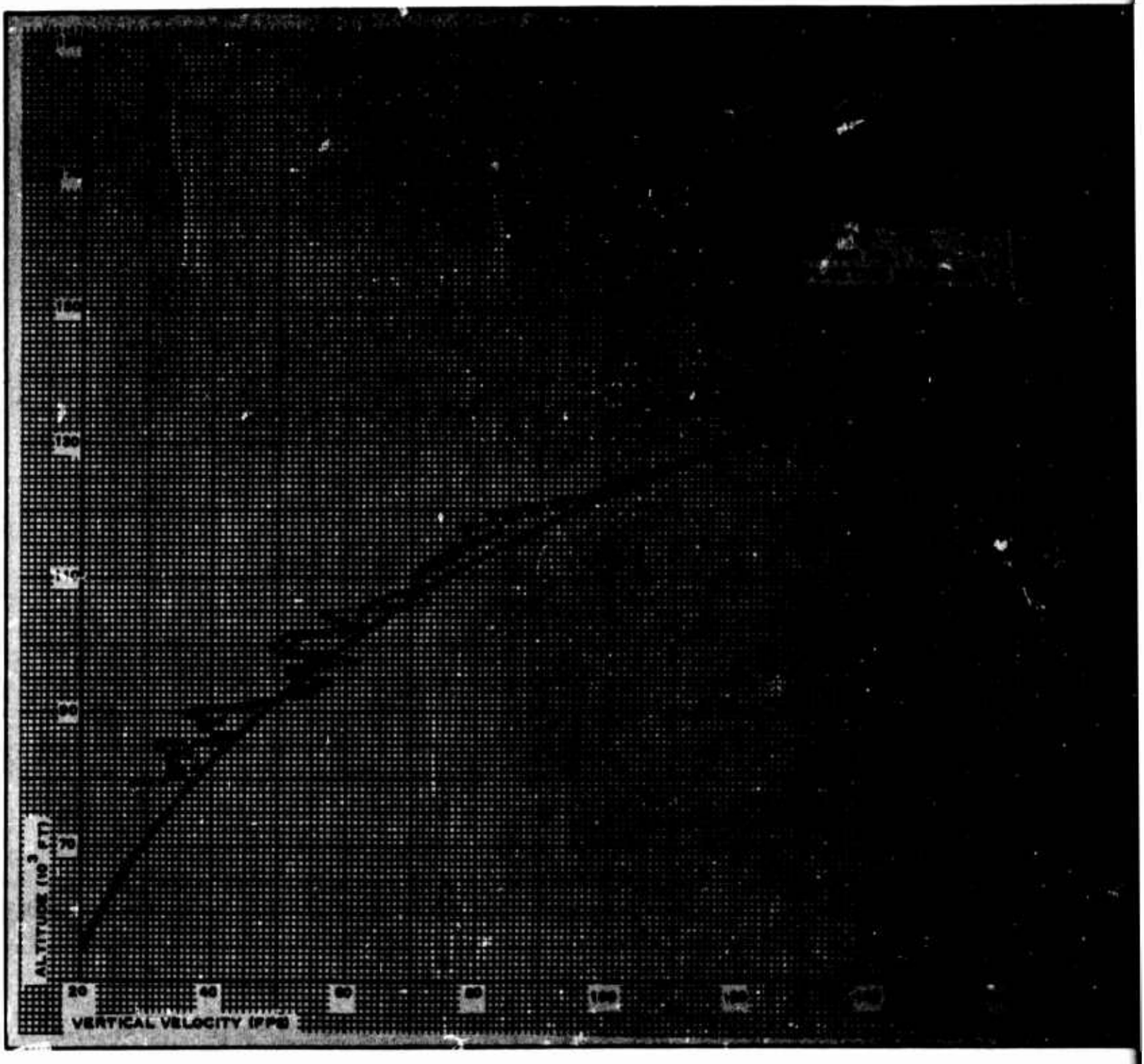
ALTITUDE (10^3 FT)
VERTICAL VELOCITY (FPS)

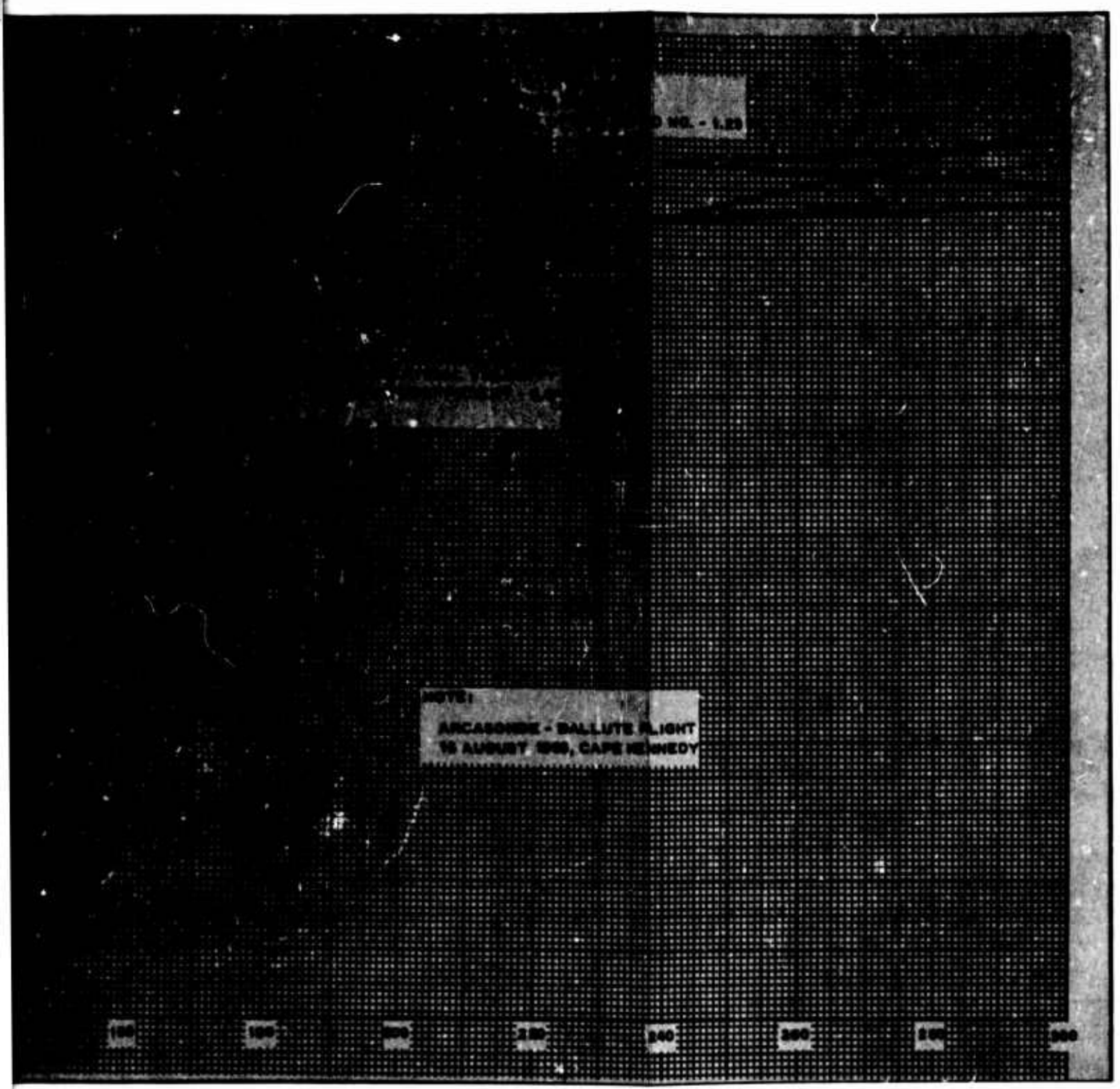

Figure 20. Descent Rate, BALLUTE

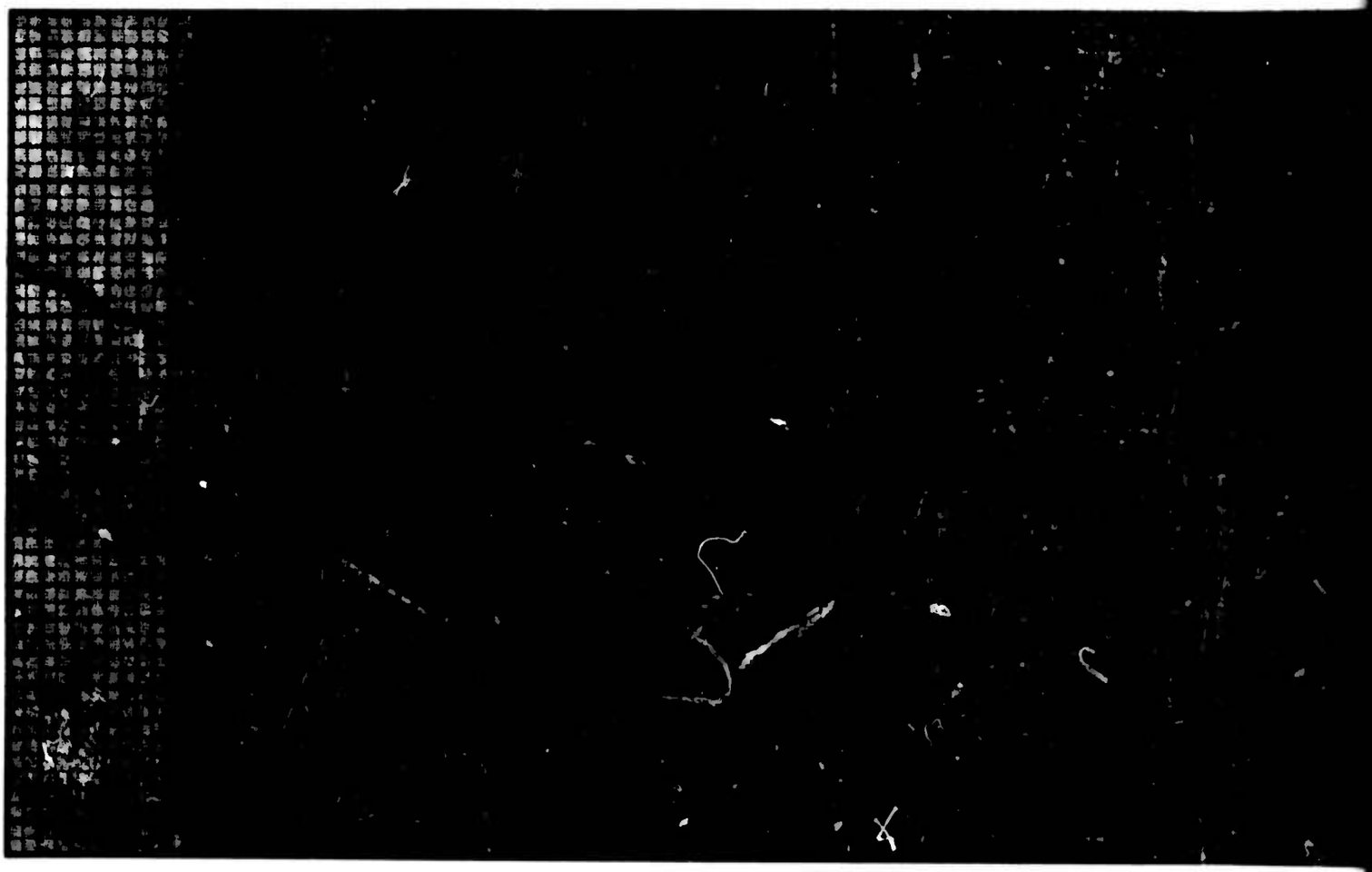

Figure 21. Horizontal Excursions, Test 906

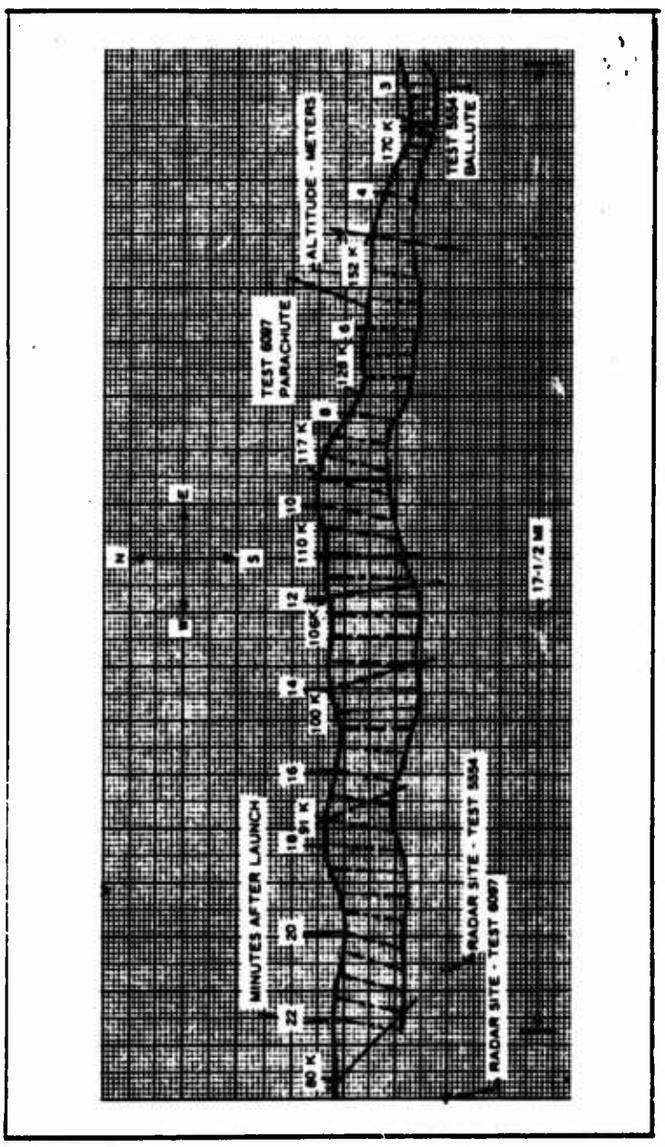

Figure 22. Wind Sensitivity Schematic

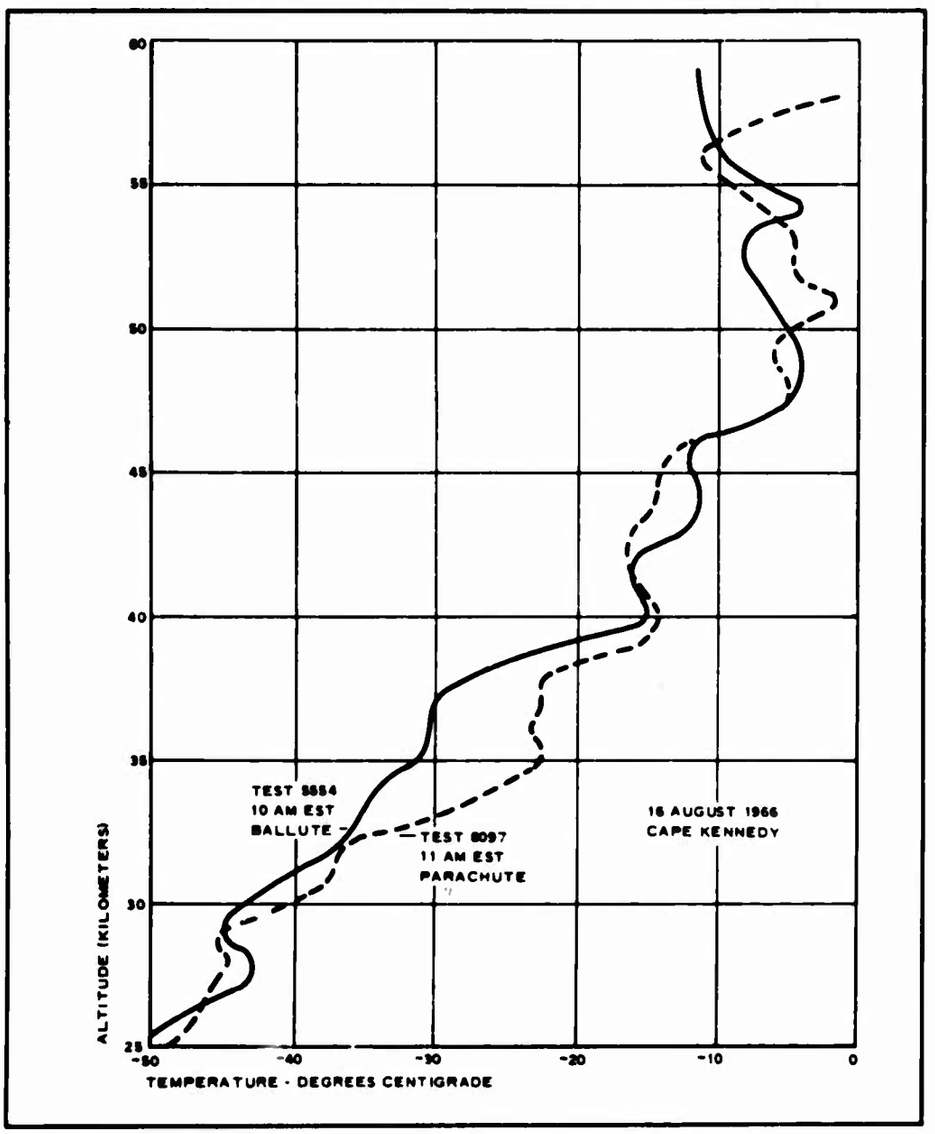

Figure 23. Temperature Versus Altitude, Tests 6097 and 5554

Figure 24. Eighteen-Percent Burble Fence

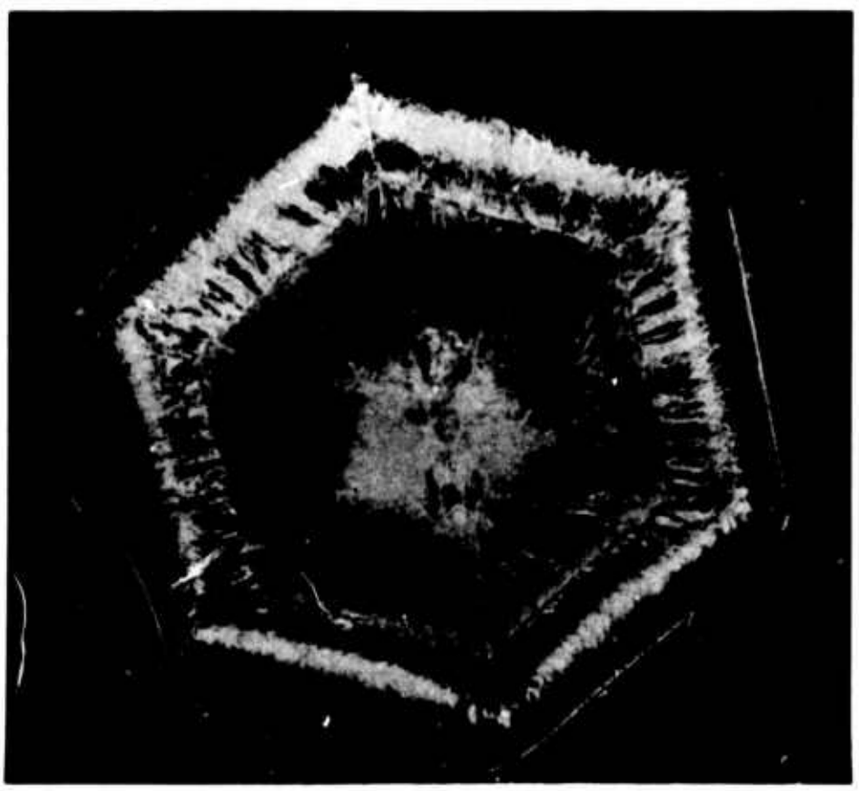

Figure 25. Twenty-Five Percent Burble Fence

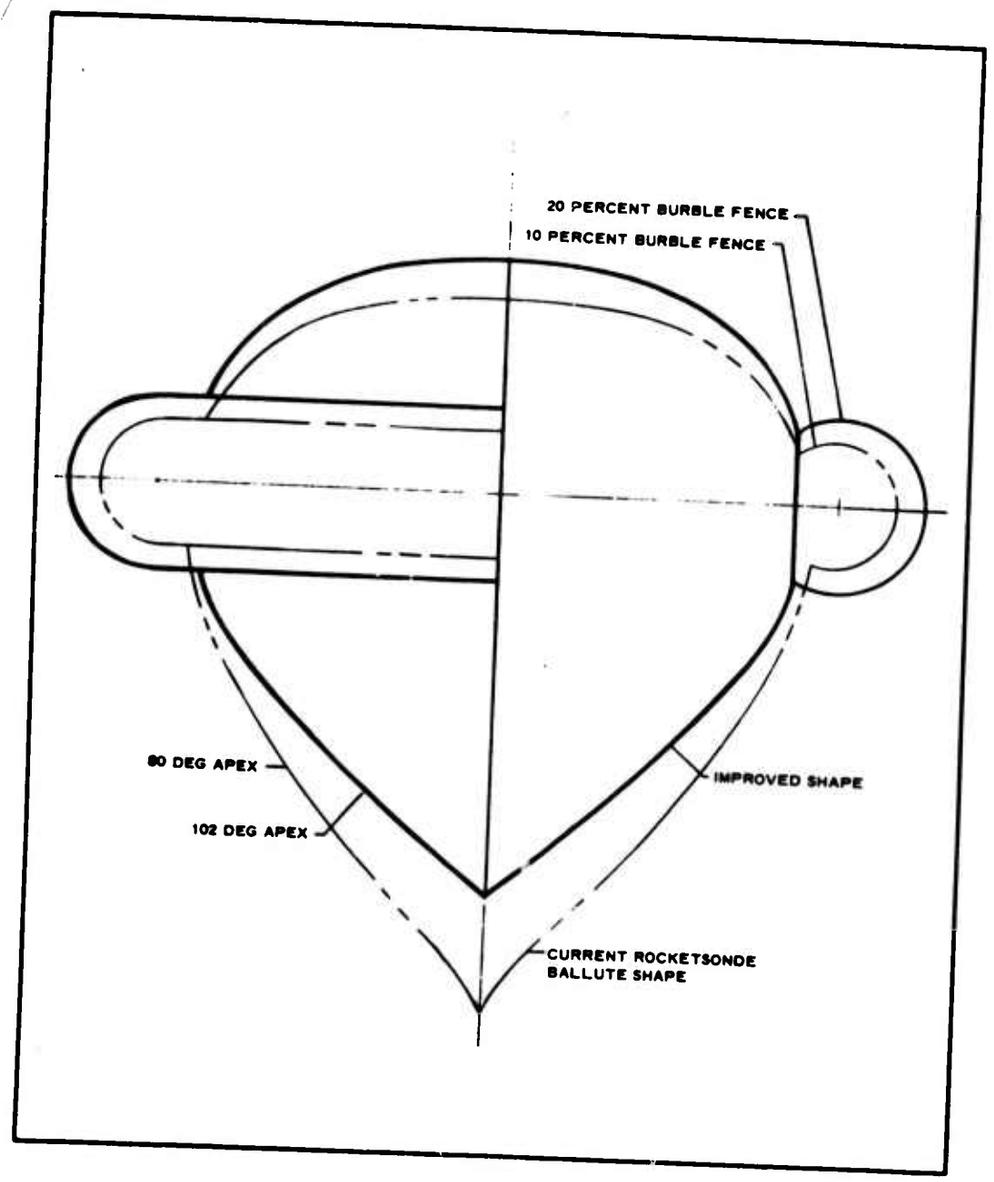

Figure 26. Twenty-Percent Burble Fence

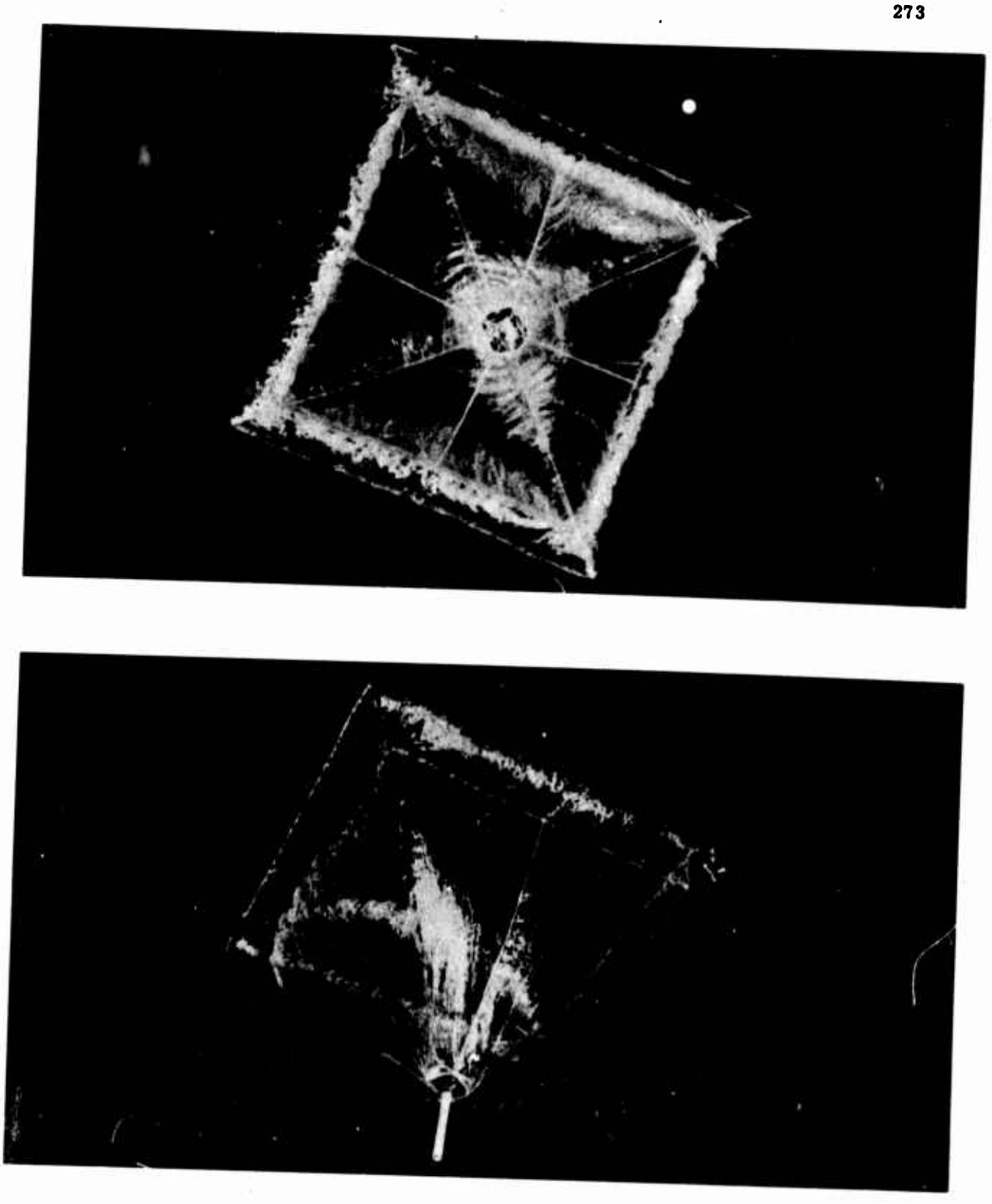

Figure 27. Square BALLUTE

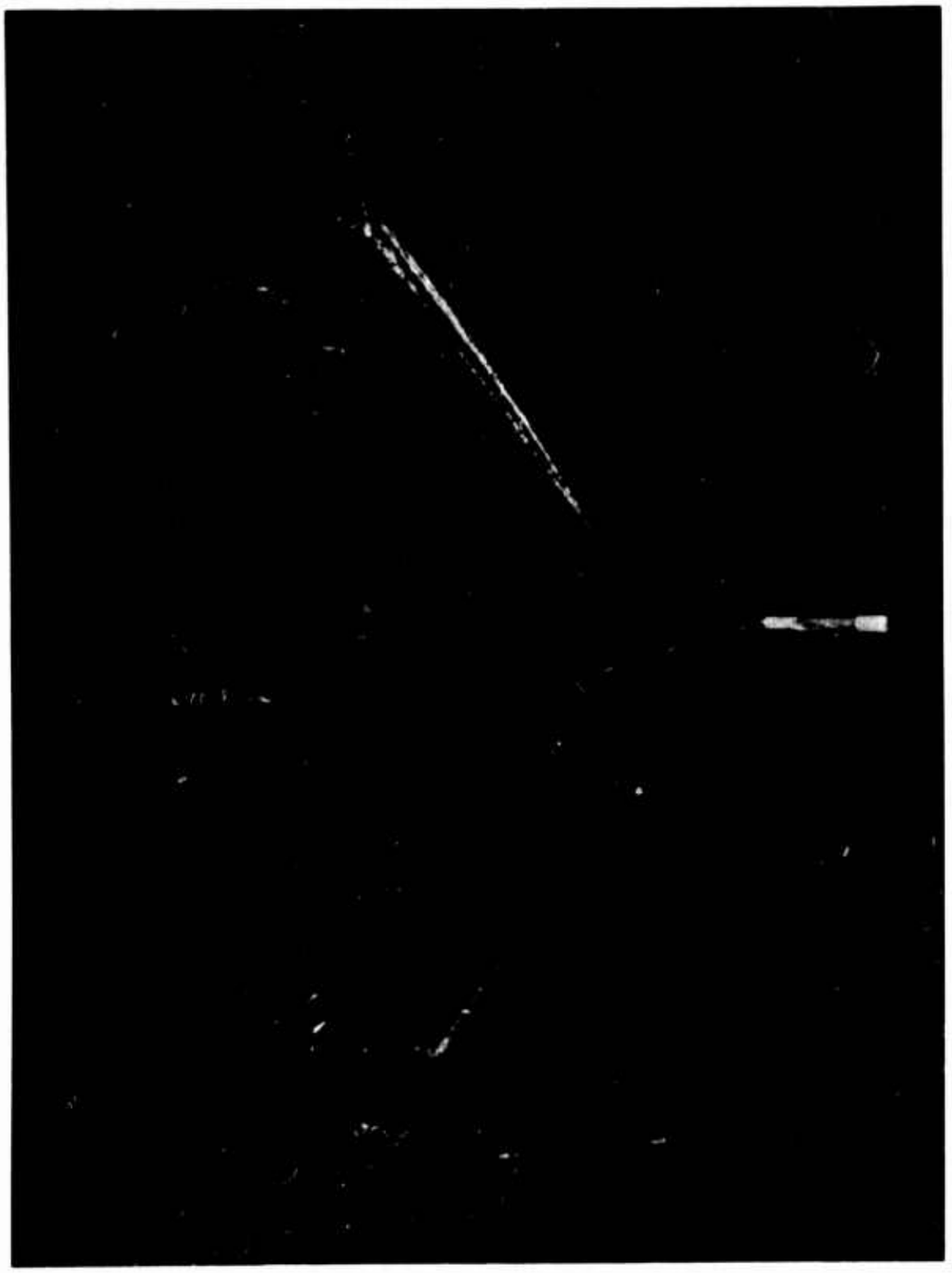

Figure 28. Square Flat BALLUTE

9. ADVANCED BALLUTE CONCEPTS FOR METEOROLOGICAL MISSIONS

In addition to work being done for AFCRL in the rocketsonde programs, GAC has a continuing research program in the decelerator field. Some facets of this research may have meteorological applications.

Figure 29 shows a ram-air-inflated one-meter sphere in free fall. Inflation is accomplished through a series of baffled inlets. Orientation of the inlets into the air stream is accomplished by minute ballasting. Because the sphere is an aerodynamically unstable configuration at subsonic velocities, the inlet positions oscillate in and out of the stagnation pressure zone, causing cyclic recurrence of the concave dimple that can be seen in the photograph.

Figure 30 shows the Goodyear Aerospace spinning BALLUTE in free fall. This demonstration model shows the segmented burble fence that imparts the spin. Because this BALLUTE is stable, the canted segments are maintained at a constant angle of attack. Each segment has a constant lift-drag ratio and the spin rate is directly proportional to the rate of fall. If fall rate is a valid method for the determining density, and if spin rate is a linear function of fall rate, density may be defined as a function of spin rate.

One simple method of monitoring BALLUTE rotation is using a partial internal corner reflector that, as it turns, modulates the gain of the tracking radar.

Any BALLUTE with sufficient forward ballast to maintain orientation might be used for density sensing once the drag coefficient value has been established.

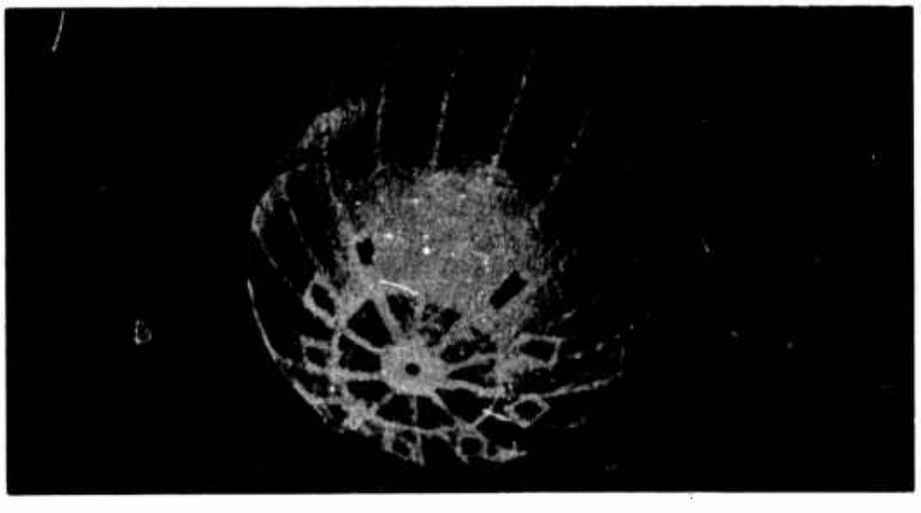

Figure 29. Ram-Air Sphere

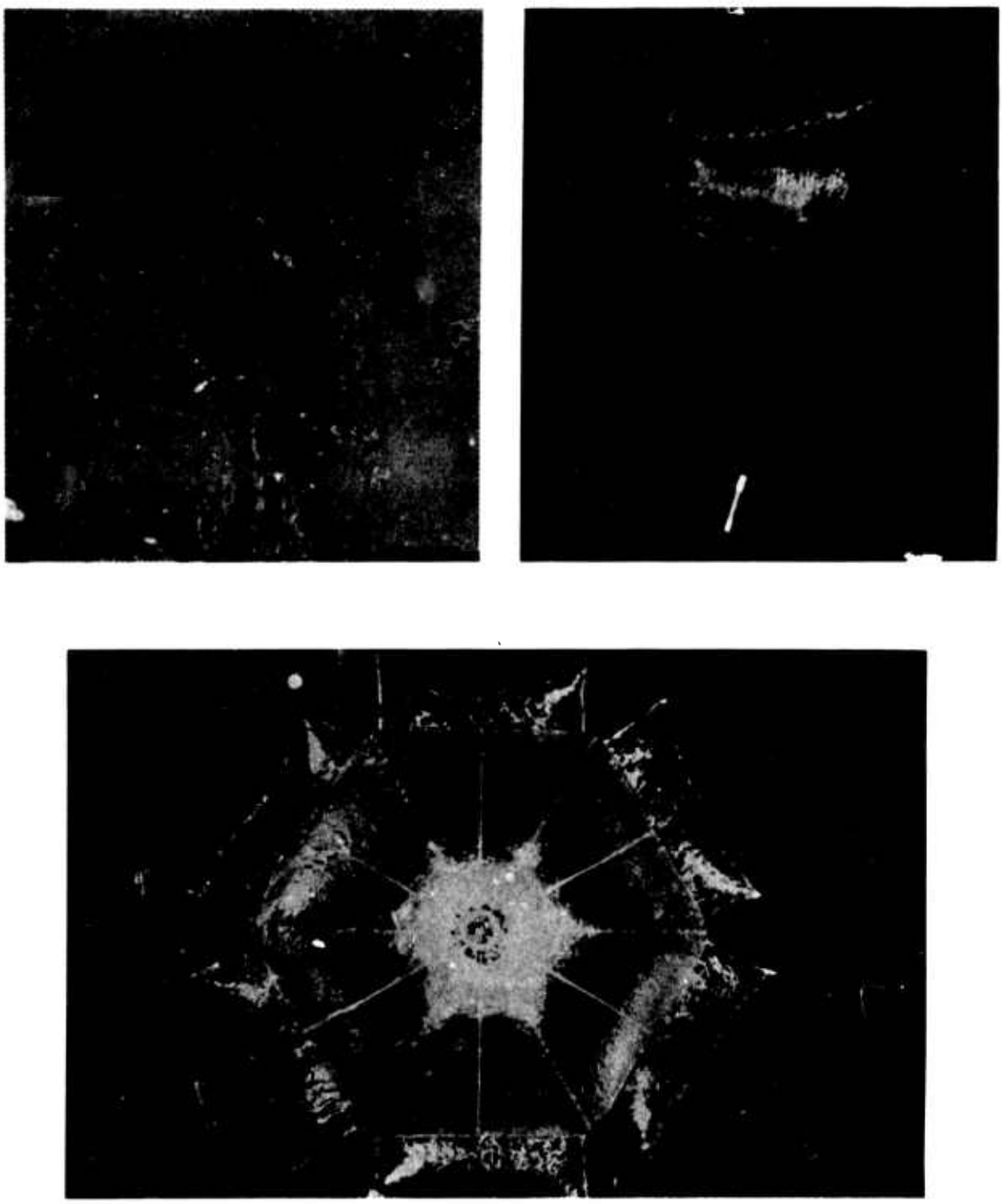

Figure 30. Spinning BALLUTE, Three Views

References

Heinrich, H.G. and Haak, E.L. (1962) Stability and Drag of Parachutes with Varying Effective Porosity, Wright-Patterson Air Force Base, Air Systems Division, ASD-TDR-62-100.

Houtz, N.E. (1962) The Application of Isotensoid Membranes to the Design of Inflatable Drag Bodies, Goodyear Aircraft Corporation, Akron, Ohio, GER-10770.

Leviton, R. and Lalley, V.E. (1958) Accuracy of Wind Determination From the Track of Falling Objects, AFCRL, Air Force Surveys in Geophysics No. 93.

Murrow, H.N. and Whillock, C.H. (1964) Performance Characteristics of a Pre-Formed Elliptical Parachute at Altitudes Between 200,000 and 100,000 ft Obtained by In-Flight Photography, Langley Air Force Base, Virginia, NASA TND-2183.

XXII. The Measurement of High-Altitude Balloon Gas Temperature

R. M. Lucas and G. H. Hall
Arthur D. Little, Inc.
Cambridge, Massachusetts

Abstract

A mathematical model of the vertical motion of high-altitude zero-pressure balloons, programmed for a digital computer, has been in operation for several years. Correlation of input and output data of the program with the measured data of actual flights has been good, but incomplete, because of the lack of simultaneous measurements of balloon gas and air temperature. Ambient air data, a vital program input, has been questionable due to either the timing or geographical location of an associated radiosonde flight or the local effects which occur when the radiosonde and thermometer are placed near the flight hardware. Also, limited information is available on transient gas temperatures. Therefore, a test flight was conducted to obtain balloon gas and air temperatures. The necessary flight parameters were then used to fly the mathematical model and the output of this digital program, altitude, and gas temperature, were compared to the measured values. The resulting correlation indicates that the mathematical model is sufficiently accurate to predict the vertical motion of high-altitude balloons providing the local air temperature profile is known. A preliminary test program was conducted to evaluate the thermistor characteristics, to provide the necessary calibrations, and determine the possible measuring errors.

1. INTRODUCTION

The vertical motion of high-altitude balloons may be calculated by solving a series of equations which relate to the acceleration of the gas-fabric system (the equation of motion), the energy equations for the fabric and gas, and the consideration of air and helium as perfect gases. The equations have been integrated numerically and programmed on an IBM 7090 computer in FORTRAN II (Dingwell, Sepetoski, and Lucas, 1963; Germeles, 1966). Good correlations have been made with the Stratoscope II and Stargazer altitude-time histories.

Among the several inputs and outputs of this program is the air temperature vs altitude profile as an input, and the helium gas temperature vs time as an output or calculated quantity. In order to establish a better correlation than was heretofore available, an instrumented flight was made from Page, Arizona on October 18, 1964.

2. BALLOON SYSTEM

The balloon, helium, telemetry system, ground support and flight conduct were provided by the National Center for Atmospheric Research (NCAR). The general configuration and dimensions of the balloon system are shown in Figure 1.

There were two major differences between this balloon manufactured by Raven Industries and the usual high-altitude vehicles. The top fitting was a 14-in.-diam collar with an 8-in. opening and cover plate for insertion of the thermistors at the launch site. The balloon material, 1.4-mil polyethylene was not dusted with the usual lubricating powder in order to prevent contamination of the surface radiation properties of the thermistors and the hardware inside the balloon. The gross load of the balloon and payload was 514 lb. With a gross lift of 548 lb, the free lift was 6.75 percent. The theoretical ceiling was 80,000 ft.

3. INSTRUMENTATION

3.1 Telemetry System

The telemetry system was designed and built by NCAR (Anonymous, 1964) as a permanent system adaptable to a wide variety of sensor parameters.

The system operates as an FM/FM data transmission system. The unit has 41 channels for signal transmission and 6 channels for synchronization control, time and balloon controls, and so forth. It has an analog-to-digital converter which converts the voltage signals to a 3-digit decimal number expressed in binary code. The output of the encoder is an FM signal. The system has a second modulating

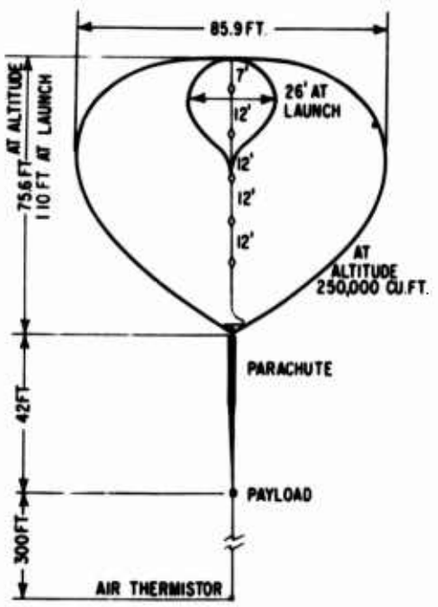

Figure 1. Balloon Configuration

unit for control use and it is a "return-to-zero" type for operation as a "pulse duration modulation" of a "pulse coded system".

The ground station components employ a variety of data recorders and read-out equipment. For this flight, a Flexowriter was chosen for real-time printout as most convenient for immediate assessment of the data.

The temperature data appeared as a 3-digit number and each thermistor occupied 3 channels of information that provided overlapping data in 3 temperature ranges. With this arrangement, the numerically largest number has the greatest accuracy. The entire system was scanned at a rate to give a complete set of temperature readings every 15 sec.

The other channels, in addition to providing pressure/altitude information by means of a hypsometer (Conover and Stroud, 1958), provided telemetry system checks and circuit calibrations.

3.2 Sensors

In choosing a temperature sensor, the more important requirements are:

(1) Measure the temperature of helium gas over a range of +40°C to -80°C and in helium atmosphere pressure range of 20 to 1000 mb.

(2) Be accurate to within ± 0.1°C with a time constant of less than 10 msec.

(3) Provide high enough signal so that the telemetry system could detect a change of 0.01°C.

(4) Exhibit no drift or loss of accuracy after repeated temperature cycling and exposure to simulated solar radiation.

(5) Be unaffected by solar radiation, and when connected to leads, be insensitive to electromagnetic radiation associated with the balloon system.

(6) Be small, lightweight, and capable of being physically protected during flight.

In order to accurately measure the gas temperature within a balloon at low pressures, it is necessary to thermally couple the temperature sensor to the surrounding gas and to thermally decouple the sensor from radiative effects caused by solar energy transmitted through the balloon fabric and by infrared radiation emitted by the balloon fabric, other internal equipment, the atmosphere, and the earth. Self-heating in a thermistor – for example, by internal power dissipation – must be made negligibly small. In addition, it is usually desirable to design the temperature sensor to have a small thermal time constant.

The advantages of using small temperature sensors such as thermistor beads less than 20 mils in diameter have been discussed by Ney, et al. (1961). For sensors of small diameter, the Nusselt number, which is the ratio of heat transfer by natural convection to that by conduction, is very small; therefore, the heat loss from the sensor is controlled by conduction to the surrounding gas. Furthermore, it can be shown that the ratio of heat loss by conduction to that lost by radiation for a spherical sensor immersed in an infinite medium of thermal conductivity K is:

$$\frac{K}{\epsilon r \sigma \bar{T}^3} \tag{1}$$

where

K = thermal conductivity of the gas

r = radius of sensor

ϵ = emittance of sensor

$\bar{T}$ = mean temperature of sensor

σ = Stefan Boltzman constant.

From Eq. (1) it can be seen that radiative effects are made small by using a sensor of small diameter and low emittance. For a small spherical sensor whose heat loss is controlled by conductive effects, the error due to incident radiation from sunlight (for example) and to self-heating is given by the simple equation

$$T - T_{\infty} = \frac{r \alpha S}{K} + \frac{p}{4 \pi r K} \qquad (2)$$

where:

- T = sensor temperature
- T_{∞} = true gas temperature
- r = sensor radius
- K = gas conductivity
- α = absorptance for incident radiation
- S = incident radiant flux per unit surface area
- p = internal power dissipation.

Equation (2) shows that the errors due to radiant heating may be made small by using a sensor of small radius and a low absorptance. In addition, the bias power dissipated in the sensor must be made small to reduce the self-heating error.

The thermal time constant of a spherical sensor losing heat by conduction is

$$\tau = \frac{\rho r^2 c}{3K} \qquad (3)$$

where:

- ρ = density of sensor
- c = specific heat of sensor
- τ = thermal time constant (sec) .

The equation also shows that a small radius will result in a short time constant.

In summary, the accuracy of gas temperature measurements is enhanced by use of sensors with a small radius, low emittance, and low absorptance for incident radiation provided that internal power dissipation is made small. However, there is a limitation to the minimum size sensor that can be used. At the minimum pressures which exist in balloons, the characteristic dimension of the sensor must be large with respect to the mean free path in the gas so that the sensor can lose heat effectively by conduction. The thermistor sensor used in this investigation had a diameter of 9 mils which is roughly 20 times the mean free path in helium at the pressure of 18 mb — encountered at 80,000 ft.

Ney, et al. (1961) have shown that a 15-mil-diam, aluminized thermistor having an emittance and absorptance of 0.1 can be used to measure gas temperatures to within approximately 0.7°C, with an internal dissipation of 8 microwatts. This figure includes errors associated with infrared and solar radiation. The aluminized thermistor used in the present investigation had an internal power dissipation of less than 10 microwatts. Therefore, we expect that the reduced diameter and power dissipation used in the present thermistor arrangement would lead to errors of considerably less than 0.5°C.

The final sensor selection was a 9-mil aluminized bead thermistor (VECO TX819D), made by Victory Engineering Corporation, Springfield, New Jersey.

3.3 Circuitry

The circuit that was used to measure thermistor resistance is shown in Figure 2. The output voltage from the telemetry encoder is given by

$$E_o = E_{in} R_{fb}/R_{th}$$

where

E_o = output voltage

E_{in} = input voltage (0.166 volt) = output from thermistor metering circuit

R_{fb} = feedback resistance

R_{th} = thermistor resistance.

Three feedback resistors were required to cover the range of thermistor resistance change.

In selecting the feedback resistors, values were chosen such that E_o would not exceed 10 V and could be read to three significant digits up to values of 9.99 V. Each thermistor was coupled sequentially to each of the three feedback resistors; thus three readings were obtained for each thermistor.

As a further check on the accuracy of the system, four pairs of fixed, standard resistors were inserted periodically in the measuring circuit. The values of resistance covered the same range the thermistors would experience during the flight. This procedure provided a continuous check on the complete telemetry system. The actual readings were within one digit of each other, indicating excellent stability.

3.4 Calibration and Test Procedures

For most of the test and calibration procedures a sealed brass vessel, 6-in. on a side, was used. The vessel had feedthroughs to mount the thermistors and two window ports for introducing radiation. It could be evacuated by means of small tubing, and was immersed in a dry-ice bath for low-temperature tests.

For the thermal tests, the thermistor was mounted on two copper supports of the feedthroughs and heaters were placed on the exterior ends of the supports to simulate warm leads. The thermistors required thermally nonconducting leads to isolate them for the planned configuration. To accomplish this, the thermistors were connected to the copper mounting rods by means of a 0.003-in.-diam nichrome wire, 4-in. long. With a temperature differential of 15°C between the copper supports and the helium, the thermistor indicated an error greater than 1°C. Placing

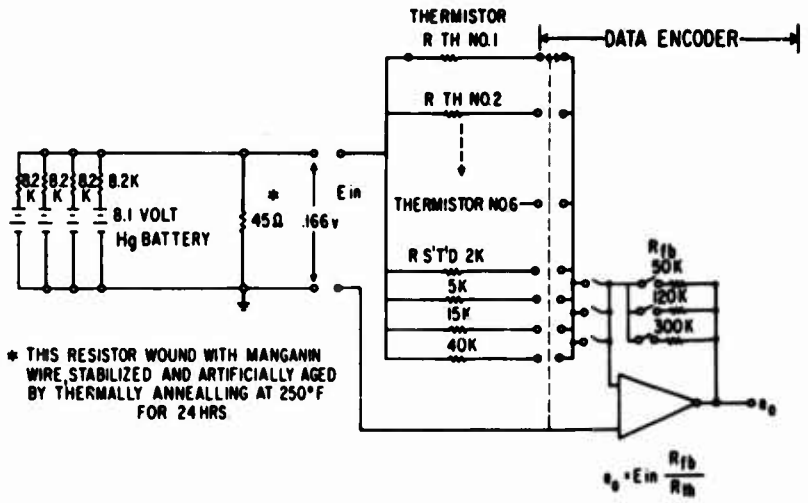

Figure 2. Thermistor Circuitry

a 4-in. length of 0.0015-in.-diam nichrome wire in series between the support and the thermistor, the error was less than 0.1°C for the same temperature differential at the 20-mb level.

The capacitance effect of 160 ft of twisted copper leads was also investigated and the time constant of the thermistor and leads was found to be much less than 5 msec. This was less than the fixed 10 msec delay time after switch closing prior to signal processing.

To minimize self-heating, resistance change with current level was established for the 20 to 1000-mb helium pressure range. The current level was also established for the temperature range of +25°C to -80°C. The maximum current level was determined which corresponded to a temperature change of 0.25°C, the maximum allowable error. The worst case occurred at the 20-mb level with a 0.1-deg error and a power dissipation of 10 microwatts. For the radiation tests, solar simulators were used which would produce a spectrum and energy level equal to that expected at the 80,000-ft level. Errors from these tests did not exceed 0.1°C.

4. MECHANICAL INSTALLATION

Since the gas temperature varies with location in a balloon, thermistors ideally should be arranged in a space array within the balloon. However, such an array would be difficult to install, be susceptible to in-flight failure, and a simple approach was preferred. Consequently, the sensors were arranged vertically (Figure 1) so that the two top sensors would be exposed to the gas at a launch, and as the balloon ascended, successive sensors would be exposed as the balloon fabric deployed.

The thermistor cage (Figure 3) is 9-in. long and 6-in. at the largest diameter. The solid stainless steel rod that carries the main load is threaded at both ends for aircraft type fittings swaged to 1/16-in.-diam preformed wire rope. The other elements are 1/8-in.-diam stainless steel tubing bent to shape and silver-soldered to form an open protective structure for the thermistor. In this manner, the thermistors are always in an active position but are physically protected from damage, for example, from insertion into the balloon on the ground or the action of the undeployed balloon fabric during launch and ascent. The tubing serves as mechanical conduits for the twisted pairs of teflon-coated copper leads. At each cage, one pair of leads terminates at the thermistor while the remaining pairs pass through the tubing and continue on to the next cage. All five pairs exit from the balloon through the bottom fitting, run along the suspension system, and terminate at the telemetry unit in the payload. To thermally isolate the cages and thermistors from the support cable and leads, the cages were flashed with a thin coating of gold. This coating reduced the thermal absorption of the cages without any appreciable increase in axial thermal conductivity. The thermistor bead, located approximately 5-in. from the centerline of the load-carrying rod and support cable, is beyond the boundary layer associated with any convective flow around the vertical cable support inside the balloon.

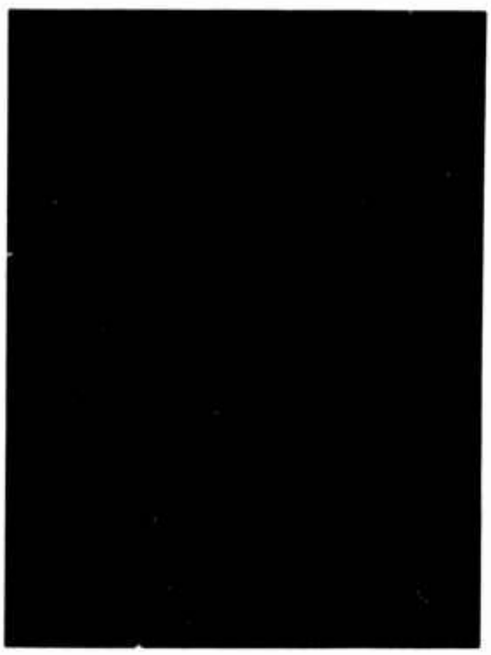

Figure 3. Thermistor Cage

In order to reduce the conduction of heat from the copper leads, which probably are warmer than the helium gas, to the thermistors, the leads were isolated from the thermistors by 4-in. of 0.0015-in.=diam nichrome wire welded at the connections. The result was the thermistor acted as a central weight on a thin beam and was most sensitive to mechanical shock and vibration. Probably this was the reason the two lower thermistors were lost during the launch preparations. However, the thermal characteristics could not be sacrificed for improved resistance to the mechanical environment.

All leads after exiting the balloon were threaded through the release squibs along with the balloon-to-parachute connector to completely separate all connections at cut-down.

5. LAUNCH AND FLIGHT

5.1 Site and Weather Requirements

An earlier launch attempt was made at the Palestine, Texas, balloon site of NCAR. Many of the preflight electromagnetic interference tests (radar, tracking beacon) and thermal radiation tests were also made at this location.

After a close-up witnessing of several "dynamic" balloon launchings, with this thermistor payload requirement in mind, it was decided that the only acceptable launch would be a "static" launch with no surface winds and zero cloud coverage. Although cloud coverage can be taken into account, the computer program also requires a knowledge of the times of in-flight shadowing which was impossible to obtain in a simple experiment of this type.

Therefore, the launch was made at a secondary site, Page, Arizona. The flight was continued after ceiling was reached, and until the received data indicated that the system was in thermodynamic equilibrium. The trajectory covered the southwestern area below Page, over parts of Grand Canyon; cutdown occurred near Tuba City, Arizona. There were no clouds and little upper altitude winds to seriously affect the system.

5.2 Installation and Erection

The balloon was uncrated and laid full length with the gores separated into two bundles, to expose one slightly inflated central gore. A preinstalled nylon line between the top fitting and the bottom fitting was attached to the lower end of the thermistor cables and carefully drawn through the top fitting. The top connector of the support cable was attached to the cover plate of the top fitting and the cover sealed to complete the enclosure of the balloon.

The helium was initially introduced slowly through the inflation tubes to avoid high-velocity, turbulent gas flow that could cause the thermistor beads to oscillate severely and the structure to fail. As the balloon envelope expanded, the helium gas flow was increased to normal inflation rates. It was somewhere during this inflation and gradual erection of the balloon that the two lower thermistors were lost.

The last operation was the attachment of the air thermistor to the 300-ft of conductor. For this installation, the strength of the lead wire was important and #27, hard-drawn magnet wire was chosen. The wire terminated in a pretzel-shaped open-cage of stainless steel tubing which was also gold flashed. Nichrome leads were also employed for this sensor.

Protection of the thermistor was less important and the bead was quite exposed to the air flow. The air thermistor was hung about 5 ft away from the centerline of the flight payload and about 10 ft away from the trailing wire, beacon antenna which was 150-ft long. Thus, there was no thermal interaction with the balloon external air flow (Ney, et al., 1961) and no electromagnetic interaction with the antenna.

5.3 System Performance

In general the entire system performed as expected. Data reception was excellent and uninterrupted except for a 30-min loss in the air-temperature measurement during ascent. However, enough data was received to establish this important parameter for the computer program. Although never fully ascertained, we concluded that the cause was a faulty reed relay in the airborne telemetry system.

6. DATA REDUCTION

The data was received in digital form in three significant decimal digits. The circuitry was designed to compare, proportionally, the resistance of the thermistor to three calibrated resistors. The highest ratio was used as the reference because the errors due to digital conversion were minimized. For instance, at tropopause, the air thermistor digital read-outs were 033, 081, 207, which, when compared with the highest reference resistor and the calibrated temperature resistance curve of the thermistor, gave a temperature of 382.5°R. An error of ±1 decimal digit in the 207 reading will give an error of ± 0.2°R in the data reduction process.

For computation of altitude, the hypsometer data was reduced to pressure and the altitude was calculated by constructing a model atmosphere from the measured temperature and pressure.

The data received totalled 250,000 decimal digits and was reduced by means of a digital computer program which was written to accept directly the output from the telemetry equipment.

7. RESULTS

7.1 Air Temperature Measurements

The temperature measured by the standard radiosonde was greater than the temperature measured by the thermistor which was suspended 300 ft below the payload. This data is presented on Figure 4. Analysis of the data indicates that the radiosonde data is, at times, 40°F greater than the air thermistor data. We believe that this temperature is due to local air heating due to absorption of thermal radiation by the uninflated balloon fabric. During ascent this mass of fabric undoubtedly warms air locally and this air temperature is measured by the radiosonde. We make this tentative conclusion since the inflated fabric temperature and the helium temperature which is computed (see Figures 5 and 6) is usually less than the radiosonde air temperature.

The temperatures measured by the air thermistor indicates that there are gradients in the atmosphere which are rather abrupt and choppy over small temperature excursions. The amplitudes of temperature measured are too high to be attributed to data transmission noise or errors in the data reduction process. The "choppiness" results in local changes in air density which can create transient changes in ascent velocity of the balloon system. Figure 5 shows two velocity bands above tropopause where the balloon ascent rate suddenly doubled. We believe that this occurred as the balloon entered stratified, cold layers.

7.2 Helium Gas Temperatures

The helium gas temperatures showed generally less scatter than the air temperature data. However, during ascent, there were significant changes in the local temperatures over four temperature samples taken at 15-sec intervals. We attribute this scatter to local flow patterns.

In Figure 5, the difference between helium and air temperatures (superheat) are plotted during ascent. Also plotted is the ascent velocity profile. Because this flight occurred in the daytime under full sunlight, there is little difference between the air and gas temperature, generally the "negative" superheat was less than 10°C. The maximum deviation occurred at the greatest ascent velocity as the balloon attained ceiling. As altitude was reached, the gas superheated to +24°C as a result of the solar radiation absorbed by the polyethylene fabric.

7.3 Computer Correlation

The correlation of computed and actual flights is excellent. Unfortunately, the thermistor measuring air temperature ceased to function properly after the balloon reached its ceiling and, therefore, correlation to the end of the ceiling phase could not be done. Four hours and 20 min after launch the flight was terminated.

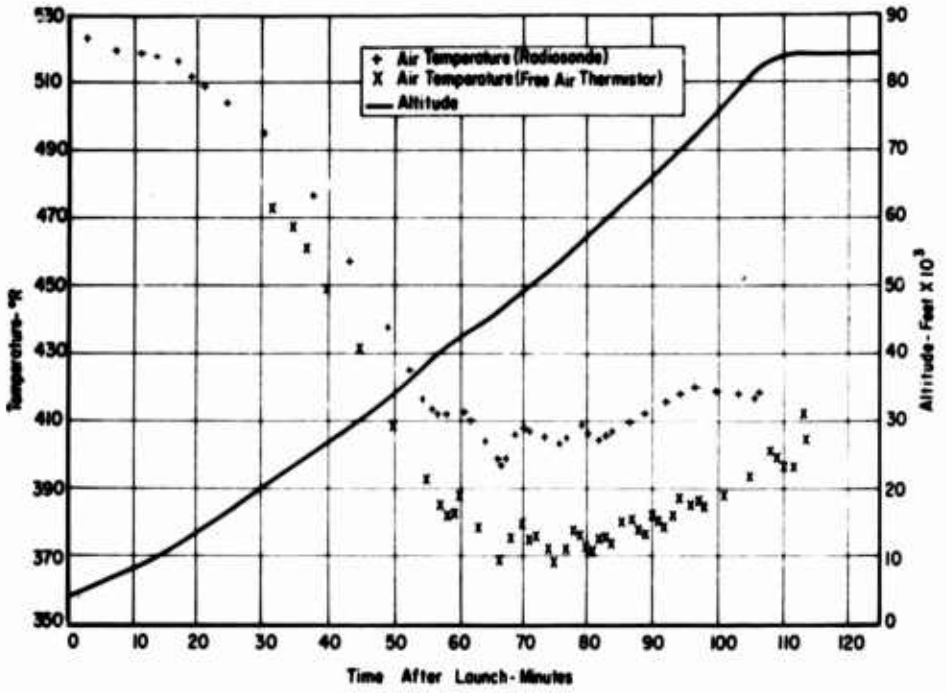

Figure 4. Air Temperature and Altitude Trajectory

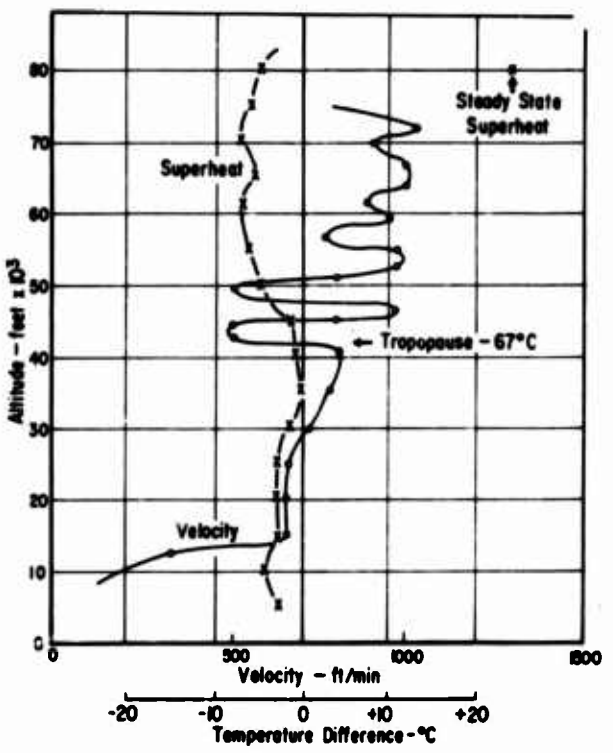

Figure 5. Helium Gas Superheat and Balloon Velocity During Ascent

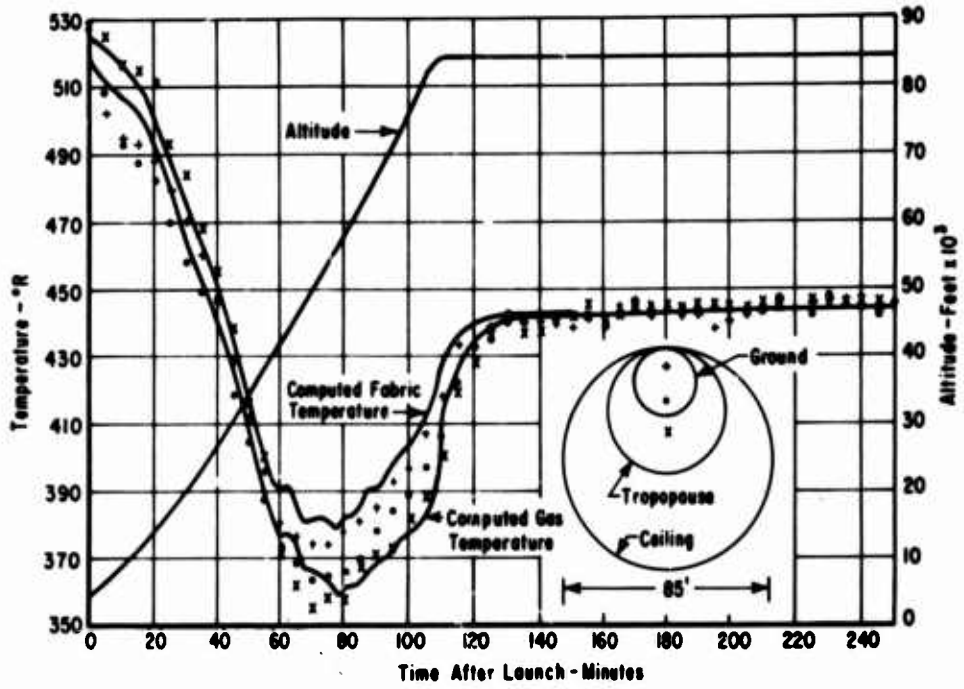

Figure 6. Temperature Correlation. Sketch shows thermistor position with respect to theoretical spherical volume

The correlation of computed and measured temperatures is shown in Figure 6. The relation of the temperature of each thermistor to the average temperatures of the gas and fabric depends, of course, on the position of the thermistor with respect to the volume of the balloon. The position of each thermistor during the flight can be deduced roughly from the sketch on the lower right of Figure 6, in which the balloon is represented grossly by a sphere. The diameter of the balloon was about 26, 46, and 80 ft at ground, tropopause, and ceiling, respectively. Thus, at ground, the lower thermistor was buried in the loose fabric.

With the aid of this sketch, a careful examination of Figure 6 shows that the correlation of computed average temperatures and measured temperatures is very good. The maximum deviation, at some parts of the flight, is less than 10°R. During most of the flight, the deviation is much less than 10°R.

The upper thermistor was coupled more closely to the fabric temperature, as might be expected. Also the average or bulk temperature of the helium is followed most closely by the thermistor which is most centrally located in the volume at an instant of time. That is, the computed gas temperature initially follows the upper thermistor. Just before tropopause, it follows the middle thermistor, and near ceiling the lower thermistor. There is a toroidal mixing of the gas upward along the balloon fabric and downward in the center along the thermistor string so this location for the sensors appears appropriate. The rotational symmetry of the mixing results

from the radiative absorption of the fabric on the far as well as near side to the sun and the fact that balloons tend to oscillate in rotation through much of their flight (Germeles and Lucas, 1963).

We think that this flight has given considerable support to the validity of our analysis, and that it has verified our long-held view that the fabric of balloons experiences rather low temperatures through tropopause. The temperature of the top thermistor must be closely coupled to the fabric temperature.

The small oscillations in the computed temperatures at tropopause are due to corresponding oscillations in the input air temperature data.

7.4 Fabric Temperature

As the computed gas temperatures closely followed the measured gas temperatures, we can deduce that the computed fabric temperatures are representative of the actual fabric temperatures. We estimate that the minimum fabric temperature was -62°C or about 5°C higher than the minimum air temperature. As this flight occurred during sunlight the fabric temperature during an evening ascent may be equal or less than the temperature encountered at tropopause.

8. CONCLUSIONS

The results of this investigation, the good correlation of computed and experimental gas temperatures, have demonstrated the validity and accuracy of the computed model.

Great care must be taken in the choice, application, and calibration of a temperature sensor. Additional effort and caution must also be taken in designing the sensor into a proper circuit and system in order to obtain data within acceptable limits of accuracy.

The tentative conclusion is reached that a thermistor placed near the balloon fabric in the helium gas boundary layer will give a representative measurement of the actual fabric temperature.

Fabric temperatures can be expected to approach the minimum air temperature during ascent.

The correct measurement of air temperature in an ascending balloon must be performed at some distance from the balloon and flight train.

References

Anonymous (1964) Scientific Ballooning, National Center for Atmospheric Research, Newsletter No. 14.

Conover, Walter C. and Stroud, W.G. (1958) A high-altitude radiosonde hypsometer, J. Meteorol. 15:63-68.

Dingwell, I.W., Sepetoski, W.K, and Lucas, R.M. (1963) Vertical Motion of High Altitude Balloons, Arthur D. Little, Inc., Contract No. Nonr-3164(00), Tech Rpt II.

Germeles, A.E. (1966) Vertical Motion of High-Altitude Balloons, Arthur D. Little, Inc., Contract No. Nonr 3164(00), Tech Rpt No. IV.

Germeles, A.E. and Lucas, R.M. (1963) Rotation of Balloons at Floating Altitude, Arthur D. Little, Inc., Contract No. Nonr 3164(00), Tech Rpt No. III.

Ney, E.D., Maas, R.W., and Huch, W.F. (1961) The measurement of atmospheric temperature, J. Meteorol. 18:60-80.

XXIII. A Search for Destructive Forces at the Tropopause

Dr. A. H. Howell
Tufts University
Medford, Massachusetts

Abstract

Anomalous behavior at the tropopause for several types of measurements was reported at the Balloon Symposium in 1964. AFCRL followed this up by sponsoring the assembly of a "Burst Information Collector" package which hopefully will produce fundamental information about the kind of ride that a balloon experiences in passing through the tropopause. A first version of such a BIC package has been successfully flight-tested and during the coming year will be hitchhiked whenever opportunity permits. What has been done is discussed, and suggestions for additional measurements are solicited.

XXIV. Some Meteorological Results of the Southern Hemisphere GHOST Experiment 20 min

Samuel B. Solot
National Center For Atmospheric Research
Boulder, Colorado

Abstract

Since the inception of the Southern Hemisphere GHOST Experiment in March 1966 a vast storehouse of wind data at 200 mb is being accumulated which is at present being processed. These data will eventually lead to hitherto unattainable description of the Southern tropospheric circulation on a hemispheric scale.

This paper discusses the quality of the data, the methods of computing wind and position, and shows some preliminary results of analysis.

Appendix A

Publications of Proceedings of Past AFCRL Balloon Symposia and Workshops

Due to interest expressed in the proceedings of past AFCRL balloon symposia and workshops, and because the report series for these reports has been changed, a listing of the proceedings of all past AFCRL balloon symposia and workshops follows.

TITLE	AFCRL REPORT NO. AND DATE
Proceedings of the AFCRL Balloon Symposium	AFCRL-63-919 December 1963
Proceedings, 1964 AFCRL Scientific Balloon Symposium	AFCRL-65-486 July 1965
Proceedings, AFCRL Scientific Balloon Workshop, 1965	AFCRL-66-309 May 1966

Unclassified
Security Classification

DOCUMENT CONTROL DATA - R&D

(Security classification of title, body of abstract and indexing annotation must be entered when the overall report is classified)

1 ORIGINATING ACTIVITY *(Corporate author)* Hq AFCRL, OAR (CRE) United States Air Force Bedford, Massachusetts 01730	2a. REPORT SECURITY CLASSIFICATION Unclassified 2b. GROUP

3 REPORT TITLE

Proceedings, Fourth AFCRL Scientific Balloon Symposium

4 DESCRIPTIVE NOTES *(Type of report and inclusive dates)*

Scientific Report. Interim.

5 AUTHOR(S) *(Last name, first name, initial)*

DWYER, James F., Editor

6 REPORT DATE	7a. TOTAL NO. OF PAGES	7b. NO. OF REFS
January 1967	292	105

8a. CONTRACT OR GRANT NO.	9a. ORIGINATOR'S REPORT NUMBER(S) AFCRL-67-0075 Special Reports No. 57
b. PROJECT AND TASK NO. 6665-01	
c. DOD ELEMENT 65402124	9b. OTHER REPORT NO(S) *(Any other numbers that may be assigned this report)* AFCRL-67-0075
d. DOD SUBELEMENT 632800	

10 AVAILABILITY/LIMITATION NOTICES

Distribution of this document is unlimited. It may be released to the Clearinghouse, Department of Commerce, for sale to the general public.

11 SUPPLEMENTARY NOTES	12 SPONSORING MILITARY ACTIVITY
	Hq AFCRL, OAR (CRE) United States Air Force Bedford, Massachusetts 01730

13 ABSTRACT

This document is comprised of a series of papers presented at the Fourth AFCRL Scientific Balloon Symposium in September 1966. The range of subject matter was purposely selected to cover both the major branches of balloon technology and a limited number of topics having a common disciplinary background. It was intended to provide, thereby, the exchange of information on capabilities and requirements essential to the orderly advancement of this technology.

DD FORM 1 JAN 64 1473

Unclassified
Security Classification

Unclassified
Security Classification

14. KEY WORDS	LINK A		LINK B		LINK C	
	ROLE	WT	ROLE	WT	ROLE	WT
Balloon, Inflatables Instrumentation **Ballon Systems, Materials**						

INSTRUCTIONS

1. ORIGINATING ACTIVITY: Enter the name and address of the contractor, subcontractor, grantee, Department of Defense activity or other organization *(corporate author)* issuing the report.

2a. REPORT SECURITY CLASSIFICATION: Enter the overall security classification of the report. Indicate whether "Restricted Data" is included. Marking is to be in accordance with appropriate security regulations.

2b. GROUP: Automatic downgrading is specified in DoD Directive 5200.10 and Armed Forces Industrial Manual. Enter the group number. Also, when applicable, show that optional markings have been used for Group 3 and Group 4 as authorized.

3. REPORT TITLE: Enter the complete report title in all capital letters. Titles in all cases should be unclassified. If a meaningful title cannot be selected without classification, show title classification in all capitals in parenthesis immediately following the title.

4. DESCRIPTIVE NOTES: If appropriate, enter the type of report, e.g., interim, progress, summary, annual, or final. Give the inclusive dates when a specific reporting period is covered.

5. AUTHOR(S): Enter the name(s) of author(s) as shown on or in the report. Enter last name, first name, middle initial. If military, show rank and branch of service. The name of the principal author is an absolute minimum requirement.

6. REPORT DATE: Enter the date of the report as day, month, year, or month, year. If more than one date appears on the report, use date of publication.

7a. TOTAL NUMBER OF PAGES: The total page count should follow normal pagination procedures, i.e., enter the number of pages containing information.

7b. NUMBER OF REFERENCES: Enter the total number of references cited in the report.

8a. CONTRACT OR GRANT NUMBER: If appropriate, enter the applicable number of the contract or grant under which the report was written.

8b, 8c, & 8d. PROJECT NUMBER: Enter the appropriate military department identification, such as project number, subproject number, system numbers, task number, etc.

9a. ORIGINATOR'S REPORT NUMBER(S): Enter the official report number by which the document will be identified and controlled by the originating activity. This number must be unique to this report.

9b. OTHER REPORT NUMBER(S): If the report has been assigned any other report numbers *(either by the originator or by the sponsor)*, also enter this number(s).

10. AVAILABILITY/LIMITATION NOTICES: Enter any limitations on further dissemination of the report, other than those imposed by security classification, using standard statements such as:

(1) "Qualified requesters may obtain copies of this report from DDC."

(2) "Foreign announcement and dissemination of this report by DDC is not authorized."

(3) "U. S. Government agencies may obtain copies of this report directly from DDC. Other qualified DDC users shall request through

_____."

(4) "U. S. military agencies may obtain copies of this report directly from DDC. Other qualified users shall request through

_____."

(5) "All distribution of this report is controlled. Qualified DDC users shall request through

_____."

If the report has been furnished to the Office of Technical Services, Department of Commerce, for sale to the public, indicate this fact and enter the price, if known.

11. SUPPLEMENTARY NOTES: Use for additional explanatory notes.

12. SPONSORING MILITARY ACTIVITY: Enter the name of the departmental project office or laboratory sponsoring *(paying for)* the research and development. Include address.

13. ABSTRACT: Enter an abstract giving a brief and factual summary of the document indicative of the report, even though it may also appear elsewhere in the body of the technical report. If additional space is required, a continuation sheet shall be attached.

It is highly desirable that the abstract of classified reports be unclassified. Each paragraph of the abstract shall end with an indication of the military security classification of the information in the paragraph, represented as *(TS), (S), (C), or (U).*

There is no limitation on the length of the abstract. However, the suggested length is from 150 to 225 words.

14. KEY WORDS: Key words are technically meaningful terms or short phrases that characterize a report and may be used as index entries for cataloging the report. Key words must be selected so that no security classification is required. Identifiers, such as equipment model designation, trade name, military project code name, geographic location, may be used as key words but will be followed by an indication of technical context. The assignment of links, rules, and weights is optional.

Unclassified
Security Classification